DEVELOPMENT OF A YARN CAPABLE OF MEASURING LOCALISED TEMPERATURE

Pasindu Lugoda

A thesis submitted in partial fulfilment of the requirements of

Nottingham Trent University for the degree of Doctor of Philosophy

February 2018

Copyright statement

Acknowledgement

I would firstly like to thank my supervisor and the director of studies Professor Tilak Dias for providing me with this life changing opportunity. You have been a tremendous mentor to me and your advice on this research and on my career has been priceless. Thanks a lot for encouraging me and allowing me to grow as a research scientist. It would have been impossible to complete this research successful without your great supervision.

I would also like to express my thanks to my second supervisor Dr. Rob Morris. You have also been an incredible mentor to me and guided me throughout the research. I want to also thank Dr. Theodore Hughes-Riley and Dr. Christophe Trabi for their support and guidance. I am extending my thanks to all the past and present members of the Advanced textiles research group, they have offered incredible support during this study, Dr. Colin Cork, Dr. Ekael Mbise, Dr. Dorothy Hardy, Richard Arm, Carlos Oliveira, Dr. Anura Rathnayaka, Dr. Dilusha Rajapaksha, Ioannis Anastopoulos, Will Hurley, Gayani Nandasiri, Achala Satharasinghe, Dr Arash Shahidi, Dr. Varindra Kumar.

This research would not have been possible if not for the Vice Chancellor's Bursary awarded by Nottingham Trent University for which I am extremely honoured and grateful.

I wish to give a very special thanks to my parents (Susantha Lugoda and Tilani Lugoda), brother (Uwin Lugoda) and grandmother (Matilda Suwadaratne) they have made countless sacrifices for me. I would like to dedicate this dissertation to them. I would also like to thank all my friends and family including Dr. Buddhike Neminda, Valerio Salis, Dr. Heshan Ariyasena and Manjula Ariyasena for their advice and suggestions that has made my stay in Nottingham more enjoyable. Lastly, I would like to thank all my friends for cheering me up and inspiring me to strive for my goals.

Abstract

In this research an electronic temperature sensor (ETS) yarn has been developed by embedding a commercially available thermistor chip into the fibres of a yarn. A polymer resin is used to encapsulate the thermistor creating a micro-pod which protects the thermistor from mechanical and chemical stresses during use, and also allows the ETS yarn to be washed. The thermistor micro-pod and interconnects were then encased within a warp knitted braid to from the ETS yarn.

Temperature is the most widely measured physiological bio-marker in medicine. Temperature changes can indicate underlying pathologies such as wound infections or the formation of ulcers in diabetic patients. A temperature sensor capable of providing remote, continuous and localised (temperature at a given point) temperature measurements could provide clinicians with a powerful tool when handling such complications. Even though there are many flexible temperature sensors they lack true textile characteristics making them unsuitable in many situations. The existing textile-based temperature sensors are incapable of providing localised measurements and can suffer from hysteresis.

At the start of the project a geometrical model of the ETS yarn was developed in-order to understand its design parameters. Then the crafting of the ETS yarn was achieved in three key stages. Hardware and software necessary to obtain temperature from the ETS yarn have been developed. Thereafter work has been conducted to characterise the behaviour of the thermistor and understand the design rules for the micro-pod. Theoretical models were created in COMSOL in-order to study the heat flow through the micro-pod and warp knitted braid, and the effect they have on the response and recovery times of the thermistor. The model has been validated using experiments. Results have shown that encapsulating the thermistor in a micro-pod and making it into a yarn has a minimal effect on the thermal time constant and that the resin of the micro-pod and fibres of the warp knitted braid have no significant impact on the accuracy of the temperature readings. The research into calibrating the ETS yarn has shown that the resistance-temperature conversion equation provided by the thermistor manufacturer provided the most accurate temperature measurement with 63 % of the readings being within ± 0.5 °C accuracy. Cyclic tests have been carried out on the ETS yarn to ensure that its performance is not effected by mechanical strain. Thereafter an evaluation of the response of the ETS yarn to operational conditions (ambient temperature, moisture content, wind speed) was studied.

Finally, prototype temperature sensing garments have been produced using a network of ETS yarns. The necessary hardware and software to capture the temperature data from these prototypes has been developed. Finally, two prototypes have been created, a temperature sensing sock with five ETS yarn for detecting non-freezing cold injuries and a dressing with 16 ETS yarns to provide a temperature map of a wound. The temperature sensing sock was tested on volunteers. Both the

wound dressing and the sock can provide remote, continuous and localised temperature measurements without compromising the textile characteristics of the fabric.

Table of Contents

List of Figures and Tables

List of Figures

List of tables

1. Introduction

The thesis demonstrates the scientific study carried out to develop wearable temperature sensing textiles for monitoring skin temperature. The temperature sensing textiles were created by embedding miniature semiconductor sensors, thermistors, within the fibres of yarn, which enables a high degree of integration of sensors in a textile fabric.

1.1 Brief Background

1.1.1 Importance of Body Temperature measurement

Body temperature is widely considered as one of the main vital signs that must be measured and monitored in hospital patients (Louise McCallum and Dan Higgins, 2012). It is also an established bio-marker of infection in wounds (Nakagami et al., 2010), (Mufti et al., 2015), (Chaves et al., 2015) and could be used to manage the occurrence of foot ulcers in diabetic high risk patients (Armstrong et al., 2007), (Yusuf et al., 2015). Pathology is determined from a difference in skin temperature relative to other regions of the skin and not from an absolute temperature measurement as this will change depending on other external parameters. Extensive work in the literature has determined that a temperature difference of 2.2 °C is sufficient to identify diabetes foot ulcer formation (Armstrong et al., 2007), (Lavery et al., 2007), (Lavery et al., 2004), (Peregrina-Barreto et al., 2014). Ulcer formation takes place over the course of a week with previous studies taking temperature measurements twice-daily (Armstrong et al., 2007). Traditional thermometers are not well suited for ambulatory temperature measurement or regular contact measurements of a single point on the skin.

Wound care has become one of the leading health challenges in the 21st century and the cost is expected to escalate to an annual US$20 billion in the coming years (John O'Connor, 2012). Chronic wounds require frequent dressing changes to determine possible infections, an activity which creates a burden in terms of health care costs, nursing care, patient outcomes and hospitalization time (Hilton et al., 2004).

A sensor capable of providing remote localised temperature (temperature at a given point) measurements could also be used to determine Non-Freezing Cold Injury, monitoring temperature in infants (Chen et al., 2010) and breast cancer detection (Lawson and Chughtai, 1963)

1.2 Research Motivation

The development of a wearable medical device capable of providing localised temperature measurements is therefore prudent. The field of wearable medical devices has grown in recent years due to reducing costs of electronics, with revenues of US$2.8 billion in 2014, which are predicted to rise to US$8.3 billion by 2019 (Mordor Intelligence, 2014). A wearable temperature

sensor capable of providing remote continuous temperature measurements while the patients are in the comforts of their own homes, would provide the clinicians with a powerful tool when dealing with diabetic high risk patients and patients with ulcers. A textile structure is the ideal solution for creating a framework for a comfortable and conformal wearable temperature measuring fabric. An ideal way to achieve this is by using a yarn embedded with a temperature sensor such as a thermistor that could be knitted or woven into a wearable textile which is the focus of this work.

1.3 Aims and Objectives

The aim of this project was to create a new generation of temperature sensing textiles by fully embedding a semiconductor sensor within the core of yarns. The temperature sensing textile should be capable of monitoring temperature at different points therefore giving clinicians a powerful tool when dealing with complications such as wound care. In-order to achieve this aim and to focus and simplify the process, the aim was broken down into the following objectives:

- To design and construct the Electronic Temperature Sensing (ETS) yarn from a commercially available thermistor;
- Create the software and the most appropriate hardware to capture temperature from the ETS yarn;
- Study the effects of the polymer resin and yarn filaments (that are used to craft the ETS yarn) on the response and recovery time of the thermistor;
- Understand the errors that might occur due to the polymer resin and the yarn filaments used on the accuracy of the ETS yarn;
- Find an appropriate method to calibrate the ETS yarn;
- To understand the effects of tensile stress on ETS yarn;
- Investigate the influence of external conditions such as ambient temperature and moisture content on the temperature recorded by the ETS yarn;
- Create temperature sensing textiles using ETS yarn capable of monitoring temperature in individuals;
- Develop the software and hardware to capture and present the temperature recorded with the temperature sensing textiles;
- Carry out a small-scale user trial using the developed temperature sensing textiles.

The aims and objectives have been derived from the gap in knowledge identified in chapter 2 section 2.7.

1.4 Research Methodology

In order to achieve the research aim the proposed methods and outcome of the research will be discussed in this section. A quantitative approach has been utilized where scientific theories and formulas have been used to design and develop a temperature sensing textile capable of providing remote, localised temperature measurements. The literature search presented in chapter 2 has identified the importance of such a textile in the field of health and wellbeing. Most of the temperature measuring devices that are currently available in the market are not textile-based and do not exhibit textile characteristics such as the ability to bend, shear and drape. The few textile-based temperature sensors that exist in the market are not capable of giving remote, continuous and localised (temperature at a given point) temperature measurements.

Thereby using an approach where semiconductor packaged dies and their associated interconnects are embedded within the fibres of a yarn (Colin Cork et al., 2013), a commercially available surface mounted negative temperature coefficient (NTC) thermistor chip was incorporated into a yarn. The Murata 10 kΩ 100 mW 0402 surface-mount devices NTC thermistor (NCP15XH103F03RC, Murata, Kyoto, Japan) was chosen due to its small size (0.5 mm × 0.5 mm × 1 mm) and sensitivity to the temperature range of interest (20^{o}C - 40^{o}C). The thermistors were soldered onto an eight strand copper wire ((34.60 ± 0.24) µm x 8) which was then encapsulated with a conformable polymer resin with polyester carrier fibres to form a micro-pod surrounding the thermistor. The micro-pod thus formed protected the thermistor from mechanical and chemical stresses the ETS yarn would be subjected to during the subsequent post-processes and eventual use in a medical environment. Finally, the micro-pod was covered using packing fibres and a braided sheath to form the ETS yarn.

First a geometrical model of the ETS yarn was created to identify the necessary design rules for the ETS yarn. The geometrical model looked into the minimum amount of polymer resin required to encapsulate the thermistor; the thickness and volume fraction of the packing fibres and the braiding sheath. Thereafter a jig was created to make the ETS yarn. Then an interface hardware was made to capture the temperature from the ETS yarn, subsequently a software program was developed to present the data in a user-friendly manner.

The incorporation of additional layers between the sensing element and the outer surface of the yarn will retard the flow of heat and therefore will influence the performance of the thermistor in the ETS yarn. The effect of encapsulating a sensing element is a well-known consideration in the field of sensor design (Clausen and Sveen, 2007), (J. Liu et al., 2012).

A theoretical simulation was conducted to determine the effect of the micro-pod and yarn filaments on the thermistor's response and recovery time. The theoretical results were validated using experiments. It was critical to ensure that the response time and recovery time of the thermistor when encapsulated in the yarn was at most on the order of minutes in order to allow multiple

reliable measurements to be taken daily. Similarly, the effect of the thermally resistive barrier caused as a result of the micro-pod on the absolute temperature measurements needed to be understood. While determining the absolute temperature was not necessary for detecting the possibility of foot ulcer formation in diabetes patients (diabetic ulcer formation was detected by comparing temperature measurements at different foot sites), knowing that the temperatures recorded were correct ensured that the relative temperatures measured were accurate. Since the detection of foot ulcer formation presents a change of > 2 ˚C, it was important that the temperature sensing yarn developed could detect changes with an accuracy of around ± 0.5 ˚C. Hence the effects of resin and yarn filaments on the accuracy of the thermistor was tested using a specially developed test rig. Thereafter the most appropriate method to calibrate the ETS yarn was identified. Finally, the temperature captured by the ETS yarn was compared to that of a calibrated thermistor to determine the true accuracy of the yarn.

Textile yarns are subjected to mechanical stresses during their conversion to fabrics and garments, and when it is worn as a garment. Therefore cyclic tests were carried out on the ETS yarn to study the effects of mechanical stress on its temperature measurements.

Once the tests on the ETS yarn were completed it was important to identify the effects of external factors such as ambient temperature and moisture content on the temperature measured by the ETS yarn. Skin contact temperature measurement is a complex process which can be influenced by ambient temperature, sensor shape, contact of its sensing area to the surface and the thermal conductivity of the surface used to hold the sensor (Psikuta et al., 2013) (Soukup et al., 2014)

Finally using multiple ETS yarns, two prototypes were created. It was important to develop an interface hardware; a robust method of connection between the interface hardware and the ETS yarn; and a software interface for the prototypes, a temperature sensing sock and a temperature sensing wound dressing. A small-scale user trial was carried out with the temperature sensing sock. User trials could not be conducted on the wound dressing as clinical approval is required for such a trial.

Ultimately this work presents an innovative solution for the on-line temperature monitoring of diabetes foot ulcers and the infection of wounds with a new generation of temperature sensing textiles. This offers a significant uplift in the capabilities offered by existing technology.

The proposed research methodology is given in the figure 1.1 below

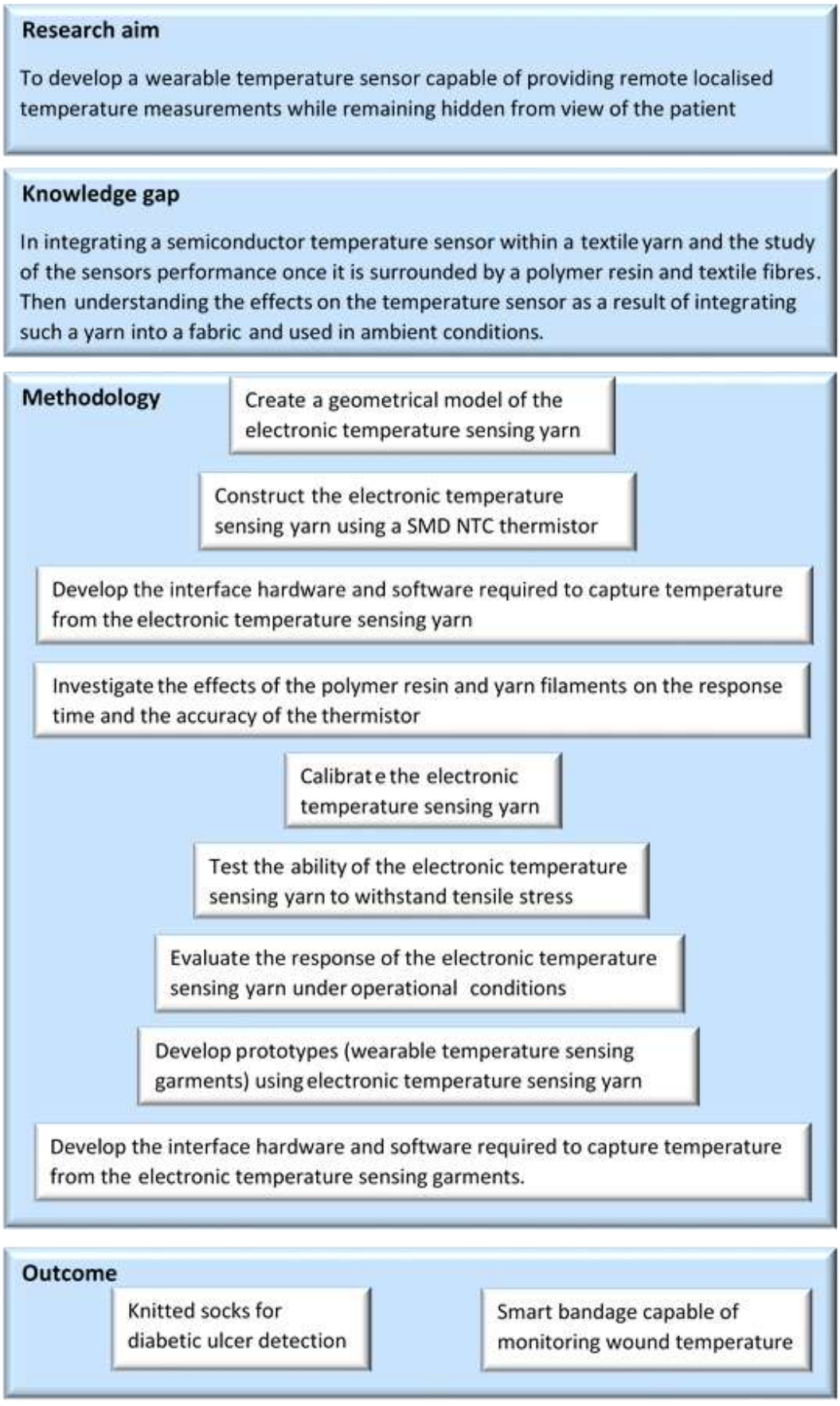

Figure 1-1: Proposed methodology for the project

1.5 Structure of the thesis

The thesis comprises of 8 chapters and the contents of the chapters are summarised below.

Chapter 1 -Introduction which would contain a brief background of the research project followed by the knowledge gap and motivation to do the research. Thereafter the research aims and objectives will be discussed. Then the research methods and steps applied to full fill the research question and objectives will be discussed followed by a brief introduction of the chapters in the thesis.

Chapter 2 – Literature Review will be the intellectual context of the study. The first section will give a brief background on temperature measurement. Then it will look at applications that can benefit from remote continuous temperature measurement; where an in-depth study will be done on wound monitoring, early detection of ulcer and non-freezing cold injury detection. Thereafter the modes of heat transfer in humans would be looked at. Then the next section will look at the different devices and methods used for temperature measurement. This will be followed by an extensive study on thermistors. The next section would be a comparison of the different types of temperature sensors. Then the next section would be on wearable temperature sensor. A brief background history on wearable electronics will be presented. Followed by a thorough analysis of the existing wearable temperature sensors which have been divided into three sections depending on their construction. The last section will identify the gap in knowledge.

Chapter 3- Developing the Electronic Temperature Sensing (ETS) yarn looks at the construction of the Electronic Temperature sensing (ETS) yarn. Initially it looks at the calibration of the thermistors that is going to be embedded within the fibres to make the ETS yarn. Then a geometrical model of the ETS yarn is created using the software MATLAB, in-order to calculate the minimum volume of solder-paste and Polymer Resin required to make the ETS yarn. Thereafter the process of making the ETS yarn has been described in three key steps. Finally the interfacing hardware and software developed to capture the temperature from the ETS yarn would be analysed.

Chapter 4- Performance analysis of the ETS yarn the chapter investigates the effects of the polymer resin and the yarn filaments on the thermistor's response time, accuracy and lastly at the tensile strength of the ETS yarn. Initially it looks at the thermistor's response and recovery times. In-order to do this the effects on the thermal time constant of the chip due to the polymer resin and yarn filaments are studied using a theoretical model created in COMSOL and validated using practical experiments. Then the effects of the polymer resin and yarn filaments on the accuracy of the ETS yarn was analysed using a test-rig which has been developed using Fabroc® heaters. Then the most appropriate method to calibrate the final ETS yarn has been identified. Thereafter the true accuracy of the ETS yarn has been assessed by comparing the temperature captured by the ETS yarn to that of a thermistor which has been calibrated to a high degree of accuracy. Finally cyclic tests were conducted on a standard tensile testing equipment with ETS yarn, to ensure that its readings are not effected by mechanical strain.

Chapter 5- Evaluating the ETS yarn response under operational conditions analyses the effects of environmental factors on the surface temperature measurements provided by the ETS yarn. The study focused on the effects of ambient temperature on the ETS yarn readings. The chapter also analyses the effects on the temperature captured by the ETS yarn when it is not in direct contact with the surface being measured. It also looks at the effects of including the ETS yarn in a textile fabrics to create a temperature sensing fabric. It then investigates the effects of insulating the temperature sensing fabric with different materials. Thereafter it looks at how the orientation of the temperature sensing fabric would impact its measurements. Thereafter experiments have been conducted to investigate the effects of moisture content and relative humidity on the temperature measurements. Finally the effects of wind speed on the temperature measured by the temperature sensing textile has been investigated.

Chapter 6- Design and manufacture of temperature sensing apparel looks closely at using ETS yarn to capture temperature in humans. Initially the ETS yarn was tested on the hand to identify whether the position of the yarn would impact the temperature measurements. Then two prototype garments (arm bands and a glove) were created using ETS yarns. The software and the interconnecting hardware were developed for each prototype and the most appropriate method of connection between the ETS yarn and the interconnecting hardware was sought. Then the final two prototypes were created, a sock for early detection of diabetic ulcer and a wound dressing to monitor wound temperature. Both of them were capable of providing remote temperature measurements. The sock was tested on volunteers and the effects on the temperature measurements due to insulating the sock and the effects of movement when wearing the sock were studied.

Chapter 7-Conclusion is the final chapter of the thesis and it summarizes and concludes the study. It also suggests future work that should be undertaken in order to use these temperature sensing textiles in clinical environments. It lastly looks at the problems encountered during the course of the research and how they have been overcome.

1.6 References

- Armstrong, D.G., Holtz-Neiderer, K., Wendel, C., Mohler, M.J., Kimbriel, H.R., Lavery, L.A., 2007. Skin Temperature Monitoring Reduces the Risk for Diabetic Foot Ulceration in High-risk Patients. Am. J. Med. 120, 1042–1046. doi:10.1016/j.amjmed.2007.06.028.
- Chaves, M.E.A., Silva, F.S. da, Soares, V.P.C., Ferreira, R.A.M., Gomes, F.S.L., Andrade, R.M. de, Pinotti, M., Chaves, M.E.A., Silva, F.S. da, Soares, V.P.C., Ferreira, R.A.M., Gomes, F.S.L., Andrade, R.M. de, Pinotti, M., 2015. Evaluation of healing of pressure ulcers through thermography: a preliminary study. Res. Biomed. Eng. 31, 3–9. doi:10.1590/2446-4740.0571.

- Chen, W., Dols, S., Oetomo, S.B., Feijs, L., 2010. Monitoring Body Temperature of Newborn Infants at Neonatal Intensive Care Units Using Wearable Sensors, in: Proceedings of the Fifth International Conference on Body Area Networks, BodyNets '10. ACM, New York, NY, USA, pp. 188–194. doi:10.1145/2221924.2221960.
- Clausen, I., Sveen, O., 2007. Die separation and packaging of a surface micromachined piezoresistive pressure sensor. Sens. Actuators Phys., Selected Papers from the 9th International Conference on Materials for Advanced TechnologiesICMAT 2005 SISelected Papers from the 9th International Conference on Materials for Advanced Technologies 133, 457–466. doi:10.1016/j.sna.2006.05.011.
- Cork, C., Dias, T., Acti, T., Ratnayake, A., Mbise, E., Anastasopoulos, I., Piper, A., 2013. The next generation of electronic textiles. Presented at the Digital Technologies for the Textile Industries, Manchester, UK.
- Giansanti, D., Maccioni, G., Bernhardt, P., 2009. Toward the design of a wearable system for contact thermography in telemedicine. Telemed. J. E-Health Off. J. Am. Telemed. Assoc. 15, 290–295. doi:10.1089/tmj.2008.0105.
- Hilton, J.R., Williams, D.T., Beuker, B., Miller, D.R., Harding, K.G., 2004. Wound Dressings in Diabetic Foot Disease. Clin. Infect. Dis. 39, S100–S103. doi:10.1086/383270.
- Husain, M.D., Kennon, R., Dias, T., 2013. Design and fabrication of Temperature Sensing Fabric. J. Ind. Text. 1528083713495249. doi:10.1177/1528083713495249.
- O'Connor, J., 2012. Higher wound care costs are driving treatment research. McKnight's. URL https://www.mcknights.com/news/higher-wound-care-costs-are-driving-treatment-research/ (accessed 8.04.2014).
- Krzysztof, G., Gołębiowski Jacek, 2009. Temperature Measurements in a Textronic Fireman Suit and Visualisation of the Results. Fibres Text. East. Eur. 97–101.
- Lavery, L.A., Higgins, K.R., Lanctot, D.R., Constantinides, G.P., Zamorano, R.G., Armstrong, D.G., Athanasiou, K.A., Agrawal, C.M., 2004. Home monitoring of foot skin temperatures to prevent ulceration. Diabetes Care 27, 2642–2647. doi:10.2337/diacare.27.11.2642.
- Lavery, L.A., Higgins, K.R., Lanctot, D.R., Constantinides, G.P., Zamorano, R.G., Athanasiou, K.A., Armstrong, D.G., Agrawal, C.M., 2007. Preventing diabetic foot ulcer recurrence in high-risk patients: use of temperature monitoring as a self-assessment tool. Diabetes Care 30, 14–20. doi:10.2337/dc06-1600.
- Lawson, R.N., Chughtai, M.S., 1963. Breast Cancer and Body Temperature. Can. Med. Assoc. J. 88, 68–70. PMID: 20327365.
- Liu, J., Shi, Y., Li, P., Tang, J., Zhao, R., Zhang, H., 2012. Experimental study on the package of high-g accelerometer. Sens. Actuators Phys. 173, 1–8. doi:10.1016/j.sna.2011.09.004.

- McCallum, L., Higgins, D., 2012. Body temperature is a vital sign and it is important to measure it accurately. This article reviews and compares the various methods available to nurses Measuring body temperature. Nurs. Times 108, 20–22.
- Werff, L. 2011. Heat sensitive bandage could combat infection, Monash University [WWW Document]. Monash Univ. URL http://monash.edu/news/show/heat-sensitive-bandage-could-combat-infection (accessed 7.2.14).
- Mordor Intelligence, 2014. Global Wearable Medical Device Market - Growth, Trends and Forecasts (2014-2019), HealthCare.
- Moser, Y., Gijs, M.A.M., 2007. Miniaturized Flexible Temperature Sensor. J. Microelectromechanical Syst. 16, 1349–1354. doi:10.1109/JMEMS.2007.908437.
- Mufti, A., Coutts, P., Sibbald, R.G., 2015. Validation of commercially available infrared thermometers for measuring skin surface temperature associated with deep and surrounding wound infection. Adv. Skin Wound Care 28, 11–16. doi:10.1097/01.ASW.0000459039.81701.b2.
- Nakagami, G., Sanada, H., Iizaka, S., Kadono, T., Higashino, T., Koyanagi, H., Haga, N., 2010. Predicting delayed pressure ulcer healing using thermography: a prospective cohort study. J. Wound Care 19, 465–472. doi:10.12968/jowc.2010.19.11.79695.
- Nasir Mehmood, A.H., 2015. A flexible and low power telemetric sensing and monitoring system for chronic wound diagnostics. Biomed. Eng. OnLine 14. doi:10.1186/s12938-015-0011-y.
- Peregrina-Barreto, H., Morales-Hernandez, L.A., Rangel-Magdaleno, J.J., Avina-Cervantes, J.G., Ramirez-Cortes, J.M., Morales-Caporal, R., 2014. Quantitative Estimation of Temperature Variations in Plantar Angiosomes: A Study Case for Diabetic Foot. Comput. Math. Methods Med. 2014. doi:10.1155/2014/585306.
- Psikuta, A., Niedermann, R., Rossi, R.M., 2013. Effect of ambient temperature and attachment method on surface temperature measurements. Int. J. Biometeorol. 58, 877–885. doi:10.1007/s00484-013-0669-4.
- Thomas Klien, 2015. Spanish Researchers Test Patient Reactions to Wearables for Parkinson Monitoring | EMDT - European Medical Device Technology [WWW Document]. Eur. Med. Device Technol. URL http://www.emdt.co.uk/daily-buzz/spanish-researchers-test-patient-reactions-wearables-parkinson-monitoring (accessed 3.4.15).
- University of Tokyo, 2015. Fever alarm armband: A wearable, printable, temperature sensor -- ScienceDaily [WWW Document]. ScienceDaily. URL http://www.sciencedaily.com/releases/2015/02/150223084343.htm (accessed 2.25.15).
- Webb, R.C., Bonifas, A.P., Behnaz, A., Zhang, Y., Yu, K.J., Cheng, H., Shi, M., Bian, Z., Liu, Z., Kim, Y.-S., Yeo, W.-H., Park, J.S., Song, J., Li, Y., Huang, Y., Gorbach, A.M., Rogers, J.A., 2013.

Ultrathin conformal devices for precise and continuous thermal characterization of human skin. Nat. Mater. 12, 938–944. doi:10.1038/nmat3755.

- Yusuf, S., Okuwa, M., Shigeta, Y., Dai, M., Iuchi, T., Rahman, S., Usman, A., Kasim, S., Sugama, J., Nakatani, T., Sanada, H., 2015. Microclimate and development of pressure ulcers and superficial skin changes. Int. Wound J. 12, 40–46. doi:10.1111/iwj.12048.
- Ziegler Stefan, Frydrysiak Michał, 2009. Initial Research into the Structure and Working Conditions of Textile Thermocouples. Fibres Text. East. Eur. 17, 84–88.

2. Literature Review

2.1 Introduction

This chapter summarises the findings of the in-depth literature search carried out to determine the existing knowledge on textile-based sensing of skin temperature. The chapter consists of following subsections:

- the history and the benefit of continuous skin temperature sensing for patients;
- the modes of heat transfer important for skin temperature measurement;
- types of sensors and the temperature measuring technologies;
- background history on wearable electronics;
- state-of-the-art on wearable temperature monitoring;
- Critical analysis of current knowledge on skin temperature measurement in order to identify the gaps in knowledge.

2.2 Temperature measurement

Temperature is the quantity of thermal energy in a substance and is the indirect measure of the kinetic energy of its molecules (Howells, 2015). Max Planck defined temperature as the degree of hotness or coldness of an object. In organisms the rate and quality of biochemical processers are affected by the temperature. The survival of multicellular organisms are restricted to a temperature range of 0-45 °C. Above this range the proteins denature and cell membranes become unstable due to the aggregation of lipids, and below this range the processes are too slow to sustain life (Anbar et al., 1998). Humans are capable of sensing and regulating body temperature and it is a key feature in human survival. A change in the body temperature of +/- 3.5 °C from the resting temperature of 37 °C would cause physiological impairments and even fatality.

Body temperature, inarguably, is one of the four main vital signs that must be measured and monitored in a patient and accurately measuring it has an impact on diagnosis and treatment (Louise McCallum and Dan Higgins, 2012). Body heat was recognized early by ancient philosophers as an important indicator of health. Assessment of bodily heat dates back to pre-Hippocratic medicine (600-400BC) (Anbar et al., 1998). Hippocrates (460–377 BC) is regarded as the first person to obtain thermograms in patients. It was carried out by covering the patient's thorax with an earth-soaked cloth. Since warmer areas of the body dry faster, the enlargement pattern of the dry area showed the temperature distribution (Otsuka and Togawa, 1997).

The first attempt of making a temperature scale was carried out by a Greek scientist and physician, Galen 170 A.D. ("Temperature and Temperature Scales – FREE Temperature and Temperature Scales information | Encyclopedia.com: Find Temperature and Temperature Scales research," 2003). However the first air thermoscope was described only in the late 16th century in the four

books of magic by Giovanni Battista Della Porta (Zittel, 2008). Astronomer Galileo is credited for the invention of the first air thermoscope in 1595 (McGee, 1988). Later in 1612 the first thermometer (mouth thermometer) was invented by an Italian physiologist, professor at Padua Santorio (1561–1636) (Pearce, 2002).

The three main temperature scales used for temperature measurement are the Fahrenheit, Celsius and Kelvin scales. In 1724 the German Physicist Gabriel Fahrenheit developed the mercury thermometer and introduced the Fahrenheit scale. The scale used a mixture of salt, ice and ammonium chloride as 0 °F. In 1742 the Swedish astronomer Anders Celsius introduced the Celsius scale. He divided the fixed points of freezing and boiling of water into 100. The Kelvin scale introduced by the Irish physicist William Thomson uses the fixed point of absolute zero as 0 K and the scale is the same as the Celsius scale (Howells, 2015). In this thesis only the Celsius scale has been used to prevent confusion.

Carl Wunderlich made great progress in clinical thermometry in 1871 and is regarded as the father of clinical thermometry (Mackowiak and Worden, 1994). He systematically recorded the temperature of 25,000 patients and established the normal temperature range as 36.3 to 37.5 ^{o}C (Pearce, 2002). He argued for routine temperature measurements in patients and also wanted to establish a graphic record for each patient (Wunderlich, 1871), (Ring, 2004). Thereafter temperature has become one of the most measured vital signs in patients (Louise McCallum and Dan Higgins, 2012).

2.2.1 Remote continuous localised temperature measurement

Unobtrusive 24/7 continuous monitoring of patient's temperature benefits many branches in medical science. Continuous and accurate monitoring of patient's temperature can lead to early detection of diseases and also provide patients with the ability to spend time in the comforts of their own homes (Boano et al., 2011). The importance of localised temperature measurement (measuring temperature at specific points) for monitoring changes, treatment outcomes and predicting potential complications have been identified in medicine (Kelechi et al., 2006).

There are many applications which can benefit greatly from remote continuous localised temperature measurement, such as monitoring temperature in infants (Chen et al., 2010), breast cancer detection (Lawson and Chughtai, 1963). However the literature review will focus on three application that require continuous remote localised temperature measurement. The three applications are wound temperature measurement, early detection of ulcer formation and non-freezing-cold injury detection.

2.2.1.1 Wound temperature measurement

Wound care has become one of the leading health challenges in the 21st century and the global wound care cost is expected to escalate to an annual US$20 billion in the coming years (John O'Connor, 2012). When wounds are not treated properly or when the human biochemical healing mechanism fails, wounds can end up being chronic or hard to heal (Salvo et al., 2015). The burden of treating chronic wounds is growing rapidly due to the aging population and the rise in the number of individuals with obesity and diabetics worldwide (Sen et al., 2009). Chronic wounds are posing a heavy burden on the health care budgets (Nixon et al., 2014). They require frequent dressing changes, an activity which creates a burden in terms of health care costs, nursing care, patient outcomes and hospitalization time (Hilton et al., 2004).

Diabetes/Diabetes mellitus is a major cause of chronic wounds. Diabetes is a metabolic disease that can be characterised by hyperglycemia which can occur due to defects in insulin action, insulin secretion or both. Long term complications of diabetics could lead to peripheral neuropathy (Association, 2013). Diabetic neuropathy affects up to 50% of people with diabetes. This can be defined as the presence of signs and/or symptoms of damage of the peripheral nerves system which connects the brain and the central nervous system to the rest of the body (Diabetic Neuropathy, 2009). Frequently diabetic neuropathy would contribute to foot ulcers that could lead to amputation if not treated (Sen et al., 2009). It is reported that every 30 seconds a limb is lost to diabetics (Vuorisalo et al., 2009). The main advantages of wound sensing include prevention of amputations, reduction of hospitalisation time and acquiring a good understanding of the process which impair wound healing (Dargaville et al., 2013).

In medicine measuring the temperature of a wound is considered an useful way to optimize the diagnosis of chronic wounds (V et al., 2015). The wound bed temperature critical for normal cellular activity has been identified as 33 °C (V et al., 2015), (McGuiness et al., 2004). When the temperature of a wound falls below 33 °C the neutrophil, fibroblast and epithelial cell activity reduces which hinders wound repair (McGuiness et al., 2004). However results from the study done by Chaves et al on pressure ulcer patients has shown a relationship between the wound area and temperature variation of pressure ulcers. Patients with lower pressure ulcer temperature (32-33 °C) showed an increase in wound area compared to those with higher temperatures (34-35 °C). However this clinical study has been conducted on a small sample of patients (Chaves et al., 2015).

Temperature is also an established marker of infection in wounds (Nakagami et al., 2010), (Fierheller and Sibbald, 2010). By using quantitative measurements Fierheller et al have found a relationship between the increased periwound temperature and wound infection (Fierheller and Sibbald, 2010). The cohort study done by Nakagami et al on 35 patients with pressure ulcers contradicts shows that an increase in wound site temperature when compared to periwound skin

temperature could imply colonisation or other factors that can disrupt wound healing (Nakagami et al., 2010).

Contact thermography has also been used on patients with surgical wounds. A study carried out by Horzic (Horzic et al., 1996) has shown that the temperature of a wound and its surrounding would rise during the first three days after the operation, and then gradually decrease from day 4 to day 8. The authors have concluded from the results that if the temperature remained high after four days the wound was getting infected (Horzic et al., 1996). Thermography has also been used to examine nociceptive pain due to inflammation in venous leg ulcers. The pain intensity ratings have been higher in patients with higher wound temperatures (Goto et al., 2014).

2.2.1.1.1 Existing technologies for wound temperature measurement

Generally non-contact temperature measurement using handheld IR thermographic scanners are used to judge the wound temperature (Fierheller and Sibbald, 2010), (Mufti et al., 2015). However this requires the bandage or the wound dressing to be removed in order to obtain the measurement and also this method does not provide continuous measurements to the physicians.

Colour changing heat sensitive fibres have been developed for wound management by Monash University and CSIRO, but they are unable to present or store the data in an electronic manner (Louise van der Werff, 2011). Ultrathin conformable devices have been produced at MIT (Webb et al., 2013) and miniature flexible sensors have also been developed for wound temperature sensing (Moser and Gijs, 2007), however they are not textile-based nor they exhibit textile characteristics (ability to bend, shear and drape). A stretchable hydrogel that can be used to bond hard electronics has been developed by Lin et al (Lin et al., 2015) at MIT, and this has been used to create a smart wound dressing. Even though the smart hydrogel based wound dressing containing sensors and drug delivery channels is ideal for future implantable devices, when used in a wound dressing it is visible to the wearer and it also needs to be placed in between the wound dressing and the wound as an additional layer (“Stretchable hydrogel electronics,” n.d.).

A printed wearable temperature sensor has been developed by Honda et el as part of a smart bandage capable of monitoring touch and temperature, it also has a wireless signal transmission coil and a micro-pump for drug delivery, and functions as a curing system. The temperature sensor has been printed on a flexible Kapton substrate using screen printing and shadow mask printing methods. The temperature sensor has been made by using carbon nanotubes (CNTs) and synthesizing poly (3, 4-ethlenedioxythiophene) poly (styrenesulfonate) (PEDOT:PSS) composition ink. However it too is visible to a wearer and has to be placed in between the wound bandage and the wound (Honda et al., 2014). A wireless temperature data logger was developed by Matzeu et el by using temperature sensitive resistive film and an RFID tag. The temperature resistive film was

made of carbon nanotubes. However this has not been tested on wound conditions (Matzeu et al., 2011).

A conformal skin like Electronic System has been developed by Lee et al and tested on wound conditions. This has been made by transferring a fabricated electronic device on a carrier substrate to an elastomeric membrane. Thereafter it has been enclosed using a silicone coating and flexible cables, then it has been laminated and used for wound management (Lee et al., 2015). However this sensor too, is visible to the wearer and requires the sensor to be worn as an additional accessory on the skin surface next to the wound.

The flexible and low power telemetric sensing and monitoring system for chronic wounds developed by Nasir (Nasir Mehmood, 2015) contains only one moisture and one temperature sensor, therefore it is unable to provide a temperature distribution graph of the wound site. It also is visible to the wearer and needs to be placed in between the wound and the bandage.

As it can be seen most of the devices that are in the market or the ones that are been developed are not textile-based and, therefore, do not exhibit textile characteristics. Most of the sensors are also unable to provide localised temperature measurements while remaining hidden from the view of the patient.

2.2.1.2 Early detection of ulcer formation

Early detection of ulcer formation is a complicated process. Most of the ulceration occurs in diabetic patients. Diabetes could cause a loss of connection between the muscles and the nerves (sensory denervation) and this affects mechanoreceptors and thermoreceptors by depriving the patient from feeling any kind of symptoms (pain or swelling) when an injury has occurred (Peregrina-Barreto et al., 2014).

Temperature could be used to predict and prevent ulcers in diabetic high risk patients (Armstrong et al., 2007) (Yusuf et al., 2015). Armstrong et al studied 225 diabetic patients that were divided into two groups. In one group the temperature of six foot sites were measured twice daily. It required the patients in this group to contact the nurses and reduce activity until the temperature has stabilised, if the temperature measured showed a difference exceeding 4 °F (2.2 ^{o}C) between the corresponding sites of the left and the right feet. In the other group the standard therapy was carried out. The results showed that in only 4.7 % of the patients whose foot temperature were monitored formed ulcers compared to 12.2 % of the patients in the standard therapy group. In the patients that ulcerated, an average temperature difference of 4.8 ^{o}F was observed on the site of ulceration in the week prior to formation of an ulcer when compared to the 7 consecutive-day sample of fifty other candidates that did not ulcerate. This study showed that temperature difference between the two feet can be a warning signal for formation of foot ulcers (Armstrong et

al., 2007). Also a study done by Lavery et al has shown that foot ulceration in high-risk patients could be reduced by 4.37 times by monitoring the temperature of their feet , when compared to those patients whose foot temperatures have not been monitored (Lavery et al., 2007).

The systematic review and meta-analysis of all the literature from 1960 to 2011 by Houghton et al on the topic of increase in skin temperature compared with the same site on the contralateral limb and predicting foot ulcers has shown that temperature monitoring is an effective way to predict and prevent ulcers (Houghton et al., 2013). Therefore it is safe to say that temperature differences between the feet can be used to predict neuropathic ulceration and by monitoring the temperature the risk of ulceration can be reduced.

Localised measurements has also been used to predict a stage 1 pressure ulcer by detecting an increase or decrease in temperature in-between areas of erythema (superficial reddening of the skin, usually in patches, as a result of injury or irritation causing dilatation of the blood capillaries) and surrounding healthy tissue. The results have shown that in 23 % of patients the erythematic sites were cooler than the surrounding tissue and in 63 % of them the erythematic sites were warmer, and only in 15% the temperature remained similar (Sprigle et al., 2001).

2.2.1.2.1 Existing temperature sensing technologies for early detection of ulcers

An overview of temperature monitoring devices for early detection of foot ulcers has been carried out by Roback (Roback, 2010). It has shown three major commercially available technologies that are used for early detection of diabetic ulcers. They are scanning the foot using an infrared thermometer, Liquid Crystal Thermography and temperature sensors integrated in a weighing scale.

Non-contact temperature measurement using infrared cameras has generally been used for foot temperature measurement in diabetic high risk patients(Netten et al., 2013) (Armstrong et al., 2007). A Low cost, light weight screening systems using infrared sensors for foot neuropathy has been developed by Iven et al (Iven et al., 2014). However non-contact temperature sensors do not provide continuous real time temperature measurements.

Liquid crystal thermography has also been used to monitor diabetic ulcers (Benbow et al., 1994), (Stess et al., 1986). They are unable to store or present data in an electronic manner.

A temperature sensing weighing scale has been invented by thermoscale® that required the wearer to stand in the weighing scale to obtain the temperature measurements. Recently another weighing scale capable of monitoring hot spots in feet was developed by Morovati and Maclean by using thermistors (Morovati and Maclean, 2016). The scale was capable of identifying hot spots by capturing the temperature between the two feet and comparing to see if the difference exceeded 2.2 °C. Even though the temperature measuring weighing scales (Figure 2.1) can be used for early

detection of ulcers they are unable to provide remote temperature measurements and the user must always get on the weighing scale to observe a change in temperature.

Figure 2-1: Thermoscale from Thermoscale®

In the recent past an optical fibre integrated sock has been developed by Najafi et al. The sensors were placed on the heel, midfoot, big toe, 1st and 5th metatarsal heads (figure 2.2). Even though the study done on the 21 diabetic patients showed how the technology can be used to predict foot ulcers and also the wearers found the socks comfortable, (Najafi et al., 2014) optic fibres are expensive and fragile.

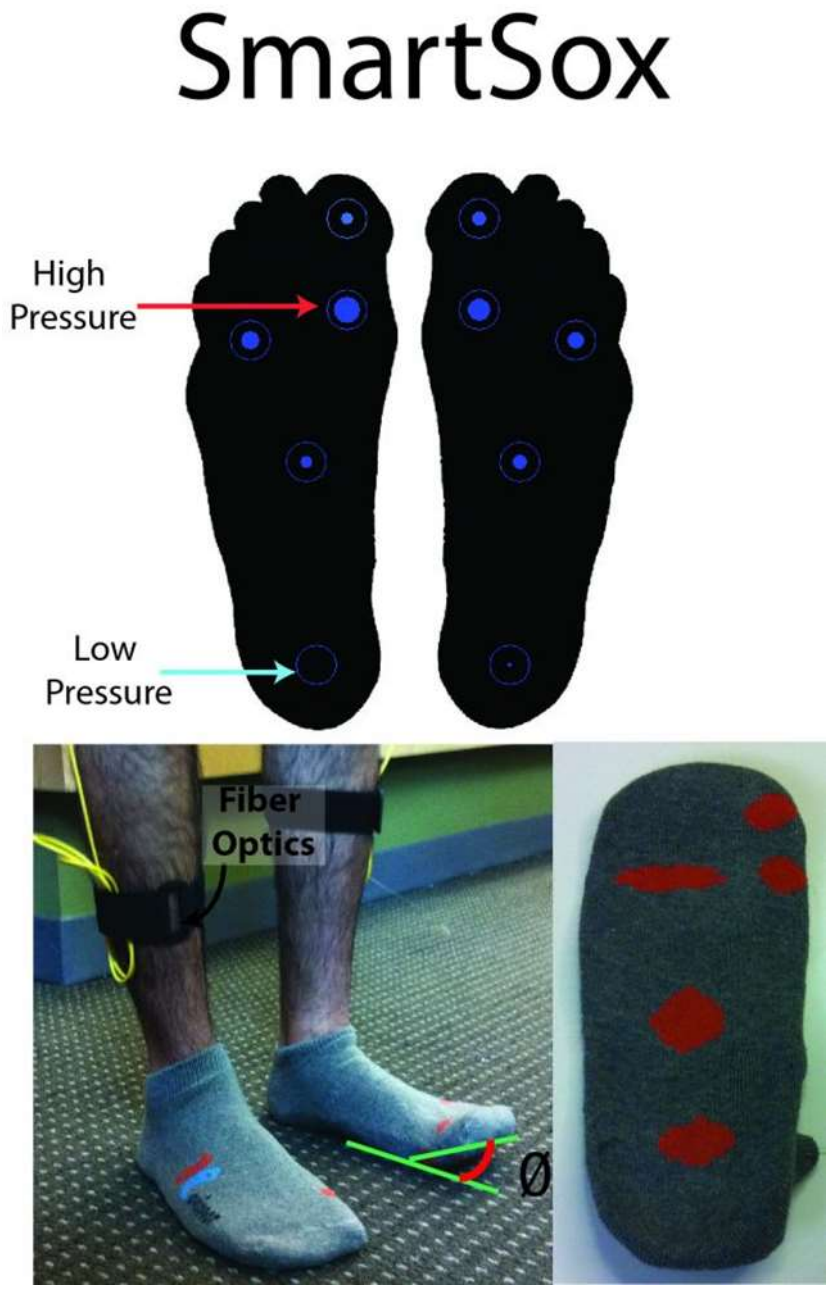

Figure 2-2: Temperature sensing sock using optical fibres (Najafi et al., 2014)

2.2.1.3 Non Freezing Cold Injury

Non-freezing cold injury (NFCI) occurs when limbs generally the feet are exposed to cold and damp conditions for a long period of time (Irwin et al., 1997). Generally it occurs when exposed to temperature just above freezing (-0.55°C to 15°C) (Irwin, 1996). Freezing of the tissues does not occur and it is this which distinguishes NFCI from freezing cold injury (frostbite), although the two conditions may occur together in the same limb (Hope et al., 2014). In the initial stage, the limb feels numb. After removal from the cold, abnormal sensations are felt. A further stage sees the onset of pain and finally symptoms can last a few weeks or a lifetime. Long-term effects are cold-sensitivity and 5% of patients will suffer chronic pain (Imray et al., 2009). An additional problem is the development of more severe cold injuries on subsequent exposure to cold (Hope et al., 2014).

Pain is most common at night and typically occurs at the soles of the feet and base of the toes, figure 2.3 (Imray et al., 2009). NFCI can lead to amputation in severe cases (Imray et al., 2009).

Figure 2-3: Feet of a 40 year old man effected by NFCI (Irwin et al., 1997)

NFCI is most common in military personal, however it can also be seen in individuals who take part in mountain climbing, adventure training (Marcus, 1979) diving (Laden et al., 2007). It is also common in people working in hostile environments (agricultural workers, fishing industry and etc). It has also been reported in elderly (Ramstead et al., 1980) and homeless (King et al., 1958) individuals (Hope et al., 2014).

The prevention of NFCI has benefits for the military. NFCI has been a significant medical, logistical and operational problem for centuries (Hope et al., 2014).. NFCI was a common reason for evacuating to a hospital ship in the Falklands war (Tek and Mackey, 1993). It is also a major threat during expeditions in cold wet climates (Tek and Mackey, 1993) and today it mostly occurs during winter training exercises (Golden et al., 2013). NFCI causes swelling of the feet and hence the soldier may not be able to put their boots back on (Imray et al., 2009) resulting in military consequences. In most cases the condition could lead to expensive litigation which divert military resources. NFCI frequently leads to medical discharge of army trainees (Izard and Bilzon, 2008), may reach epidemic proportions in war zones (Jia and Pollock, 1997) and can also lead to long-term consequences (Imray et al., 2009).

The human body is subject to its own microclimate characterised by the temperature found next to the skin. By monitoring the microclimate that would encourage the onset of NFCI, a better

understanding of the condition, its causes and prevention could be achieved, if the temperature of the foot could be monitored under a range of environmental conditions with different footwear in the laboratory. Subsequently, a threshold could be set for the temperature and the length of exposure. This would work in a similar manner to the badges worn by radiologists that monitor exposure to ionising radiation. There are no NFCI detecting technologies in the market.

2.4 Modes of heat transfer in humans

Heat is transferred from the skin to the atmosphere and vice versa through the known four heat transfer mechanisms Conduction, Radiation, Convection and Evaporation.

Conduction is the transfer of heat from a body at higher temperature to a body of lower temperature or the transfer of heat from one part of a body at higher temperature to another part which is at lower temperature. This process takes place at the molecular level, where higher energetic molecules transfer energy to the lower energetic molecules. It can be observed in solids, gases and liquids (Rohsenow et al., 1985).

The Fourier's law of heat conduction (Equation 2.1) states that the heat transfer (Q_{cond}) through conduction is directly proportional to the temperature difference (ΔT) between the two bodies and also directly proportional to the heat transfer area (A). But inversely proportional to the length of the body (x).

$$Q_{cond} = \frac{kA(\Delta T)}{x} \qquad (2.1)$$

Where k is a transport property known as the thermal constant defined for a material.

Convection is the transfer of heat from bounding surface to a fluid or the heat transfer across the flow plane within the interior of a flowing fluid. Convection can be divided into two sections, forced convection and natural convection. Forced convection is when fluid motion is induced by an external force such as fans, blowers or pumps (Rohsenow et al., 1985).

Free and natural convection occurs when the fluid motion is bought about by a density difference produced by the heat transfer itself (Rohsenow et al., 1985). It occurs when a hot surface heats up the air adjacent to it by conduction causing the adjacent air to have a lower density. At constant pressure the density of a gas is inversely proportional to its temperature. This causes the lower density air to rise allowing high dense cooler air to take its place. This process repeats itself cooling the surface. The opposite happens if a cold object is placed in a hot room (Cengel, 2002). The heat transfer from convection (Q_{conv}) can be identified by using the Newton's law of cooling given below in equation 2.2.

$$Q_{conv} = h_c A_s (T_s - T_a) \quad (2.2)$$

Where A_s - heat transfer surface area and h_c - average heat transfer coefficient of the surface

Radiation/Thermal Radiation is defined as the electromagnetic radiation emitted by a body using its internal energy by virtue of its temperature (Rohsenow et al., 1985). The heat exchange between an object and its surrounding is proportional to the temperature, surface area and the nature of the object. The heat exchange due to radiation (Q_{rad}) between a surface and its surrounding can be explained by the following equation 2.3 (Freedman and Young, 2007):

$$Q_{rad} = A\sigma e(T^4 - {T_s}^4). \qquad (2.3)$$

Where,

σ - Stephan-Boltzmann constant ($\sigma = 5.669 * 10^{-8} \frac{W}{m^2K^4}$),

e - Emissivity of the surface (a value between 0 and 1),

A - Surface area of the object,

T - Absolute temperature of the body,

T_s - Temperatures of its surrounding.

Evaporation and condensation are transport phenomena in which vapours (gas at a lower temperature than its critical temperature) or vapour mixtures are in contact with liquids, and a large amount of heat is absorbed or released with the phase change, this is known as latent heat (Asano, 2006). The rate of transfer of heat due to evaporation (Q_{evap}) between a skin and its environment can be expressed by Parsons Equation 2.4:

$$Q_{evap} = h_e\left(P_{sk,s} - P_a\right). \qquad (2.4) \text{ (Parsons, 2014)}$$

Where:

$P_{sk,s}$ - the saturated water pressure at skin temperature;

P_a - partial vapour pressure in air;

h_e - the evaporative heat transfer coefficient that relates by the Lewis Relation to the convective heat transfer coefficient (h_e=16.5h_c, h_c is the convective heat transfer coefficient).

2.5 Temperature Sensors

There are over 20 different types of temperature sensors that can be used for temperature measurement (Lipták et al., 2004). These can be divided into two major groups, contact temperature sensors and non-contact temperature sensors.

2.5.1 Non-contact temperature sensors

Non-contact temperature sensors are based on measuring radiation of thermal energy from heated bodies. These also can be further divided into two, those that provide direct measurement and those that use interrogative methods (Michalski, 2001). Generally non-contact sensors aren't used

in wearable applications and not geared towards providing continuous measurements of patient's temperature.

2.5.2 Contact sensors

Contact sensors operate under conductive and convective temperature transfer conditions. The contact sensors can be further broken down into two, electrical and non-electrical contact sensors depending on the energy form of the output (Michalski, 2001).

2.5.2.1 Non-Electrical contact temperature sensors

Non-electrical contact sensors are sensors that use the change in the physical properties of solids, liquids and gases to indicate the temperature and they are listed below.

2.5.2.1.1 Liquid in glass thermometers

Liquid in glass type thermometers depend on the variation of the volume of liquid being used for temperature measurements (Michalski, 2001). Mercury or alcohol are generally used as the liquid in most of these thermometers. Mercury exist in liquid form between temperatures -38 °C to 356.7 °C, and therefore it can be used to measure temperatures within that range. It expands with increasing temperature and the expansion is linear, therefore it can be calibrated (Lipták et al., 2004). Mercury glass thermometers (Figure 2.4) were widely used until recently to measure the body temperature of patients by the medical community.

Figure 2-4: Mercury in glass thermometer ("5 Weird Nursing Rules You Might Have Never Heard of," n.d.)

2.5.2.1.2 Dilatation thermometers

These thermometers are constructed using two different materials with different thermal expansions. The material with the higher expansion coefficient is used as a tube with a coaxial rod made from the material with the lower expansion coefficient. Since the expansion of the two materials is small for reasonable length, the difference must be amplified by using a mechanical system. They can be used to measure temperatures below 1000 °C to an accuracy of 1 °C to 2 °C (Michalski et al., 2001a).

2.5.2.1.3 Bimetallic thermometers

A Bimetallic thermometer is made by welding/hot rolling two dissimilar metals with different expansion coefficients. The metal with the high coefficient value is called the active metal whereas the other is the passive. A bimetallic strip is designed to be at straight at neutral temperatures but bends at higher temperatures generally towards the passive side (Michalski, 2001). They can be used to measure temperature over a range of about –73 °C to about 537 °C. When produced into a coil or helix its movement with change in temperature can be used as a pointer on a dial scale to show temperature. They range from pocket size to 127 mm depending on the application (Lipták et al., 2004).

2.5.2.1.4 Manometric Thermometers

These thermometers can be classified into two types, variable volume thermometers and variable pressure type thermometers. The variable volume type thermometers are liquid filled thermometers whereas, pressure type depends on the thermometric behaviour of vapours or gases (Michalski et al., 2001a). The design for a liquid filled thermometer consists of a thermal cylinder, capillary tube and a sensing element (membrane box, bellow spring) (Sychev, 1961). It is filled with a thermometric liquid that is considered incompressible. When the temperature increases the liquid expands to dilate the elastic element. The pointer is moved as a result of this dilation. A vapour pressure manometric thermometer uses the vapour pressure as a function of temperature. Vapour pressure thermometers have a similar structure to liquid filled thermometers. However, it is filled with a thermometric liquid and its saturated vapour. Gas manometric thermometers uses the change in gas pressure to indicate the temperature. They have a larger bulb compared to vapour thermometers and are generally filled with helium or nitrogen (Michalski et al., 2001a).

2.5.2.1.5 Temperature Indicators

There are different types of temperature indicators like Pyrometric cones, thermochromic paints, temperature indicating crayons, self-adhesive indicators and liquid crystals (Michalski, 2001). Most of these sensors use heat sensitive fusible crystalline solids which change from solid to liquid with a different colour at fixed temperatures, the temperature depends on the blend of ingredients. They provide a low-cost method of visual verification of temperature within an accuracy of 0.6 °C (Lipták et al., 2004).

2.5.2.1.6 Discussion on non-electrical contact temperature sensors

The non-electrical contact sensors are unable to record/store/transfer data in an electronic manner. Therefore the measurements have to be physically taken. Hence they are unable to provide temperature readings remote to the measurement point except in the case of manometric thermometers. They are also bulky therefore not ideal for wearable electronic applications.

2.5.2.2 Contact Electrical Temperature sensors

Contact electrical temperature sensors change its electrical properties relative to the temperature. The measurement instrument used, measures the electrical effect with regard to the temperature of the sensor. The electrical signals that are produced can be processed and manipulated using digital and analogue techniques (Michalski, 2001).

2.5.2.2.1 Thermocouples

A thermocouple consists of two wire legs which are made from different conductors. The two conductors are welded together to form a junction. When the two junctions (points of connection of the two conductors) are placed in different temperatures a weak electromotive force is produced. The value and the direction of the force is vital with the temperature and the materials of these two conductors. This is called the thermoelectric effect and the two conductors are known as heated electrodes. The thermoelectric voltage produced is proportional to the temperature difference in between the conductors (Liu et al., 2012). One junction of the thermocouple is called the reference junction and it is held at constant known temperature. Whereas the other is called the measuring junction and is used to measure the temperature.

Even though thermocouples can be made from several different combinations of materials, a number of standard types (shown in table 2.1) are used because they have large temperature gradients and predictable output voltage (Alan Tong, 2001).

Table 2:1: Types of thermocouples

Thermocouple type	Typical Accuracy (°C)	Overall range (°C)
Type B (platinum/rhodium)	5 (at 1,000 °C)	100 - +1,800
Type E (chromel/constantan)	1.7	-200 - +900
Type J (Iron Constantan)	2.2	-40 - +760
Type K (chromel/alumel)	2.2	-200 - +1,300
Type N (nicrosil/nisil)	2.2	-200 - +1,300
Type R (platinum/rhodium)	1.5	-50 - +1,760
Type S (platinum/rhodium)	1.5	-50 - +1,760
Type T (copper/constantan)	1	-200 - +400

2.5.2.2.2 Resistance temperature detectors (RTD)

Resistant thermometers are made of metals. When metals are heated the amplitude and the frequency of vibration in their lattice structure increases, and this obstructs the flow of electrons through a metal influencing the electrical resistance of the metal. The electrical resistance of a metal is obtained using Ohms law (V=IR), by applying a fixed voltage V to the metal and by

measuring the current flowing through it. The resistance is then used to calibrate the temperature of the metal. Platinum is generally used to make RTD's since its electrical resistance varies linearly with change in temperature over a wide range (15 ^{o}K-900 ^{o}K) and due to its inert nature. Copper and Nickel can also be used for different ranges of temperature (Howells, 2015). The temperature coefficient of RTD's which is the relative change in resistance with temperature, is about 0.4 %/°C (Anonymous, 1995). Therefore to obtain a high degree of accuracy a Wheatstone bridge must be used to measure the change in resistance (Howells, 2015).

2.5.2.2.3 Quartz, Ultrasonic and Noise thermometers

A Quartz thermometer uses the property of a piezoelectric crystal's natural frequency of vibration dependence on temperature to provide temperature measurements (Ghosh, 2012). The output signal is generally produced as a frequency output. The frequency-temperature characteristics are non-linear, therefore the polynomial equation 2.5 can be used to get the resonant frequency of a quartz oscillator (f(v)) as a function of temperature (Michalski et al., 2001b).

$$f(v) = f_0(1 + \alpha v + \beta v^2 + \gamma v^3) \quad (2.5)$$

Where f_0 - frequency at a reference temperature; and α, β and γ are coefficients.

An **Ultrasonic** thermometer uses the effect of the temperature of a medium on the velocity of sound waves in that medium to provide temperature measurements. **Noise** thermometers use a thermal noise voltage or current from a sensing resistor to sense the temperature (Michalski et al., 2001b).

However quartz thermometers are not small enough to be used in wearable applications. The ultrasonic thermometers are not mass produced therefore they are not ideal to be used in textiles. Noise thermometers are normally used for temperature sensing in extreme conditions such as very low temperatures in nuclear reactors and has never been used to monitor body skin temperature (Michalski et al., 2001b).

2.5.2.2.4 Fibre Optic thermometers

Dielectric optical fibres are made of a light guide which is made of a rod core surrounded by a sheath. The core with a refractive index of n1 conducts the electromagnetic waves. The sheath has a refractive index of n2, to ensure that the electromagnetic waves are constrained within the fibre core, it is necessary to ensure that the refractive index n1>n2 (Michalski et al., 2001c). There are many types of fibre optic sensors that can be used depending on the application. The most common type of fibre optic sensors are stated below; a detailed description is summarised in Appendix 1 (Hoffmann et al., 2007):

- Fibre Bragg gratings, that use the temperature dependence of distributed optical reflection;

- Raman scattering distribution temperature sensors, where the temperature dependence of inelastic scattering on optical phonons are used;
- Temperature sensing with an interferometric probe, extrinsic interferometric optical structures show a temperature dependent behaviour;
- Semiconductor band gap technology which depends on the band gap of semiconductor crystals;
- Brillouin Scattering distributed temperature sensors which use scattering on acoustic phonons.

However most of the temperature sensors that use fibre optic are expensive and fragile therefore not ideal for wearable electronic applications.

2.5.2.2.5 Transistor and diode thermometers

Transistors and diodes are PN junction semiconductor devices and their current vs voltage characteristics are determined by the electrical charge carriers on each side of the semiconductor junction. The carrier density is temperature dependent. Diode thermometers are made from semiconductor Germanium (Ge), Silicon (Si) or GaAs. However in diode thermometers to obtain highly accurate readings, a digital voltmeter has to be combined with special circuitry. Also measures have to be taken to ensure proper earthing and screening (Michalski et al., 2001d).

Transistor thermometers use the permissible collector and base junction temperatures and the linear range of the thermometric characteristics to give the temperature measurement. They are more sensitive than diode thermometers. However they require circuitry to amplify the signals and linearization to obtain high accuracy (Michalski et al., 2001d).

2.5.2.2.6 Thermistors

The thermistor can be regarded as the optimum sensor for applications within a temperature range of -50 °C - +150 °C due to its high sensitivity, accuracy and repeatability (Gregg Lavenuta, 1997).

2.5.2.2.6.1 Process of manufacturing thermistors

Thermistor is a temperature-dependent resistor made of semi-conductor materials. It can be separated into two distinct classes; metal oxides (e.g. oxide of manganese, cobalt, nickel, copper, iron or titanium) or single-crystal (Germanium and Silicon) semiconductors.

Metal oxide thermistors are formed using fine powders, which are compressed and sintered at high temperatures (Ng, 2009). The Resistance/temperature characteristics and the R25 value (the electrical resistance at 25 °C) of the thermistor depends on the formulation of the oxides. Even though there are many different configurations of thermistors (e.g. bead, chip, discs) the ceramic processing techniques used to manufacture thermistors are similar in most of them. The “green”

body of the thermistor is formed by milling and blending the formulated and prepared metal oxide powder in a binder. Thereafter it is heat treated to form the ceramic material. Then the additional electrical contacts are put in place for the different shapes (disc or chip type) of thermistors (Gregg Lavenuta, 1997) .

Single-crystal Ge and Si thermistors are produced by doping a few percentage of compensating dopants into the semiconductor. The sensing temperature range of a thermistor will depend on the energy gap of the material (Ng, 2009).

Table 2:2: Temperature ranges of the different types of thermistors

Thermistor type	Temperature range
Germanium Thermistors	-272.15 ^{o}C to -173.15 ^{o}C
Silicon Thermistors	Less than -23.15 ^{o}C
Metallic oxide thermistors (Mn_20_3, NiO, Co_20_3, Fe_20_3, Cu_20, U_20_3, and $Ti0_2$)	-73.15 ^{o}C to 426.85 ^{o}C
Metallic oxide thermistors ($A1_20_3$, BeO, $Zr0_2$, MgO, Dy_20_3 , ,and Y_20_3.)	Higher temperatures

2.5.2.2.6.2 Bead Thermistors

They have lead wires embedded in ceramic material (shown in figure 2.5). They are produced by combining powders of metal oxides in a binder to form a slurry. A minute amount of this slurry is then applied to two parallel platinum alloy wires which are held in place using a fixture. The number of beads can be adjusted depending on the wire length. Once the beads are dried they are sintered in a furnace at 1100 °C-1400 °C. In the process of sintering an intimate electrical and physical bond is made; due to the metal oxide particles bonding together and shrinking down around the platinum alloy leads, this also causes the ceramic body to become denser. Once the sintering process has been concluded the wires can be cut to produce individual devices (Gregg Lavenuta, 1997). The bead thermistors are only a few millimetres in diameter (0.25mm to 1.5mm) and some even have the bead enclosed in a capsule (Bishop, 2011). Generally a glass coating is applied to provide protection, long term stability and also a strain relief to the ceramic-lead interphase (Gregg Lavenuta, 1997). They respond almost immediately to change in temperature due to its minute size (Bishop, 2011).

Figure 2-5: Bead thermistor (Corleto, 2016)

2.5.2.2.6.3 Disc thermistors

They are manufactured by preparing different metal oxide powders and blending them in a binder and thereafter compressing minute amounts of the mixture in a die beneath several tons of pressure. Then the ceramic bodies are made by firing the discs at high temperature. Next the contacts for the lead wires are made by applying a thick film of electrode material, generally silver, on either side of the disc. Finally a thin coating of glass, epoxy, or phenolic is applied to it to provide protection against environmental and mechanical stresses. The coated disc thermistors are generally about 0.25 mm-1.5 mm in diameter whereas an uncoated thermistor will be about 1.3 mm-2.5 mm in diameter (Gregg Lavenuta, 1997). The larger disc thermistors generally work in the self-heating mode (Self-heating mode is discussed further in section 2.5.2.2.6.10.1) (Vishay Dale, 2002).

2.5.2.2.6.4 Washer shaped thermistors

Washer shaped thermistors can be regarded as a variation of disc thermistors, they have a hole in the middle and are leadless therefore are used for surface mount devices (Gregg Lavenuta, 1997).

2.5.2.2.6.5 Rod thermistors

Rod thermistors are manufactured by extruding a viscous oxide binder mixture through a die. Thereafter it is heat treated to form a ceramic material, then the electrodes are applied and leads are attached. Rod thermistors are used for applications demanding high power dissipation and/or high resistance (Gregg Lavenuta, 1997).

2.5.2.2.6.6 Chip thermistors

They are made by using the tape casting method where an oxide-binder slurry (like in the manufacture of bead thermistors) are poured into a fixture which allows a tight controlled thickness of the material to be cast onto a movable carrier or a belt. Thereafter the cast material is left to dry into a flexible ceramic tape. This is cut into small sections and then sintered at high temperatures to form wafers. Next a thick film electrode material is applied on the wafers and they are cut into chips. The chips can be made into surface mount thermistors or separate units by attaching leads and covering with a protective glass, epoxy or phenolic layer (Gregg Lavenuta, 1997). The chip style

smaller thermistors change their temperature (i.e. resistance) by absorbing the surrounding's temperature (Vishay Dale, 2002).

2.5.2.2.6.7 Single crystal semiconductor thermistors

There are two types of semiconductor thermistors, NTC (negative temperature coefficient) and PTC (positive temperature coefficient) thermistors. NTC thermistors are the most common type of thermistors and the resistance of the thermistor decreases with increasing temperature (Bishop, 2011). Generally in practice NTC thermistors are used for temperature measurement and PTC thermistors are only used for binary detection of a given temperature (Michalski et al., 2001d).

2.5.2.2.6.8 NTC Thermistors

NTC thermistors like their name suggests have a negative resistance to temperature coefficient. Generally NTC thermistors are made from pure oxides of metals such as nickel, copper, manganese, tin, cobalt, uranium, iron, zinc, titanium and magnesium which are sintered at temperatures exceeding 982 °C. The temperature coefficient and the resistance of the thermistor depends on the sintering temperature and the sintering atmosphere; the type, proportion of the oxides used (Liptak, 2003). They are shaped into discs or chips depending on the application (Vishay Dale, 2002).

In some NTC thermistors the change in resistance is high as 6 %/°C however in most it is about 1 %/°C. They can have very high accuracy and resolution when measuring temperatures in between -100 °C and 300 °C. NTC thermistors are used more commonly when compared to PTC thermistors (Du, 2014). However they are highly non-linear and this makes them extremely sensitive to narrow span measurements but challenging when measuring a wide temperature span (Liptak, 2003).

2.5.2.2.6.8.1 How do NTC thermistors function

Thermistors generally provide a temperature measurement with a large resolution within a narrow range of temperature. The thermistor can be regarded as a resistor; therefore its conductance (σ) can be given by the equation 2.6 (Ng, 2009).

$$\sigma = \frac{1}{\rho} = (nq\mu_n) + (pq\mu_p) \qquad (2.6)$$

Where:

μ_p and μ_n are the mobility's of the holes and electrons respectively;

q is magnitude of the electron charge and is given as 1.6 X 10^{-19} coulomb;

n and p are the concentrations of the free electrons and holes respectively.

Thermistors operate in the temperature range in which the ionized concentration (p or n) is a function of temperature and is given by the equation 2.7 (Ng, 2009).

$$Concentration\ \alpha\ \exp(-\frac{E_a}{Tk}) \qquad (2.7)$$

Where:

E_a is the activation energy and it is related to the energy gap and the impurity level of the semiconductor;

k is the Boltzmann's constant;

T is the temperature in Kelvin.

For NTC thermistors as the temperature goes up the number of active charge carriers in the semiconductor increases and when the number of charge carriers increase, the more current the material is able to conduct hence the resistance decreases. Therefore the resistance of the thermistor changes as an exponential function with temperature and it is given below in equation 2.8 (Nawrocki, 2005).

$$R_t(T) = R_{298}\exp[B\left(\frac{1}{T} - \frac{1}{298}\right)] \quad (2.8)$$

Where:

R_t(T) is the resistance of the thermistor as a function of temperature;

R_{298} is Thermistor reference temperature at 298 ^{o}K (25 °C);

B is the material constant of the thermistor (typically with in a range of 2500 ^{o}K- 4500 ^{o}K);

T is the temperature given in the Kelvin scale.

The temperature dependent temperature-resistance coefficient α of the thermistor is calculated using the following equation 2.9 (Nawrocki, 2005)

$$\alpha = \frac{1}{R_t}\frac{dR_t}{dT} = -\frac{B}{T^2} \quad (2.9)$$

2.5.2.2.6.9 PTC thermistors

A PTC thermistor is normally composed of a polycrystalline ceramic material made of carbonate or oxyalate with added doping materials. They show only a small change in resistance with regards to temperature up until the switching point is reached thereafter a resistance changes exponentially over a few tens of Degrees (Vishay Dale, 2002), (TDK, 2012).

PTC thermistors can fall into two major categories; the thermally sensitive silicon resistors also called silistors and the other is known as a switching PTC thermistor (Digi-Key, n.d.), (John, 2011).

2.5.2.2.6.9.1 Silistors

Silistors are sensitive silicon resistors which rely on the properties of doped silicon. They are manufactured from high quality silicon wafers, which are made in different shapes. They have a positive temperature coefficient of about 0.8 %/°C. If the temperature goes beyond a certain temperature (usually 150 °C) the device automatically changes to a negative coefficient region (John, 2011), (Du, 2014). Silistors have a more linear resistance-temperature characteristic curve however there not as sensitive as NTC thermistors (Liptak, 2003). They are generally used for

temperature compensation of silicon semiconductor devices in a temperature range of -60 °C to 150 °C (Du, 2014).

2.5.2.2.6.9.2 Switching PTC thermistor

The switching PTC thermistors are made from poly crystalline ceramic material. Ceramics are usually regarded as good insulating material with high electrical resistances. Semi-conduction and therefore a low resistance is attained by doping the ceramic with atoms of a higher valency than that of the lattice structure (TDK, 2012). They are mostly made of barium, strontium titanates and lead in the crystal lattice with additives as manganese, yttrium, silica and tantalum (TDK, 2012), (Digi-Key, n.d.).

The material is made of individual crystallites. At the ends of each of the mono-crystallites also known as grain boundaries, potential barriers are formed. These prevent electrons from flowing into the adjacent areas. This causes high resistance in the boundaries. This effect decreases at lower temperatures. At low temperatures grain boundaries get polarised and the high dielectric constants prevent the boundary barriers from forming and this allows smooth flow of electrons (TDK, 2012).

After a certain temperature (Ferroelectric Curie temperature) the polarization and the dielectric constant reduces significantly, therefore there is a strong growth in potential barriers causing the resistance to increase significantly (TDK, 2012). For a certain temperature range above the Curie temperature (transition temperature) the resistance increases exponentially by factors of 10^5-10^6 (Downie, 2012). After this range of the positive temperature coefficient (α), the natural features of a semiconductor start exhibiting itself due to free charge carriers increasing as a result of thermal expansion (TDK, 2012).

Most switching PTC thermistors are made like NTC disk and chip type thermistors. Disc is the most common body shape of these thermistors however they can be as chips and surface mount packages. These thermistors are commonly designed to operate at transitional temperatures of 60 °C and 120 °C but it can made to switch as high as 200 °C or as low as 0 °C (Digi-Key, n.d.). The graph below in figure 2.6 shows the change in resistance with change in temperature for switch type PTC thermistors and silistors.

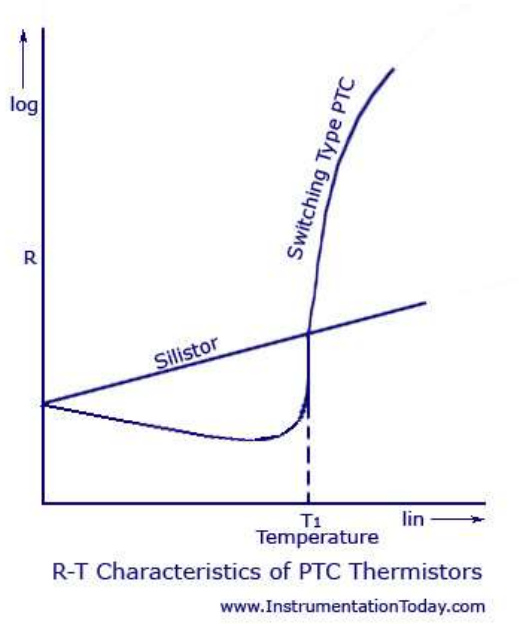

Figure 2-6: Temperature vs resistance characteristics for a switch type PTC thermistor and a silistor (John, 2011)

2.5.2.2.6.10 Self-heating

When the resistance of a resistance based temperature sensor is measured by using an electrical current the effect known as self-heating occurs. It causes a temperature rise in the sensor above the ambient temperature, which is caused due to the heat loss on the resistance of the sensor, due to the flow of the current through the sensor. The self-heating effect on the thermosensitive part (semiconductor bead) can have a significant effect on the thermistor measurement. However this effect can be calculated using the following equation 2.10, given the self-heating coefficient, K_s (Nawrocki, 2005).

$$\Delta T = \frac{P}{K_s} = \frac{R_t I^2}{K_s} \qquad (2.10)$$

Where:

ΔT is the thermometry error caused due to self-heating;

R_t is the sensor resistance;

I is the current flowing through the sensor;

P is the electrical power that causes the temperature rise in the sensor;

K_s is the self-heating coefficient of the sensor.

2.5.2.2.6.10.1 Self-heating mode

The resistance of a thermistor can be changed externally by a variation in ambient temperature or internally by self-heating which occurs as a result of the heat produced by passing a large current through the device (Nikolic et al., 2011). Self-heating can be bought about by using a constant current or voltage supply. For applications based on self-heating the thermal Dissipation constant (D.C.) is an important factor. The D.C. of a thermistor is the amount of power required to raise the

body temperature of the thermistor by 1 °C in a particular measurement medium (BetaTHERM Sensors, n.d.).

D.C. can be used to monitor levels or flow rates of gases and liquids, for example when the thermistor is placed in a fluid path as the flow rate of the fluid increases the D.C. will increase and the change in resistance will correlate to the flowrate (BetaTHERM Sensors, n.d.). Thermistors in self-heating mode can also be used for applications that depend on the current-time characteristic which include time delay, overload protection, surge suppression, and sequential switching (Sapoff and Oppenheim, 1963).

2.5.3 Comparison of temperature sensors

Devices that are traditionally used to measure the body temperature which give measurements more of a static nature are not generally geared for continuous ambulatory temperature measurement. Non-contact sensors are unable to provide continuous remote temperature measurements if the patient is not in line of sight of the sensors. Among contact temperature sensors, most of the non-electric temperature sensors are not able to store temperature measurements in an electronic manner. In contact electrical sensors the most commonly used sensors are thermistors, thermocouples and RTD's (Husain, 2012), (MINCO, n.d.). Therefore a comparison between these three sensors have been carried out to identify the most appropriate sensor for the application.

2.5.3.1 Accuracy

The accuracy of thermistors and RTD are high +/-0.1 °C and +/-0.01 °C respectively. Thermocouples are not as accurate as thermistors and RTD's, however they too can have an accuracy of +/-0.5 °C (Baker, 1998).

2.5.3.2 Temperature range

The thermocouples have the highest temperature range when compared to RTD's and thermistors. The temperature range of the thermocouples are from -272 °C- +2760 °C (Lipták et al., 2004). RTD's can have a temperature range of about -250 °C- +900 °C. Whereas thermistors have a limited temperature range of about -100 °C to 450 °C (Baker, 1998). The measurement range of a human body temperature sensor can be considered as narrow, since the skin temperature does not vary over tens of degrees Centigrade.

2.5.3.3 Step Response time

The response time is the time taken to respond to a step change in temperature. The step response time is the smallest in thermocouples, they have a response time of less than 1 s. Whereas thermistors have a step response time of 1-5 s and RTD's can have a step response time of 1-10 s (Baker, 1998). A step response time of a few seconds can be regarded as negligible for applications discussed in the thesis.

2.5.3.4 Linearity

Linearity of a temperature sensor shows how consistently the output of the sensor changes with temperature. Thermistors are nonlinear therefore they provide very good accuracy over a narrow range of temperatures (Lipták et al., 2004). Since RTD's use metal sensing they are more linear therefore they are stable at high temperatures (Anonymous, 1995).

2.5.3.5 Sensitivity

Sensitivity can be defined as the minimum change in temperature (input) that can bring about a detectable change in the output. Thermocouples produce a voltage difference corresponding to a difference in temperature and they have a medium sensitivity of 10s of μV / ˚C. In RTD's and thermistors the resistance changes as a result of change in temperature. Platinum RTD's have a sensitivity of 0.00385 Ω / Ω / ˚C. Whereas thermistors have a sensitivity of several Ω / Ω / ˚C (Baker, 1998). Thermistors have the best sensitivity out of the three sensors (National Instruments, 2010). Since the sensor variations with respect to temperature is high and also the resistance change with regard to lead resistances is high in thermistors, a simple voltage divider circuit can be used instead of a bridge completion circuit when connecting the thermistor to an analogue to digital converter (Anonymous, 1995).

2.5.3.6 Drift/Stability

Drift/Stability is the ability of a sensor to give reproducible results for a period of time. It includes retaining the step response time, selectivity and sensitivity of the sensor (V. Bochenkov and G. Sergeev, 2010). A problem with low cost thermocouples is that they tend to drift when measuring high temperatures. However the ones made of nickel and platinum are more stable. Thermocouples are the least stable sensors (Anonymous, 1995). The stability of RTD's is extremely high and they drift by less than 0.1 °C/year (Wilson et al., 2008). Thermistors are also known for good stability and glass bead thermistors have been reported to have RMS fitted drift rates as small as 0.19+/-0.08 μK per week (Lawton and Patterson, 2002).

2.5.3.7 Lead resistance

RTD's have low resistances that changes slightly with temperature (0.4 Ω/°C). In order to measure such small resistances complex circuits are required and long leads will lead to errors. Thermistor can be used to provide remote measurements using long wires since the resistance of the wires are insignificant when compared to the high resistance of the thermistors (Wilson et al., 2008) (SENSORAY, n.d.). When fabrics are made using temperature sensing yarn the length of the leads will vary depending on the position of the sensor therefore thermistors are ideal for wearable applications.

2.5.3.8 Electrical Noise

Electrical and magnetic noise can be a problem when using thermocouples to measure temperature, since they produce signals in microvolts and typically stray magnetic and electrical signals have magnitudes greater than the measurements. Small signals from an RTD is also prone to noise like thermocouples therefore precautions should be taken to prevent noise. Thermistors have the lowest effect from noise from the three sensors (pico Technology, n.d.).

2.5.3.9 Self-Heating

Self-heating is common in thermistors and RTDs. When powering an RTD it is important to find the smallest possible excitation current. With higher current levels RTD's go into self-heating mode causing measurement errors and with lower current levels produce lower outputs susceptible to noise (Rajanish K. Kamat and Gourish M. Naik, 2002). When a thermistor self-heats the resistance of the thermistor becomes less than it is and this causes an error (Wilson et al., 2008).

2.5.3.10 Excitation

Thermocouples do not need any excitation whereas thermistors and RTD's are powered by a voltage/current source (Baker, 1998).

2.5.3.11 Output

Thermocouples output a voltage whereas thermistors and RTD's output a resistance (Baker, 1998).

2.5.3.12 Ruggedness

Ruggedness is the ability to withstand shock and vibrations. Thermocouples are known to be rugged temperature sensors (Rajanish K. Kamat and Gourish M. Naik, 2002) whereas thermistors are known to be most fragile out of the three. However most thermistors can handle mechanical and thermal shock and vibrations better than other types of sensors (Wilson et al., 2008).

2.5.3.13 Size

Size of the sensor is an important parameter for wearable electronic applications**.** Thermistors come in very small sizes (Wilson et al., 2008). Therefore thermistors can provide point sensing due to its small size.

2.5.3.14 Cost

Thermistors can be considered as the cheapest out of the three. Thermocouples can range from cheap to moderate. RTD's are expensive when compared to the other two sensors (Baker, 1998). If the sensors are to be included in textiles, they must be reasonably priced.

2.5.3.15 Summary

Table 2:3: Comparison of thermistors, thermocouple and RTD's (MINCO, n.d.), (Baker, 1998)

	Thermocouple	RTD	Thermistor
Accuracy	**Low (±0.5 °C)**	**High (±0.01 °C)**	**Moderate (±0.1 °C)**
Temperature range	**-260 to 850°C**	**-270 to 1800°C**	**-80 to 150°C (typically)**
Response time	**Fastest (less than 1 s)**	**Moderate (1-5 s)**	**Slowest (1-10 s)**
Linearity	**Moderate**	**Best**	**Poor**
Stability	**Low**	**Best**	**Moderate**
Sensitivity	**Low**	**Moderate**	**Best**
Effects of Lead Resistance	**-**	**High**	**Low**
Ruggedness	**Most Rugged**	**Moderate**	**Moderate**
size	**Bead diameter = 5 x wire diameter**	**Moderate**	**Smallest 0.3 x 0.3mm (package die)**
Cost	**Low**	**high**	**Low to moderate**

When comparing the temperature sensors it can be seen that for small temperature ranges (variation in body temperature) the thermistor is the most suitable sensor. It comes in small sizes and at very low costs. Also the high sensitivity and resistance of the thermistor ensures that complex circuitry is not needed to measure temperature using a thermistor and this can be beneficial because integrating complex circuits into a textile can be difficult. It also provides a good accuracy, relatively fast response time and a good stability at a low cost.

2.6 Wearable sensors

Traditional ways of obtaining temperature do not provide clinicians with a powerful tool when dealing with diseases such as wound care. Wound care requires remote continuous real time temperature measurement. To provide the patients with the ability to spend time in the comfort of their own homes while being diagnosed, the sensors must be worn. A recent study done by researchers from the Polytechnic University of Madrid (Thomas Klien, 2015) has revealed that patients have a strong preference for wearable sensors in which the sensors and semiconductor devices remain hidden from view. In-order to obtain remote continuous real time temperature measurements while the sensors remain hidden from view, the sensors must be wearable and able to fit into the day to day lives of the patients without any kind of hassle. The integration of sensors into clothing is driven by the growing convergence between new forms of fibres, textiles and electronics (McGrath and Scanaill, 2013). Smart clothing (wearable electronics) can be explained as

the interdisciplinary research from different disciplines and Suh et al (Suh et al., 2010) states that it is the combination of textile technology (Electronic Textiles), design research and physiology (shown in figure 2.7).

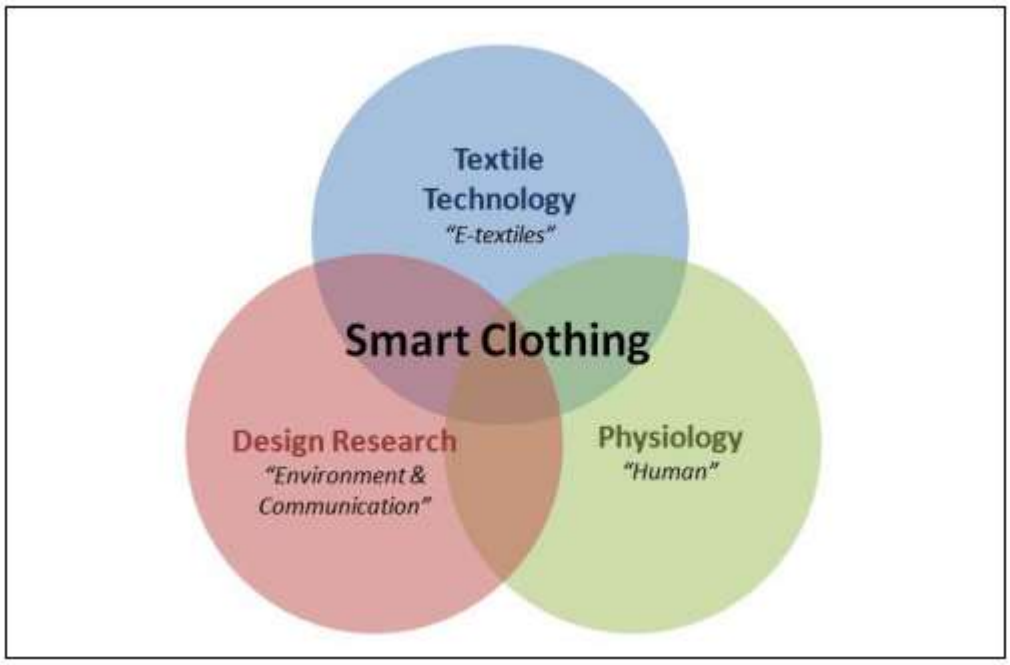

Figure 2-7: Multidisciplinary approach to smart clothing (Suh et al., 2010)

2.6.1 Background on Wearable Electronics

Wearable electronics is the interdisciplinary, common scientific branch which is created by the connection of the three disciplines: textile science, electronics, and computer science. The major problems in wearable arise due to the flexibility, washability, and resistance against cyclic mechanical deformations (Gniotek and Izabela, 2004). The global annual wearable technology market is predicted to reach $47.4 billion by 2019 according to a report by ON World (Hatler et al., 2014). The revenues of wearable medical devices, which were US$2.8 billion in 2014 are predicted to rise to US$8.3 billion by 2019 according to the market analyst firm Mordor Intelligence (Mordor Intelligence, 2014).

The first Electronic textiles garment appeared as early as 1883, in the form of an electric Corset that claimed to benefit "ladies in all stages of their life" (Fishlock, 2001). Thereafter there have been few inventions in the early – mid 20th century. A patent search revealed that the first patent on electrical textiles was filed in the first quarter of the last century, the electrically heated glove for "drivers of Aeroplanes" in 1911 (Carron, 1911) followed by electric conductors embodied in quilts, blankets and clothing for heating in the 1930s; in the 1940s a heated clothing and equipment was developed by incorporating electrical resistance heating elements made from wire gauze and press stud fasteners (Hardman, 1942). Another patent for a heated glove for aviators appeared during the Second World War (Summers, 1945). This glove contained a fastening device attached to it, this

ensured that the movement of the wearer was not hampered, due to its ability to easily connect and disconnect from the power. A heated baby carriage blanket was patented in 1961 (Ellis, 1961); another method of making an electric blanket using two inner layers of synthetic plastics material and a heating element consisting of conductor wires was patented in 1965 (Owers, 1965); electrically heated sock was patented in the 1968 (Balz and Murphy, 1968). The above patents show that most of the developments in electronic wearable textiles were limited to heated textiles until late 1960.

However, the invention of semiconductor diodes and transistors paved the way for adding these to textiles in the late 1970's. In 1979 an illuminating clothing were patented by Miller and Dalke (Miller and Dalke, 1979). Even more heated textiles were patented in the 1980. The electrical heating element that can be incorporated into an inner lining (Courvoisier and Arieh, 1987) and controllably heated clothing (Kerr, 1983) in the 1983 being two of them. The US army proposed a more sophisticated technologies using sensors to monitor living casualties on the battlefield in 1983 (Geddes and Tacker, 1983). In 1990 academic institutions started showing interest in wearable technology. Massachusetts Institute of Technology developing a wearable computer (Post and Orth, 1997) and Georgia Institute of Technology developing a wearable motherboard (Gopalsamy et al., 1999) being among the first academic institutions to work in this area. Textiles with electronic boxes added (Hong et al., 1999), (Carroll, 1996) or attached (Janik, 2000), (Baudhuin, 1996) were patented and developed in the late 1990's. Systems with conductive wires integrated into fabrics were also proposed in 1999 (Lebby and Jachimowicz, 1999).

By the start of the new millennium first electronic integrated textiles rather than electrical textiles started to appear, the ICD+Jacket (Andrew Tuck, 2000) developed by Levi and Philips were one of the first in the market. There were many patents filled by Deutsche (Trinkel, 2002), Infineon (Dangelmaier et al., 2006), Sennheiser (Niehoff, 2007) and Philips (Bhattacharya, 2009) for electronics textiles. Energy harvesting concepts using motion energy from persons respiration were also patented (Muglia et al., 2005). Clothing + claimed to have the integrated sensors onto clothing (Mischke, 2012) and now more than half of the world's heart rate belts are claimed to be created by clothing+ (McGrath and Scanaill, 2013).

Functional elements have also been included into textiles structures. The Burton Amp jacket made for snowboarders by the collaboration of Apple and Burton™. Snowboards consist of an IPod that can be controlled using textile switches on the sleeve of the jacket (Leigh Ault and Alicia Awbery, 2003). The seamless Heart Rate Monitoring Sports Bra NuMetrex developed by Textronics with sensor electrodes knitted into the fabric is another example ("adidas miCoach Seamless Sports Bra," n.d.). In 2004 a paper on the construction of a fabric-mesh transducer capable of capturing motion and gesture together with ECG measurements was published (Wijesiriwardana et al., 2004)

thereafter another paper in relation to this was published describing capacitive fibre-meshed transducers for touch and proximity sensing in 2005 (Wijesiriwardana et al., 2005).

Several textile switches have been patented by France Telecom (Deflin et al., 2003), Daimlerchrysler Ag (Kübler and Seidel, 2005), Sentrix Technology Limited (Leftly, 2006). A fully integrated textile switch has been patented (Dias et al., 2006) and described in 2008 (Dias et al., 2008). In 2009 a linear fabric transducer for strain measurement has been patented (Dias and Hurley, 2011). In 2008 (Dias and Fernando, 2010) a key patent appeared which described the encapsulation of semiconductor devices within the fibres of the yarn.

Fibretronics which is the construction of electronic capabilities on textile fibres (Devanand Uttam, 2014) has become an important part of wearable electronics. Soft switches have been made using International fashion Machines (Maggie Orth's, 2009). Heating products have been developed by Marktek (Marktek Inc., 2006) using conductive textiles. Textile conductors, connectors and sensors have also been made by Ohmatex (Ohmatex, n.d.). Polar (Polar, n.d.) makes fitness trackers and heart rate monitors. Physiological measurement devices for sports, defence and healthcare has been produced by Smart Life (Smart Life, n.d.).

The I-Garment Project funded by the European Space Agency (ESA) has made an integrated system for management of Civil Protection Units (ESA, 2008). Philips has used LED technology to produce illuminating textiles (PHILIPS, n.d.). Forster Rohner has developed conductors, heaters, sensors and illuminated textiles using conductive material and modern embroidery techniques (Forster Rohner, n.d.). Wearable computing has been investigated by the WearIT@work (Boronowsky et al., 2006). It has been funded by the European Commission, which has also funded the STretchable ELectronics for Large Area applications (STELLA) which looks into integration of electronics in stretchable substrate (CORDIS, 2012).

By using Fabroc heaters made using polymer Fabroc yarn® (Mbise et al., 2015) EXO technologies have produced heated gloves that can be used by skiers, motorists and the military (EXO^2, n.d.). NIKE and iPod have combined to produce a shoe that tracks your runs and tracks distance, pace, time and calories (NIKE+, n.d.). Adidas has produced something similar known as MICOACH (adidas, n.d.). Another wireless physiology monitoring system has been made by Zephyr supply wearables (Medtronic, n.d.). Google glasses (Google Glass, 2016) and apple watches (Apple, n.d.) are also considered wearables but they are not textile-based. CUTECIRCUIT (Cutecircuit, n.d.) and Lucentury also produce Illuminating clothing. Flexible embroidery antennas for mega frequency communication has been reported (Acti et al., 2011), (Chauraya et al., 2012). Also by use of $Sn0_2$-microtube a flexible tin dioxide cloth self-powered photo detector has been developed (Hou et al., 2013). Another group of researchers have also developed Flexible Asymmetric Supercapacitors on a woven carbon substrate (Xu et al., 2013). Google has started project Jaquard where they integrate

touch and interactivity into textiles. The Jacquard yarn structures combine thin, metallic alloys with natural synthetic yarns like polyester, cotton (Project Jacquard, n.d.).

Battery power has been an issue with wearable electronic applications, but developments like LG Chem flexible cable batteries (Jon Fingas, 2012) and the Elastic and Wearable Wire-Shaped Lithium-Ion Battery (Ren et al., 2014) could provide solutions to this problem. A report done by the US army Research Laboratory speaks about the potential of graphene based nano-electronics in wearable electronic applications (Osama M. Nayfeh et al., 2011).

2.6.1.1 Electronically functional yarns

The work done at Nottingham Trent University under Professor Dias has embedded semiconductor devices within the core of a textile yarn (Dias and Rathnayake, 2016), (Rathnayake, 2015). The process of making these yarns can be broken down into three stages (A detailed description of the manufacturing process of the yarn is given in chapter 3);

- Interconnection formation stage- where the semiconductor chips have been soldered onto fine copper strands.
- Micro-pod creation stage- where the semiconductor chip, it's interconnects and carrier fibers have been encapsulated with a polymer resin to create a micro-pod.
- Covering stage – where the carrier fibers containing the micro-pod has been sent through a knit-braider to create the final yarn (process is shown in figure 2.8).

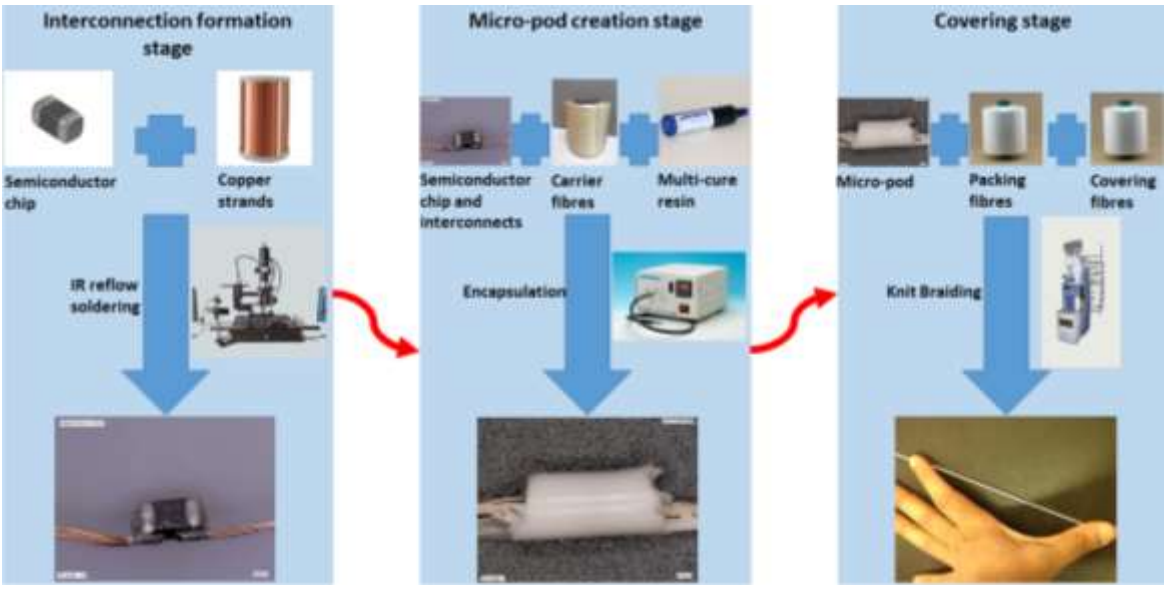

Figure 2-8: Three stages of the electronic yarn creation: interconnection formation stage, Micro-pod creation stage, Covering stage

This technology would provide an ideal candidate to embed temperature sensors within a textile fabric. However the effects on a temperature sensor due to the micro-pod creation stage and covering stage have not been studied.

2.6.2 Existing Wearable Temperature Sensors

There are many wearable temperature sensors that have been developed by the industry and academia. They can be divided into three sections depending on their construction. The three sections are wearable sensors not based on textiles; fabrics embedded with external sensors; and textile-based temperature sensors

2.6.2.1 Wearable sensors not based on textiles

These sensors are not textile-based, they either use stretchable and flexible substrates to obtain their flexibility or comes in the form of an additional device such as earphone/wristband. There are many such wearable temperature sensors in the market. For example the *cosinuss one* ear piece of Cosinuss GmbH, Munich, Germany;, Biovotion AG in Zurich, Switzerland has developed a health monitoring armband; temperature monitoring phone *Kito+ case* has been developed by Azoi Inc. (California, U.S.A) and baby monitoring stamps developed by *Stemp™* and patch thermometer from Fever Smart (Philadelphia, U.S.A.) are a few of them (Brown, 2015). Although many flexible temperature sensors are available none of these are hidden from view (University of Tokyo, 2015), (Giansanti et al., 2009).

The development of a wearable temperature sensor based on graphene nanowalls and Polydimethylsiloxane is reported by Yang et al (Yang et al., 2015). Even though it is stretchable it is not textile-based and does not exhibit other textile characteristics such as shear behaviour vital for drapability. Also the length of the samples tested were 10 mm and 20 mm which makes the sensor visible to the wearer. The printable flexible temperature and tactile pressure sensor developed by Kanao et al (Kanao et al., 2015) is able to bend but does not show any other textile characteristics.

Giansanti et al has developed a wearable thermograph using 4×4 silicon sensor thermometers shown in Figure 2.9 (*Integrated Thermometer*). Even though the thermograph is flexible due to the sponge material used it does not provide all the other textile characteristics. In-order to provide measurements the patient has to wear the thermograph as an additional piece of kit making it difficult and uncomfortable to the wearer (Giansanti et al., 2009), (Giansanti and Maccioni, 2007), (Giansanti et al., 2006).

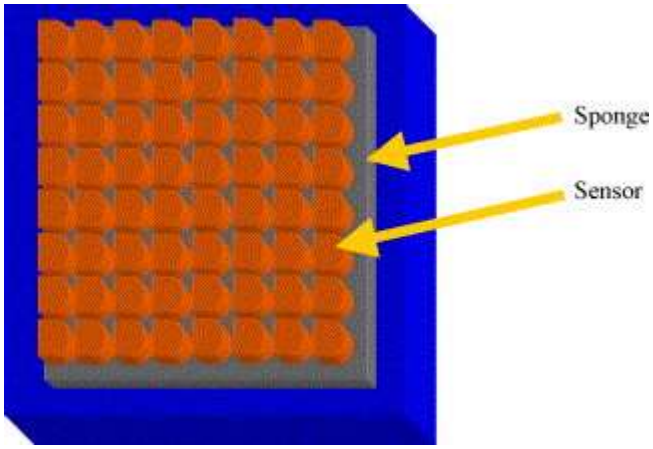

Figure 2-9 Wearable thermograph developed by Giansanti et al (Giansanti et al., 2006)

The wearable sensors not textile-based do not display all the textile characteristics as the ability to bend, shear and drape. Textiles conform to the body shape and these characteristics help to increase the level of comfort to the wearer. Few of the major problems in wearables arise due to the flexibility and resistance against cyclic mechanical deformations (Gniotek and Izabela, 2004). They also are required to be worn as an additional piece of kit which can be troublesome to the wearers.

2.6.2.2 Fabrics embedded with external sensors

Adidas-Textronics have integrated DS18B20 programmable resolution 1-wire digital thermometers, with the fabric of their sportswear garments, in order to measure the body skin temperature of lead athletes. However, it is reported that the way in which the DS18B20 chips are integrated with the garment influences the flexibility and the darpability of the sportswear product negatively (Krzysztof and Gołębiowski Jacek, 2009).

The flexible polymer foil developed by Kinkeldie (Kinkeldei et al., 2011) that could be integrated into textiles has degraded and delaminated during washing of the system. Therefore it is not ideal since garments have to be washed regularly. Humidity sensor and temperature sensors on plastic foil has also being developed by Ataman et al for textile integration (Ataman et al., 2011). However these sensors have to be fabricated in vacuum conditions using expensive clean room equipment (Mattana et al., 2013). Therefore Mattana et al has suggested a method of printing on the flexible substrate using an inkjet printer (Mattana et al., 2013). Nevertheless these sensors can only be woven into fabrics and they are visible to the wearer. The flexibility of these sensors when used in a garment is also questioned, see Figure 2.10.

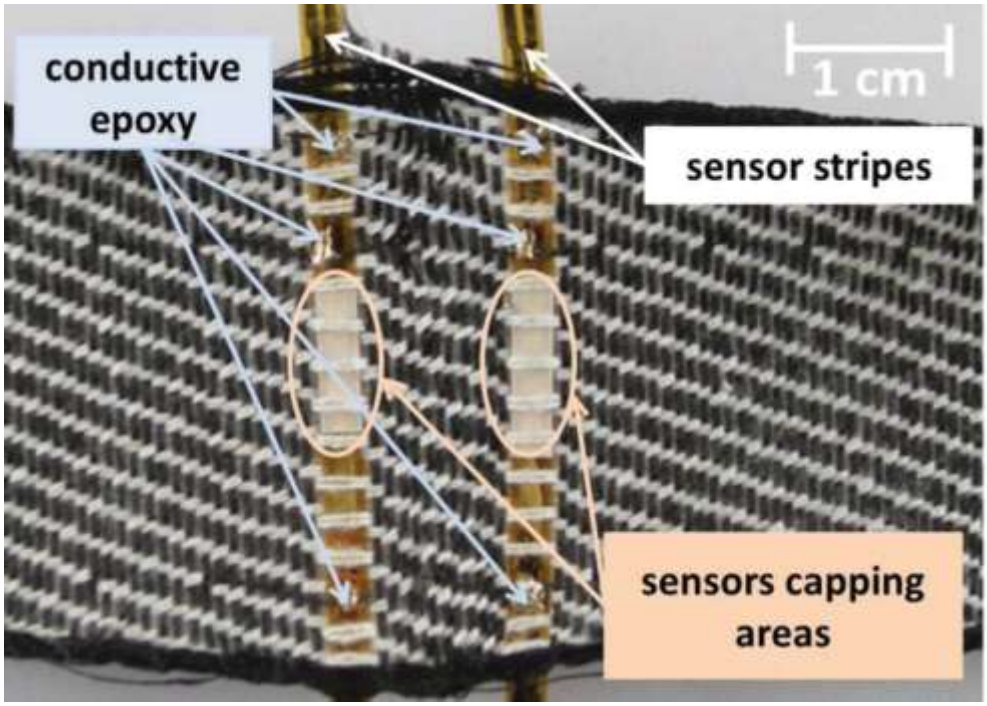

Figure 2-10: Woven sensors realized on polyimide stripes developed by Mattana et al (Mattana et al., 2013)

Optical fibres have been used for temperature measurement in garments by researchers (Li et al., 2012), (Kersey and Berkoff, 1992), however they do not provide the same flexibility as textile fibres. Bending is a major problem with fibre optics, this can induce mechanical damage leading to loss of signal in the fibre (Tao, 2005). In the recent past an optical fibre integrated sock has been developed by Najafi et al. Even though the study done on the wearer trail showed how the technology can be used to predict foot ulcers (Najafi et al., 2014) optic fibres prove to be expensive and fragile. Therefore this is not ideal for mass manufacturing smart clothing.

A thermistor yarn has been developed by Sibinski et al (see figure 2.11). The yarn has been made by depositing thermo-resistive polyvinylidene fluoride PVDF monofilament as the sensor substrate, and a thermo-sensitive paste made of multi-walled carbon nanotube polymer was used to form the active area of the sensor. It has also been reported that the initial resistance of the thermistor depends on the carbon nano-tube content, sensor length and by matching the temperature profile (Sibinski et al., 2010). However this yarn has not been used to manufacture any fabrics therefore its elasticity has not been tested.

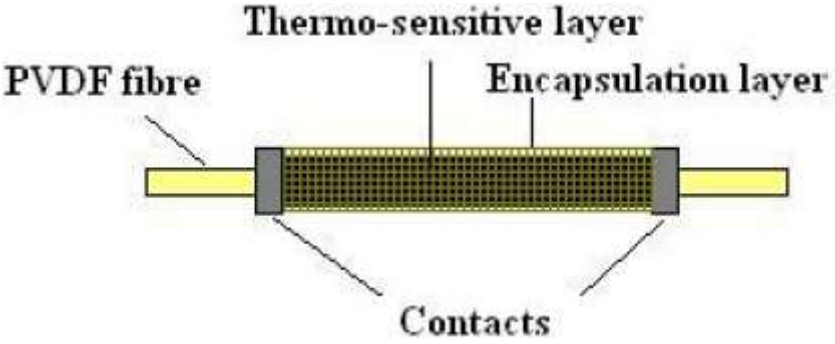

Figure 2-11: Structure of the thermistor developed by Sibinski et a l (Sibinski et al., 2010)

It has been claimed that until each part of technology has been produced out of textile material without functional limitations, technical components cannot be completely integrated into textiles. In-order to empower appearance the electronics have to be completely invisible or if not it has to be attractive and fashionable accessory of the clothing (button/zipper) (Suh et al., 2010). The problem with these types of sensors is that the external sensors effect the textile characteristics since they do not seamlessly integrate into the fabric.

2.6.2.3 Textile-based temperature sensors

These type of temperature sensors have been developed using textile materials. Ziegler et. al. report the development of textile-based thermocouples (Ziegler Stefan and Frydrysiak Michał, 2009), but these are found to be effected by the relative humidity of the environment, and, therefore, are not ideal for wound management or any other application effected by moisture. Also the manufacture of a textile thermocouple is a manual process which can add errors to the temperature measurement.

The temperature sensing fabric developed at Manchester (Husain et al., 2013) by using an inlaid metal wire in the middle of a rib knitted structure measures the average temperature along the wire but is unable to provide localised temperature measurements (Figure 2.12).

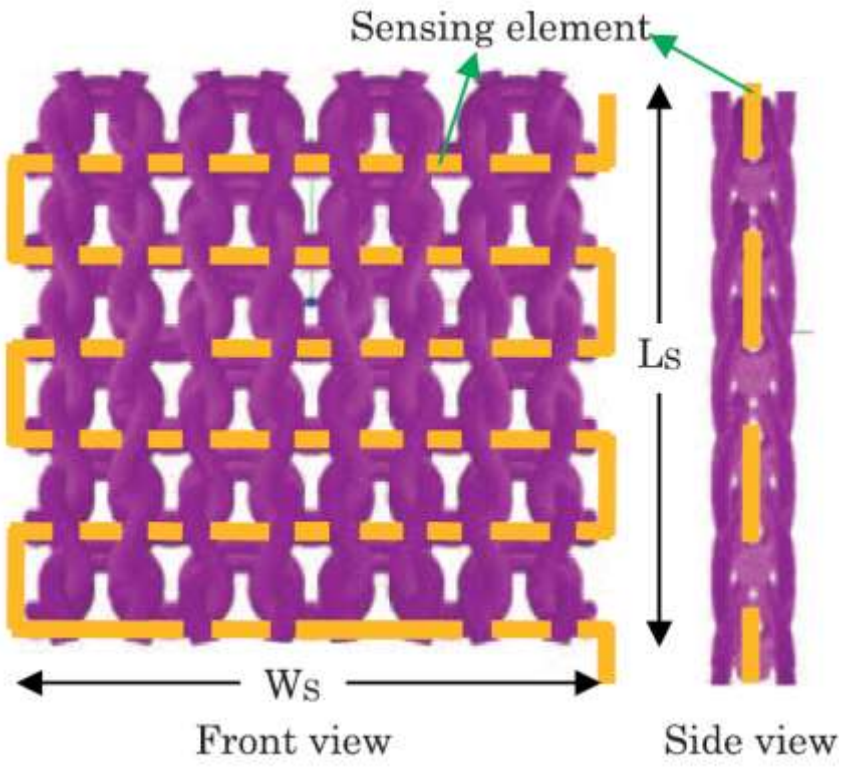

Figure 2-12: Temperature Sensing Fabric showing inlaid sensing wire in a rib knitted structure

A textile-based temperature and humidity sensor has been created by embroidering metal wires containing nickel (Soukup et al., 2014). The temperature coefficient of resistance of the wire has been used to obtain the measurements. The embroidered metal wires are also unable to provide localised temperature readings. In addition, the temperature coefficient of resistance of the wires seem to change when subjected to artificial (placed in a temperature chamber at 200 °C for 44 hours) aging.

An all fabric temperature regulating system has been developed by Roh et al (Roh and Kim, 2015) by using a metal composite embroidery yarn to form an embroidery circuit. The heating is carried out by providing a voltage drop across the circuit. The temperature sensing is carried out by measuring the resistance of the circuit. This too, however, provides an average temperature measurement and does not provide a localised temperature reading.

The textile-based sensors have all the textile characteristics however they are unable to provide localised temperature measurements.

2.7 Knowledge gap

The in-depth literature search carried out has shown the importance of a wearable temperature sensor that can provide continuous, remote, localised temperature measurements. Continuous temperature monitoring can be a powerful tool for clinicians when dealing with complications such as chronic wounds (Nakagami et al., 2010), (Mufti et al., 2015), (Chaves et al., 2015); early detection

of foot ulcers (Armstrong et al., 2007), (Yusuf et al., 2015) and non-freezing cold injury detection (Hope et al., 2014), (Imray et al., 2009). Even though temperature measurement is considered to be one of the most measured and monitored vital signs in hospitalized patients (Louise McCallum and Dan Higgins, 2012), there are not many methods to continuously remotely monitor patients once they are in the comfort of their own homes. A wearable temperature measuring device that can be seamlessly integrated into a patient's life would greatly benefit both the patient and the clinicians. The importance of localised temperature measurement has been highlighted when predicting ulcer formation in diabetic high risk patients (Armstrong et al., 2007), (Lavery et al., 2007), (Lavery et al., 2004), (Peregrina-Barreto et al., 2014). The literature has determined that a temperature difference of 2.2 °C in between the two feet at specific points is sufficient to identify diabetes foot ulcer formation (Armstrong et al., 2007),(Lavery et al., 2007), (Lavery et al., 2004), (Peregrina-Barreto et al., 2014).

Although many flexible temperature sensors are available on the market which are suitable for temperature measurements most of them are not easily concealed (University of Tokyo, 2015), (Giansanti et al., 2009), (Nasir Mehmood, 2015). A recent study undertaken by researchers from the Polytechnic University of Madrid has revealed that patients have a strong preference for wearables that remain hidden from view (Thomas Klien, 2015). A further issue with existing wearable sensors is that they do not exhibit textile characteristics such as the ability to bend and shear, which are needed to allow truly discrete sensing (Krzysztof and Gołębiowski Jacek, 2009), (Webb et al., 2013), (Moser and Gijs, 2007), (Kersey and Berkoff, 1992), (Li et al., 2012). Additionally, some sensors are affected by the relative humidity of the environment making them unsuitable for wearable applications where variations in humidity would cause false readings (Ziegler Stefan and Frydrysiak Michał, 2009).

A textile structure is the ideal solution to create a conformable and comfortable wearable temperature sensor. There are several possible ways to develop temperature measuring fabrics and garments. The simplest method is to add electronic temperature sensors to garments by insertion of components into pockets, however this effects the flexibility and the drapability of the textile. One could also incorporate fine metal wires into fabric during manufacture to create a textile-based temperature sensor. The textile-based sensors that are currently available are unable to provide localised temperature measurements (Ziegler Stefan and Frydrysiak Michał, 2009),(Husain et al., 2013), (Roh and Kim, 2015), (Soukup et al., 2014), which is essential for a medical application where the temperature difference between two regions are sort. The hysteresis of textile materials is another major limiting factor of such transducers and electrodes. Some of these sensors are also incapable of storing data in an electronic manner (Louise van der Werff, 2011) as is needed for centralised management of medical data.

A textile-based wearable temperature sensor capable of providing remote continuous localised temperature measurements has not been created. The research done at Nottingham Trent University under Professor Tilak Dias (Dias and Rathnayake, 2016), (Colin Cork et al., 2013) where surface-mount devices (SMD) were embedded within the fibres of the yarn provides an ideal solution. There are several advantages to incorporating semiconductor microchips into yarns. First, the temperature sensors are not visible on either face of the resultant fabric. Second, the temperature sensor fabrics can then be produced using conventional textile equipment. Third, the required textile characteristics of softness, comfort and conformability are not compromised. When a fabric conforms to a shape some regions bend and others go into shear mode. Paper and thin plastic films bend, but will not shear, so will crumple rather than conform to shape. In woven and knitted textile fabrics the yarns are either interlaced or interloped but neither thermally nor chemically bonded together so can readily shear. Incorporating semiconductor chips into the heart of yarns retains this property.

A SMD thermistor embedded within the fibres of the yarn to create an electronic temperature sensing yarn which can be knitted or woven into a fabric would provide a textile-based temperature sensor which is able to provide localised temperature measurements. The thermistors were chosen as the temperature sensor mainly due to them being available in small packages, so that it can be easily concealed within the core of the yarn. The high resistance and sensitivity of the thermistors when compared to the lead resistance ensures that complex circuitry is not required when obtaining the resistance measurements (which relates to the temperature) from the thermistor. The high accuracy and low cost are also added advantages.

A knowledge gap is present in understanding the effects on the thermistor's performance due to the micro-pod creation and covering stages (shown in figure 2.8). It is important to understand and optimize the micro-pod in-order to minimize its effects on the temperature measurements. This will be a major focus of this thesis. It is also vital to understand the effects on the thermistor measurements due to integrating such a yarn in a textile fabric and being used in ambient conditions, this will also be studied in this thesis.

2.8 Summary

In this chapter an intense literature search was carried out to identify the knowledge gap for a wearable temperature sensor capable of giving remote localised temperature measurements. In the beginning a literature search was done to identify the history and importance of temperature sensing for humans. Thereafter wound care and non-freezing cold injury (NFCI) detection were identified as key areas that can benefit from remote and continuous temperature measurement. It also looked at the various types of sensors that have been developed for wound temperature measurement and early detection of ulcers. This gave a broad understanding of all the available

types of sensors in the market. This also highlighted the importance of a wearable temperature measuring device that can be integrated into a patients day to day activities. The modes of heat transfer from skin to the ambient was discussed next.

Then it looked at the temperature sensors that have been traditionally used for monitoring temperature and an in-depth study was done on thermistors. A comparison of all the temperature sensors were carried out where it was observed that most of the sensors were not geared for continuous temperature measurement. From the temperature sensors that were geared for continuous temperature measurement, most of them were unable to provide electronic data which could be processed and analysed. The most suitable sensors were identified as the thermocouples, thermistors and RTDs. The comparison between the three revealed that the thermistor was the optimum sensor for the applications mentioned in this project.

The next section gave an overall view about the history of wearable devices. Thereafter a brief overview was carried out on the electronically functional yarn developed at Nottingham Trent University. Then it looked at wearable temperature sensors that have been developed and the once in the market. The wearable temperature sensors were divided into three sections depending on their construction. Then finally the knowledge gap was identified after critically analysing the literature for a textile-based temperature sensor capable of providing remote, continuous and localised temperature measurements.

The next chapter will look at the construction of the electronic temperature sensing yarn which is capable of providing remote, continuous and localised temperature measurements.

2.9 References

- 5 Weird Nursing Rules You Might Have Never Heard of, n.d. . Afford. Nurs. Sch.
- Acti, T., Zhang, S., Chauraya, A., Whittow, W., Seager, R., Dias, T., Vardaxoglou, Y., 2011. High performance flexible fabric electronics for megahertz frequency communications, in: Antennas and Propagation Conference (LAPC), 2011 Loughborough. Presented at the Antennas and Propagation Conference (LAPC), 2011 Loughborough, pp. 1–4. doi:10.1109/LAPC.2011.6114088.
- adidas, n.d. miCoach Digital Fitness, Workout, Personal Coach | adidas UK [WWW Document]. Adidas U. K. URL http://www.adidas.co.uk/micoach (accessed 5.25.16).
- adidas miCoach Seamless Sports Bra [WWW Document], n.d. . NuMetrex.com. URL http://shop.numetrex.com/product/adidas-micoach-seamless-sports-bra/ (accessed 5.23.16).
- Alan Tong, 2001. Improving the accuracy of temperature measurements. Sens. Rev. 21, 193–198. doi:10.1108/02602280110398044.

- Albert Victor Summers, 1945. Improvements relating to electrical heated clothing, flying equipment and the like. GB571985 (A).
- Anbar, M., Gratt, B., Hong, D., 1998. Thermology and facial telethermography. Part I: history and technical review. Dentomaxillofacial Radiol. 27, 61 – 67. doi: 10.1038/sj/dmfr/4600314.
- Andrew Tuck, 2000. The ICD+ jacket: Slip into my office, please [WWW Document]. The Independent. URL http://www.independent.co.uk/news/business/analysis-and-features/the-icd-jacket-slip-into-my-office-please-694074.html (accessed 7.2.14).
- Anonymous, 1995. Thermocouples, RTDs, and thermistors. Mach. Des. 67, 74.
- Apple, n.d. Apple Watch [WWW Document]. Apple U. K. URL http://www.apple.com/uk/watch/ (accessed 5.25.16).
- Armstrong, D.G., Holtz-Neiderer, K., Wendel, C., Mohler, M.J., Kimbriel, H.R., Lavery, L.A., 2007. Skin Temperature Monitoring Reduces the Risk for Diabetic Foot Ulceration in High-risk Patients. Am. J. Med. 120, 1042–1046. doi:10.1016/j.amjmed.2007.06.028
- Asano, K., 2006. Evaporation and Condensation, in: Mass Transfer. Wiley-VCH Verlag GmbH & Co. KGaA, pp. 177–208.
- Association, A.D., 2013. Diagnosis and Classification of Diabetes Mellitus. Diabetes Care 36, S67–S74. doi:10.2337/dc13-S067.
- Ataman, C., Kinkeldei, T., Vasquez-Quintero, A., Molina-Lopez, F., Courbat, J., Cherenack, K., Briand, D., Tröster, G., de Rooij, N.F., 2011. Humidity and Temperature Sensors on Plastic Foil for Textile Integration. Procedia Eng., EurosensorsXXV 25, 136–139. doi:10.1016/j.proeng.2011.12.034.
- Baker, B., 1998. Temperature Sensing Technologies (No. AN679). Microchip Technology Inc.
- Balz, C.F., Murphy, D.J., 1968. Electrically heated sock with battery supporting pouch. US3396264 A.
- Baudhuin, E.S., 1996. Telemaintenance applications for the WearableTMPC, in: , 15th AIAA/IEEE Digital Avionics Systems Conference, 1996. Presented at the , 15th AIAA/IEEE Digital Avionics Systems Conference, 1996, pp. 407–413. doi: 10.1109/DASC.1996.559193.
- Benbow, S.J., Chan, A.W., Bowsher, D.R., Williams, G., Macfarlane, I.A., 1994. The Prediction of Diabetic Neuropathic Plantar Foot Ulceration by Liquid-Crystal Contact Thermography. 17, 835-839. PMID: 7956627.
- BetaTHERM Sensors, n.d. NTC Thermistor theory [WWW Document]. URL http://www.betatherm.com/ (accessed 10.12.17).
- Bhattacharya, R., 2009. Textile-based electronic device and manufacturing method therefore. WO2009037667 A2.

- Bishop, O., 2011. Topic 30 - Temperature Sensors, in: Electronics: A First Course (Third Edition). Newnes, Oxford, pp. 117–118.
- Boano, C.A., Lasagni, M., Romer, K., Lange, T., 2011. Accurate Temperature Measurements for Medical Research Using Body Sensor Networks, in: 2011 14th IEEE International Symposium on Object/Component/Service-Oriented Real-Time Distributed Computing Workshops (ISORCW). Presented at the 2011 14th IEEE International Symposium on Object/Component/Service-Oriented Real-Time Distributed Computing Workshops (ISORCW), pp. 189–198. doi:10.1109/ISORCW.2011.28.
- Bochenkov, V., Sergeev, G. 2010. Metal Oxide Nanostructures and their applications. Laboratory of Low Temperature Chemistry, Department of Chemistry, M. Lomonosov Moscow State University, Moscow, Russia.
- Boronowsky, M., Herzog, O., Knackfuß, P., Lawo, M., 2006. Empowering the mobile worker by wearable computing - wearIT@work. J. Telecommun. Inf. Technol. nr 2, 9–14.
- Brown, A., 2015. Investigating Temperature. Wearable Technol.
- Carroll, D.W., 1996. Wearable personal computer system. US5555490 A.
- Carron, A.L., 1911. Electric-heated glove. US1011574 A.
- Cengel, 2002. Heat Transfer: A Practical Approach, 2nd Ed edition. ed. Higher Education, Boston.
- Chauraya, A., Zhang, S., Whittow, W., Acti, T., Seager, R., Dias, T., Vardaxoglou, Y.C., 2012. Addressing the challenges of fabricating microwave antennas using conductive threads. IEEE, pp. 1365–1367. doi:10.1109/EuCAP.2012.6205910.
- Chaves, M.E.A., Silva, F.S. da, Soares, V.P.C., Ferreira, R.A.M., Gomes, F.S.L., Andrade, R.M. de, Pinotti, M., Chaves, M.E.A., Silva, F.S. da, Soares, V.P.C., Ferreira, R.A.M., Gomes, F.S.L., Andrade, R.M. de, Pinotti, M., 2015. Evaluation of healing of pressure ulcers through thermography: a preliminary study. Res. Biomed. Eng. 31, 3–9. doi:10.1590/2446-4740.0571.
- Chen, W., Dols, S., Oetomo, S.B., Feijs, L., 2010. Monitoring Body Temperature of Newborn Infants at Neonatal Intensive Care Units Using Wearable Sensors, in: Proceedings of the Fifth International Conference on Body Area Networks, BodyNets '10. ACM, New York, NY, USA, pp. 188–194. doi:10.1145/2221924.2221960.
- Cork, C., Dias, T., Acti, T., Ratnayake, A., Mbise, E., Anastasopoulos, I., Piper, A., 2013. The next generation of electronic textiles. Presented at the Digital Technologies for the Textile Industries, Manchester, UK.
- CORDIS, 2012. European Commission : CORDIS : Projects & Results Service : Stretchable Electronics for large area applications [WWW Document]. URL http://www.cordis.europa.eu/project/rcn/80720_en.html (accessed 5.25.16).

- Corleto, J., 2016. Measuring Temperature with an NTC Thermistor [WWW Document]. URL https://www.allaboutcircuits.com/projects/measuring-temperature-with-an-ntc-thermistor/ (accessed 12.6.17).
- Courvoisier, G., Arieh, S., 1987. Electrical heating element intended to be incorporated in an inner lining of an item of clothing or accessory intended to be placed against a part of the human body. US4665308 A.
- Cutecircuit [WWW Document], n.d. . CUTECIRCUIT. URL http://cutecircuit.com/ (accessed 5.25.16).
- Dangelmaier, J., Pressel, K.D., Theuss, H.D., 2006. Article of clothing for attaching e.g. ID systems and blue tooth modules comprises electrical internal and external components arranged on the surface of the article so that electrical lines extend between the external components. DE102004039765 A1.
- Dargaville, T.R., Farrugia, B.L., Broadbent, J.A., Pace, S., Upton, Z., Voelcker, N.H., 2013. Sensors and imaging for wound healing: A review. Biosens. Bioelectron. 41, 30–42. doi:10.1016/j.bios.2012.09.029.
- Deflin, E., Weill, A., Bonfiglio, J., ATHIMON-PILLARD, B., 2003. Flexible textile structure for producing electric switches. WO2003050832 A1.
- Devanand Uttam, 2014. E-Textiles: A Review. Int. J. IT Eng. Appl. Sci. Res. 3.
- Diabetic Neuropathy, 2009. Oxford University Press, Oxford, GBR.
- Dias, T., Fernando, A., 2010. Operative devices installed in yarns. EP1882059 B1.
- Dias, T., Hurley, W., 2011. Linear electronic transducer. EP2245223 B1.
- Dias, T., Hurley, W., Monaragala, R., Wijeyesiriwardana, R., 2008. Development of Electrically Active Textiles. Adv. Sci. Technol. 60, 74–84. doi: 10.4028/www.scientific.net/AST.60.74
- Dias, T., Hurley, W., Wijesiriwardana, R., 2006. Switches in textile structures. WO2006045988 A1.
- Dias, T.K., RATHNAYAKE, A., 2016. Electronically functional yarns. WO2016038342 A1.
- Digi-Key, n.d. PTC Thermistors.
- Dini, V., Salvo, P., Janowska, A., Di Francesco, F., Barbini, A., Romanelli, M., 2015. Correlation Between Wound Temperature Obtained With an Infrared Camera and Clinical Wound Bed Score in Venous Leg Ulcers. Wounds Compend. Clin. Res. Pract. 27, 274–278. PMID: 26479211.
- Downie, N.A., 2012. The Ultimate Book of Saturday Science: The Very Best Backyard Science Experiments You Can Do Yourself. Princeton University Press.
- Du, W.Y., 2014. Resistive, Capacitive, Inductive, and Magnetic Sensor Technologies. CRC Press.

- Ellis, H.G., 1961. Heated baby carriage blanket. US2993979 A.
- ESA, 2008. Final presentation of the I-GARMENT project [WWW Document]. Eur. Space Agency. URL http://www.esa.int/Our_Activities/Space_Engineering_Technology/Space_for_health/Final_presentation_of_the_I-GARMENT_project (accessed 5.24.16).
- EXO2, n.d. EXO2 [WWW Document]. URL http://www.exo2.co.uk/ (accessed 5.25.16).
- Fierheller, M., Sibbald, R.G., 2010. A clinical investigation into the relationship between increased periwound skin temperature and local wound infection in patients with chronic leg ulcers. Adv. Skin Wound Care 23, 369–379; quiz 380–381. doi: 10.1097/01.ASW.0000383197.28192.98
- Forster Rohner, n.d. Technical embroideries for Smart Fabrics and Intelligent Textiles - Forster Rohner Textile Innovations [WWW Document]. URL http://www.frti.ch/en/home/ (accessed 5.24.16).
- Freedman, Y., Young, H.D., 2007. University of Physics with modern Physics, 12th ed. Pearson International Edition.
- Geddes, L.A., Tacker, W.A., 1983. Sensing of Living Casualties on the Modern Integrated Battlefield.
- Ghosh, A.K., 2012. INTRODUCTION TO MEASUREMENTS AND INSTRUMENTATION. PHI Learning Pvt. Ltd.
- Giansanti, D., Maccioni, G., 2007. Development and testing of a wearable Integrated Thermometer sensor for skin contact thermography. Med. Eng. Phys. 29, 556–565. doi: 10.1016/j.medengphy.2006.07.006.
- Giansanti, D., Maccioni, G., Bernhardt, P., 2009. Toward the design of a wearable system for contact thermography in telemedicine. Telemed. J. E-Health Off. J. Am. Telemed. Assoc. 15, 290–295. doi: 10.1089/tmj.2008.0105.
- Giansanti, D., Maccioni, G., Gigante, G.E., 2006. A comparative study for the development of a thermal odoscope for the wearable dynamic thermography monitoring. Med. Eng. Phys. 28, 363–371. doi: 10.1016/j.medengphy.2005.07.003.
- Gniotek, K., Izabela, K., 2004. The Basic Problems of Textronics. FIBRES Text. East. Eur. 12.
- Golden, F.S.C., Francis, T.J.R., Gallimore, D., Pethybridge, R., 2013. Lessons from history: morbidity of cold injury in the Royal Marines during the Falklands Conflict of 1982. Extreme Physiol. Med. 2, 23. doi: 10.1186/2046-7648-2-23.
- Google Glass, 2016. . Wikipedia Free Encycl.
- Gopalsamy, C., Park, S., Rajamanickam, R., Jayaraman, S., 1999. The Wearable MotherboardTM: The first generation of adaptive and responsive textile structures (ARTS) for medical applications. Virtual Real. 4, 152–168. doi:10.1007/BF01418152.

- Goto, T., Naito, A., Tamai, N., Nakagami, G., Mo, M., Sanada, H., 2014. Objective evaluation for venous leg ulcer-related nociceptive pain using thermography. Chronic Wound Care Manag. Res. 23. doi: 10.2147/CWCMR.S67054.
- Gregg Lavenuta, 1997. Negative Temperature Coefficient Thermistors.
- Hardman, T.E., 1942. Electrically heated clothing and equipment. US2287915 A.
- Hatler, M., Darryl, G., Chi, C., 2014. Mobile Sensing Wearables A Market Dynamics Report.
- Hilton, J.R., Williams, D.T., Beuker, B., Miller, D.R., Harding, K.G., 2004. Wound Dressings in Diabetic Foot Disease. Clin. Infect. Dis. 39, S100–S103. doi: 10.1086/383270.
- Hoffmann, L., Müller, M.S., Krämer, S., Giebel, M., Schwotzer, G., Wieduwilt, T., 2007. Applications of fibre optic temperature measurement. Temp. Mõõtmise Fiiberoptiliste Meetodite Raken. 13, 363–378.
- Honda, W., Harada, S., Arie, T., Akita, S., Takei, K., 2014. Printed wearable temperature sensor for health monitoring, in: 2014 IEEE SENSORS. Presented at the 2014 IEEE SENSORS, pp. 2227–2229. doi: 10.1109/ICSENS.2014.6985483.
- Hong, P.S., Jenkins, M.D., Ronzani, P.A., Williams, J.W., 1999. Wearable computer. EP0918276 A3.
- Hope, K., Eglin, C., Golden, F., Tipton, M., 2014. Sublingual glyceryl trinitrate and the peripheral thermal responses in normal and cold-sensitive individuals. Microvasc. Res. 91, 84–89. doi:10.1016/j.mvr.2013.11.002.
- Horzic, M., Bunoza, D., Maric, K., 1996. Contact Thermography in a study of primary healing of surgical wounds. Ostomy. Wound Manage. 42, 36–38, 40–42, 44. PMID: 8703289.
- Houghton, V.J., Bower, V.M., Chant, D.C., 2013. Is an increase in skin temperature predictive of neuropathic foot ulceration in people with diabetes? A systematic review and meta-analysis. J. Foot Ankle Res. 6, 31. doi: 10.1186/1757-1146-6-31.
- Hou, X., Liu, B., Wang, X., Wang, Z., Wang, Q., Chen, D., Shen, G., 2013. SnO2-microtube-assembled cloth for fully flexible self-powered photodetector nanosystems. Nanoscale 5, 7831. doi: 10.1039/c3nr02300a.
- Howells, E.B., 2015. Measuring temperature. Anaesth. Intensive Care Med., Intensive Care / Transplantation 16, 358–362. doi: 10.1016/j.mpaic.2015.04.011.
- Husain, M.D., 2012. Development of Temperature Sensing Fabric (PhD thesis). University of Manchester.
- Husain, M.D., Kennon, R., Dias, T., 2013. Design and fabrication of Temperature Sensing Fabric. J. Ind. Text. 1528083713495249. doi: 10.1177/1528083713495249.
- Imray, C., Grieve, A., Dhillon, S., Caudwell Xtreme Everest Research Group, 2009. Cold damage to the extremities: frostbite and non-freezing cold injuries. Postgrad. Med. J. 85, 481–488. doi: 10.1136/pgmj.2008.068635.

- Irwin, M.S., 1996. Nature and mechanism of peripheral nerve damage in an experimental model of non-freezing cold injury. Ann. R. Coll. Surg. Engl. 78, 372–379. PMID: 8712655.
- Irwin, M.S., Sanders, R., Green, C.J., Terenghi, G., 1997. Neuropathy in non-freezing cold injury (trench foot). J. R. Soc. Med. 90, 433–438. PMID: 9306996.
- Iven, G., Chekh, V., Luan, S., Mueen, A., Soliz, P., Xu, W., Burge, M., 2014. Non-contact Sensation Screening of Diabetic Foot Using Low Cost Infrared Sensors, in: 2014 IEEE 27th International Symposium on Computer-Based Medical Systems (CBMS). Presented at the 2014 IEEE 27th International Symposium on Computer-Based Medical Systems (CBMS), pp. 479–480. doi: 10.1109/CBMS.2014.99.
- Izard, R.M., Bilzon, J.L.J., 2008. Risk Factors for Non-Freezing Cold Injury in British Army Infantry Recruit Training: 1504. Med. Sci. Sports Exerc. 40, S229. doi: 10.1249/01.mss.0000322484.42167.4e.
- Janik, C.M., 2000. Flexible wearable computer. US6108197 A.
- Jia, J., Pollock, M., 1997. The pathogenesis of non-freezing cold nerve injury. Observations in the rat. Brain J. Neurol. 120 (Pt 4), 631–646. PMID: 9153125.
- John, 2011. Thermistor-Construction,Temperature Sensors,Types-NTC,PTC Thermistors. Instrum.-Electron.
- O'Connor, J., 2012. Higher wound care costs are driving treatment research. McKnight's. URL https://www.mcknights.com/news/higher-wound-care-costs-are-driving-treatment-research/ (accessed 8.04.14).
- Jon Fingas, 2012. LG Chem develops very flexible cable batteries, may leave mobile devices tied up in knots [WWW Document]. Engadget. URL http://www.engadget.com/2012/09/02/lg-chem-develops-very-flexible-cable-batteries/ (accessed 5.25.16).
- Kanao, K., Harada, S., Yamamoto, Y., Honda, W., Arie, T., Akita, S., Takei, K., 2015. Printable flexible tactile pressure and temperature sensors with high selectivity against bending, in: 2015 28th IEEE International Conference on Micro Electro Mechanical Systems (MEMS). Presented at the 2015 28th IEEE International Conference on Micro Electro Mechanical Systems (MEMS), pp. 756–759. doi:10.1109/MEMSYS.2015.7051068.
- Kelechi, T.J., Michel, Y., Wiseman, J., 2006. Are Infrared and Thermistor Thermometers Interchangeable for Measuring Localized Skin Temperature? J. Nurs. Meas. 14, 19–30. doi:10.1891/jnum.14.1.19.
- Kerr, J.F., 1983. Controllably heated clothing. US4404460 A.
- Kersey, A.D., Berkoff, T.A., 1992. Fiber-optic Bragg-grating differential-temperature sensor. IEEE Photonics Technol. Lett. 4, 1183–1185. doi:10.1109/68.163773.

- King, R.C., Parrish, J.A., Allibone, A., 1958. Trench-foot in Peacetime England. Br. Med. J. 1, 1099–1102.
- Kinkeldei, T., Zysset, C., Cherenack, K.H., Tröster, G., 2011. A textile integrated sensor system for monitoring humidity and temperature, in: Solid-State Sensors, Actuators and Microsystems Conference (TRANSDUCERS), 2011 16th International. Presented at the Solid-State Sensors, Actuators and Microsystems Conference (TRANSDUCERS), 2011 16th International, pp. 1156–1159. doi:10.1109/TRANSDUCERS.2011.5969238.
- Krzysztof, G., Gołębiowski Jacek, 2009. Temperature Measurements in a Textronic Fireman Suit and Visualisation of the Results. Fibres Text. East. Eur. 97–101.
- Kübler, S., Seidel, F.-P., 2005. Textile with built-in electrical switches is used as internal lining or seat covering in vehicles. DE102004009189 A1.
- Laden, G.D.M., Purdy, G., O'Rielly, G., 2007. Cold injury to a diver's hand after a 90-min dive in 6 degrees C water. Aviat. Space Environ. Med. 78, 523–525. PMID: 17539448.
- Lavery, L.A., Higgins, K.R., Lanctot, D.R., Constantinides, G.P., Zamorano, R.G., Armstrong, D.G., Athanasiou, K.A., Agrawal, C.M., 2004. Home monitoring of foot skin temperatures to prevent ulceration. Diabetes Care 27, 2642–2647. PMID: 15504999.
- Lavery, L.A., Higgins, K.R., Lanctot, D.R., Constantinides, G.P., Zamorano, R.G., Athanasiou, K.A., Armstrong, D.G., Agrawal, C.M., 2007. Preventing diabetic foot ulcer recurrence in high-risk patients: use of temperature monitoring as a self-assessment tool. Diabetes Care 30, 14–20. doi: 10.2337/dc06-1600.
- Lawson, R.N., Chughtai, M.S., 1963. Breast Cancer and Body Temperature. Can. Med. Assoc. J. 88, 68–70. PMID: 20327365.
- Lawton, K.M., Patterson, S.R., 2002. Long-term relative stability of thermistors: Part 2. Precis. Eng. 26, 340–345. doi: 10.1016/S0141-6359(02)00110-1.
- Lebby, M.S., Jachimowicz, K.E., 1999. Textile fabric with integrated electrically conductive fibers and clothing fabricated thereof. US5906004 A.
- Lee, W., Kwon, O., Lee, D.S., Yeo, W.-H., 2015. Fabrication and Characterization of a Conformal Skin-like Electronic System for Quantitative, Cutaneous Wound Management. J. Vis. Exp. Doi: 10.3791/53037.
- Leftly, S.A., 2006. Switches and devices for textile artcles. WO2006030230 A1.
- Leigh Ault, Alicia Awbery, 2003. Apple - Press Info - Burton and Apple Deliver the Burton Amp Jacket [WWW Document]. URL https://www.apple.com/pr/library/2003/01/07Burton-and-Apple-Deliver-the-Burton-Amp-Jacket.html (accessed 5.23.16).

- Li, H., Yang, H., Li, E., Liu, Z., Wei, K., 2012. Wearable sensors in intelligent clothing for measuring human body temperature based on optical fiber Bragg grating. Opt. Express 20, 11740–11752. doi: 10.1364/OE.20.011740.
- Lin, S., Yuk, H., Zhang, T., Parada, G.A., Koo, H., Yu, C., Zhao, X., 2015. Stretchable Hydrogel Electronics and Devices. Adv. Mater. 28, 4497-4505. doi: 10.1002/adma.201504152.
- Liptak, B. (Ed.), 2003. Instrument Engineers' Handbook, Fourth Edition, Volume One: Process Measurement and Analysis: Process Measurement and Analysis Vol 1, 4 edition. ed. CRC Press, Boca Raton, FL.
- Lipták, B., Rall, D., Moore, L.W., Adler, B., 2004. Temperature sensors. InTech 51, 61–62.
- Liu, H.T., Shao, D., Li, B.Q., 2012. Theory Analysis of Thermocouple Temperature Measurement. Appl. Mech. Mater. 239-240, 749–753. doi: 10.4028/www.scientific.net/AMM.239-240.749.
- Louise McCallum, Dan Higgins, 2012. Body temperature is a vital sign and it is important to measure it accurately. This article reviews and compares the various methods available to nurses Measuring body temperature. Nurs. Times 108, 20–22.
- Louise van der Werff, 2011. Heat sensitive bandage could combat infection, Monash University [WWW Document]. Monash Univ. URL http://monash.edu/news/show/heat-sensitive-bandage-could-combat-infection (accessed 7.2.14).
- Mackowiak, P., Worden, G., 1994. Carl Reinhold August Wunderlich and the Evolution of Clinical Thermometry. Clin. Infect. Dis. 18, 458–467. PMID: 8011836.
- Maggie Orth's, 2009. International Fashion Machines [WWW Document]. URL http://www.ifmachines.com/ (accessed 5.24.16).
- Marcus, P., 1979. "Trench foot" caused by the cold. Br. Med. J. 1, 622.
- Marktek Inc., 2006. Electrically Conductive Textiles - Conductive Fabrics - Conductive Foams - EMI / RFI / EMC / ESD Conductive Textiles [WWW Document]. URL http://www.marktek-inc.com/eeontexconductextiles.htm (accessed 5.24.16).
- Mattana, G., Kinkeldei, T., Leuenberger, D., Ataman, C., Ruan, J.J., Molina-Lopez, F., Vasquez Quintero, A., Nisato, G., Troster, G., Briand, D., de Rooij, N.F., 2013. Woven Temperature and Humidity Sensors on Flexible Plastic Substrates for E-Textile Applications. IEEE Sens. J. 13, 3901–3909. doi: 10.1109/JSEN.2013.2257167.
- Matzeu, G., Losacco, M., Parducci, E., Pucci, A., Dini, V., Romanelli, M., Di Francesco, F., 2011. Skin temperature monitoring by a wireless sensor, in: IECON 2011 - 37th Annual Conference on IEEE Industrial Electronics Society. Presented at the IECON 2011 - 37th Annual Conference on IEEE Industrial Electronics Society, pp. 3533–3535. doi: 10.1109/IECON.2011.6119881.

- Mbise, E., Dias, T., Hurley, W., 2015. Design and manufacture of heated textiles, in: Dias, T. (Ed.), Electronic Textiles Smart Fabrics and Wearable Technology. Woodhead Publishing, Nottingham.
- McGee, T., 1988. Principles and Methods of Temperature Measurement. John Wiley & Sons.
- McGrath, M., Scanaill, C., 2013. Sensor Technologies: Healthcare, Wellness and Environmental Applications. Apress.
- McGuiness, W., Vella, E., Harrison, D., 2004. Influence of dressing changes on wound temperature. J. Wound Care 13, 383–385. doi: 10.12968/jowc.2004.13.9.26702.
- Medtronic, n.d. Zephyr Technology Corporation - Measure Life... Anywhere! Zephyr is a global leader in real-time physiological and biomechanical monitoring, or Physical Status Monitoring (PSM) solutions for mHealth, Defense, First Responder, Training and Research markets. [WWW Document]. Zephyr Technol. Corp. URL http://zephyranywhere.com/ (accessed 5.25.16).
- Michalski, L., 2001. Temperature Measurement. John Wiley & Sons.
- Michalski, L., Eckersdorf, K., Kucharski, J., McGhee, J., 2001a. Non-Electric Thermometers, in: Temperature Measurement. John Wiley & Sons, Ltd, pp. 19–36.
- Michalski, L., Eckersdorf, K., Kucharski, J., McGhee, J., 2001b. Quartz, Ultrasonic and Noise Thermometers and Distributed Parameter Sensors, in: Temperature Measurement. John Wiley & Sons, Ltd, pp. 139–150.
- Michalski, L., Eckersdorf, K., Kucharski, J., McGhee, J., 2001c. Fibre Optic Thermometers, in: Temperature Measurement. John Wiley & Sons, Ltd, pp. 125–138.
- Michalski, L., Eckersdorf, K., Kucharski, J., McGhee, J., 2001d. Semiconductor Thermometers, in: Temperature Measurement. John Wiley & Sons, Ltd, pp. 103–124.
- Miller, G.E., Dalke, M., 1979. Illuminated article of clothing. US4164008 A.
- MINCO, n.d. RTD, Thermocouples, or thermistors? [WWW Document]. URL http://www.minco.com/Sensors-and-Instruments/Support-and-Tools/Sensor-FAQs (accessed 5.6.16).
- Mischke, J., 2012. Sensors add a new basic function to garments. Wearable Technol. URL https://www.wearable-technologies.com/2012/03/sensors-add-a-new-basic-function-to-garments/(accessed 5.5.16).
- Mordor Intelligence, 2014. Global Wearable Medical Device Market - Growth, Trends and Forecasts (2014-2019), HealthCare.
- Morovati, R., Maclean, I., 2016. Development of Foot Temperature Measuring Device for Diabetes1. J. Med. Devices 10, 020919–020919. doi: 10.1115/1.4033219.
- Moser, Y., Gijs, M.A.M., 2007. Miniaturized Flexible Temperature Sensor. J. Microelectromechanical Syst. 16, 1349–1354. doi:10.1109/JMEMS.2007.908437.

- Mufti, A., Coutts, P., Sibbald, R.G., 2015. Validation of commercially available infrared thermometers for measuring skin surface temperature associated with deep and surrounding wound infection. Adv. Skin Wound Care 28, 11–16. doi:10.1097/01.ASW.0000459039.81701.b2.
- Muglia, H.A., Refeld, J., Eiselt, H., 2005. Generator device for converting motion energy of person's respiration into electrical energy is integrated into clothing item normally arranged at one or more positions on person that undergoes change in dimensions during respiration. DE10340873 A1.
- Najafi, B., Singh Grewal, Gurtej, Parvaneh, S., Lee-eng Jacqueline, A. Menzies, R., K Talal, T., G Armstrong, D., 2014. Validation Of An Optical Fiber Based Smart Textile: A Clinical Tool For Predicting Diabetic Foot Ulceration. Qatar Found. Annu. Res. Conf. Proc. HBPP0345. doi: 10.5339/qfarc.2014.HBPP0345.
- Nakagami, G., Sanada, H., Iizaka, S., Kadono, T., Higashino, T., Koyanagi, H., Haga, N., 2010. Predicting delayed pressure ulcer healing using thermography: a prospective cohort study. J. Wound Care 19, 465–472. doi: 10.12968/jowc.2010.19.11.79695.
- Nasir Mehmood, A.H., 2015. A flexible and low power telemetric sensing and monitoring system for chronic wound diagnostics. Biomed. Eng. OnLine 14. doi: 10.1186/s12938-015-0011-y.
- National Instruments, 2010. RTD, Thermistor, Thermocouple Comparison Chart - National Instruments [WWW Document]. URL http://digital.ni.com/public.nsf/allkb/C50FA55B3B2F85D9862572D00083350E (accessed 1.3.18).
- Nawrocki, W., 2005. Measurement Systems and Sensors. Artech House, Norwood, MA, USA.
- Netten, J.J. van, Baal, J.G. van, Liu, C., Heijden, F. van der, Bus, S.A., 2013. Infrared Thermal Imaging for Automated Detection of Diabetic Foot Complications. J. Diabetes Sci. Technol. 7, 1122–1129. doi:10.1177/193229681300700504,
- Ng, K.K., 2009. Thermistor, in: Complete Guide to Semiconductor Devices. John Wiley & Sons, Inc., pp. 528–535.
- Niehoff, W.D., 2007. Textile material for an article of clothing comprises electrical and/or electronic components and/or lines embedded in the material. DE102005033643 A1.
- NIKE+, n.d. Join me on Nike+ [WWW Document]. URL https://secure-nikeplus.nike.com/plus/products/ipod_nano/ (accessed 5.25.16).
- Nikolic, M.V., Radojcic, B.M., Aleksic, O.S., Lukovic, M.D., Nikolic, P.M., 2011. A Thermal Sensor for Water Using Self-Heated NTC Thick-Film Segmented Thermistors. IEEE Sens. J. 11, 1640–1645. doi: 10.1109/JSEN.2010.2103309.

- Nixon, M., D, M., Moore, C., 2014. Evidence-Based Wound Surveillance A Three-Dimensional Approach To Measuring, Imaging and Documenting Wounds. ARANZ Med. Ltd.
- Ohmatex, n.d. ohmatex | smart textile and technologyohmatex | smart textile and technology. URL https://www.ohmatex.dk/products_textile-_cables_connectors/ (accessed 10.12.16).
- Nayfeh, O., Chin, M., Ervin, M., Wilson, J., Ivanov, T., Proie, R., Nichols, B., Crowne, F., Kilpatrick, S., 2011. Graphene-based Nanoelectronics (No. ARL-TR-5451). Army Research Laboratory.
- Otsuka, K., Togawa, T., 1997. Hippocratic thermography. Physiol. Meas. 18, 227. doi: 10.1088/0967-3334/18/3/007.
- Owers, L.C., 1965. Method of making an electric blanket. US3213521 A.
- Parsons, K., 2014. Human Thermal Environments: The Effects of Hot, Moderate, and Cold Environments on Human Health, Comfort, and Performance, Third Edition. CRC Press.
- Pearce, J.M.S., 2002. A brief history of the clinical thermometer. QJM Int. J. Med. 95, 251–252. doi: 10.1093/qjmed/95.4.251.
- Peregrina-Barreto, H., Morales-Hernandez, L.A., Rangel-Magdaleno, J.J., Avina-Cervantes, J.G., Ramirez-Cortes, J.M., Morales-Caporal, R., 2014. Quantitative Estimation of Temperature Variations in Plantar Angiosomes: A Study Case for Diabetic Foot. Comput. Math. Methods Med. 2014. doi: 10.1155/2014/585306.
- PHILIPS, n.d. Luminous textile [WWW Document]. URL http://www.largeluminoussurfaces.com/luminoustextile (accessed 5.24.16).
- Pico Technology, n.d. Improving the accuracy of temperature measurements [WWW Document]. URL https://www.picotech.com/library/application-note/improving-the-accuracy-of-temperature-measurements (accessed 4.22.16).
- Polar, n.d. Heart Rate Monitors, activity trackers and bike computers [WWW Document]. Polar Glob. URL http://www.polar.com/en (accessed 5.24.16).
- Post, E., Orth, M., 1997. Smart fabric, or "wearable clothing," in: , First International Symposium on Wearable Computers, 1997. Digest of Papers. Presented at the , First International Symposium on Wearable Computers, 1997. Digest of Papers, pp. 167–168. doi: 10.1109/ISWC.1997.629937.
- Project Jacquard [WWW Document], n.d. URL https://atap.google.com/jacquard/ (accessed 5.25.16).
- Rajanish K. Kamat, Gourish M. Naik, 2002. Thermistors – in search of new applications, manufacturers cultivate advanced NTC techniques. Sens. Rev. 22, 334–340. doi: 10.1108/02602280210444654.

- Ramstead, K.D., Hughes, R.G., Webb, A.J., 1980. Recent cases of trench foot. Postgrad. Med. J. 56, 879–883. PMID: 6115374.
- Rathnayake, A., 2015. Development of the core technology for the creation of electronically active, smart yarn (PhD thesis). Nottingham Trent University.
- Ren, J., Zhang, Y., Bai, W., Chen, X., Zhang, Z., Fang, X., Weng, W., Wang, Y., Peng, H., 2014. Elastic and Wearable Wire-Shaped Lithium-Ion Battery with High Electrochemical Performance. Angew. Chem. 126, 7998–8003. doi: 10.1002/ange.201402388.
- Ring, E., 2004. The historical development of thermal imaging in medicine. Rheumatology 43, 800–802. doi: 10.1093/rheumatology/keg009.
- Roback, K., 2010. An overview of temperature monitoring devices for early detection of diabetic foot disorders. Expert Rev. Med. Devices 7, 711–8. doi: http://dx.doi.org/10.1586/erd.10.35.
- Roh, J.-S., Kim, S., 2015. All-fabric intelligent temperature regulation system for smart clothing applications. J. Intell. Mater. Syst. Struct. 1045389X15585901. doi: 10.1177/1045389X15585901.
- Rohsenow, W.M., Hartnett, J.P., Ganić, E.N., 1985. Handbook of heat transfer fundamentals. McGraw-Hill.
- Salvo, P., Dini, V., Di Francesco, F., Romanelli, M., 2015. The role of biomedical sensors in wound healing. Wound Med., Special Issue: Wound Diagnostic 8, 15–18. doi: 10.1016/j.wndm.2015.03.007.
- Sapoff, M., Oppenheim, R.M., 1963. Theory and application of self-heated thermistors. Proc. IEEE 51, 1292–1305. doi: 10.1109/PROC.1963.2560.
- Sen, C.K., Gordillo, G.M., Roy, S., Kirsner, R., Lambert, L., Hunt, T.K., Gottrup, F., Gurtner, G.C., Longaker, M.T., 2009. Human Skin Wounds: A Major and Snowballing Threat to Public Health and the Economy. Wound Repair Regen. Off. Publ. Wound Heal. Soc. Eur. Tissue Repair Soc. 17, 763–771. doi: 10.1111/j.1524-475X.2009.00543.x.
- SENSORAY, n.d. Comparison of Thermocouples, RTDs, and Thermistors [WWW Document]. URL http://www.sensoray.com/support/appnotes/thermocouples_rtds_thermistors.htm (accessed 1.3.18).
- Sibinski, M., Jakubowska, M., Sloma, M., 2010. Flexible Temperature Sensors on Fibers. Sensors 10, 7934–7946. doi: 10.3390/s100907934.
- SMART LIFE, n.d. SmartLife [WWW Document]. SmartLife. URL http://www.smartlifewearabletech.com/#home (accessed 5.24.16).
- Soukup, R., Hamacek, A., Mracek, L., Reboun, J., 2014. Textile based temperature and humidity sensor elements for healthcare applications, in: Proceedings of the 2014 37th International Spring Seminar on Electronics Technology. Presented at the Proceedings of

the 2014 37th International Spring Seminar on Electronics Technology, pp. 407–411. doi: 10.1109/ISSE.2014.6887634.

- Sprigle, S., Linden, M., McKenna, D., Davis, K., Riordan, B., 2001. Clinical skin temperature measurement to predict incipient pressure ulcers. Adv. Skin Wound Care 14, 133. PMID: 11905978.
- Stess, R., Sisney, P.C., Moss, K.M., Graf, P.M., Louie, K.S., Gooding, G.A.W., Grunfeld, C., 1986. Use of Liquid Crystal Thermography in the Evaluation of the Diabetic Foot. Diabetes Care 9, 267–272. doi: 10.2337/diacare.9.3.267.
- Stretchable hydrogel electronics [WWW Document], n.d. . MIT News. URL http://news.mit.edu/2015/stretchable-hydrogel-electronics-1207 (accessed 1.28.16).
- Suh, M., Carroll, K.E., Cassill, N.L., 2010. Critical Review on Smart Clothing Product Development. J. Text. Appar. Technol. Manag. 6.
- Sychev, I.A., 1961. Temperature error of liquid manometric thermometers and methods for compensating it. Meas. Tech. 4, 803–810. doi: 10.1007/BF00980865.
- Tao, X.M., 2005. Wearable Electronics and Photonics. Elsevier.
- TDK, 2012. PTC thermistors, general technical information.
- Tek, D., Mackey, S., 1993. Non-freezing cold injury in a Marine infantry battalion. J. Wilderness Med. 4, 353–357. doi: 10.1580/0953-9859-4.4.353.
- Temperature and Temperature Scales – FREE Temperature and Temperature Scales information | Encyclopedia.com: Find Temperature and Temperature Scales research [WWW Document], 2003. . World Earth Sci. URL http://www.encyclopedia.com/doc/1G2-3437800603.html (accessed 1.15.16).
- Thomas Klien, 2015. Spanish Researchers Test Patient Reactions to Wearables for Parkinson Monitoring | EMDT - European Medical Device Technology [WWW Document]. Eur. Med. Device Technol. URL http://www.emdt.co.uk/daily-buzz/spanish-researchers-test-patient-reactions-wearables-parkinson-monitoring (accessed 3.4.15).
- Trinkel, M., 2002. Intelligent clothing item provided with sensor e.g. for monitoring vital functions of wearer, has sensor electrical line acting as antenna. DE10047533 A1.
- University of Tokyo, 2015. Fever alarm armband: A wearable, printable, temperature sensor -- ScienceDaily [WWW Document]. ScienceDaily. URL http://www.sciencedaily.com/releases/2015/02/150223084343.htm (accessed 2.25.15).
- Vishay Dale, 2002. NTC and PTC thermistors. URL https://www.vishay.com/docs/33016/engnote.pdf (accessed 6.4.14).
- Vuorisalo, S., Venermo, M., Lepäntalo, M., 2009. Treatment of diabetic foot ulcers. J. Cardiovasc. Surg. (Torino) 50, 275–91. PMID: 19543189.

- Webb, R., Bonifas, A., Behnaz, A., Zhang, Y., Yu, K., Cheng, H., Shi, M., Bian, Z., Liu, Z., Kim, Y., Yeo, W., Park, J., Song, J., Li, Y., Huang, Y., Gorbach, A., Rogers, J., 2013. Ultrathin conformal devices for precise and continuous thermal characterization of human skin. Nat. Mater. 12, 938–944. doi: 10.1038/nmat3755.
- Wijesiriwardana, R., Mitcham, K., Dias, T., 2004. Fibre-meshed transducers based real time wearable physiological information monitoring system, in: Eighth International Symposium on Wearable Computers, 2004. ISWC 2004. Presented at the Eighth International Symposium on Wearable Computers, 2004. ISWC 2004, pp. 40–47. doi: 10.1109/ISWC.2004.20.
- Wijesiriwardana, R., Mitcham, K., Hurley, W., Dias, T., 2005. Capacitive fiber-meshed transducers for touch and proximity-sensing applications. IEEE Sens. J. 5, 989–994. doi: 10.1109/JSEN.2005.844327.
- Wilson, J., Ball, S., Huddleston, C., Ramsden, E., Ibrahim, D., 2008. Test and Measurement: Know It All. Newnes. 1st Ed. Elsevier.
- Wunderlich, C., 1871. On the Temperature in Diseases: A Manual of Medical Thermometry. New Sydenham Society. 2D German ed. The New Sydenham society.
- Xu, J., Wang, Q., Wang, X., Xiang, Q., Liang, B., Chen, D., Shen, G., 2013. Flexible Asymmetric Supercapacitors Based upon Co9S8 Nanorod//Co3O4@RuO2 Nanosheet Arrays on Carbon Cloth. ACS Nano 7, 5453–5462. doi: 10.1021/nn401450s.
- Yang, J., Wei, D., Tang, L., Song, X., Luo, W., Chu, J., Gao, T., Shi, H., Du, C., 2015. Wearable temperature sensor based on graphene nanowalls. RSC Adv. 5, 25609–25615. doi: 10.1039/C5RA00871A.
- Yusuf, S., Okuwa, M., Shigeta, Y., Dai, M., Iuchi, T., Rahman, S., Usman, A., Kasim, S., Sugama, J., Nakatani, T., Sanada, H., 2015. Microclimate and development of pressure ulcers and superficial skin changes. Int. Wound J. 12, 40–46. doi: 10.1111/iwj.12048.
- Ziegler Stefan, Frydrysiak Michał, 2009. Initial Research into the Structure and Working Conditions of Textile Thermocouples. Fibres Text. East. Eur. 17, 84–88.
- Zittel, C., 2008. Philosophies of Technology: Francis Bacon and His Contemporaries. BRILL.

3. Development of an electronic temperature sensing yarn

3.1 Introduction

This chapter describes the design and development of a yarn capable of measuring temperature by means of semiconductor electronics and it has been broken down into the following subsections to provide a clear overview of the process:

- E-yarn technology developed in the Advanced Textiles Research Group of Nottingham Trent University;
- Selection of the temperature sensor;
- Geometrical model of the electronic temperature sensing yarn (ETS yarn);
- Fabrication of ETS yarn;
- Development of hardware and software necessary to determine the temperature with ETS yarn;
- Summary.

3.2 Construction of electronic temperature sensor yarn

Electronic textiles can be produced using several methods, however it is important to maintain the textile characteristics when producing the textile. Textiles are produced using fibres and yarns. By using the E-yarn technology pioneered by Dias at UK's Nottingham Trent University (NTU) (Dias et. al., 2016), (Colin Cork et al., 2013) where semiconductor packaged dies are embedded within the fibres of yarn, commercially available thermistors can be integrated within the fibres of a yarn in order to craft an electronic temperature sensor yarn, named ETS yarn thereafter. A negative temperature coefficient (NTC) thermistor was soldered onto a fine copper wire consisting of eight strands of 34.60 ± 0.48 µm diameter copper wires (copper content more than 85% according to the wire supplier), which was then wrapped in either polyester or Zylon® fibres depending on the experiment to be conducted to provide mechanical strength to the fine copper wire interconnects. The microchip, interconnects and yarn fibres were then encapsulated to form a micro-pod using an UV curable polymer resin, Dymax 9-20801 (Dymax Corporation, Torrington, CT, United States). This micro-pod was then covered using packing fibres and a warp knitted tube to form the ETS yarn as shown in figure 3.1. The above construction ensured that the thermistor microchip and copper interconnects are maintained in the centre of ETS yarn, thus making them not visible on the ETS yarn surface. The polymer micro-pod safeguarded the microchip from mechanical and thermal stresses ETS yarn could be subjected to during fabric and garment manufacturing processes.

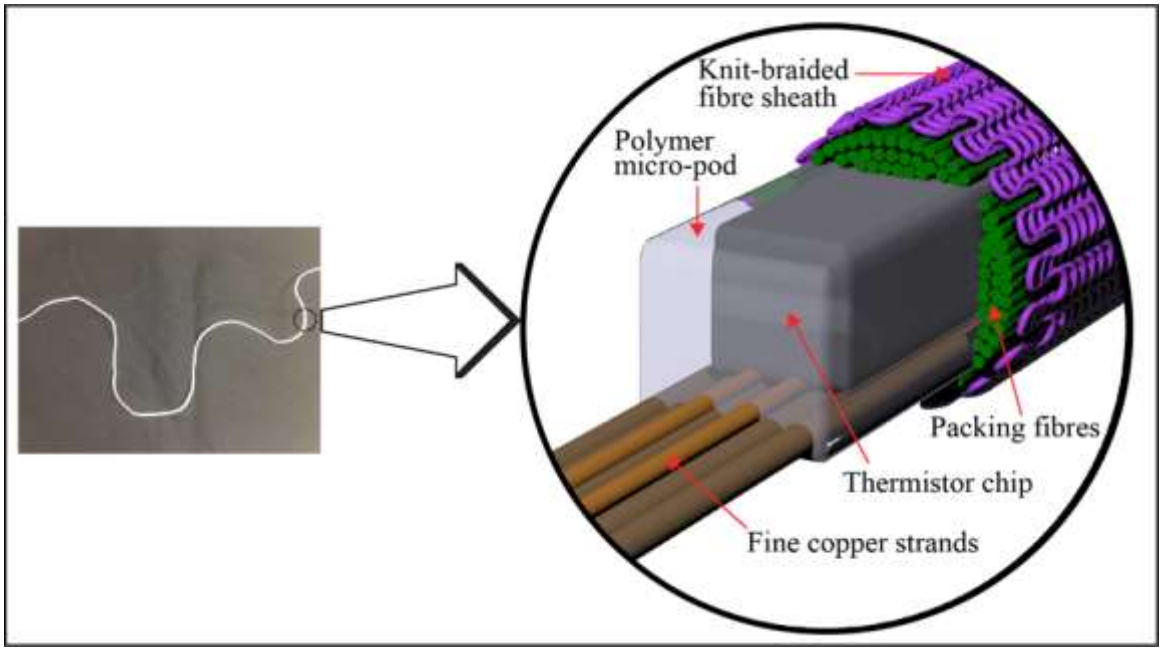

Figure 3-1: Photograph of electronic temperature sensing yarn (left) and a schematic of the cross section of the electronically active yarn (right)

3.3 Selection of temperature sensor

A surface mount device (SMD) thermistor was chosen for the application due to its miniature size and low cost. Even though they are non-linear they provide accuracy over a narrow range of temperature, and since the temperature variation in skin of a healthy human is approximately 31–37 °C (Liu et al., 2013) a thermistor is sufficient for the required application. The high sensitivity and high lead resistance of the thermistor enabled its resistance to be measured by using a two wire configuration and a simple voltage divider circuit.

The Murata 10 kΩ, 100 mW 0402 surface-mount device (SMD) Negative Temperature Coefficient (NTC) thermistor (NCP15XH103F03RC; Murata, Kyoto, Japan), with geometrical dimensions of 1.0 x 0.5 x 0.5 mm was chosen due to its miniature size. The electrical resistance (R_t) of the thermistor would respond to a change in temperature. The temperature in Kelvin (T) can be calculated using equation 3.1 provided by the manufacturer. According to the information provided by the manufacturer the thermistor has a 10 KΩ ± 1 % resistance (R_0) at 298.15 K (25 °C) (T_0) and a material constant B of 3380 ± 1 %.

$$B = \ln(\frac{R_t}{R_0})/(\frac{1}{T} - \frac{1}{T_0}) \qquad (3.1)$$

The manufacturer also provided the tolerance in resistances for different temperatures of the thermistor, given in table 3.1.

Table 3:1: Resistance tolerance of the thermistor provided by Murata

Temperature/°C	Rmin/Ω	Rtyp/Ω	Rmax/Ω	R.min. tol	R.max. tol
0	26.68	27.22	27.77	-2%	2%
10	17.64	17.93	18.21	-2%	2%
20	11.94	12.08	12.22	-1%	1%
30	8.22	8.31	8.41	-1%	1%
40	5.74	5.83	5.92	-2%	2%
50	4.08	4.16	4.24	-2%	2%
60	2.95	3.01	3.08	-2%	2%
70	2.17	2.23	2.28	-2%	3%

An important factor to be considered when using thermistors is that they are prone to self-heating errors and, therefore a small electrical current must be passed through the device when measuring the resistance of a thermistor. This results in dissipation of heat which would cause a small temperature increase, and this is called the self-heating error (BIPM, 2014). The self-heating effect on the thermosensitive part (semiconductor bead) can have a significant effect on the electrical resistance of the thermistor. However, this effect can be calculated using the following equation 3.2, given the self-heating coefficient, K_s (Nawrocki, 2005).

$$\Delta T = \frac{P}{K_S} = \frac{R_t I^2}{K_S} \quad (3.2)$$

Where ΔT is the increase in temperature, R_t is the resistance of the thermistor and I is the current flowing through the thermistor. According to the data sheets provided by Murata for their 10kΩ 100mW 0402 NTC Thermistor for a rated power of 100mW the thermistor's temperature could rise to 125 °C due to self-heating, at ambient temperature of 25 °C.

Murata provides a design software SimSurfing that enable end users to simulate the thermistor behaviour and the temperature errors that can occur when using 0402 NTC thermistors. A voltage divider circuit was used for the simulations to obtain the resistance of the thermistor (the reason to use the voltage divider circuit is discussed in detail in section 3.6.1.1). The simulation parameters were set as follows, the load resistance R1 was set to 10kΩ and the Voltage In (V_{in}) was set to 5V. The simulation results are given in figure 3.2; the error caused on the temperature measurement due to self-heating is given in figure 3.2d

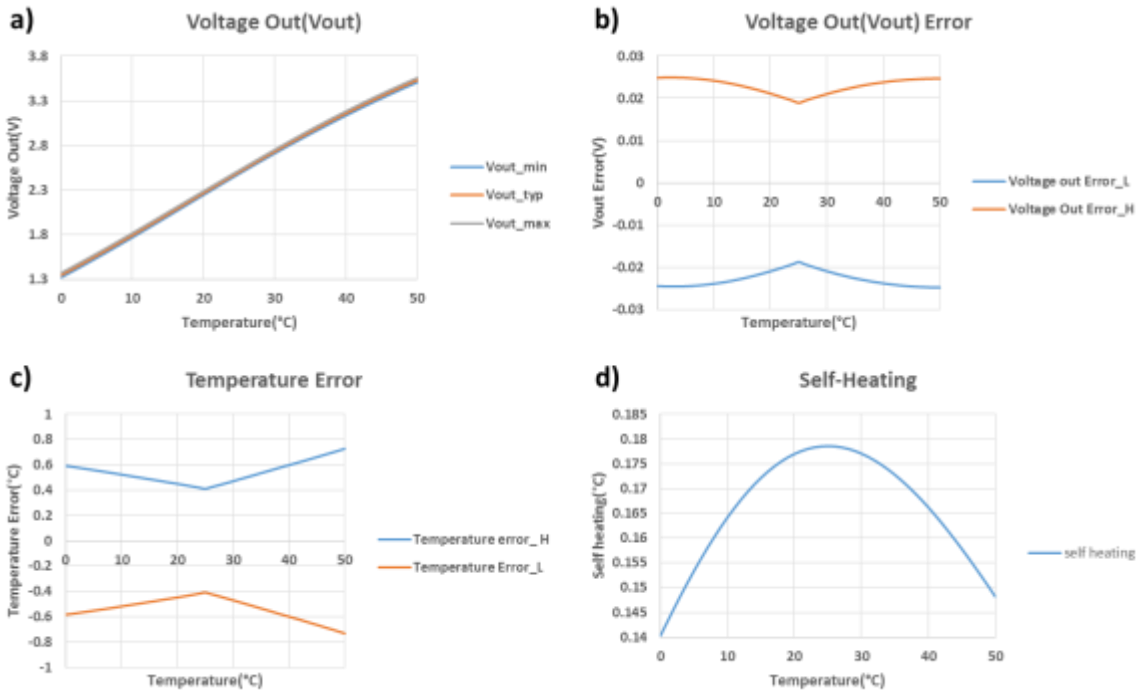

Figure 3-2: The SimSurfing simulation results where a) was the Voltage out (Vout) of the voltage divider circuit, b) was the Vout error, c) was the Temperature error caused due to the Vout error and the equation provided by the manufacturer and d) was the Self heating error.

As it can be seen from figure 3.2c when measuring a temperature in the range of 20 °C to 40 °C the maximum temperature error would be ±0.6 °C. This temperature range can be considered as acceptable because the wound bed temperature critical for normal cellular activity has been identified as 33 °C (V et al., 2015) (McGuiness et al., 2004), and literature suggests that the temperature of a wound when left uncovered could drop to temperatures in the range of 24 °C to 26 °C (M. Romanelli et al., 2002). The simulation also shows a maximum self-heating error of 0.18 °C for this temperature range (shown in figure 3.2d). These errors were considered acceptable as miniature SMD thermistors from other manufacturers have similar tolerances.

3.3.1 Testing the thermistor

Once the thermistor was chosen it was necessary to determine whether the selected thermistor can be used for accurate surface temperature measurements. For this purpose an ECHOTHERM™ IC50 digital, electronic chlling/heating dry bath (TORREY PINES SCIENTIFIC®, California, USA) (henceforth called the dry bath) was used (information about the dry bath is given in appendix 16). Six 0402 NTC thermistors were used for the experiment. The two solder pads of each of the thermistors were soldered onto two 50 cm long eight strand copper wires (16 Ωm^{-1} (data in appendix 3)) copper alloy, Red House Global, Colmworth, UK), each copper strand had a diameter of 34.60 ± 0.48 µm (data is given in Appendix 3) measured using an Olympus BX41 microscope (OLYMPUS, Tokyo, Japan). The thermistors were soldered onto the copper strands (the process of

soldering the copper strands onto the thermistor is discussed in-depth in section 3.5.1) and fixed on to the dry bath surface using insulating tape (RS Stock No.134-7319, RS, Corby, UK).

The resistance of the thermistor was measured by using a voltage divider circuit connected to a 12 bit NI DAQ USB 6008 (National Instruments™, Newbury, UK). A 10kΩ load resistance (R1) was used for the potential divider circuit and its resistance was measured to a precision of 0.01% using an Agilent 34410A 6 ½ Digital multi-meter (Agilent Technologies, California, USA). Software was written using the visual programing language from National Instruments LabVIEW to capture the voltage out (Vout) and calculate the resistance of the thermistor (Rt). The voltage divider circuit used and the LabVIEW program is discussed in detail in section 3.6 of this chapter.

The temperature of the dry bath was varied from 0 °C to 50 °C in steps of 1 °C and at each step the temperature was maintained for 5 minutes. The LabVIEW program recorded 159 resistance measurements a minute for each of the thermistors. The average resistance readings were calculated for each of the thermistors after it reached its steady state (average of the resistance measurements from 3-5 minutes after changing the temperature of the dry bath). Thereafter, using these averages the average resistance of all the thermistors were calculated and plotted in blue on figure 3.3. The average measurements of the samples were used to calculate the confidence intervals for 95% confidence and this was plotted as the error bars (Appendix 4 contains the Resistance vs Temperature graphs of the six thermistors).

Thereafter using the temperature indicated on the dry bath and by using equation 3.1 provided by the manufacturer the expected resistance values for the corresponding temperature values were calculated and plotted in orange in figure 3.3.

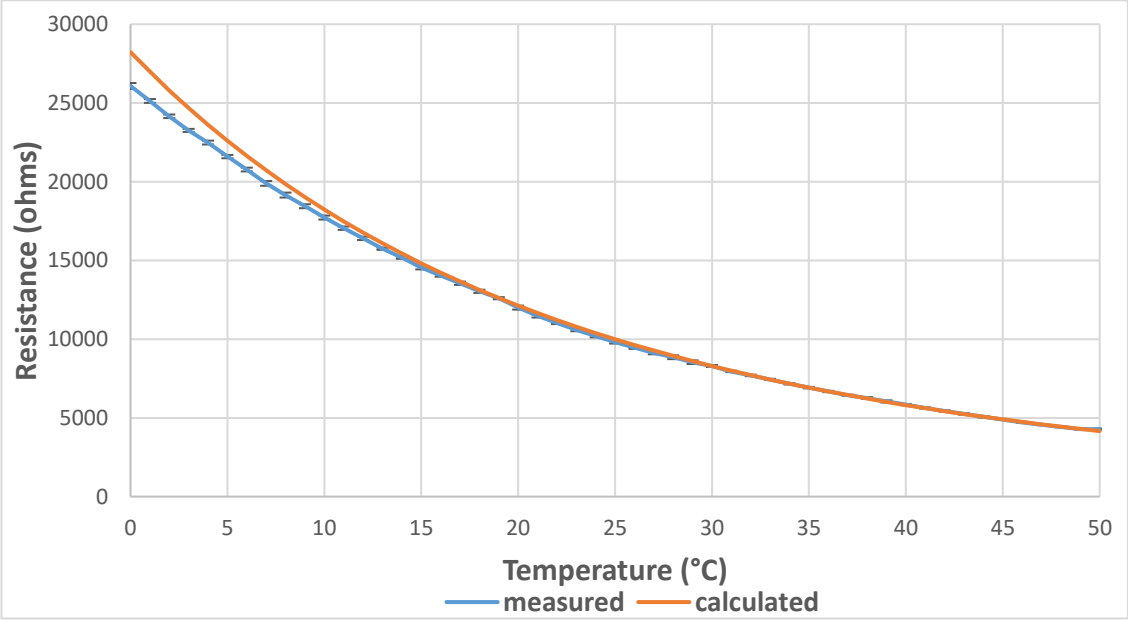

Figure 3-3: Comparing the average measured resistance values from the six thermistors against the calculated resistance values from the temperature indicated on the dry bath by using equation 3.1.

The results given in figure 3.3 suggest that the calculated resistance values are within the confidence intervals of the measured resistance values from 16 °C to 50 °C. A difference in resistance of 2147–273 Ω between the measured and the calculated thermistor resistance was observed within the temperature region of 0 °C to 15 °C. This may be due to the effects of ambient temperature on the temperature measurements or due to the inability of the dry bath surface to reach the set temperature at low temperatures. However this was not investigated further since in wound care, temperatures are not expected to go as low as 15 °C (V et al., 2015). The literature also demonstrates that the temperature of the wounds in chronic leg ulcers would range between 24 °C to 26 °C even when the wound is left uncovered (M. Romanelli et al., 2002).

3.4 Geometrical Model of the Electronic Temperature Sensing Yarn

It is important to understand the design rules for constructing ETS yarn. It is important to determine the minimum levels of solder paste required to form a robust solder joint between the strands of fine copper wires (the interconnects) and the solder pads of the thermistor and the minimum amount of polymer resin required to protect the microchip with a cylindrical micro-pod. Due to the manner in which its been created the ETS yarn is a composite yarn consisting of different components, i.e. packing fibres, polymer micro-pod formed to protect the thermistor and circular warp knitted fibre covering, and it is important to estimate the thickness and the volume fraction of each of these layers. Therefore, a geometrical model of ETS yarn structure was constructed to study how the different layers could influence the temperature measurement of the thermistor. This model was also used to estimate the effects on heat flow to the thermistor through the micro-pod and yarn fibres (this is given in Chapter 4 section 4.2.2).

The geometrical model of the yarn was constructed in MATLAB (Mathworks®, Massachusetts, USA) and MATLAB was also used to do the calculations stated in the equations 3.3-3.5. MATLAB is a multi-paradigm numerical computing environment. MATLAB's ability to implement algorithms, do mathematical calculations and create three dimensional images made it an ideal software for creating the geometrical model (MathWorks, 2018). The images obtained in MATLAB are given in figure 3.4. Appendix 5 contains the MATLAB program used for the calculations and images.

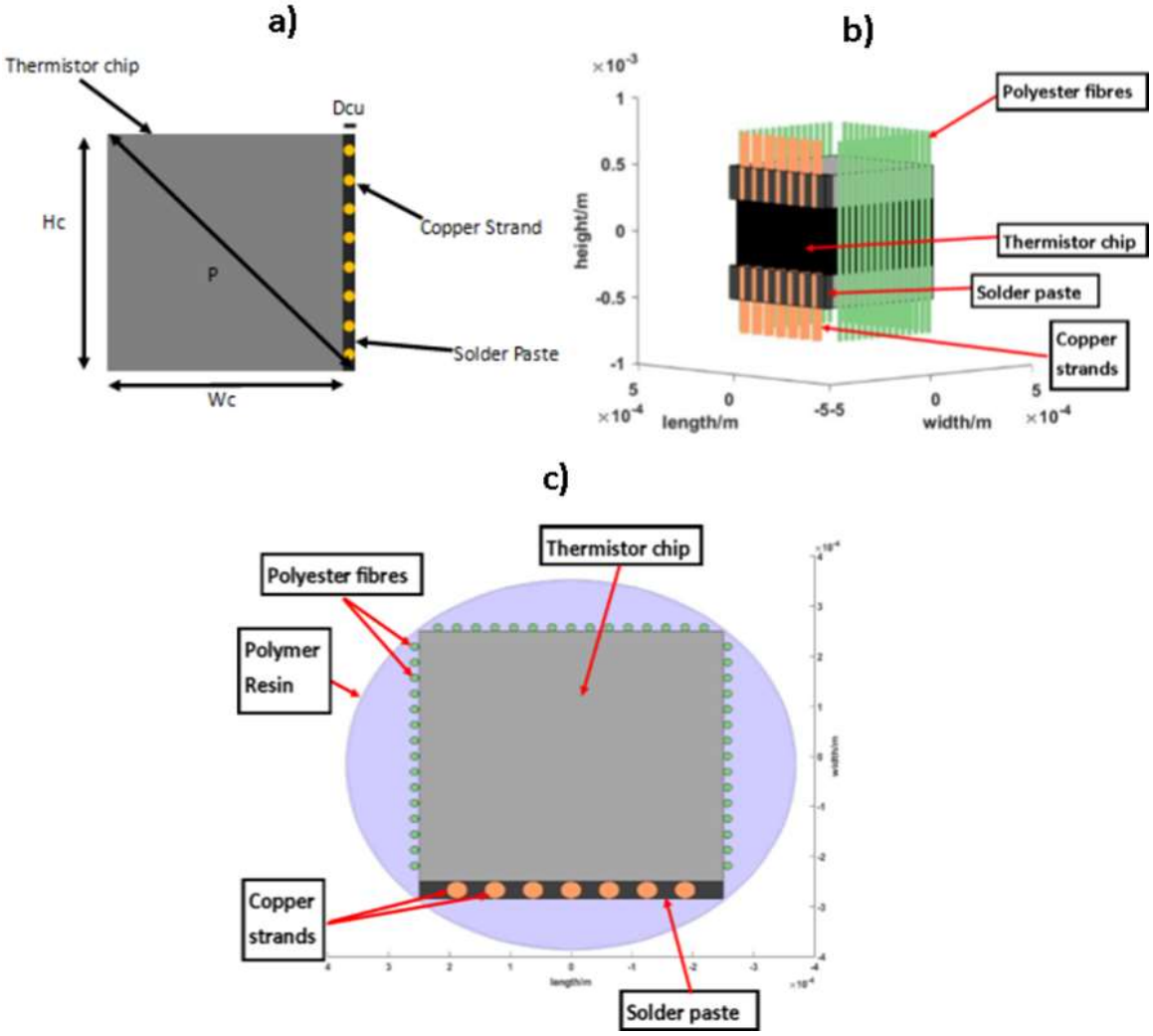

Figure 3-4: a) Simulation model of thermistor with soldered copper strands. b) 3D model of thermistor chip with soldered copper strands and polyester fibres surrounding the chip. c) Cross-sectional view of the micro-pod in the simulation.

In order to create the geometrical model initially the average diameter of a single strand of copper in the eight strand copper wire, which is used to create the interconnects, was measured to be 34.60 ± 0.48 µm using a Olympus BX41 microscope. The average diameter of a single polyester fibre in the 167 dtex/48 polyester yarn, which is used as the carrier fibres inside micro-pod, as packing fibres and also the circular warp knitted outer sheath, was measured to be 14.46 ± 0.62 µm (data is given in Appendix 6) using the Olympus BX41 microscope.

The amount of solder paste required for the soldering process was calculated by assuming:

- The solder paste formed an uniform layer on top of the solder pads of the chip as shown in figure 3.4 (a);
- The thickness of the solder paste is equal to the diameter of a copper filament;
- All copper filaments are in contact with the solder pad.

$$V_{solder} = V_t - V_{tcu} = (H_c * L_s * D_{cu}) - \left(\pi * \left({}^{D_{cu}}/_{2}\right)^2 * L_s * N_f\right) \qquad (3.3)$$

Where:

- R_{cu} and D_{cu} are the radius and diameter of the copper respectively;
- L_s is the Length of the solder pad;
- H_c is the height of the thermistor chip;
- V_{solder} is the total volume of solder paste;
- V_{tcu} is the volume of the copper strands in the solder joint;
- N_f is the number of strands of the copper wire;
- V_t is the total volume of solder paste and copper strands when combined.

After the soldering process the thermistor chip and the copper wire were wrapped around two 167 dTex/48 polyester yarns. This makes the polyester experience more force when a strain is applied to the yarn compared to the copper filaments. It was assumed for the calculation that the polyester fibres were aligned along three sides of the thermistor and the soldered copper strands were soldered onto the fourth side. However, in reality it is extremely difficult to align all the polyester filaments along the sides of the thermistor during the wrapping process.

Finally the thermistor has to be encapsulated, in order to protect it and the solder bonds from mechanical and thermal stresses and washing. This is achieved with a polymer micro-pod that is formed around the thermistor by using an UV curable conformable resin, and the amount of resin required to form the micro-pod was also calculated.

It was assumed that the resin used for the encapsulation process formed a perfect cylinder around the microchip making the micro-pod. A cylindrical shape was chosen, because the general shape of a yarn is cylindrical. It was also assumed that the minimum radius of the micro-pod will occur when the structure created by the microchip and solder paste is inscribed in the micro-pod. The diagonal length P (shown in figure 3.4a) represents the widest point. Hence the minimum radius of the cylindrical micro-pod (R) was calculated as 366 µm (diameter 732 µm) using the equation 3.4 given below.

$$R = \sqrt{\left((W_c + D_{cu})^2 + {H_c}^2\right)}/2 \qquad (3.4)$$

Where:

- W_c is the width of the thermistor chip;
- D_{cu} is the diameter of a copper strand;
- H_c is the height of the thermistor chip.

The minimum length of the cylinder was estimated as the length of the thermistor and the minimum diameter of the cylindrical micro-pod was calculated as 732 µm. By using this information the minimum volume of the micro-pod was calculated. To find the ideal volume of resin (V_r) needed for the encapsulation, the volumes of the chip, the solder paste, the polyester filaments and the copper filaments have to be deducted from the estimated minimum volume of the micro-pod. It was also assumed that the polyester fibres did not absorb the polymer resin and the wicking of polymer resin by polyester filament was neglected for the calculation of the volume of resin required to form the micro-pod. The ideal volume of resin required for the encapsulation is calculated in equation 3.5.

$$V_r = V_w - V_c - V_{ts} - V_{tp} = \pi L_c \left(\sqrt{\frac{((W_c + D_{cu})^2 + Hc^2)}{2}} \right)^2 - L_c W_c H_c - 2H_c L_s D_{cu} - \frac{\pi {D_p}^2 L_c N_y N_{pf}}{4} \quad (3.5)$$

Where:

- V_w is the whole volume of the encapsulation;
- V_c is the volume of the thermistor chip;
- V_{ts} is the volume occupied by the solder paste and copper strands;
- V_{tp} is the volume occupied by the polyester filaments that is in the yarn used for wrapping the copper strands;
- D_p is the diameter of a single polyester filament;
- N_y is the number of polyester yarns used;
- N_{pf} is the number of filaments in a single polyester yarn.

By using the equation 3.5 the minimum volume of resin was estimated at $4.21*10^{-10}$ m^3. In reality the volume of resin used will be more than the Ideal amount calculated due to the wicking of resin between polyester filaments. The higher the volume of resin used the better the mechanical strength of the encapsulation. However using larger volumes of polymer resin for the encapsulation increases the size of the micro-pod and increases the thickness of the ETS yarn.

The micro-pod is then protected and covered using polyester packing fibres and an outer sheath made of polyester yarn which is formed using a small diameter circular warp knitting machine from Rius-Comatex. The average thickness of the outer sheath (T_{os}) was measured at 0.24±0.01 mm using a micrometre screw gauge. However obtaining the thickness of the outer sheath accurately is extremely challenging due to compression in textile yarns. The outer sheath is made out of polyester fibres and air, and the volume fraction of a braided structure has been estimated to be 0.5 (Shishoo, 2008).

The diameter of the sensing yarn can be varied by changing the cylinder sizes of the circular warp knitting machine (RIUS MC braiding machine, RIUS, Spain). Increasing the cylinder size increases the

thickness of the ETS yarn but it makes the micro-pod more untraceable to the wearer. However a thicker yarn will be more visible in a garment. For this geometrical model a six needle cylinder was used to make the ETS yarn. The average diameter of the ETS yarn (D_{ETS}) was measured at 1.97±0.02 mm using the Olympus BX41 microscope.

The volume fraction V_{pf} of the packing yarn can be calculated from the following equation 3.6,

$$V_{pf} = \frac{\pi {R_p}^2 N_{pf} N_{py}}{\pi\left(\frac{D_{ETS}-2T_{os}}{2}\right)^2 - \pi R^2)} \qquad (3.6)$$

Where:

- N_{py} is the number of polyester yarn used as packing yarn;
- N_{pf} is the number of polyester filaments in a single yarn;
- R_p is the radius of each polyester filament;
- R is the radius of the micro-pod.

The results of the geometrical model are summarised in table 3.2 below.

Table 3:2: Estimated values from the geometrical model.

Parameter	***Value***
Minimum volume of solder paste	$2.44 * 10^{-12}\ m^3$
Minimum micro-pod diameter	732 μm
Minimum micro-pod volume	$4.21 * 10^{-10}\ m^3$
Minimum Resin Volume	$1.46 * 10^{-10}\ m^3$

3.5 Fabrication of the Electronic Temperature Sensing yarn

The initial step of the project was to understand the existing knowledge within the Advanced Textiles Research Group on how to embed semiconductor microchips in yarn. The Murata 0402 NTC thermistor is a two terminal analogue semiconductor device. As such preliminary experiments were carried out with LEDs of similar dimensions. LED's (Part Number: KPHHS-1005SURCK, Kingbright 630 nm Red LED, SMD package, dimensions 1000µm x 500µm x 500µm) were soldered with eight strand fine copper wires and encapsulated with additional polyester yarns using an UV curable acrylic conformable resin, Dymax 9001-E-V-3.5. Then the core yarn, consisting of copper wire interconnects, micro-pods with LEDs and polyester yarn was covered using a knit braided fibre sheath and packing fibres to produce the final electronically active yarn (see Figure 3.5).

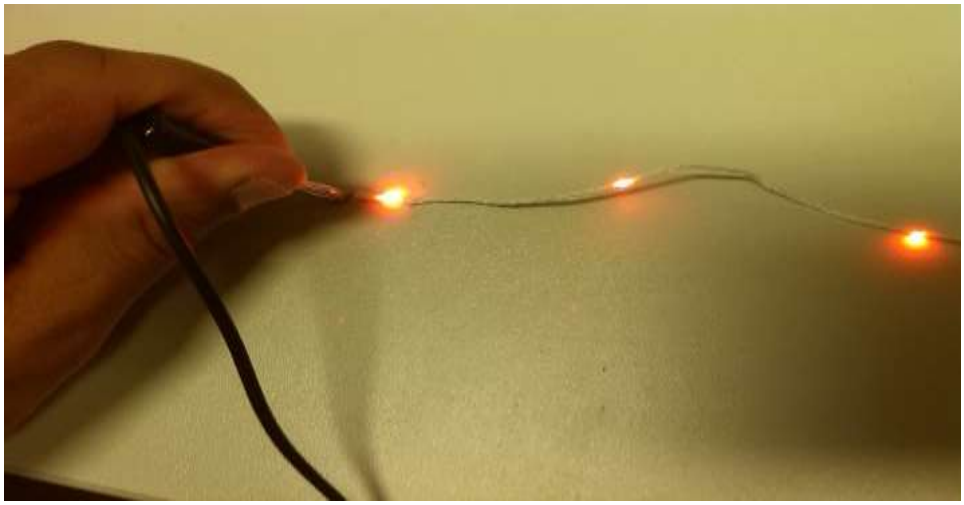

Figure 3-5: LED Embedded yarn

As the next step NTC thermistors of dimensions 1000 µm x 500 µm x 500 µm were used instead of the LEDs to make the ETS yarn. The process of making the ETS yarn can be broken down into the following three stages:

- Stage 1 – Interconnect formation – fine copper wires are soldered onto the solder pads of semiconductor package dies (in this case surface mount thermistors), shown in Fig. 3.6a;
- Stage 2 – Encapsulation – the thermistor chip and solder joints are encapsulated to form a polymer micro-pod, shown in Fig. 3.6b;
- Stage 3 – Covering – a fibre sheath is formed around the interconnects and micro-pods to conceal them, protect from mechanical damage and provide additional strength to the fibre, shown in Fig. 3.6c.

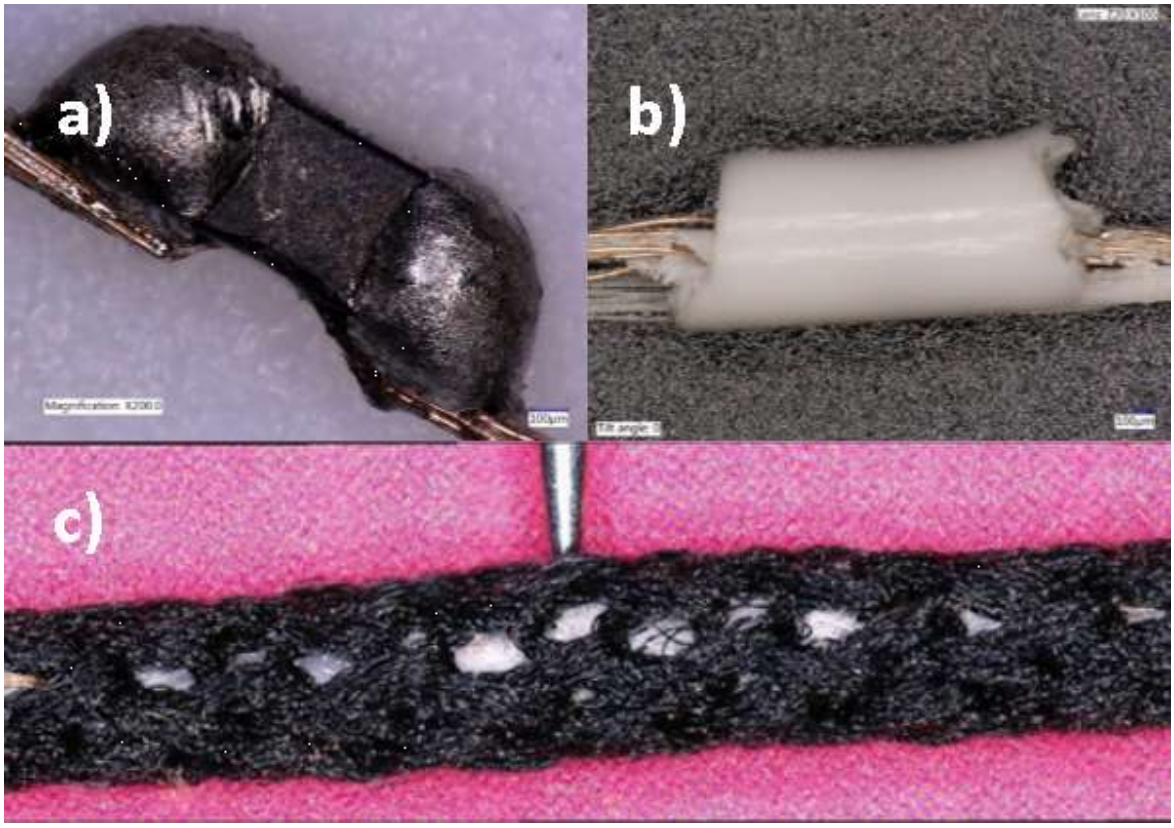

Figure 3-6: The three stages of the yarn fabrication process captured using a VHX Digital microscope (Keyence,Milton Keynes,UK): Interconnect formation (a), Micro-pod (b) and covering (the position of the chip is pointed using a needle)(c).

An in-depth exploration of each of the above stages are presented below.

3.5.1 Stage 1 - Interconnect formation

The creation of a robust and efficient bond between the solder pads of the microchip and copper wires (in this case an eight-strand copper wire) to form the interconnects is one of the key stages in the fabrication of ETS yarns. The interconnect formation was achieved using two crucial steps, the soldering step and short circuit removal step. The two steps are illustrated in figure 3.7.

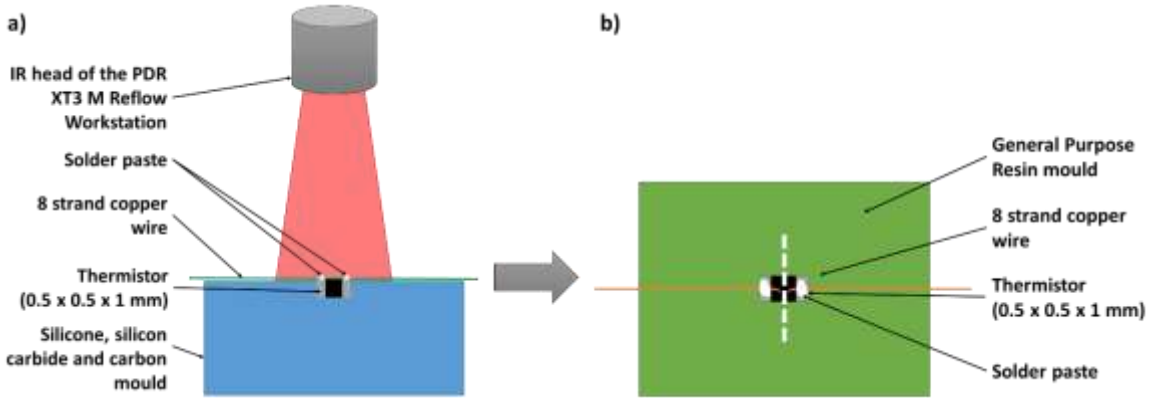

Figure 3-7: Annotated Schematic of the Interconnect formation stage where (a) The side view of the soldering step where the eight-strand copper wire is soldered on to the thermistor using the IR Reflow Work station (IR-XT3M, PDR Ltd., West Sussex, UK), and (b) shows the top view of the short circuit removal step where the short circuit was removed using a sharp blade (white dotted line demonstrates the cutting of the eight-strand copper wire using a sharp blade). The schematic is not drawn to scale.

3.5.1.1 The soldering step

The research at Advance Textiles Research Group (ATRG) has demonstrated that a metal solder bond provides mechanically strong and electrically efficient connection between fine copper wires and the solder pads of packaged dice (Rathnayake, 2015). To accommodate such small connections, a focused IR Reflow Workstation (IR-XT3M, PDR Ltd., West Sussex, UK) was used to form interconnects. To hold the microchip and eight -strand copper wire securely during the soldering process, a miniature mould was constructed using a mixture of silicone, silicon carbide and carbon (SiO, SIC, C). These materials were chosen due to their thermally conductive properties and the ease of moulding. The micro-mould was constructed by gluing a thermistor chip onto a Perspex slide before forming a thin wall of clay around the thermistor microchip. Clay was used because it does not stick on to the silicone used in the mould. Equal volumes of silicone and silicon carbide powder were mixed with 10% platinum catalyst. After stirring the mixture carefully for three minutes, the solution was left in a vacuum chamber for five minutes to prevent air bubble formation in the mould. The mixture was then poured inside the clay walls and left to harden (see figure 3.10).

The thermistor was positioned inside the micro-mould and the copper strands were laid unbroken across the solder pads. A Nordson EFD dispenser (Ultimus™ I, Nordson EFD, RI, USA) was used to dispense the solder paste accurately onto the solder pads of the thermistor. A pressure of 43.5 Psi was used for 0.1s to dispense the SolderPlus Dispensing Paste (PN: 7024454, Sn96.5/Ag3.0/Cu0.5, Nordson EFD, RI, USA) through a precision stainless steel dispensing tip of inner diameter 0.13 mm (PN:7018314, Outer diameter- 0.5 mm, Nordson EFD, RI, USA). The volume of solder paste dispensed was measured at $1.22*10^{-11}$ m^3. This was five times more than the estimated value in table 3.2 in section 3.4. The additional volume could be as a result of the solder flux; and also since in the geometrical model it is assumed that all the copper strands are touching the solder pads, however, in reality it is extremely difficult to align all the strands onto the surface of the solder pads, therefore more solder paste has to be dispensed in order to form a good connection.

Thereafter the IR reflow work station from PDR was used to solder the copper strands onto the solder pad. The Reflow soldering conditions recommended by the chip manufacturer, Murata is given in Figure 3.8.

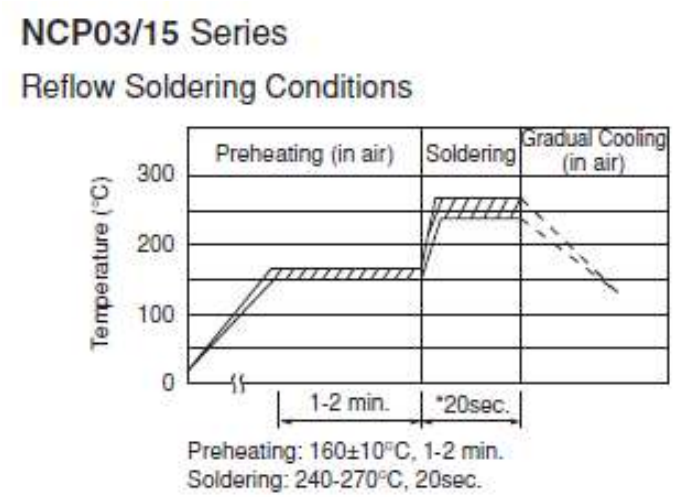

Figure 3-8: Recommended reflow conditions [shown in appendix 2]

Since the thermistors are not soldered onto a PCB board but instead onto a wire the time interval for preheating was reduced from 1-2 minutes to 34 seconds. The profile used in the PDR machine when soldering the thermistor chip onto the copper strands is given in figure 3.9.

Figure 3-9: Reflow Workstation Profile

3.5.1.2 The short circuit removal step

After completion of the soldering the short circuit created by the length of copper wires remaining between the two solder pads was removed using a sharp blade. Since the blade could damage the silicon carbide mould during cutting, a second micro-mould was constructed using General Purpose

Resin (GPR), which is a polyester resin in styrene solution ($C_6H_5CH=CH_2$, CAS No.-100-42-5, Stynolite, UK). GPR was chosen from several candidate materials, primarily because of its hardness.

It should be noted that the second micro-mould could not be used to hold the chip during the soldering process due to the low thermal stability of the GPR. The GPR mould was constructed by gluing the miniature thermistor chip onto the surface of a silicone sheet. Since superglue does not adhere well to silicone, unhardened silicone mixed with 10 % platinum catalyst was used as a glue to stick the thermistor chip on to the silicone sheet. Thereafter, the silicone was hardened using a hot air gun (HL 1810 S, STEINEL, UK). As with the silicone and silicon carbide mixture, the solution of GPR mixed with 2 % methyl ethyl ketone peroxide as a catalyst, was left in a vacuum chamber for five minutes and then poured inside the silicone walls to create the GPR mould.

Two cymbal yarn tensioners were welded on either side of an aluminium rod to hold and control the copper wire during the soldering process. The two moulds were positioned between the two tensioners. To ensure that the copper wire is in contact with the thermistor when it is positioned in the mould, the two moulds were fixed on to the aluminium rod at equal height. The copper wire was positioned in the tensioners. Figure 3.10 shows the set up used for the interconnection formation stage.

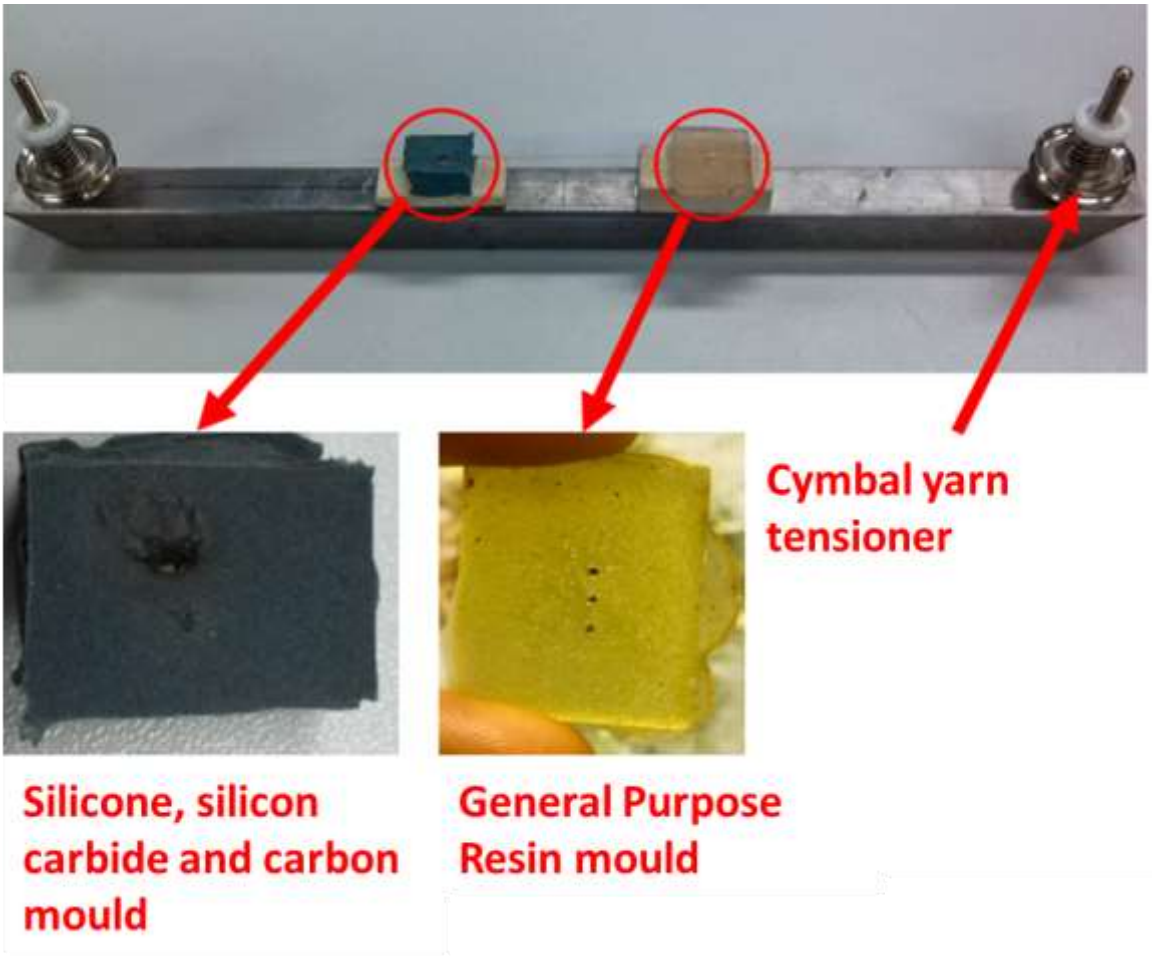

Figure 3-10: Soldering Jig developed for the interconnect formation stage

3.5.2 Stage 2- Micro-pod creation

The thermistor and the solder bonds have to be encapsulated with a polymer micro-pod to protect against mechanical, thermal and chemical stresses to which the electronic yarn would be subjected during fabric production, garment manufacturing and later during its use. The micro-pod would also protect the thermistor during washing, spinning and drying. As such the creation of the micro-pod is an important step of the creation of ETS yarn. In order to enhance the mechanical strength of the interconnects, the copper wire with soldered thermistor was wrapped around two 167 dtex/48 polyester yarns. The wrapping ensured that any strain force would influence the polyester yarn and not the copper filaments.

Thereafter the thermistor was encapsulated with a thermally conductive resin. Two types of encapsulation material were tested (Multi-Cure® 9-20801 and 9001-E-V-3.5, from Dymax Corporation, Torrington, CT, USA). The resins were dispensed by using an EFD Nordson dispenser (Ultimus™ I, Nordson EFD, RI, USA), and cured with an UV spot curing system (BlueWave™ 50, Dymax Corporation, Torrington, CT, USA), thus forming the micro-pod.

In order to control the volume and shape of the micro-pod; the thermistor, interconnects and the two polyester yarns were placed inside a hollow PTFE tube of length 5.1 cm with a 0.87 mm internal diameter. A cylindrical shape was chosen for the micro-pod as textile yarns are generally of cylindrical shape. An internal diameter of 0.87 mm was chosen because it was the closest diameter available in the market to the ideal diameter of 0.732 mm (estimated in section 3.4). The PTFE tube was held in place using two cymbal yarn tensioners. A hole was created on the PTFE Teflon tube using a sewing needle in order to inject polymer resin. To prevent the resin covering and filling the hole on the PTFE tube, the soldered thermistor was placed about 2 mm to the right of the hole. The precision tip (inner diameter- 0.20 mm, Outer diameter- 0.42 mm, PN:7018417, Nordson EFD, RI, USA) that dispenses resin was held at an angle 38.4 ° to the horizontal. The figure 3.11 shows the encapsulation jig that was developed for the encapsulation process.

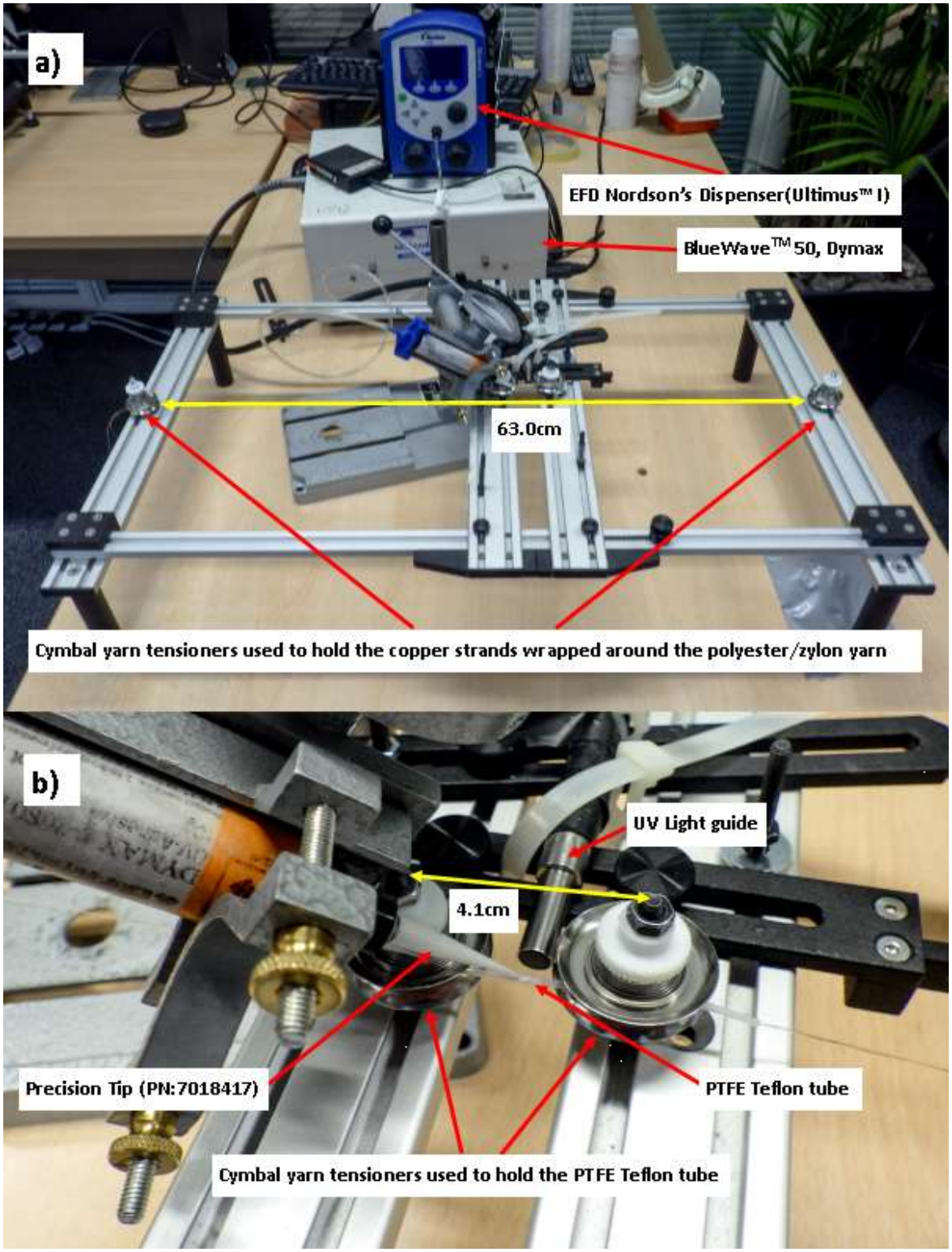

Figure 3-11: Encapsulation jig; where a) is the image of the entire encapsulation jig and b) is close up view of where the encapsulation was done.

Thereafter the resin was dispensed using a pressure of 60.5 Psi over a time of 0.6 s. The volume of multi-cure 9-20801 resin dispensed was measured at 1.504 +/- 0.10 $*10^{-9}$ m^3. This was 4.7 times greater than the estimated volume of resin for a 0.87 mm diameter of cylindrical encapsulation that can be calculated using equation 3.5 in the geometrical model section. This is because in order to ensure that the thermistor and interconnects are covered and protected by the polymer resin the

length of the PTFE tube filled with resin should be more than the length of the chip. The length of the micro-pod was measured at 2.17+/-0.07 mm using the VHX Digital Microscope (Keyence, Milton Keynes, UK). Figure 3.12 presents the images captured by the VHX Digital Microscope of the thermistor soldered onto the copper filaments and the micro-pod. This gives an indication of the length of the micro-pod with regard to the thermistor.

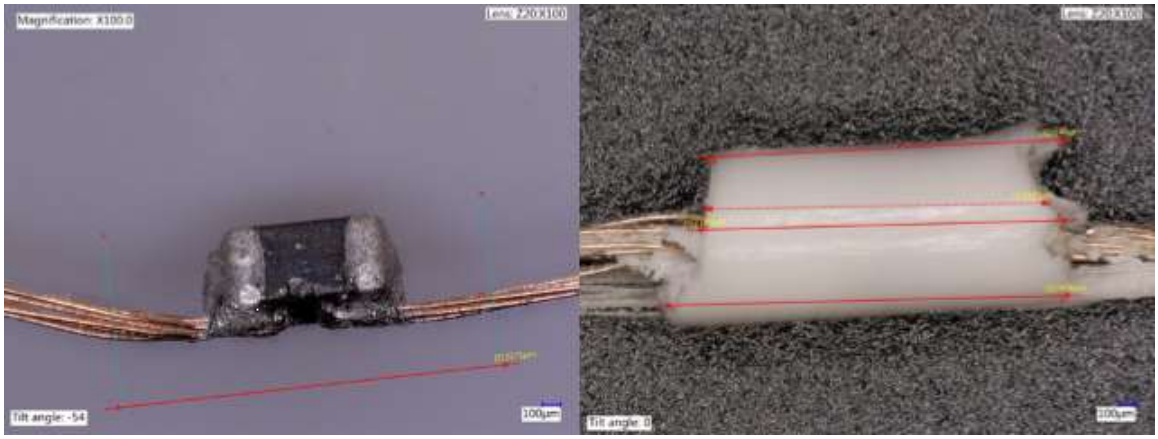

Figure 3-12: Length of the micro-pod

Once the U.V. curing was completed the core yarn was pulled out of the PTFE tube. To ensure that the copper filaments and interconnects were not damaged the pulling force was applied to the polyester filaments.

3.5.3 Stage 3- Covering

The final stage of creating an electronic yarn (E-yarn) is to surround the micro-pod and interconnects with packing fibres and a knit braided fibre sheath, in order to protect the interconnects being damaged due to mechanical stresses and to form an even yarn, i. e. without thick places. This was achieved with a small diameter circular warp knitting machine from RIUS, MC-2. The machine consists of a 10.0 mm diameter hollow needle cylinder with six latch needles, with an inner diameter of 2.0 mm. The latch needles were threaded with six 167dtex/48 polyester yarns. The carrier yarn (the core of the E-yarn) consists of micro-pods, copper interconnects and two polyester yarns was passed through the 2.0 mm bore of the needle cylinder with six additional 167dtex/48 polyester filament yarns (288 packing fibres), in order to create a tight packing of carrier yarn in the resultant ETS yarn. This technique ensures that the electronic circuitry and interconnects are hidden within the resultant yarn, and also allows all types of textile fibres, i.e. natural and synthetic fibres, to be used in-order to form the fibre sheath. The diameter of the resultant ETS yarn was measured around 1.97±0.02 mm using the Olympus BX41 microscope (shown in appendix 7) and it is defined by the dimensions of the microchip.

3.6 Hardware and Software Development for the electronic temperature sensing yarn

3.6.1 Interfacing Hardware

There are several methods to measure temperature from a thermistor.

Voltage divider circuit- The simplest way to measure a resistance is using a voltage divider circuit, also known as an electrical serial circuit. A voltage divider contains two resistors in series, with a voltage tap in between the two resistors (shown in figure 3.13). By using Kirchoff's voltage law and Ohm's law equations 3.7 (given below) can be obtained, which can then be used to calculate the resistance of the thermistor (Rt) (Recktenwald, 2013).

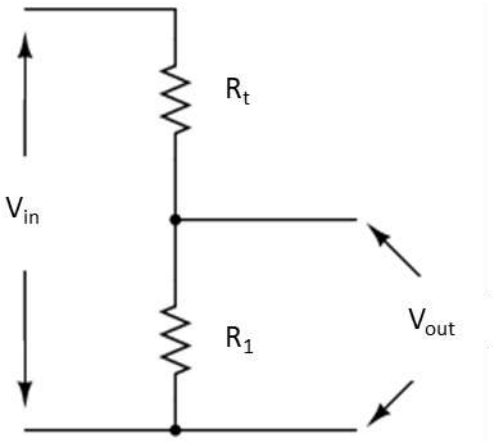

Figure 3-13:Potential divider circuit

$$R_t = \left(\frac{V_{in}}{V_{out}} - 1\right) R_1 \qquad (3.7)$$

Where Vin is the input voltage coming into the potential divider circuit, Vout is the voltage out and R1 is the constant load resistance.

Wheatstone bridge circuit- When a thermistor is connected to a Wheatstone bridge circuit as shown in figure 3.14 it provides a thermometer with high accuracy and zero indication on the initial point of the scale. However a Wheatstone bridge has a narrower measuring range (Nawrocki, 2005).

If the Wheatstone bridge is balanced then

$$\frac{R_1}{R_2} = \frac{R_3}{R_t} \qquad (3.8)$$

For measuring the temperature the out of balance voltage is measured and the resistance of the thermistor, Rt is determined by using the equation 3.9 below (AMETHERM, 2013).

$$V_{out} = V_{in}\left(\frac{R_2}{R_2+R_3} - \frac{R_t}{R_1+R_t}\right) \qquad (3.9)$$

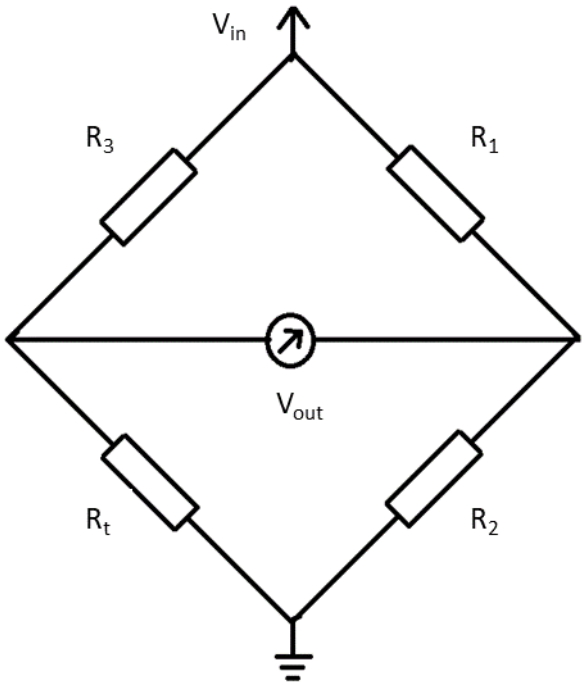

Figure 3-14: Wheatstone bridge circuit

The Wheatstone bridge has an advantage over the voltage divider circuit if the change in voltage is very small when compared to the offset voltage. Generally this can be difficult to observe when using a voltage divider circuit without using amplification. In the Wheatstone bridge circuit there is no offset at nominal offset (in practice there is a very small one) hence the saturation problem is greatly reduced or eliminated. Another disadvantage of using a voltage divider is that the initial accuracy without calibration is very limited. Since the output of the voltage divider circuit is a function of the actual values of the resistors it is important to obtain the actual values of resistors. In Wheatstone bridge circuits it depends on matching the resistances rather than absolute precision (Schweber, 2016).

Two-wire and four-wire resistant measurement-

Resistance measurements can be made using a two-wire or a four-wire configuration. It is often made using the two wire method (shown in figure 3.15a), where a test current is sent through the leads and the resistor being measured. Then the same set of leads is used to measure the voltage across the resistor, this is used to calculate the resistance. The main problem when using the two wire method to obtain the resistance occurs when obtaining small resistance measurements (resistances equal to or less than 1 kΩ). The resistance of the leads are added to the measurement, which for small resistance measurements would bring about a significant change in the measured resistance when compared the actual resistance (Janesch, 2013).

Since the two-wire method has its limitations when measuring small resistances a four-wire configuration shown in figure 3.15b is generally used for low resistance measurements. The four

wire configuration uses two sets of leads to obtain the resistance measurement. The current is sent through one set of leads and the voltage is measured through another set of leads. Even though there might be a small current that flows through the leads where the voltage is being measured this is generally regarded as negligible. This ensures that the voltage measured by the volt meter is approximately equal to the voltage across the resistor. Thereafter the resistance is calculated using the measured voltage and the current sent (Kiethley, 2012).

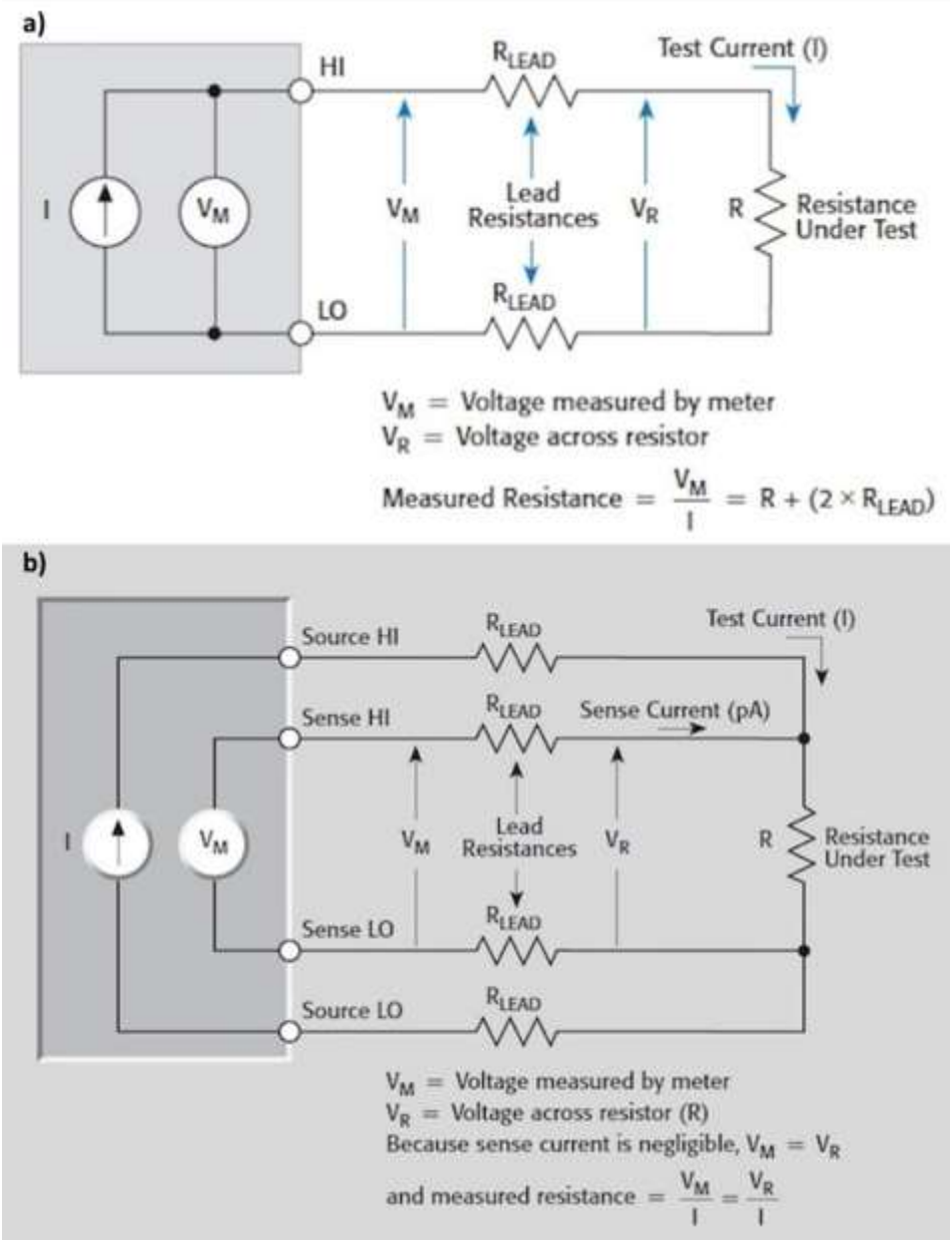

Figure 3-15: Resistance measurement using a) a two-wire configuration, b) a four-wire configuration (Janesch, 2013)

3.6.1.1 Voltage divider circuit

A Voltage divider circuit (electrical serial circuit) shown in figure 3.13, was chosen as the hardware interphase for the thermistor. This was chosen mainly due to the simplicity of the circuit and fewer number of components, which would prove easier to integrate with a textile. Also the thermistor chosen has a very high resistance of 10 kΩ at 25 °C and the resistance of the copper wire (lead

resistance) was measured at 15.95+/-0.33 Ω/m (data is given in Appendix 3). Therefore it can be seen that the wire resistance only brings about a minute change (of about 0.16 % if a meter of the copper wire is used as the lead) in the resistance of the thermistor. Hence it can be argued that a two-wire measurement is sufficient for obtaining the temperature off the thermistor. Another advantage of using a thermistor is its large temperature coefficient of about (-2 % to -6 %) therefore there is a large change in resistance when the temperature changes. Hence the change in voltage is large enough to be easily measured using a voltage divider circuit, and a Wheatstone bridge circuit is not required to obtain the measurements (Anonymous, 1995) (Kimball et al., 1993).

The thermistor resistance value was captured using the equation (3.7) given above. A 5 V was used as voltage in (Vin) for the potential divider circuit and a 10 kΩ resistor was used as R1. A 10 kΩ resistor was chosen as the load resistor due to the thermistor resistance at 25 °C being 10 kΩ. This ensured that the voltage was shared equally among the two resistors. The chosen voltage in (Vin) and resistance (R1) would bring about a maximum temperature rise of only 0.2 °C due to self-heating on the thermistor (as shown in figure 3.2d above). This was deemed expectable for this study since in pathologies like diabetic foot ulcer detections temperatures vary by about 4 °F (2.2 ^{o}C) (Armstrong et al., 2007).

Once the thermistor resistance (Rt) was calculated, it was substituted in equation 3.1 given in the manufacturer's data sheet to determine the temperature of the thermistor. The hardware setup shown in figure 3.16 was used to connect the voltage divider circuit to the computer.

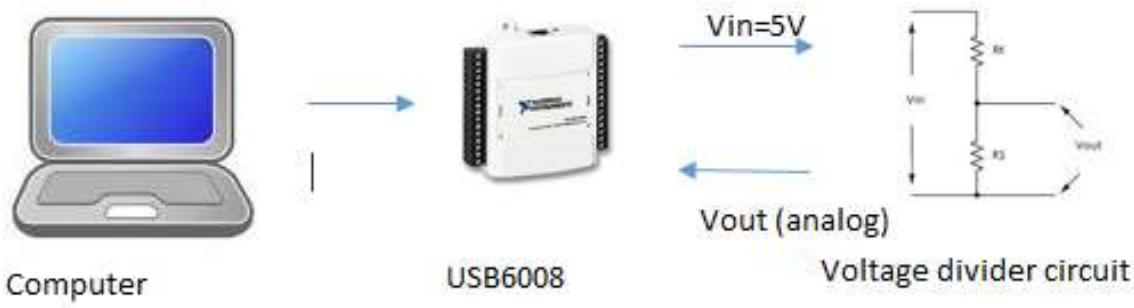

Figure 3-16: Hardware setup

A multifunctional NI-DAQ USB 6008 unit from National Instruments was used to provide the analogue voltage V_{in} for the voltage divider circuit and the corresponding analogue Voltage (V_{out}) was measured using the analogue input of the NI-DAQ.

3.6.2 Software

LabVIEW (Laboratory Virtual Instrument Engineering Workbench) was chosen as the software for this project. It was selected because of its ability to easily create professional user Interfaces and

also it could be used to automate any instrument using free instrument drivers (National Instruments, 2013). LabVIEW is a system-design platform and development environment for a visual programing language from National Instruments. It is commonly used for data acquisition, instrument control and industrial automation on a variety of platforms which include Microsoft windows ("LabVIEW," 2016).

Programs in LabVIEW are called virtual Instruments (VIs) because their operations and appearance imitate physical instruments. A VI contains three components: Front panel which is a user interface for the VI, it contains controls(input) and indicators(output); Block diagram (shown in Appendix 11 figure 8.17) which is the source code for the functionality of the program, block diagram objects include terminals, SubVIs, Express VI, functions (SubVIs, Express Vis and functions are explained in the paragraph below), constants, structures and wires that transfer data among other block diagram objects; Icon and connector pain, which identifies the interface to the VI so that the VI can itself be used in another VI (National Instruments, n.d.).

SubVIs- corresponds to a subroutine in text-based programming languages. Once you build a VI it can be used in another VI. The VI can be called in the block diagram of another VI and then its known as a SubVI (National Instruments, n.d.). Express VIs- are nodes that require minimal wiring because you configure them with dialog boxes. Express VIs give users a VI or a library of VIs for making their own applications and it is commonly used to perform measurement tasks (National Instruments, n.d.). Functions- are elementary nodes in the G programming language. They are analogous to operators or library functions in conventional languages (National Instruments, 1998).

3.6.2.1 Key steps to consider when making the program

The key steps required to capture the temperature off the thermistor and present it to the user, were identify and how the LabVIEW software was used to program them are listed below

3.6.2.1.1 Provide Voltage in (Vin) to the Potential divider circuit

The first step was to provide an input voltage (Vin) to power the potential divider circuit. This was done using a DAQ Assistant Express Vi in LabVIEW. This Express Vi can be used to create, edit and run tasks using the NI-DAQ USB 6008. Therefore this was used to generate an analogue voltage signal (Vin) from the Analogue output (AO0) of the USB 6008 unit.

3.6.2.1.2 Obtain Voltage (Vout) of the potential divider circuit

To acquire the voltage signal (Vout) from the voltage divider circuit, the DAQ Assistant Express Vi was set up to acquire analogue voltage signal from the analogue input (AI0) of the NI DAQ USB-6008.

3.6.2.1.3 Calculating the Temperature

Since the values of Vin, Vout and the resistance (R1) are known the thermistor resistance (Rt) can be calculated using the equation 3.7. The formula Express VI in LabVIEW was used to apply equations in the block diagram. Thereafter the temperature was calculated using equation 3.1 given above. This equation provides the temperature in Kelvin so to obtain the temperature in degrees Centigrade 273.15 had to be deducted from the temperature reading obtained.

3.6.2.1.4 Graphical User Interphase

The graphical user interphase has to be user friendly and provide all the information to the user. The user should be able to set the input Voltage (Vin) and the resistance (R1) of the potential divider circuit. Therefore two controls were placed on the front panel of the screen for this purpose. It is important to display the temperature captured from the ETS yarn in a graphical manner therefore the temperature reading was shown using a thermometer. It was also important to see how the temperature reading varies with time. Therefore a waveform graph was used to show this. Since this software will be used when running experiments on the ETS yarn it was considered essential that the user gets to see the voltage out (Vout) and the thermistor resistance (Rt). Therefore two indicators were placed in the front panel to give the Rt and Vout values. The graphical user interface is given below in figure 3.17.

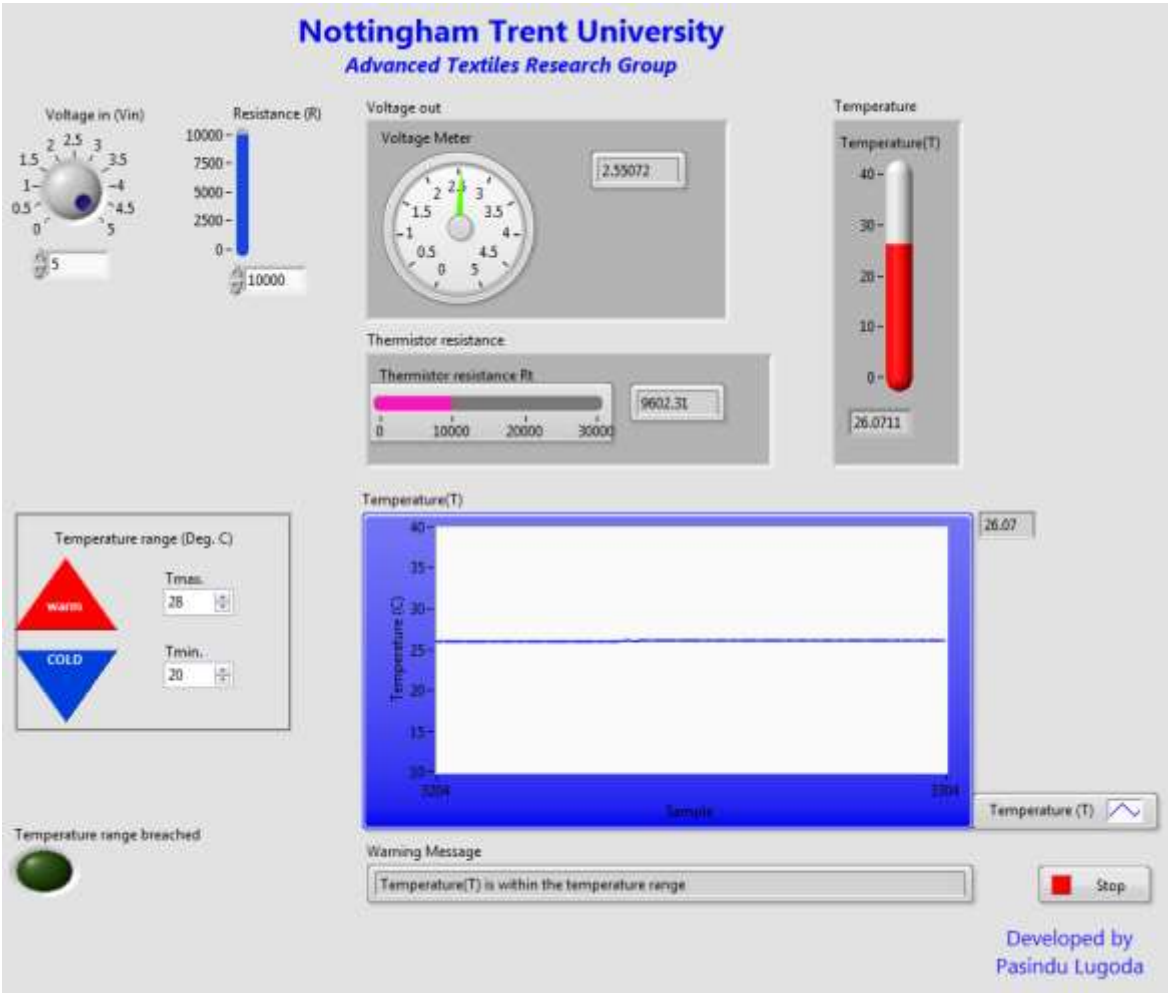

Figure 3-17: User interface for temperature measurement from the ETS yarn

3.6.2.1.5 Store data

It is important to store the temperature recorded by the thermistor yarn in order to analyse the data later on. Therefore by using the Open/Create/Replace File Function in LabVIEW an excel (.xlxs) file was created. The file dialog Express VI was used to give the user the opportunity to select a location and a name for the new file. Thereafter by using write to text file function the temperature reading, temperature range, if the temperature range has been breached, voltage out (Vout) and the thermistor resistance (Rt) were recorded on the excel file (showed in table 3.3).

Table 3:3: Excel sheet that records data from the application

	A	B	C	D	E	F	G
1	Voltage in(Vin)	Tmax.	Tmin.	Temperature range breached	temperature(T)	Voltage out(Vout)	Thermistor Resistance (Rt)
2	5	28	20	TRUE	28.079	2.645	8905.778
3	5	28	20	TRUE	28.165	2.649	8877.405
4	5	28	20	TRUE	28.295	2.655	8834.643
5	5	28	20	TRUE	28.301	2.655	8832.474
6	5	28	20	TRUE	28.418	2.66	8794.234
7	5	28	20	TRUE	28.504	2.664	8766.195
8	5	28	20	TRUE	28.519	2.665	8761.171
9	5	28	20	TRUE	28.519	2.665	8761.171
10	5	28	20	TRUE	28.55	2.667	8751.131
11	5	28	20	TRUE	28.601	2.669	8734.66
12	5	28	20	TRUE	28.689	2.673	8706.085
13	5	28	20	TRUE	28.729	2.675	8693.254
14	5	28	20	TRUE	28.738	2.675	8690.406
15	5	28	20	TRUE	28.738	2.675	8690.406
16	5	28	20	TRUE	28.74	2.675	8689.693
17	5	28	20	TRUE	28.74	2.675	8689.693
18	5	28	20	TRUE	28.74	2.675	8689.693
19	5	28	20	TRUE	28.74	2.675	8689.693
20	5	28	20	TRUE	28.74	2.675	8689.693
21	5	28	20	TRUE	28.744	2.675	8688.269
22	5	28	20	TRUE	28.742	2.675	8688.981
23	5	28	20	TRUE	28.747	2.676	8687.558
24	5	28	20	TRUE	28.742	2.675	8688.981
25	5	28	20	TRUE	28.76	2.676	8683.287
26	5	28	20	TRUE	28.747	2.676	8687.558
27	5	28	20	TRUE	28.764	2.676	8681.864
28	5	28	20	TRUE	28.775	2.677	8678.308
29	5	28	20	TRUE	28.769	2.677	8680.441
30	5	28	20	TRUE	28.782	2.677	8676.174
31	5	28	20	TRUE	28.802	2.678	8669.777
32	5	28	20	TRUE	28.815	2.679	8665.515
33	5	28	20	TRUE	28.809	2.678	8667.646

3.6.2.1.6 Additional feature

When used in experiments or in other applications (such as detecting inflammation in wounds), it would be important to see if the temperature measured goes above or below a temperature range pre-set by the user. Therefore the software also enables one to define temperature limits (Tmax. & Tmin.). If the temperature reading (T) goes above or below the temperature limit a warning signal would appear and an indicator would light up informing the user that the measured temperature (T) does not lie within the set range. The figure 3.18 below shows an image of the user interface once the temperature has breached the temperature limits set by the user.

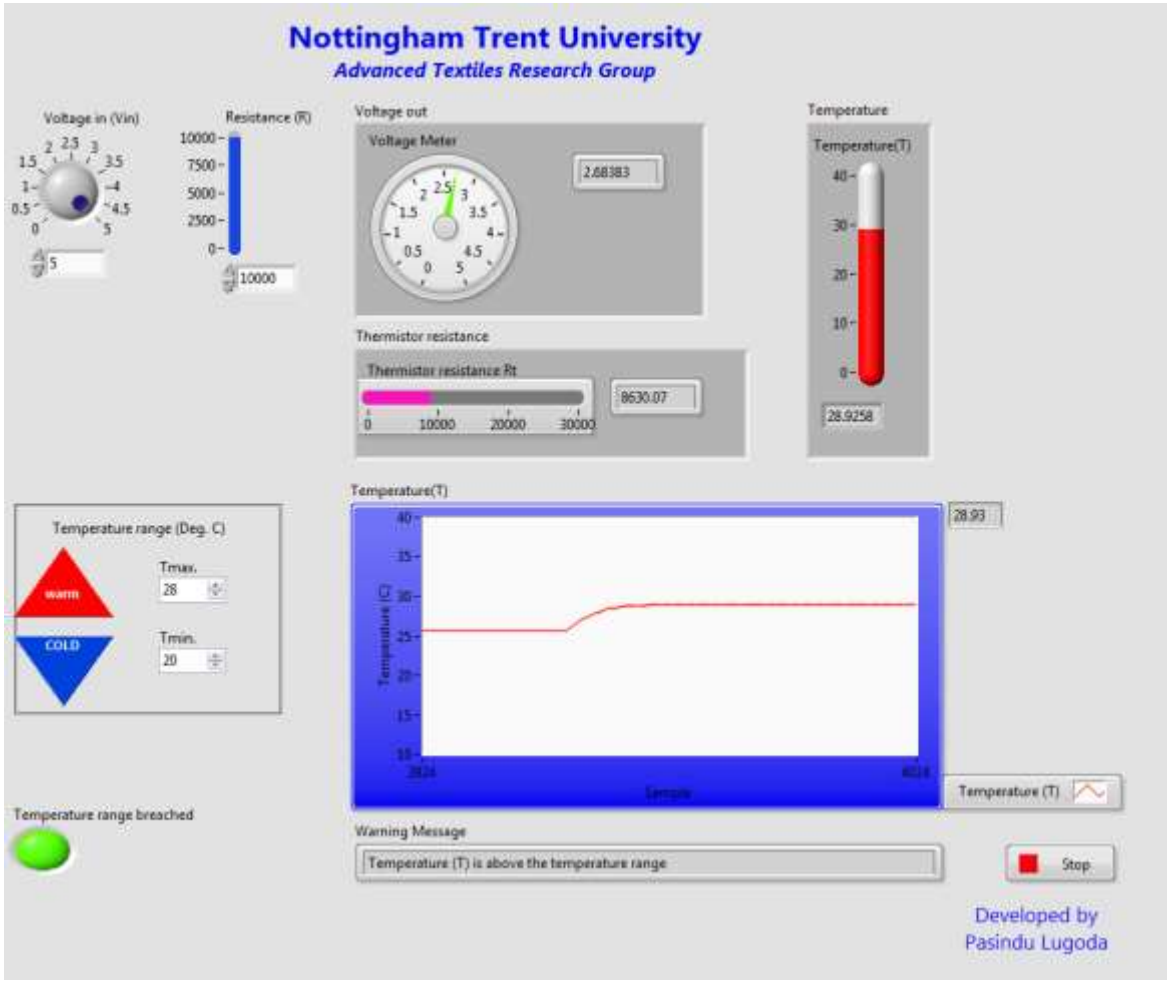

Figure 3-18: User interface with the temperature rising above the maximum limit set (The green indicator on the bottom left is lit up and there is a warning message displaying the "temperature (T) is above the temperature range" right below the graph)

3.6.2.2 Flow Chart of the Program

A detailed flowchart of how the software runs is given below. The main VI was created by calling three SubVI's. A VoltageIN SubVI was used to generate a Vin to the potential divider circuit. Capture temperature SubVI was used to capture the Voltage out (Vout) from the potential divider circuit and convert it to temperature. The check range SubVi was used to check if the temperature measured fell within or out of the temperature range set by the user.

3.6.2.2.1 Flowchart of the Main VI

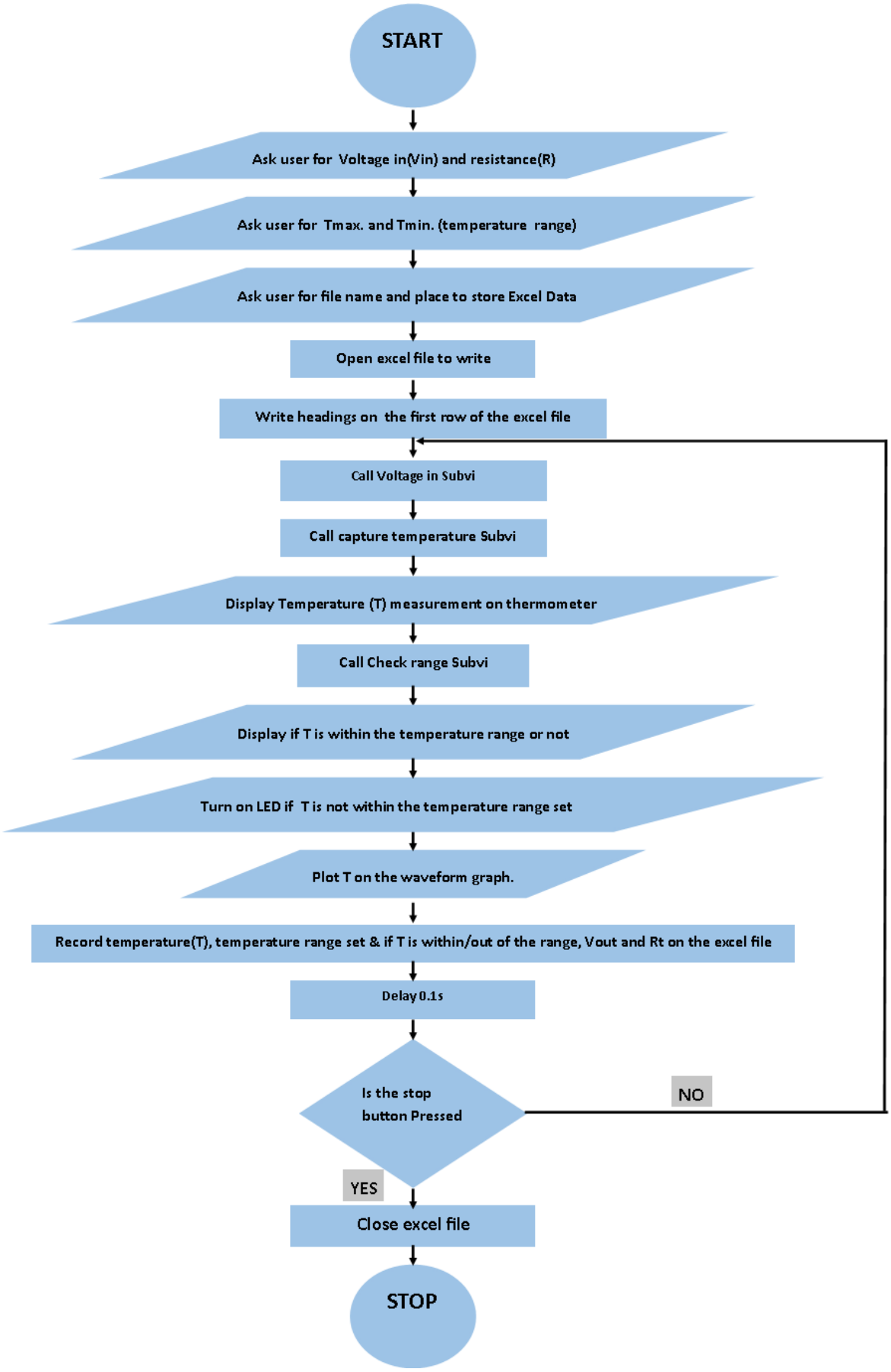

3.6.2.2.2 Flowchart of Voltage In SubVI

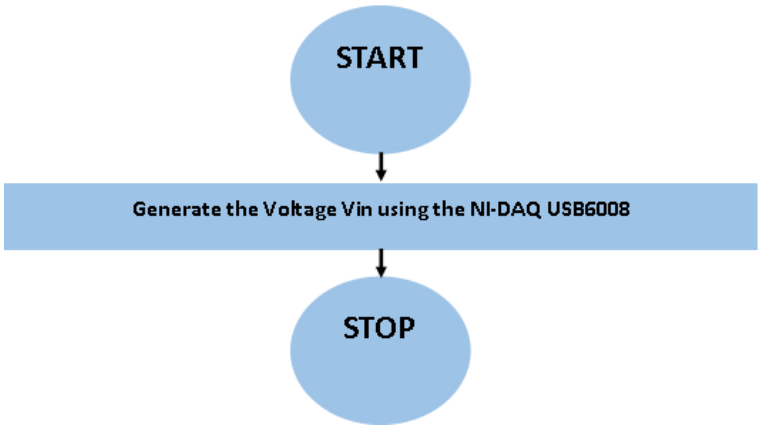

3.6.2.2.3 Flowchart of Capture Temperature SubVI

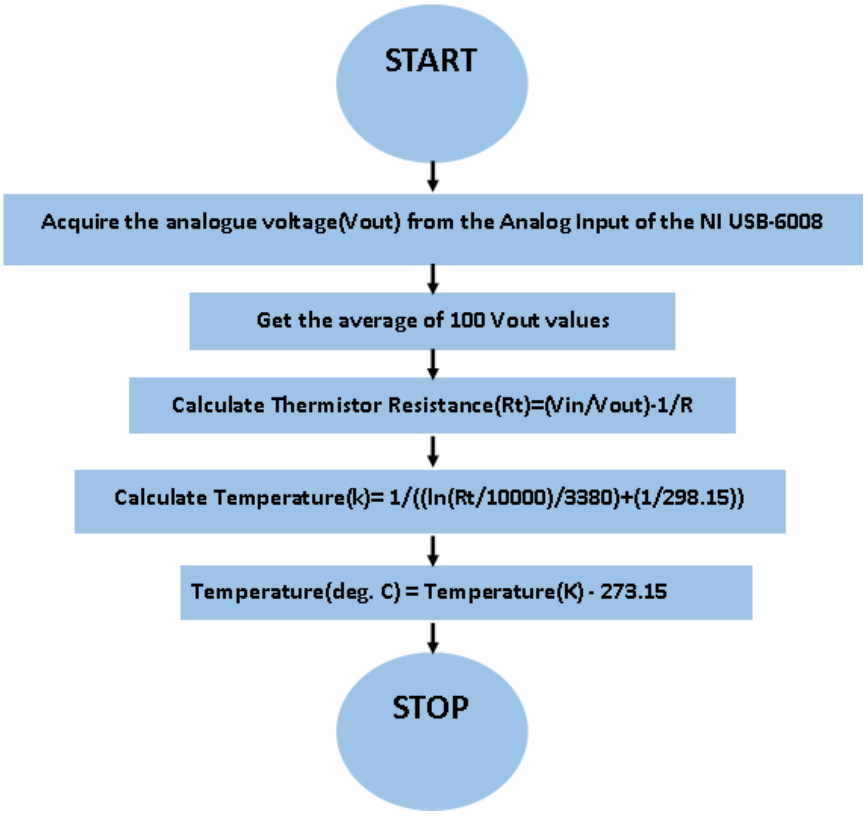

3.6.2.2.4 Flowchart of Check Range SubVI

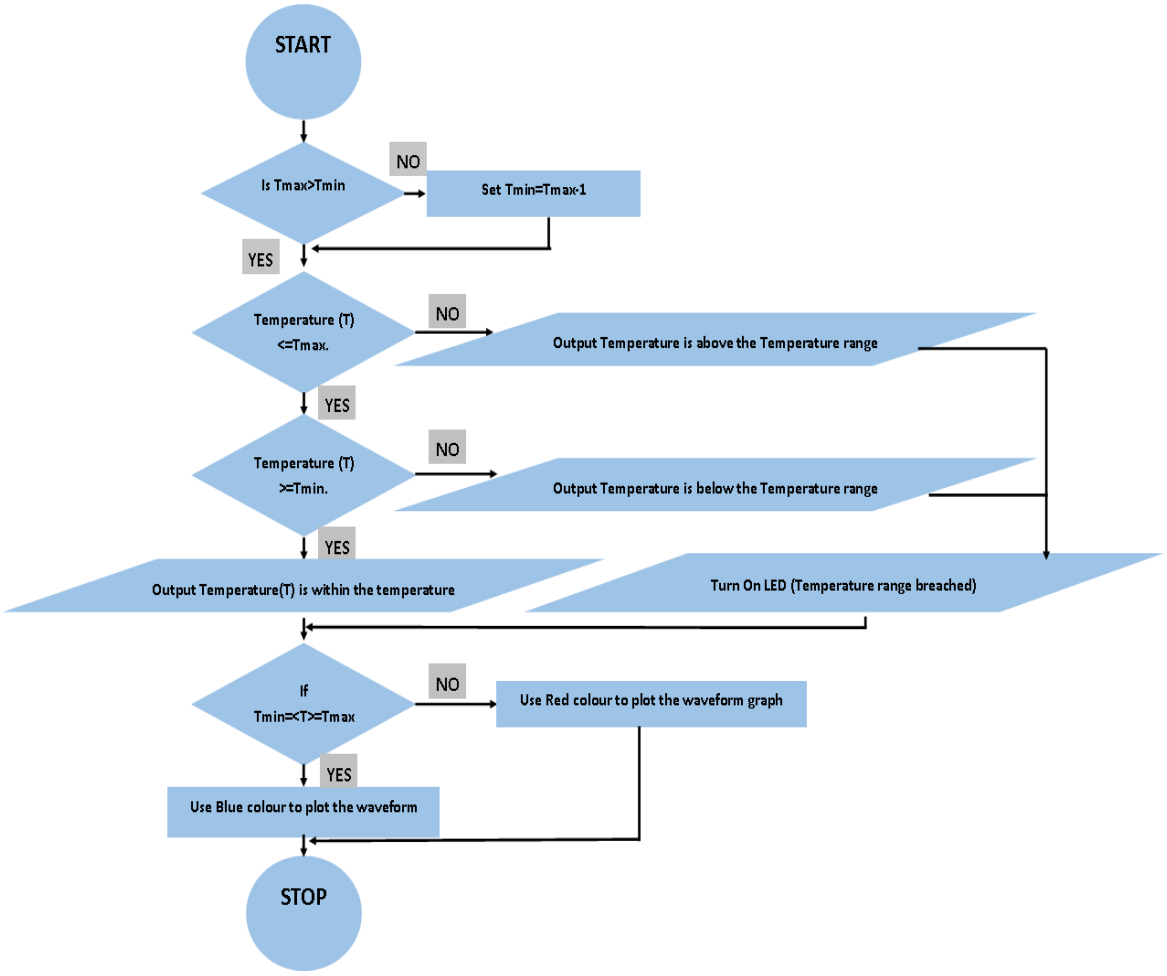

3.7 Summary

This chapter looked at the construction of the ETS yarn. The initial test done on the chosen thermistor proved that it could be used for surface temperature measurement. Thereafter the geometrical model of the ETS yarn constructed in MATLAB and it was first used to estimate the minimum volume of solder paste required for forming the interconnects as $2.44 * 10^{-12}\ m^3$. Then the micro-pod was modelled in a cylindrical shape and the minimum volume of polymer resin required for this encapsulation was estimated as $1.46 * 10^{-10}\ m^3$. The model also looked at the layers covering the micro-pod (knit braided sheath and the packing fibre layer). It also provided an equation to calculate the volume fraction of the packing fibres. This model was also used to estimate the parameters in the COMSOL model in Chapter 4 section 4.2.2.

During the construction of the ETS yarn it was proven that it was impossible to create an encapsulation with a 0.732 mm diameter and a more realistic diameter would be 0.87 mm. It also showed that the volume of solder paste required for the solder joint would be five times greater than the estimated value. It was decided that a simple voltage divider circuit would be used as the hardware for the ETS yarn. LabVIEW was chosen as the programing language to capture and present

the temperature off an ETS yarn. A complete breakdown of the LabVIEW program was also presented in this chapter.

The next stage was to test the ETS yarn, to see how the micro-pod and the yarn filaments effect the thermistor's measurements, this is described in chapter 4.

3.8 References

- AMETHERM, 2013. NTC Thermistors - Temperature Measurement With A Wheatstone Bridge | Ametherm [WWW Document]. URL http://www.ametherm.com/thermistor/ntc-thermistors-temperature-measurement-with-wheatstone-bridge (accessed 2.11.16).
- Anonymous, 1995. Thermocouples, RTDs, and thermistors. Mach. Des. 67, 74.
- Armstrong, D.G., Holtz-Neiderer, K., Wendel, C., Mohler, M.J., Kimbriel, H.R., Lavery, L.A., 2007. Skin Temperature Monitoring Reduces the Risk for Diabetic Foot Ulceration in High-risk Patients. Am. J. Med. 120, 1042–1046. doi: 10.1016/j.amjmed.2007.06.028.
- BIPM, (Bureau International des Poids et Mesures), 2014. Guide on secondary thermometry Thermistor Thermometry. Consultative Committee for Thermometry under the auspices of the International Committee for Weights and Measures. URL https://www.bipm.org/utils/common/pdf/ITS-90/Guide-SecTh-Thermistor-Thermometry.pdf. (accessed 2.11.15).
- Cork, C., Dias, T., Acti, T., Ratnayake, A., Mbise, E., Anastasopoulos, I., Piper, A., 2013. The next generation of electronic textiles. Presented at the Digital Technologies for the Textile Industries, Manchester, UK.
- Dias, T.K., RATHNAYAKE, A., 2016. Electronically functional yarns. WO2016038342 A1.
- Dini, V., Salvo, P., Janowska, A., Di Francesco, F., Barbini, A., Romanelli, M., 2015. Correlation Between Wound Temperature Obtained With an Infrared Camera and Clinical Wound Bed Score in Venous Leg Ulcers. Wounds Compend. Clin. Res. Pract. 27, 274–278. PMID: 26479211.
- Janesch, J., 2013. Two-Wire vs. Four-Wire Resistance Measurements: Which Configuration Makes Sense for Your Application? Keithley Instruments. Inc.
- Kiethley, 2012. Overview of Two-Wire and Four-Wire (Kelvin) Resistance Measurements (No. 3176). Keithley Instruments. Inc, USA.
- Kimball, B.R., Decristofano, B., Caldarella, G., 1993. Thermistor calibration procedure for simulated skin sensors (No. NATICK/TR-93/024). U.S. Army Natick Research, development and engineering center.
- LabVIEW, 2016. . Wikipedia Free Encycl. URL https://en.wikipedia.org/wiki/LabVIEW (accessed 2.3.14).

- Liu, Y., Wang, L., Liu, J., Di, Y., 2013. A study of human skin and surface temperatures in stable and unstable thermal environments. J. Therm. Biol. 38, 440–448. doi: 10.1016/j.jtherbio.2013.06.006.
- MathWorks, 2018. MATLAB Documentation - MathWorks United Kingdom [WWW Document]. URL https://uk.mathworks.com/help/matlab/?requestedDomain=true (accessed 2.5.18).
- McGuiness, W., Vella, E., Harrison, D., 2004. Influence of dressing changes on wound temperature. J. Wound Care 13, 383–385. doi: 10.12968/jowc.2004.13.9.26702.
- M. Romanelli, G. Gaggio, M. Coluccia, F. Rizzello, A. Piaggesi, 2002. Technological Advances in Wound Bed Measurements. Wounds 14.
- National Instruments, 2013. Top 10 Reasons to Use NI LabVIEW for Automating Test and Validation Systems - National Instruments [WWW Document]. URL http://www.ni.com/white-paper/8995/en/ (accessed 6.21.16).
- National Instruments, 1998. Function and VI Reference Manual.
- National Instruments, n.d. LabVIEW Environment Basics - National Instruments [WWW Document]. URL http://www.ni.com/getting-started/labview-basics/environment (accessed 6.21.16).
- Nawrocki, W., 2005. Measurement Systems and Sensors. Artech House, Norwood, MA, USA.
- Rathnayake, A., 2015. Development of the core technology for the creation of electronically active, smart yarn (PhD thesis). Nottingham Trent University.
- Recktenwald, G., 2013. Voltage Dividers and Potentiometers. URL https://cdn.sparkfun.com/assets/resources/4/4/pot_voltage_divider.pdf (accessed 6.3.14).
- Schweber, B., 2016. The Wheatstone Bridge: Still the Preferred Sensor-Interface Topology After 180 Years | Electronics360 [WWW Document]. Electron. 360. URL http://electronics360.globalspec.com/article/6522/the-wheatstone-bridge-still-the-preferred-sensor-interface-topology-after-180-years (accessed 1.22.18).
- Shishoo, R., 2008. Textile Advances in the Automotive Industry. Elsevier.

4. Performance Analysis of the Yarn

4.1 Introduction

This chapter demonstrates the performance of electronic temperature sensing yarn and the effects of the yarn filaments and micro-pod on the embedded thermistor's performance. The chapter has been broken down into the following sections:

- The theoretical and practical effects on the response and recover time of the thermistor as a result of the micro-pod and yarn filaments;
- The effects of the yarn filaments and micro-pod on the accuracy of the thermistor;
- Calibration of the electronic temperature sensing yarn;
- Effects of tensile stress on the electronic temperature sensing yarn.

4.2 Response Time and Recovery Time

The Response Time and Recovery Time are important parameters for temperature sensors (Yang et al., 2015). Since the thermistor chip in the ETS yarn is not in direct contact with the surface being measured, the heat must be transferred through the polymer resin and the polyester/zylon fibres. Therefore it is important to study the effects of the polymer resin and the yarn filaments on the response and recovery times of the sensor.

The response and recovery times of a thermistor can be analysed by studying its thermal time constant which gives a measure of the system's rate of response to an input. It is defined as the time taken for the system to reach $(1 - \frac{1}{e})$ or 63.2% of its final value (Ressler et al., 2003) .

4.2.1 Samples used for the simulations and experimentation

Initial set of experiments were carried out on thermistors soldered onto the eight strand copper wire (shown in figure 4.1a), this has not been simulated (in section 4.2.2) since the thermistor cannot be incorporated into the software COMSOL Multiphysics®. The thermal time constant is influenced by the mounting configuration and the environment the thermistor is exposed to (EPCOS, 2011). To understand the effects of the volume and thermal conductivity of the micro-pod, the thermistor and interconnects were encapsulated with different volumes of thermally conductive Multi-Cure® 9-20801 resin (data sheet in appendix 8). This was achieved by varying the diameter of the cylindrical micro-pod to 0.87 mm (shown in figure 4.1b), 1.53 mm and 5.00 mm. Given the difficulty in manufacturing a micro-pod with a 0.732 mm diameter (this optimum diameter calculated in chapter 3 section 3.4) this was investigated by simulation.

The cylindrical diameters of the micro-pods were varied by using hollow PTFE tubes having different internal diameters of 0.87 mm, 1.53 mm and 5.0 mm (the process of making micro-pods is described in chapter 3 section 3.5.2). It is important to keep the diameter of the micro-pod as small

as possible since increasing the micro-pod size increases the size of the resulting ETS yarn and this would affect the aesthetics as well as the size of a textile fabric/garment made using this yarn. It is advisable to keep the size of the ETS yarn below 2 mm. Two sizes of PTFE tubes were available containing internal diameters of 0.87 mm and 1.53 mm which was within the desired range (0.732 mm – 2.00 mm). A third diameter of 5.00 mm was also tested for research purposes. However the cross-sectional area for a 5.00 mm micro-pod was 46.6 times (shown in table 4.1) the ideal cross-sectional area estimated for the 0.732 mm diameter (shown in table 4.1).

Table 4:1: Cross-sectional area of the different sizes (0.87 mm, 1.53 mm, 5.0 mm) of micro-pod compared to the ideal cross-sectional area for the 0.732 mm diameter

Diameter of micro-pod (mm)	*Cross-sectional area of the micro-pod compared to a micro-pod constructed with the ideal diameter of 0.732 mm*
0.87±0.006	*1.4*
1.53±0.008	*4.4*
5.0±0.1	*46.6*

In order to understand the effects of the thermal conductivity of the resin, a thermally non-conductive Multi-Cure® 9001-E-V-3.5 resin (data sheet in appendix 9) was used to form the cylindrical micro-pods with different diameters (0.87 mm, 1.53 mm and 5.0 mm).

The copper strands were wrapped around two 167Dtex/48 polyester yarn to provide mechanical strength to the fine copper wire. Therefore the polymer micro-pod consists of polyester filaments (shown in figure 4.1c). Hence to understand the effects of the polyester (PE) yarns in the micro-pod, the thermistors and interconnects were twisted with two 167dtex/48 filaments PE yarns and encapsulated using Multi-Cure® 9-20801 resin to form a cylindrical micro-pod with a 0.87mm diameter; this is defined as core fibre. Thereafter for the next set of experiments two zylon filaments were included within the encapsulation instead of the two PE yarn. Finally to understand the effect of the knit-braided fibre sheath and the packing fibres on the performance of thermistor chip, it was then packed using six 167dtex/48filaments PE yarns and braided using six 167dtex/48filaments PE yarns to form the final ETS yarns (shown in figure 4.1c). Initially simulations were carried out using COMSOL before experimental validation.

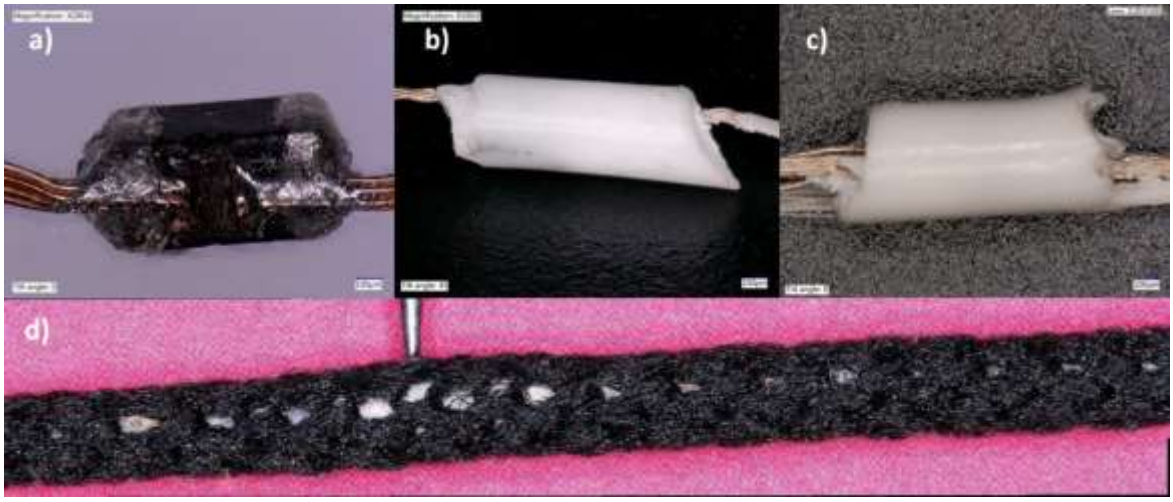

Figure 4-1: a) eight copper strands soldered onto the thermistor, b) Micro-pod of 0.87 mm diameter formed with Multi-Cure® 9-20801 resin to cover only the thermistor chip; c) shows the Micro-pod of 0.87 mm diameter formed with Multi-Cure® 9-20801 resin to cover thermistor chip with two PE yarns; d) The final yarn, the position of the embedded thermistor chip is indicated by a needle in the figure.

4.2.2 Development of a theoretical model to study the thermal time constant

A theoretical model was created using the values calculated in the geometrical model in chapter 3 (section 3.4) to study the heat flow through the micro-pod and yarn filaments, and the effect it has on the response and recovery time of the thermistor. It was built in COMSOL Multiphysics® (version 3.4, COMSOL, Stockholm, Sweden) which is a cross-platform finite element analysis, solver and Multiphysics software. This software was used because it contains a heat transfer module which comprises of simulation tools which can be used to study the mechanisms of heat transfer, such as conduction, convection and radiation (COMSOL, 2012).

The heat flow through the micro-pod and the yarn filaments was modelled using the software, this was used to simulate response and recovery times, which was then used to calculate the thermal time constant. However the thermal time constant of the thermistor cannot be integrated into the simulations and the exact construction of the thermistor is not known. Therefore for the simulations a copper block of similar dimensions was used in place of the thermistor and the average temperature measurements at the surface of the copper block was recorded for the simulation data.

It was assumed that the heat would be transferred through thermal conduction inside the micro-pod. Conduction is the transfer of heat from a body at higher temperature to a body of lower temperature or the transfer of heat from one part of a body at higher temperature to another part which is at lower temperature (Rohsenow et al., 1985). The relationship between flow of heat and the temperature field is defined using Fourier's law (Hahn and Özişik, 2012). For an isotropic and homogenous solid Fourier's law defining the conductive heat flux is given in equation 4.1.

$q = -k\nabla T$ (4.1) (Hahn and Özişik, 2012), (COMSOL, 2012)

The micro-pod with the thermistor chip and PE yarn was considered to be an immobile solid, therefore the heat transfer in solids with respect to time was obtained using the equation 4.2 given below

$\rho C_p \left(\frac{\partial T}{\partial t}\right) = \nabla(k\nabla T) + Q$ (4.2) (COMSOL, 2012)

Where:

T is the temperature in kelvin, t is the time taken from the start of the simulation, ρ is the density of the polymer resin/polyester fibres in the encapsulation, C_p is the heat capacity , k is the thermal conductivity and Q is the Heat source (surface being measured). The properties of the resins and polyester filaments are in table 4.2.

Table 4:2: Thermal Properties of material

Property	Multi-Cure® 9-20801 resin	9001-E-v3.1 Multi-Cure®	Polyester
Thermal Conductivity	0.9 $Wm^{-1}K^{-1}$	0.2 $Wm^{-1}K^{-1}$	1.009 $Wm^{-1}K^{-1}$ (Kawabata and Rengasamy, 2002)
Density	2000 kgm^{-3}	1060 kgm^{-3}	1390kgm^{-3} (Behera and Hari, 2010)
Specific Heat Capacity	1000 $JKg^{-1}K^{-1}$	1470 $JKg^{-1}K^{-1}$	1300$JKg^{-1}K^{-1}$

In these simulations the heat flow through the polyester fibres surrounding the micro-pod (packing fibres and the knit braided fibre sheath shown in figure 3.1 in section 3.2) was modelled as heat flow through a porous medium. Textile yarns are porous, containing cylindrical fibres and air (Veit, 2012). However there are no simulations done to study the heat flow through a single textile yarn. Most of the work that is in the literature (Haghi, 2011), (Yuchai Sun et al., 2010) is on textile fabrics which are made using several textile yarns. Textile fabrics have also been considered as porous media (Das et al., 2011), (Haghi, 2011), and heat transfer through a textile fabric is a complex process defined by solid conduction through fibres; conduction by intervening air; natural convection in the space between fibres; free convection due to wind flow and buoyancy flow in the surrounding environment; and radiation (Das et al., 2011), (Haghi, 2011), (Yuchai Sun et al., 2010).

However, the heat flow through a fabric has been simplified and previously modelled, by only using conduction through solid fibres and conduction through the air filling the spaces between fibres (Min et al., 2007). Hence for the simulations documented in the thesis heat flow through the packing fibres and the knit braided fibre sheath was modelled only using heat conduction through a porous medium. This was done to simplify the model and also due to the limitation in the computational power, including convection and radiation in the model caused the COMSOL model to crash. Therefore in the theoretical model the effects of convection and radiation have been ignored.

The relative humidity of the air in-between the fibres was set to 75 % (which was the average humidity during the week). Convective heat transfer does not take place if the fluid is kept stationary (Haghi, 2011). Therefore for the simulation, the air in-between the fibres in the yarn was treated as trapped dead air hence the natural convection in the spaces between fibres have been ignored. It was also assumed that there would be no forced wind flow in the environment and the buoyancy flow was negligible, hence the effects of free convection as a result of wind flow and buoyancy flow have been ignored. The effects of radiation have also been neglected since the research done on non-woven fabrics by Zhu et al has shown that the radiative heat transfer increases with pore size (Zhu et al., 2015). Therefore for these simulations, it was assumed that the packing fibres and fibres in the knit braided fibre sheath were densely packed and the pore size was small enough to not allow radiation.

The conductive heat flow through a porous medium, which was used in the simulations was defined using equation 4.3.

$$(\rho C_p)_{eq}(\partial T/\partial t) = \nabla(k_{eq}\nabla T) + Q \qquad (4.3)$$ (COMSOL, 2012)

Where $(\rho C_p)_{eq}$ is given using equation 4.4,

$$(\rho C_p)_{eq} = \theta_p \rho_p C_{p,p} + (1-\theta_p)\rho C_p \qquad (4.4)$$

And k_{eq} is given using equation 4.5,

$$k_{eq} = \theta_p k_p + (1-\theta_p)k \qquad (4.5)$$

Where C_p is the Specific heat capacity of air, ρ is the density of air and k is the thermal conductivity of air. K_p is the thermal conductivity of polyester, $C_{p,p}$ is the Specific heat capacity of polyester, ρ_p is the density of polyester and the Volume fraction is θ_p. The volume fraction of a braided structure has been estimated to be 0.5 (Shishoo, 2008).

The images of the simulations done for the samples stated in section 4.2.1 are given in Appendix 10.

4.2.3 Experimentation used to validate the theoretical model and obtain the thermal time constant from the samples

The response and recovery time experiment was done using a precision Electronic Hot Plate (Model 1000-1, Electronic Micro Systems Ltd, Salisbury, UK.). The temperature of the hot plate was set to 65 °C. Two thermocouples and the sample been tested were placed on a sensor holder made of silicon. The sensor holder consisted of three slits (3 mm apart) which were used to hold the three sensors in place. The two thermocouples were positioned on either side of the sample being tested. This was done to ensure that the hot plate temperature remained constant on either side of the sample during the experiment.

The thermocouples were connected to a PICO-TC08 unit (Pico Technology, St Neots, UK). The resistance of the thermistor was determined with a potential divider circuit by using a NI USB 6008 DAQ (National Instruments, UK) unit. The PIC0-TC08 and the NI 6008 DAQ both were interfaced to a PC. The values of the resistors used in the potential divider circuit was determined with an Agilent 34410A 6 ½ Digital multi-meter (Agilent Technologies, USA) which has a precision of 0.01 %.

Initially before the start of the experiment the sensor holder containing the three sensors was placed at room temperature away from the hot plate and left to reach equilibrium. Then the experiment was started, and the sensor holder was left in the same position for 60 seconds in-order to record the room temperature. Thereafter in-order to obtain the sudden change in temperature the sensor holder was placed on the hot plate and a weight of 1 kg was used to hold it down. The response of the sensor to being placed on the hot plate was regarded as the response time of the sample. The sensor holder was then left on the hot plate for 300 seconds to reach equilibrium. Then the thermocouples and the sample were removed from the sensor holder and the hot plate, and placed back in room temperature for 240 seconds. The samples response to being placed back in room temperature was regarded as the recovery time of the sample.

4.2.3.1 Software for the Pico TC-08 Unit

The software developed in chapter 3 section 3.6.2 was used. In-order for the LabVIEW program to communicate with the USB TC-08 labVIEW drivers were installed. In the main VI of the main program another SubVI was called to obtain the thermocouple readings. The USB_TC08 SubVI used USB_TC_08 library functions to obtain the temperature from the thermocouples (appendix 11 figure 8.18 contains the block diagram of the SubVI). The flowchart of the subVI is given below.

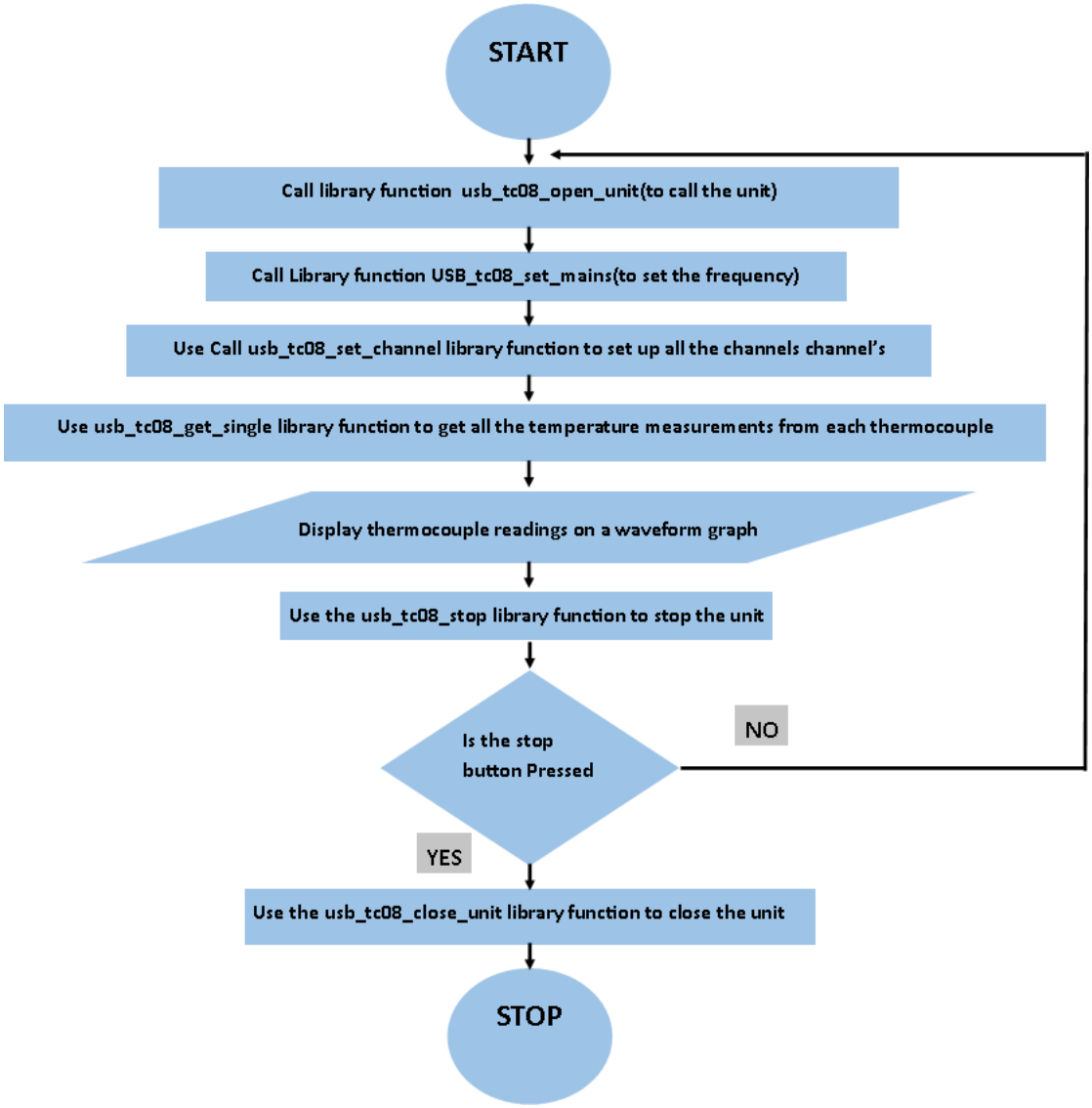

The mainVI was modified to record the thermocouple readings on the excel sheet as well as the thermistor readings, the thermocouple readings were also displayed on the waveform graph in the main VI.

4.2.4 Theoretical results

The theoretical data calculated by using equations 4.1 and 4.2 in COMSOL for the samples stated in section 4.2.1 are shown below in Figure 4.2.

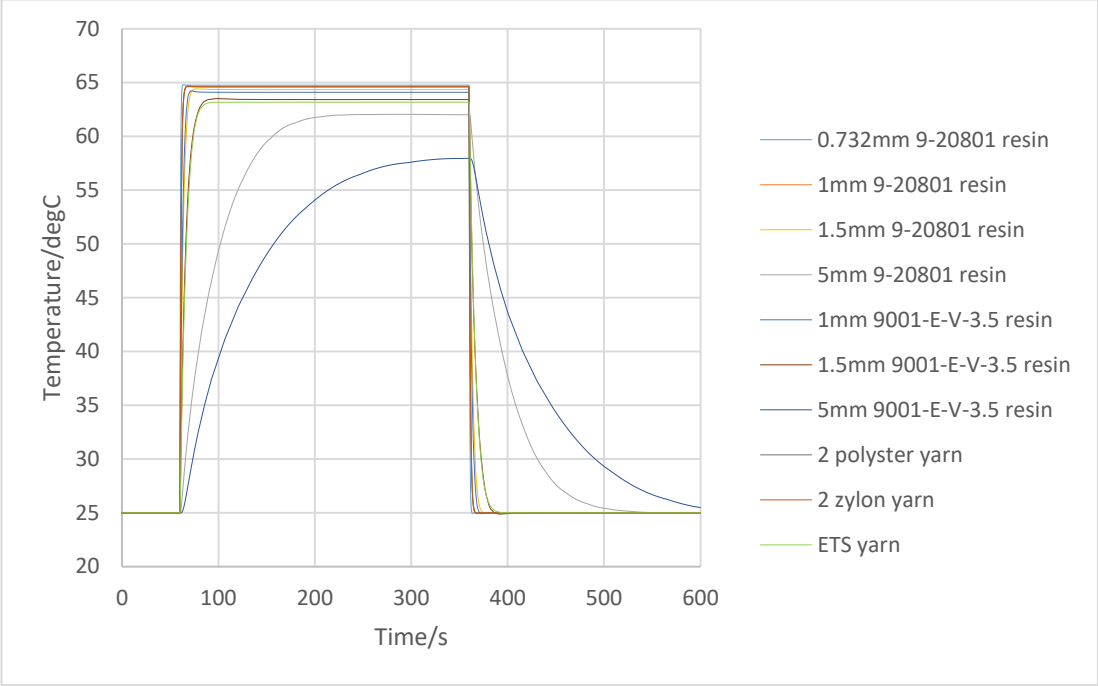

Figure 4-2:COMSOL Simulation results

The results show that the theoretical thermal time constants were less than 70 seconds for all of the samples. When the thermally conductive 9-20801 adhesive is used to form a cylindrical micro-pod of optimum diameter (0.732 mm), the thermal time constant for the heat to flow through the resin was found to be 0.7 s as shown in table 4.3 (2nd column). From the results given in table 4.3 one could deduce that increasing the diameter of the cylindrical micro-pod would result in corresponding increases in the thermal time. This is due to the increase in the thermal resistance. Due to the difficulty of creating a 0.732 mm diameter cylindrical micro-pod, 0.87 mm was considered as the minimum diameter of the micro-pod that can be manufactured to protect the thermistor. When this was the case the thermal time constant (TTC) only increased by 0.4s when compared to using the optimum diameter of 0.732 mm, making 0.87 mm an acceptable diameter. When the diameter of micro-pod was increased further to 1.53 mm and 5.0 mm the TTC increased by 3.6 s and 37.8 s respectively (see column 2 of table 4.3).

Similar results for the thermally non-conductive 9001-E-V-3.5 resin were evident from the data shown in table 4.3 giving an increase in the TTC of 0.9 s when compared to when 9-20801 resin was used to make the micro-pod of 0.87 mm diameter, however this has no impact on the desired temporal resolution which would be no less than 30 minutes. Increasing the diameter of the micro-pod formed with 9001-E-V-3.5 resin to 1.53 mm and 5.0 mm increased the TTC to 6.6 s and 69.6 s respectively. The polyester (PE) fibres placed within the micro-pod appear to have no significant impact on the TTC when compared to the TTC measured with the micro-pods without PE fibres, which were formed to a diameter of 0.87 mm from 9-20801 resin. The Zylon filaments placed within the micro-pod does not seem to impact the TTC either. The packing fibres and the knit-braid used

for covering the micro-pod, however did increase the thermal time constant by a further 5.6 s when compared to when the thermistor was encapsulated at a diameter of 0.87 mm with polyester fibres in the encapsulation, which as discussed previously does not impede the performance of the device for the intended applications.

4.2.5 Experimental results

The experimental data recorded using the NI DAQ for the samples stated in section 4.2.1 is given in figure 4.3.

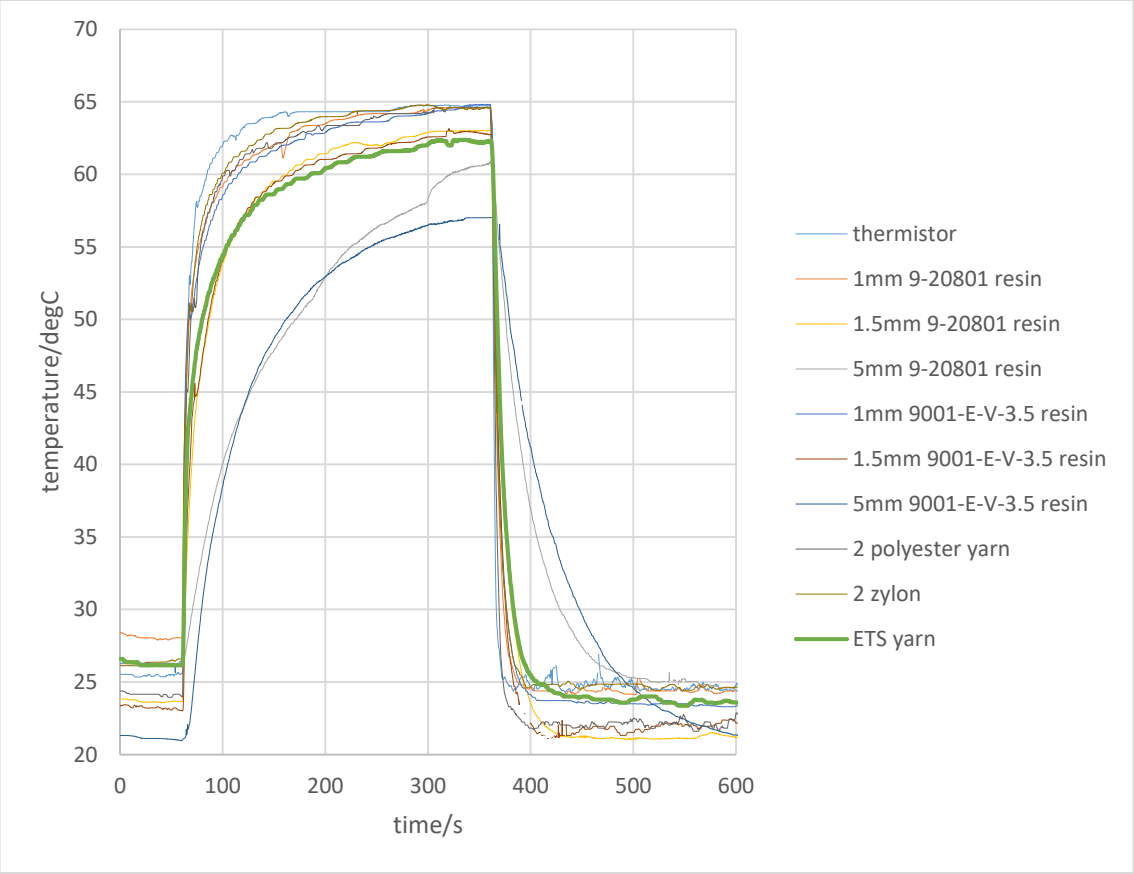

Figure 4-3: Experimental Response and Recovery time graphs

Table 4:3: Theoretical and experimental thermal time constants for the thermistor under different encapsulation conditions. Results have been extracted from the data presented in Figure 4.2 and figure 4.3. The experiments were conducted on three different samples (except for 5 mm 9001 resin encapsulation) and five ETS yarn samples. The mean and the standard deviation has been stated in the table.

	Simulated thermal time constant for response/recovery time τ_S (s)	**Measured thermal time constant for response time τ_P (s)**	**Measured thermal time constant for recovery time τ_R (s)**	**Effect of additional layers [τ_R(s)-3.9(s)*]**
Thermistor	Not Simulated	5.5 ± 1.4	3.9 ± 0.2*	0
0.732 mm 9-20801 resin	0.7	Not measured	Not measured	Not measured
0.87 mm 9-20801 resin	1.1	8.5 ± 2.2	6.4 ± 0.3	2.5 ± 0.4
1.53 mm 9-20801 resin	3.6	16.3 ± 9.4	13.4 ± 0.9	9.5 ± 0.9
5 mm 9-20801 resin	37.8	86.2 ± 17.1	34.6 ± 0.4	30.7 ± 0.4
0.87 mm 9001-E-V-3.5	2.0	8.2 ± 1.87	8.5 ± 1.2	4.6 ± 1.2
1.53 mm 9001-E-V-3.5	6.6	16.1 ± 4.3	9.6 ± 0.4	5.7 ± 0.4
5 mm 9001-E-V-3.5	69.6	59.4	32.8	28.9
Two polyester yarn (0.87 mm resin)	1.1	6.7 ± 1.0	6.4 ± 0.8	2.5 ± 0.8
Two zylon yarn (0.87 mm resin)	1.1	5.8 ± 1.3	7.6 ± 0.7	3.7 ± 0.7
Temperature sensing yarn	6.7	15.9 ± 4.1	12.1 ± 1.3	8.2 ± 1.3

The graph plotted using the experimental results shown in figure 4.3 displays a similar shape as the graph in the theoretical simulations (figure 4.2). The simulated thermal time constant for the response time and the recovery time were identical. The experimental results (table 4.3 columns 3 and 4) however show a difference between the response and recovery times of the sensor with regard to their thermal time constants. This change could be as a result of the silicon holder, which was used to restrain the samples on the hot plate. The properties (thermal conductivity, heat

capacity and density) of the silicon sample holder are clearly different to those of air. The thermal time constant is also affected by the environment its exposed to (EPCOS, 2011). Therefore the thermal time constant of the recovery is considered herein to be that of the samples.

The results of the first experiment given in the first row of table 4.3 gives the thermal time constant for the thermistor chip soldered onto the eight strands copper wire as 3.9 s which is only 0.1 s less than the value provided in the sensor datasheet. The theoretical model only gives the thermal time constant at the surface of the chip, therefore, to compare the simulation results with the experimental results the difference between the measurements of the sample and the thermistor was calculated. These values are presented on the last column on table 4.3.

As in the theoretical simulations the experimental results demonstrate the thermal time constant increases with the increase in diameter of encapsulation. The small discrepancy between the thermal time constants for simulation and experiment results are most likely due to the positioning of the thermistor chips within the micro-pod and the human error bought about when removing the samples from the hot plate.

The thermal time constant increases only by 2.5 s when the thermistor was encapsulated using 9-20801 adhesive to form a 0.87 mm diameter cylindrical micro-pod, it can be seen that the volume of resin brings about a minute increase in the thermal time constant. When the thermally non-conductive 9001E-V-3.5 resin was used to form the micro-pod the thermal time constant increases as in the theoretical simulations. For the diameter of 0.87 mm diameter there is an increase of only 2.1 s compared to the thermally conductive 9-20801 resin.

When the diameter of the micro-pod increases the TTC increases as expected, for both the 9-20801 and 9001-E-V-3.5 resin. However the TTC was much less than the theoretically estimated TTC for a 5 mm diameter micro-pod (see rows 6 and 9 in the columns 2 and 5 in table 4.3). This may be caused due to the heat being lost due to conduction along the copper wires. This has not been accounted for in the theoretical simulations. This was not investigated further since a 5 mm cylindrical micro-pod would mean that the cross-sectional area of the micro-pod will be 46.6 times the minimum cross-sectional area estimated for the minimum diameter (0.732 mm), and hence the micro-pod would be too large to be included within a yarn and placed in a fabric.

As assumed in the theoretical simulations the experimental results show polyester fibres within the micro-pod have no significant impact on the thermal time constant (row 10, column 5) compared to the experimental results when a 0.87mm 9-20801 adhesive (row 4, column 5) was used. The minute increase in the experimental results (table 4.3) of 1.2 s when 2 Zylon fibres were included in the micro-pod, maybe caused due to the positioning of the thermistor in the micro-pod. It was extremely difficult to position the sensor in the exact middle of the micro-pod during encapsulation.

Therefore it can be argued that the PE and Zylon fibres placed within the micro-pod have no significant impact on the thermal time constant.

The thermal time constant when the encapsulation was covered with packing fibres and the warp knitted outer covering (final ETS yarn) was 8.2 s (table 4.3) more than the thermal time constant of the thermistor, this was 1.5 s longer than the theoretical value estimated with COMOL, given in Table 4.3 (last row of column 2). This maybe caused due to the estimations made on the volume fractions in the theoretical model. However a total thermal time constant of 12.1 s for the ETS yarn (last row of the 4th column), can be regarded as acceptable since, as discussed earlier for long term monitoring applications, such a temporal resolution is not essential. Therefore, it can be concluded that the volume and thermal conductivity of the polymer resin and the yarn filaments have insignificant effect on the response and recovery times of the sensor.

Another way to analyse the response time is by looking at the step response time of the sensors. This is given in appendix 12 where the theoretical and experimental data has been analysed by looking at the step response times of each of the samples.

4.3 Accuracy testing using the Test Rig

In order to understand the effects of the polymer resin and yarn fibres on the accuracy of the ETS yarn a test rig had to be designed. The main focus during the design of the test rig was to develop an equipment capable of gradually increasing the temperature of the sample over a prolonged period of time. It is assumed that body/wound temperature would change gradually over time rather than having step changes. The samples stated in section 4.2.1 were tested with the custom made test Rig.

4.3.1 Developing the Test Rig

The test rig was constructed using textile-based heaters produced by the Advanced Textiles Research Group at Nottingham Trent University. Silicone was used to make the base for the test rig. Silicone was chosen because of its good thermally insulating property, to prevent the heat produced by the textile heaters escaping through thermal conduction. A mixture of silicone, silicon carbide and carbon (SiO, SIC, C) was laid on top of the silicone base. The mixture of SiO, SiC, C was chosen because of its thermally conductive and electrically insulating property. This provided an uniform temperature surface for the samples to be tested. Three commercially available k type thermocouples from Pico Technology were placed at equidistance's in-between the two layers of silicone and silicon carbide. The thermocouples were bent slightly to ensure the measuring heads were on the same level as the surface of silicon carbide. This structure was regarded as the test bed and it is shown in figure 4.4.

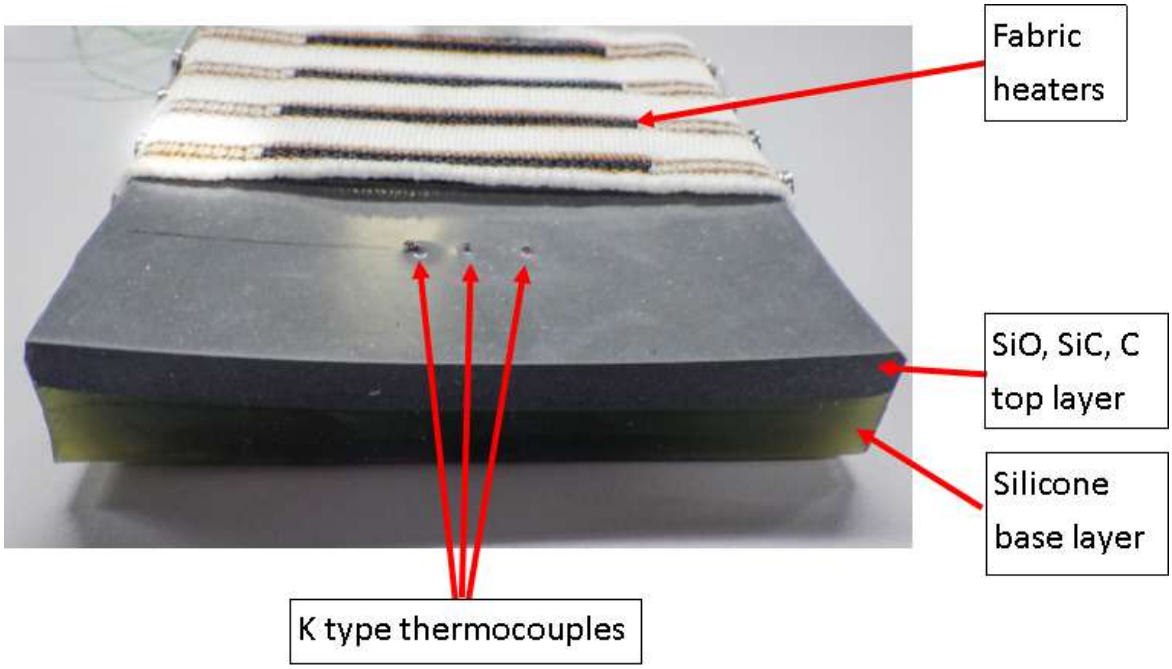

Figure 4-4: Fabric heaters positioned on top of the test bed

To hold the samples being tested and two other commercially available thermocouples a flexible sensor holder (FSH) had to be designed. A potion off the edge of the test bed was cut for this purpose. This was done to ensure that the test bed and the sensor holder had the same composition. Three slits were cut on the sensor holder at equal distances (4 mm apart) to the thermocouples on the test bed. The sample being tested was placed on the middle slit and the two thermocouples were placed on the other two.

Thereafter the sensor holder was placed directly on top of the thermocouples in the test bed. This ensures that the sample and the two thermocouples would be positioned right on top of the three thermocouples in the test bed during the experiment. A rectangular metal plate was placed on top of the sensor holder, this was done to ensure that there was an evenly distributed weight holding the sensor holder in place. The two thermocouples on the FSH were used to observe if there would be any changes in the temperature recorded by them, when compared to the temperature captured by the thermocouples on the test bed (which were positioned right underneath them).

Four two course fabric heaters were placed on the lower end of the thermally conductive SiO, SIC, C layer. Fabric heaters were made by knitting FabRoc (EXO2, USA) and interconnecting it using knitted copper filaments (Mbise et al., 2015). The heaters were knitted with a band on both sides and a Velcro strip was sewn onto its edges to ensure the heaters were held in place.

In order to eliminate the effects of room temperature on the readings the test Rig was placed inside an insulation box. The insulation box was constructed with Floor mate 300A (Dow building solutions, MI, USA) which has a very low thermal conductivity of 0.033 $Wm^{-1}K^{-1}$ (data sheet given in appendix 13). The thickness of the box was measured at 24.72 + 0.31 mm. The lid was held in place using a 5

kg metal weight. When used in a wound dressing it is assumed that the bandage would provide the insulation against room temperature and create a micro-climate. The entire test rig is given in figure 4.5.

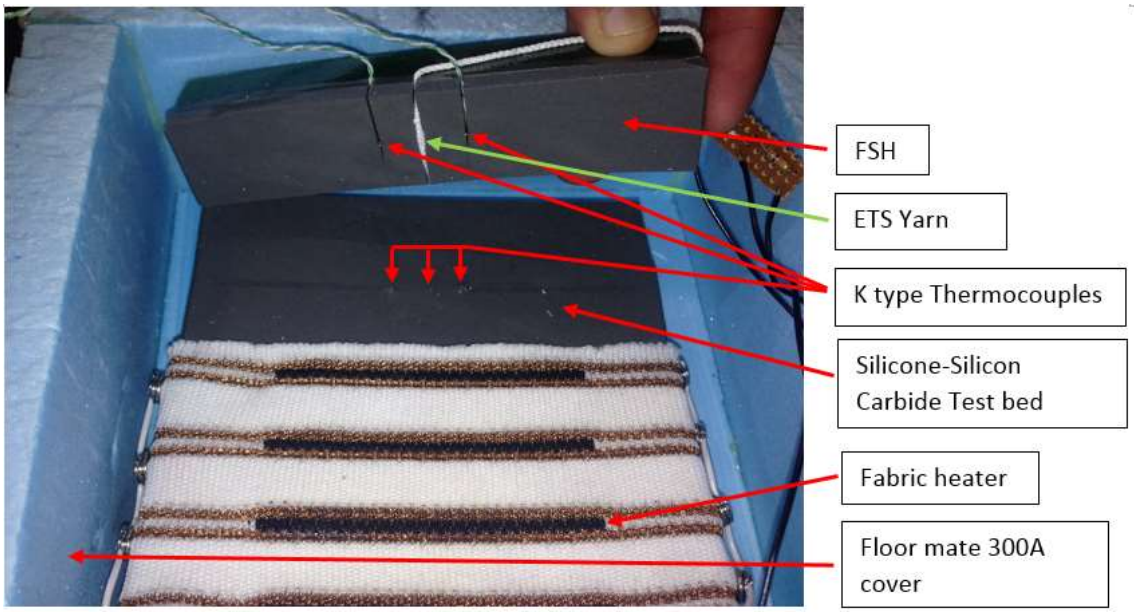

Figure 4-5: Test-Rig

The fabric heaters were powered using a laboratory power supply with 5 V, 2 A. The fabric heater elements heated the silicon carbide gradually increasing its temperature. The program was developed in LabVIEW to read the temperature off the five thermocouples and the sensing yarn (the program given above in section 4.2.3.1). The LabVIEW program was adjusted (using a time delay express VI) to record temperature measurements every minute. The results were saved onto a spread sheet.

The thermocouples were connected to a PICO-TC08 unit (Pico Technology, UK). The resistance of the thermistor was determined with a potential divider circuit by using a NI USB 6008 DAQ unit. The PIC0-TC08 and the NI 6008 DAQ both were interfaced to a computer. The values of the resistors used in the potential divider circuit was determined with an Agilent 34410A 6 ½ Digital multi-meter which has a precision of 0.01 %.

4.3.2 Results

Preliminary tests were conducted to evaluate the functionality of the test rig, whereby a thermocouple was used instead of sensing yarn. As the results were encouraging the samples mentioned in section 4.2.1 were tested using the custom made test rig.

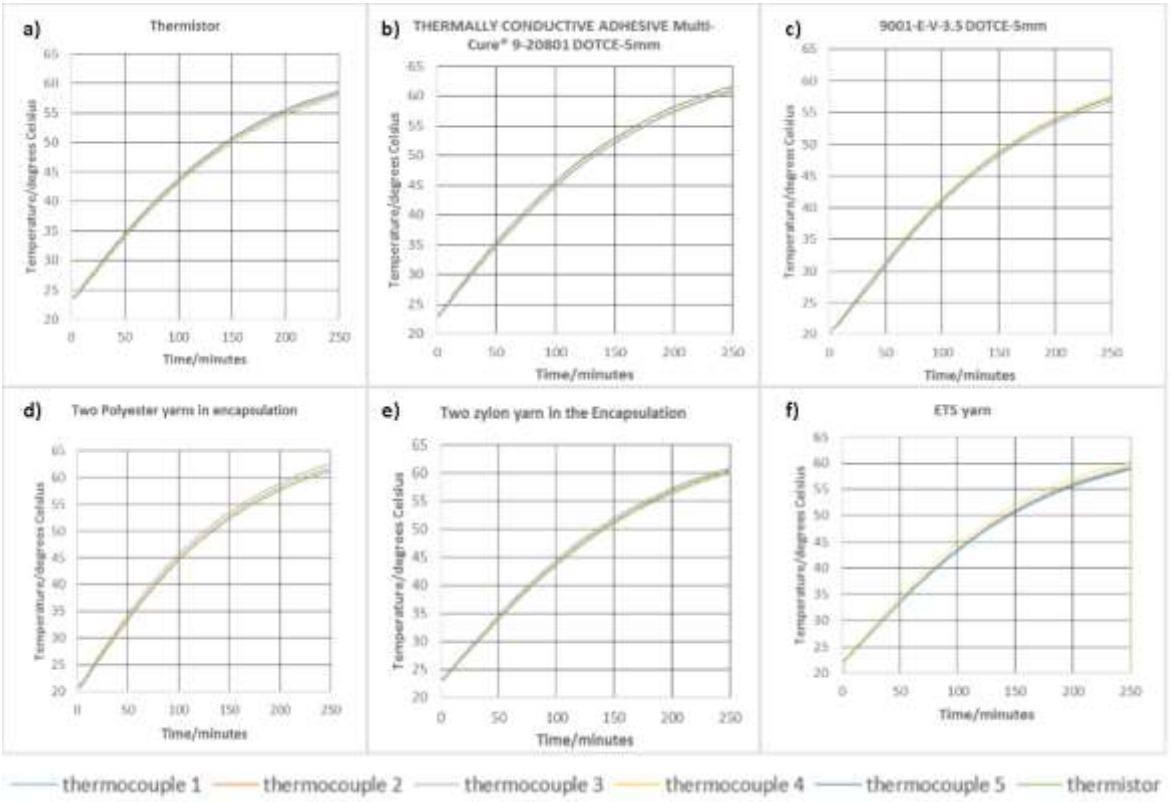

Figure 4-6: Results from the test rig. Where thermistor measurements are shown in green and the thermocouple measurements are shown using the rest of the colours. Where a) gives the results when a thermistor is tested, b) when a thermistor is encapsulated using 9-20801 resin to form a cylindrical micro-pod with a diameter of 5mm, c)When it is encapsulated using 9001-E-V-3.5 resin to form a cylindrical micro-pod with a diameter of 5mm, d) when polyester fibres are inserted within the 0.87mm diameter encapsulation created using 9-20801 resin, e) when zylon fibres are inserted within the 0.87mm diameter encapsulation created using 9-20801 resin and f)when the final ETS yarn is tested.

The thermocouples used for these experiments were of class one tolerance which means they have an accuracy of +/-1.5 °C within a temperature range of -40 to 375 °C. Therefore the accuracy of the test rig is +/-1.5 °C. The Tolerance of the Murata NTC 0402 thermistors is ±1 % according to the manufacturer. The results from the first experiment (figure 4.6a) shows that the temperature measurements obtained from the thermistor fall on top of the temperature measurements captured by the thermocouples. This suggests that there is no difference between the temperature measurements captured by the thermistor and the thermocouples.

The results from the second set of experiments (figure 4.6b) demonstrated that the thermistor readings were not significantly influenced by the quantity of multi-cure 9-20801 resin used to form the micro-pod. Even the 5 mm diameter micro-pod did not have any effect on the temperature measured by the thermistor. Therefore one could conclude that the amount of resin used for encapsulation has minor effect on the sensing ability of the thermistor.

One could conclude from the results from the third set of experiments (figure 4.6c) that the thermally non-conductive resin 9001-E-V-3.5 also has minor effect on the temperature measuring

ability of the thermistor. This may be due to the minute difference in between the thermal conductivities of the resins.

The results from the fourth (figure 4.6d) and fifth set (figure 4.6e) of experiments show that the inclusion of additional yarn fibres (PE and Zylon) within the micro-pod to enhance the mechanical strength of ETS yarns do not affect the thermistor readings significantly.

From the final results (figure 4.6f) one could conclude that the inclusion of polyester fibre sheath around the thermistor, interconnects and micro-pod through the knit-braiding process would not affect the performance of the thermistor significantly. It can be also observed that the ETS yarn can be used to measure temperature over a prolonged period of time. All the experiments were carried out for an excess of 250 minutes.

4.4 Calibration of the electronic temperature sensing yarn

A rigorous calibration was conducted on the final yarn to validate the manufacturer provided data. Here five complete ETS yarns were heated in an oil bath along with an NTC Thermistor (USP11493, US Sensor Corp. CA, accurate to ± 0.05 ˚C). The calibration experiments (Figure 4.7) used the precision electronic hotplate to heat an oil bath (80 ml; Pure Sunflower Oil, Tesco PLC, Welwyn Garden City, UK). The entire ensemble was contained within a thermally insulating polystyrene box and temperatures were held for 40 minutes to ensure that convection effects were minimised. The thermistor resistances were obtained using a digital multi-meter (Agilent 34410A 6½ digit, Agilent Technologies, California, United States) which gave a precision of 0.01%. This digital multi-meter was used to obtain the resistance of the ETS yarn because it was more accurate when compared to obtaining the resistance through a voltage divider and a NI-DAQ.

All of the data obtained from the calibration experiments were processed and plotted using Python v2.7 (Python Software Foundation, Wilmington, DE, USA) using the SciPy (Jones et al., 2001) and Matplotlib (Hunter, 2007) packages (the python code is given in appendix 14).

The resistance values from the five yarns were averaged and plotted against the reciprocal of the temperature. This data was then fit with a polynomial approximation converting thermistor resistance into temperature (Kimball et al., 1993) (Figure 4.8b), with the final calibration fitting given by equation 4.6.

$$\frac{1}{T} = 0.017598 - 0.003687\,[\ln(\mathrm{R})] + 0.002545\,[\ln(\mathrm{R})]^3 \qquad (4.6)$$

Where *T* is the temperature (in °C) and R is the resistance (in kΩ).

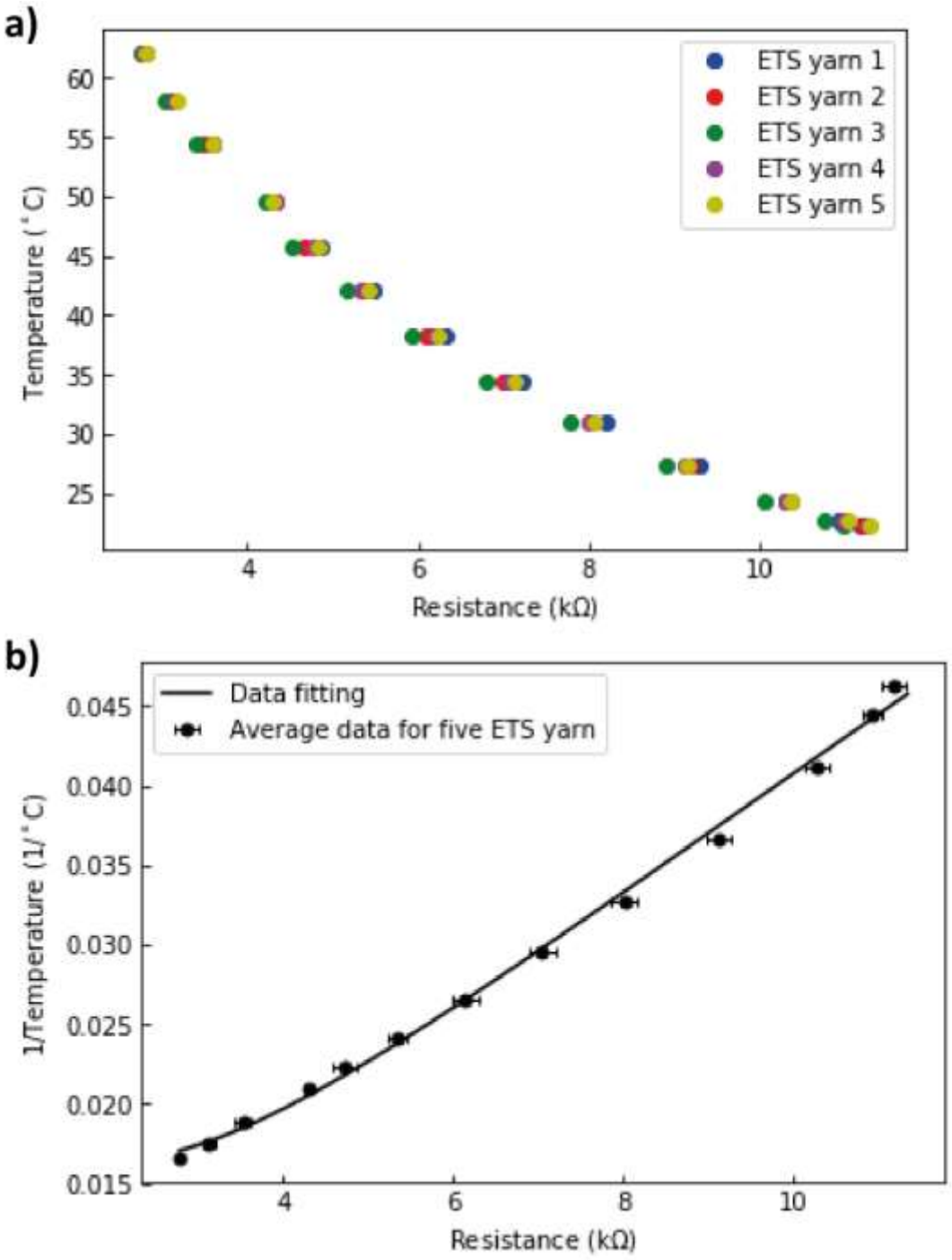

Figure 4-7: Calibration showing readings from five ETS yarns. (a) The resistance values of the five ETS yarns are plotted against the temperature of an oil bath, as determined by a high-accuracy thermistor. (b) The averaged values of the resistances of the five ETS yarns has been plotted against the reciprocal of the temperature and a polynomial fitting has been applied.

Figure 4.7a showed that all of the ETS yarn resistances were close to one another (within 300 Ω) as might be expected for thermistors of the same type. Figure 4.7b shows that the polynomial fitting fit the data well within the error bars for most data points.

Recent literature has shown a more accurate way of calibrating thermistors. The data used previously was then fit with a new polynomial approximation once again converting the thermistor

resistance into temperature (BIPM, 2014) (figure 4:8), with the new and more calibration fitting given in equation 4.7.

$$\frac{1}{T} = 0.040576 + 0.041704 \ln\left(\frac{R}{R_0}\right) + 0.030514[\ln\left(\frac{R}{R_0}\right)]^2 + 0.009980[\ln\left(\frac{R}{R_0}\right)]^3 \quad (4.7)$$

Where *T* is the temperature (in °C), R_0 is the resistance at 25 °C (in kΩ) and R is the resistance (in kΩ).

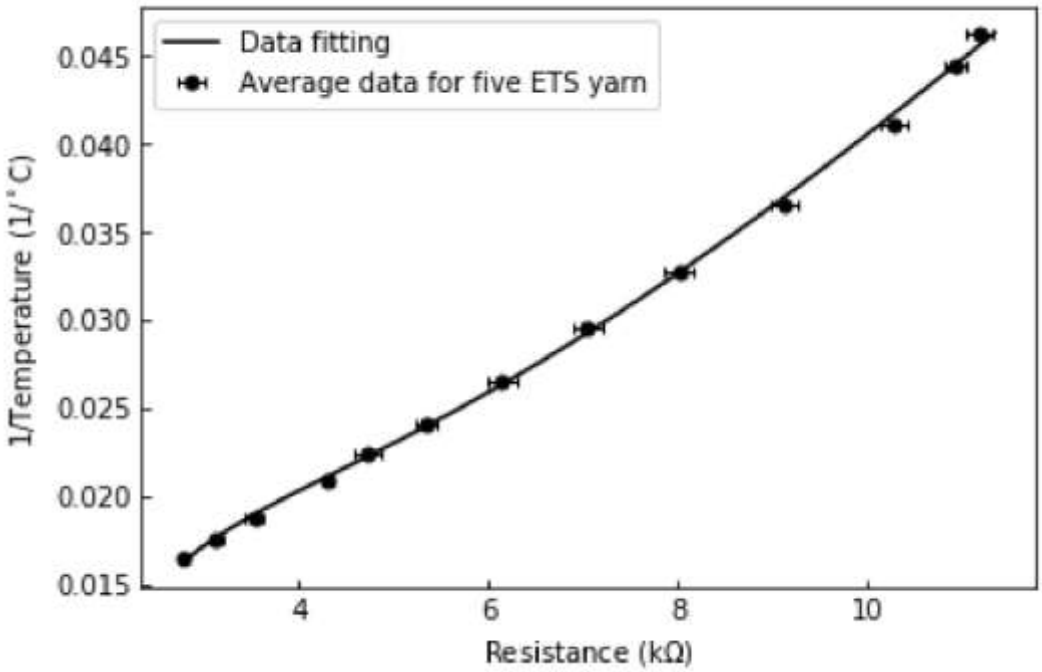

Figure 4-8: The averaged values of the resistances of the five ETS yarns has been plotted against the reciprocal of the temperature and the new polynomial fitting has been plotted

It can be seen that the new polynomial fitting (shown in figure 4:8) is more accurate when compared to the previous one (shown in figure 4:8).

It was also important to clarify if the equation given by the thermistor manufacturer can be used to provide accurate temperature measurements when using the ETS yarn. Therefore average resistance values (R_t) of the ETS yarn were used to calculate the temperature of the ETS yarn (T) using equation 4.8.

$$1/T = \left(\frac{ln\left(\frac{R_t}{R_0}\right)}{B}\right) + \left(\frac{1}{T_0}\right) \quad (4.8)$$

Where R_0 is 10KΩ±1 % resistance at 25 °C, T_0 is 298.15 K (25 °C) and B is the material constant of 3395 for the temperature range of 20-65 °C. The temperature (T) obtained is in K therefore it was converted to °C. Thereafter the reciprocal of this temperature was plotted on figure 4.8 to obtain figure 4.9.

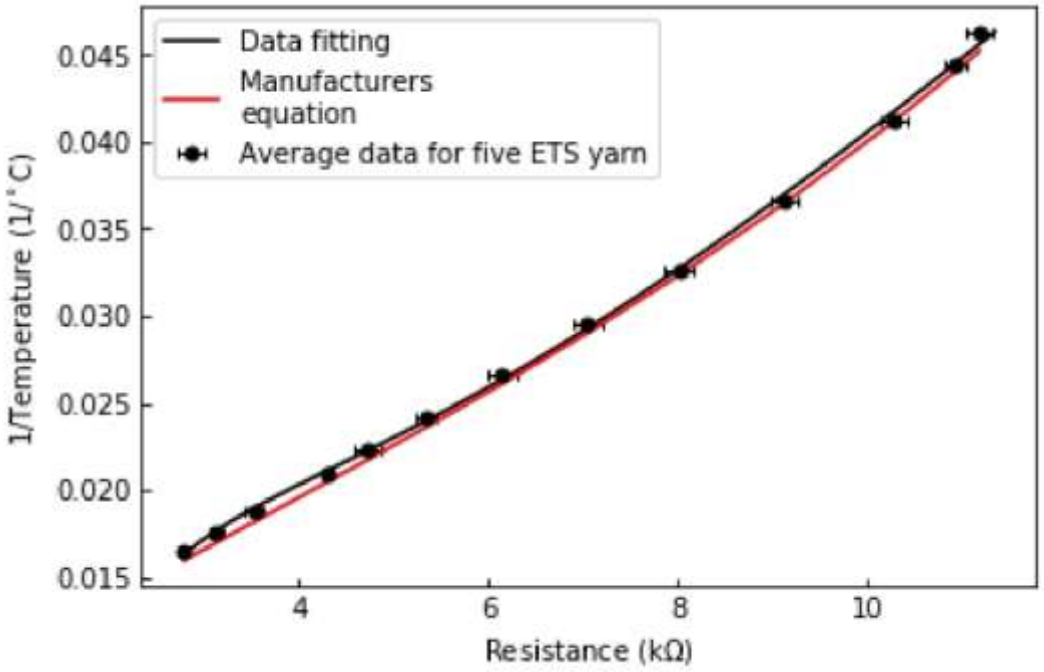

Figure 4-9: Temperature obtained from the equation provided by the thermistor manufacturer plotted in red on fig. 4.8

As it can be observed from the figure 4.9 above the equation 4.8 given by the manufacturer provided accurate temperature measurements. This further justified that the polymer resin and the yarn filaments have no significant impact on the accuracy of the thermistor.

In-order to identify which equation would provide the most accurate temperature measurements the T values for each of the equations were calculated. The T value gives the significant difference between the population mean and a hypothesized values. The T value was calculated using equation 4.9 given below

$$T = \frac{\bar{a}-\mu}{(\frac{s}{\sqrt{n}})} \qquad (4.9)$$

Where ā is the temperature calculated by the equations 4.6, 4.7 and 4.8, μ is the temperature indicated by the calibrated thermistor, s is the standard deviation (standard deviation for equation 4.7 and 4.8 have been calculated by using the information provided by the manufacturer where the error for R_0 and B has been stated as 1%). The number of yarns tested is represented by n.

The table 4.4 below gives the average T values for the three equations.

Table 4:4: T values calculated for each of the three equations

	Manufacturers equation (given in equation 4.8)	1st polynomial equation (given in equation 4.6)	2nd polynomial equation (given in equation 4.7)
Average T value	0.03554	0.2274	0.1157

It can been seen from table 4.4 that the 1st polynomial equation provided the largest T value therefore this equation 4.6 gave the largest deviation between the temperature obtained from the ETS yarn resistances' and that of the calibrated thermistor. The 2nd polynomial equation provided a lower average T value however the manufacturer's equation provide the lowest average T value. Then a graph was plotted to identify how the T value changed with regard to temperature for each of the three equations.

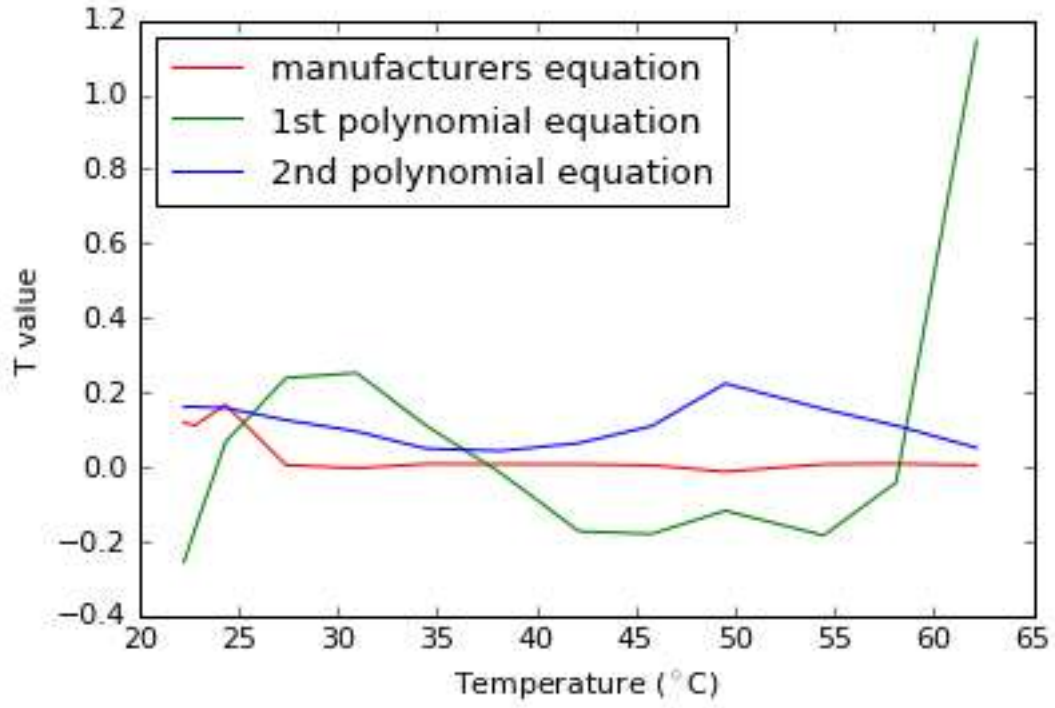

Figure 4-10: T value for different temperatures

It can be seen from figure 4.10 that the equation 4.8 provided the minimum T value therefor it can be stated that it provided the most accurate temperature measurements. Hence it can be justified to use the equation 4.8 provided by the manufacturer when temperature has to be obtained from the resistance of the ETS yarn.

At this point the true final accuracy of the ETS yarn was also assessed. It was possible that the direct conversion of the thermistor resistance tolerance to a temperature error may have been an underestimate given that the thermistors encapsulation process could have introduced additional sources of error. Equation 4.8 was used to calculate the ETS yarn temperatures and these were compared to the temperature given by the calibration thermistor (Table 4.5).

Table 4:5: Differences between the calculated ETS yarn temperatures and the temperature given by the calibration thermistor.

Thermistor (°C)	22.25	22.80	24.35	27.40	30.95	34.40	38.20	42.15	45.80	49.50	54.45	58.10	62.15
ETS yarn 1 (°C)	0.14	0.05	0.10	0.47	0.62	0.66	0.62	0.47	0.72	0.89	0.18	-0.45	-0.57
ETS yarn 2 (°C)	0.21	0.29	0.30	0.12	0.01	-0.24	-0.40	-0.28	-0.55	0.57	-1.03	-0.70	-0.32
ETS yarn 3 (°C)	-0.37	-0.35	-0.53	-0.68	-0.80	-1.05	-1.10	-1.16	-1.54	-0.02	-1.79	-1.86	-0.98
ETS yarn 4 (°C)	0.32	0.23	0.13	-0.05	0.01	-0.04	0.03	-0.17	0.09	0.92	0.16	-0.54	-0.40
ETS yarn 5 (°C)	0.38	0.32	0.27	0.10	0.23	0.29	0.27	0.27	0.52	0.67	0.07	-0.30	-0.21

It can first be noted that of the five yarns the ETS yarn 3 values differed from the calibration thermistor values the most. In the 22.25 to 62.15 °C temperature range 89 % of the yarn measurements were within 1 °C of the calibration thermistor values, and 63 % were within the desired 0.5 °C when the ETS yarn 3 data was included: Removing the ETS yarn 3 gave 98 % and 73 % for 1 °C and 0.5 °C respectively. This was deemed acceptable for this study and future work will strive to improve measurement accuracy as a 1 °C error in the absolute temperature reading from two yarns would be enough to give a false result for ulcer formation.

There were a number of potential causes for the differences seen between the ETS yarns and the calibration thermistor. The most likely reason was due to manufacturing tolerances of the thermistor. The temperature error estimated for the thermistor by the SimSurfing software in the Murata website is given in the figure 4.11. The software SimSurfing can be used to simulate the characteristics of Murata products. The simulation parameters were set as follows, the resistance R1 was set to 10 Ω because the ETS yarn was directly connected onto the multi-meter therefore R1 was taken to be the resistance of the copper wire. The voltage in (Vin) was set to 1 V because the datasheet of the Agilent multi-meter states that it produces 100 µA of current when measuring a resistance of 10 kΩ.

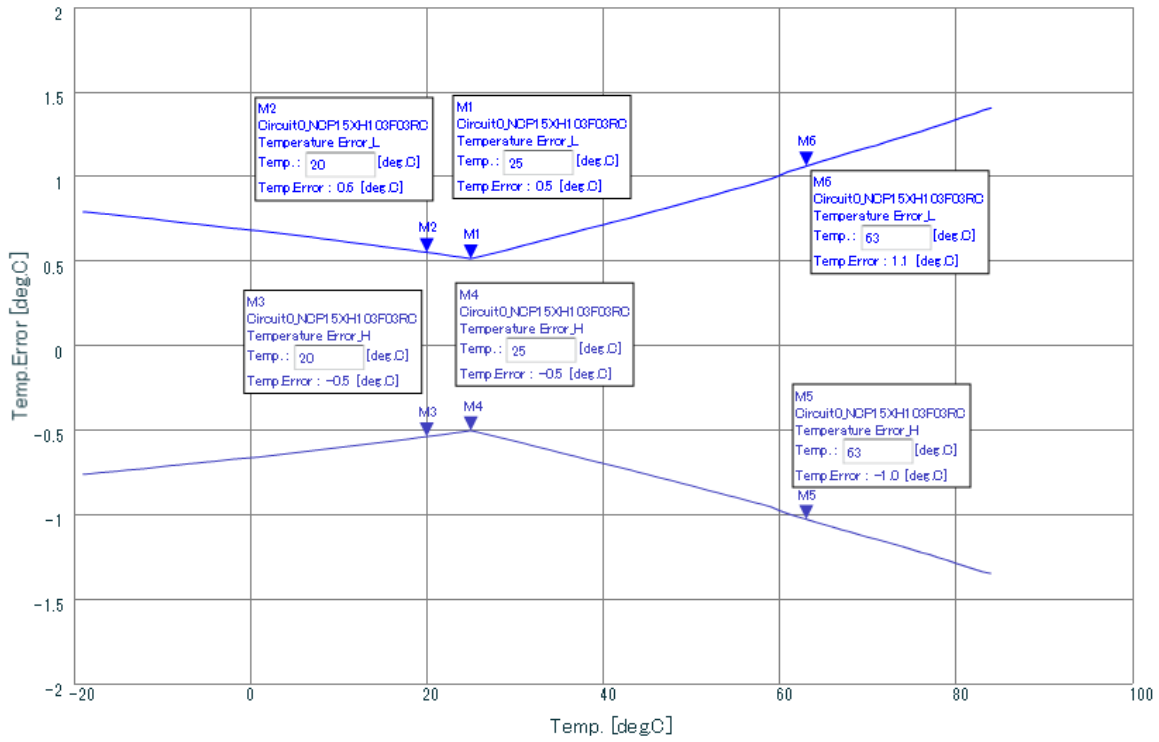

Figure 4-11: Simulated temperature error on SimSurfing software in the Murata website

The figure 4.11 shows that a temperature error of ±0.5 °C- ±1.1 °C is to be expected when obtaining temperature measurements in the temperature range of 20-63 °C when using the NCP15XH103F03RC NTC thermistor. Therefore one could argue that most of the temperature errors in the calibration experiment were due to the thermistor.

The other likely reason would have been caused due to fabrication of the ETS yarn. The ETS yarns were fabricated by hand introducing uncertainty into the both the soldering and encapsulation processes. While utmost care was taken to ensure the yarns were similar an automated manufacturing process would be more likely to produce identical yarns. ETS yarn 3 was most likely damaged during the fabrication of the yarn. This is a likely explanation because most of the temperature errors in ETS yarn 3 were greater than the simulated maximum temperature errors for the SMD NTC thermistor given in figure 4.11. The age was also a consideration, as thermistor values are known to shift with use and prolonged exposure to higher temperatures (Kimball et al., 1993). Ultimately it would also be desirable to use a thermistor for the ETS yarns that had a lower temperature error as this would reduce the error on temperature measurements.

4.5 Tensile Test

Textile yarns are subjected to mechanical stress during knitting, dyeing, wear and tear of a garment. Therefore, it is important to study the impact of strain force on the temperature measurements of the ETS yarn.

Therefore to initially understand the breaking force required for breaking the ETS yarn the Zwick/Roell Z2.5 machine (Zwick/Roell GmbH) was used. Test speed was set to 300 mm/min as specified by the skien method (British Standards, 1988). Grip to grip separation at the start position was set to 50.00 mm.

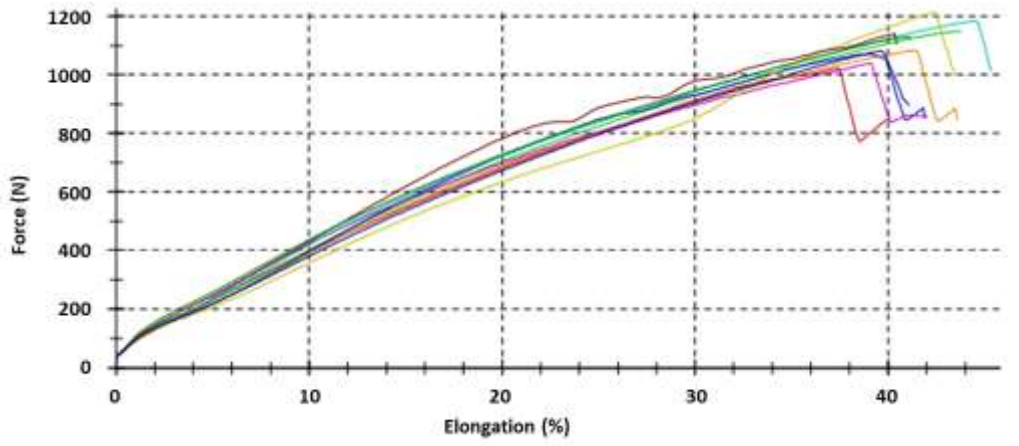

Figure 4-12: Results from the tensile test to get the breaking force (the graph was constructed using the data given in table A15.1 given in the appendix 15)

The results (figure 4.12) show the average force required to break the braided yarn as 1060 N. The average Elongation percentage of the yarn at maximum tensile force is given as 40.7 %.

Thereafter cyclical tests were carried out at 5 %, 10 %, 21 %, 42 % and 52 % of the breaking force. The yarn being tested was connected to a voltage divider circuit and then connected to the analogue input of the Zwick/Roell machine. A voltage of 5 V was supplied using an ISO-TECH IPS3303 Bench Power Supply (ISO-TECH) and a 10 kΩ resistor was used for the potential divider circuit.

The Vout of the voltage divider circuit was measured and recorded using the software provided for the Zwick/Roell machine. Figure 4.13 demonstrates that there is only a minute change in voltage when the ETS yarn is subjected to the cyclic test. The voltage changes by about 0.034 V for 100 cycles, which implies that the resistance of the ETS yarn remains almost constant during the tests. The minute increase of 0.7 ^{o}C bought about by the change in resistance may be due to friction in between the fibres and the encapsulation during the cyclic test or due to a room temperature variation. Therefore, it can be confirmed that the ETS yarn responds well to a strain force and hence can be used to make temperature sensitive garments.

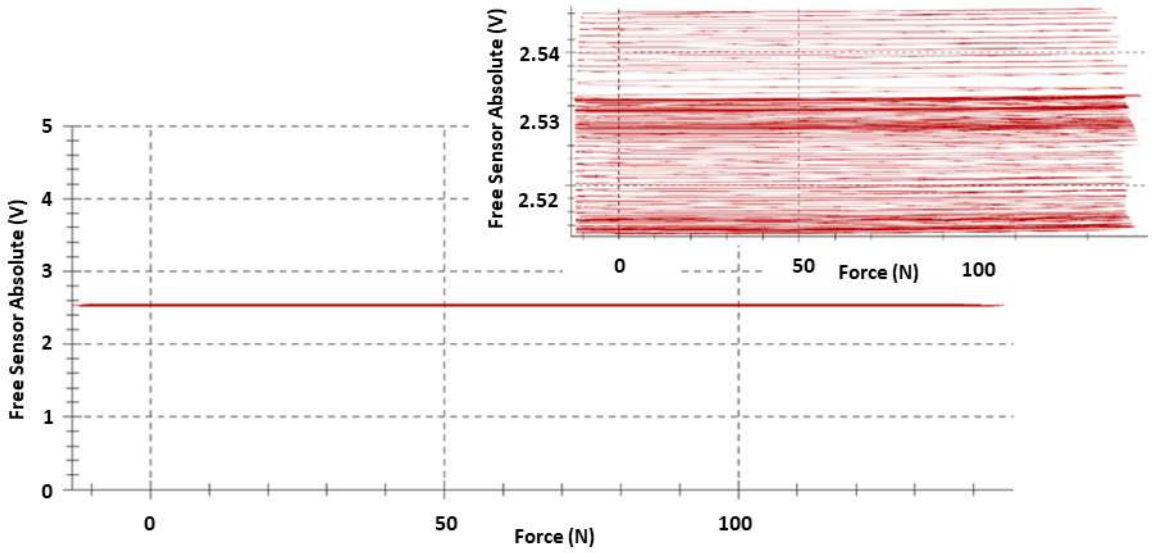

Figure 4-13: Tensile test results

4.6 Summary

In this chapter a theoretical model has been created to study the heat flow in ETS yarn and it has been used to look at the effects the polymer resin and yarn filaments have on the response and recovery times of the embedded thermistor. The theoretical model has been validated by using experiments. The response and recovery times of the thermistor has been analysed by looking at its thermal time constant (TTC). The results have shown that the volume of the micro-pod used to protect the thermistor has insignificant effect on the TTC of the sensor which also holds true in the presence of filaments within the micro-pod. The packing fibres and the braided yarn sheath however increases the TTC by 300% although the final thermal time constant of 12.1 s can be regarded as negligible when the yarn is used for applications that monitor body, wound temperature or indeed any other process which takes place over a time course of more than five minutes. Another way to look and analyse response time of a sensor is by looking at the step response time of that sensor and this is given in the appendix 12.

A test rig was designed and developed to demonstrate that temperature measurements made using the ETS yarn are comparable to traditional temperature measurements, and that the ETS yarn is well suited to make temperature measurements over a long period of time. However the test rig eliminated the effects of ambient temperature and other external variables that might affect surface temperature measurement.

The calibration carried out on the ETS yarn showed that the thermistor manufacturer's equation provided the most accurate temperature readings when compared to the two polynomial equations generated, which are generally used for calibration. The ETS yarns accuracy was determined to be accurate within ± 0.5 °C, which was suitable for detecting difference of 2 °C, for 63% of measurements taken. The percentage of measurements within the ± 0.5 °C range can be

increased by using thermistors with a lower temperature error (lower resistance tolerances) and by automating the production of the ETS yarn hence reducing the fabrication errors.

The break force of the ETS yarn was calculated at 1060 N. The polymer micro-pod was shown to protect the thermistor from applied strain (proven using cyclical strain tests) which is essential as garments are subjected to constant strain during the manufacturing process and during general wear.

In conclusion, the novel electronic temperature sensing yarn developed has been shown to be well suited for making long term measurements of temperature which could be incorporated into a textile fabric or garment. The next chapter will look at the effects of external conditions (ambient temperature, wind speed) on the temperature measurements.

4.7 References

- Behera, B.K., Hari, P.K., 2010. Woven Textile Structure: Theory and Applications. Elsevier.
- BIPM, (Bureau International des Poids et Mesures), 2014. Guide on secondary thermometry Thermistor Thermometry. Consultative Committee for Thermometry under the auspices of the International Committee for Weights and Measures.
- British Standards, 1988. Textiles — Yarns from packages — Method of test for breaking strength of yarn by the skein method (No. BS ISO 6939:1988).
- COMSOL, 2012. The Heat Transfer Module User's Guide - HeatTransferModuleUsersGuide.pdf [WWW Document]. URL http://www.ewp.rpi.edu/hartford/~collir5/MP/OTHER/Reference/HeatTransferModuleUsersGuide.pdf (accessed 7.16.15).
- Das, A., Alagirusamy, R., Kumar, P., 2011. STUDY OF HEAT TRANSFER THROUGH MULTILAYER CLOTHING ASSEMBLIES: A THEORETICAL PREDICTION. AUTEX Res. J. 11.
- Ding, D., Tang, T., Song, G., McDonald, A., 2011. Characterizing the performance of a single-layer fabric system through a heat and mass transfer model - Part I: Heat and mass transfer model. Text. Res. J. 81, 398–411. doi: 10.1177/0040517510388547
- EPCOS, 2011. SMD NTC thermistors, General technical information - pdf-general-technical-information.pdf [WWW Document]. TDK. URL http://de.tdk.eu/blob/188468/download/4/pdf-general-technical-information.pdf (accessed 9.15.15).
- Haghi, A.K., 2011. Heat & Mass Transfer in Textiles, Second Edition. ed. WSEAS Press, Montreal Canada.
- Hahn, D.W., Özişik, M.N., 2012. Heat Conduction Fundamentals, in: Heat Conduction, Third Edition. John Wiley & Sons, Inc., pp. 1–39.

- Hunter, J.D., 2007. Matplotlib: A 2D Graphics Environment. Comput. Sci. Eng. 9, 90–95. doi: 10.1109/MCSE.2007.55.
- Jones, E., Oliphant, T., Peterson, P., 2001. SciPy: Open Source Scientific Tools for Python. [WWW Document]. URL http://www.scipy.org/ (accessed 4.5.17).
- Kawabata, S., Rengasamy, R.S., 2002. Thermal conductivity of unidirectional fibre composites made from yarns and computation of thermal conductivity of yarns. NISCAIR-CSIR India 217–223.
- Kimball, B.R., Decristofano, B., Caldarella, G., 1993. Thermistor calibration procedure for simulated skin sensors (No. NATICK/TR-93/024). U.S. Army Natick Research, development and engineering center.
- Mbise, E., Dias, T., Hurley, W., 2015. Design and manufacture of heated textiles, in: Dias, T. (Ed.), Electronic Textiles Smart Fabrics and Wearable Technology. Woodhead Publishing, Nottingham.
- Min, K., Son, Y., Kim, C., Lee, Y., Hong, K., 2007. Heat and moisture transfer from skin to environment through fabrics: A mathematical model. Int. J. Heat Mass Transf. 50, 5292–5304. doi: 10.1016/j.ijheatmasstransfer.2007.06.016.
- Ressler, K., Brucker, K., Nagurka, M., 2003. A Thermal Time-Constant Experiment. Int. J. Eng. Educ. 19, 603–609.
- Rohsenow, W.M., Hartnett, J.P., Ganić, E.N., 1985. Handbook of heat transfer fundamentals. McGraw-Hill.
- Shishoo, R., 2008. Textile Advances in the Automotive Industry. Elsevier.
- Veit, D., 2012. Simulation in Textile Technology: Theory and Applications. Elsevier.
- Yang, J., Wei, D., Tang, L., Song, X., Luo, W., Chu, J., Gao, T., Shi, H., Du, C., 2015. Wearable temperature sensor based on graphene nanowalls. RSC Adv. 5, 25609–25615. doi: 10.1039/C5RA00871A.
- Yuchai Sun, Xiaogang Chen, Zhonghao Cheng, Xunwei Feng, 2010. Study of heat transfer through layers of textiles using finite element method. Int. J. Cloth. Sci. Technol. 22, 161–173. doi: 10.1108/09556221011018630.
- Zhu, G., Kremenakova, D., Wang, Y., Militky, J., Mishra, R., 2015. Study on the thermal property of highly porous nonwoven fabrics. Ind. Textila 66, 74–79.

5. Evaluating the electronic temperature sensing yarn response under operational conditions

5.1 Introduction

This chapter looks at the electronic temperature sensing (ETS) yarns performance under operational conditions, hence it is broken down into the following sub-sections to provide a clear overview:

- Brief background on contact temperature measurement;
- Identification of the steady state error that occurs when using the electronic temperature sensing yarn;
- Understanding the effects of the micro-pod and the knit braided fibre sheath on the steady state error;
- Analysing the effects on the steady state temperature measured by the ETS yarn when held at different distances away from the surface being measured;
- Identifying the steady state error when the ETS yarn is incorporated in a knitted fabric;
- Understanding the influence of external factors such as ambient temperature, insulation, orientation, moisture content, relative humidity and wind speed on the steady state error.

5.2 Brief background on contact temperature measurement

Accurately measuring skin contact temperature can be essential in clinical and thermos-physiological applications. Skin contact temperature measurement is a complex process which as shown by Psikuta et al is influenced by ambient temperature, sensor shape, contact of its sensing area to the surface and the thermal conductivity of the surface used to hold the sensor (Psikuta et al., 2013).

Temperature measurement is effected by many factors such as calibration against the absolute temperature scale, thermal disturbance due to the method of installation and instability effects (Childs et al., 2000). The effect of ambient temperature and installation type is often overlooked when measuring surface temperature. There are only few publications in which the above has been considered. The errors caused by glues and pastes on thermocouple readings have been studied by Kuznetsov and Mukhammadeev (Kuznetsov and Mukhammadeev, 2010). In a recent publication Liu and Zhang have shown the surface temperature measurement errors caused due to the ambient temperature and the installation type of the Fiber Bragg grating (FBG) sensors (Liu and Zhang, 2016). Deng and Liu have demonstrated the effects on the surface temperature measurement due to the thermal conductivity and the thickness of the material used to fix the thermocouples on the skin (Deng and Liu, 2008). However, the author could not find any publications on the effects of ambient

temperature, fabric construction and other external conditions on temperature measurements by thermistors positioned within fabrics.

The most frequent error in temperature measurement occurs when trying to measure the surface temperature of a solid body when the sensor is in contact with the surface of the body and surrounded by gas or liquid. There are three systematic errors that can occur when measuring the surface temperature of a solid body that is in a thermal steady state. The first partial error occurs as a result of the temperature sensor being in contact with the surface being measured. The sensor causes a more intense heat flow from the surface and this would cause a drop in the surface temperature. The second partial error occurs due to the thermal contact resistance in-between the sensor and the surface; this is caused due to the non-ideal contact between the sensor and the surface. The third partial error occurs due to the sensor design. Generally, the sensing element of the sensor which determines the temperature is not directly in contact with the surface being measured but enveloped inside a casing. Therefore, the temperature at sensing element is different to the temperature of the surface of the sensor casing (Michalski, 2001).

The second partial error which results due to the thermal contact resistance at the interface between the sensor and the surface; is rather difficult to calculate as the thermal contact resistance is influenced by the cleanliness and smoothness of the surface, the pressure the sensor is held on the surface, the elasticity of the surface and the sensor (Michalski, 2001). When considering the ETS yarn there are several other factors such as the micro-pod encapsulating the thermistor, type of fabric containing the ETS yarn and other external factors (wind speed, ambient temperature) that will affect the temperature measurements.

The difference between the true surface temperature and the temperature indicated by the sensor is regarded as the measurement error, and the equation given below is used to calculate the error for thermocouples (*Manual on the Use of Thermocouples in Temperature Measurement*, 1993).

$$Z = \frac{T_s - T_i}{T_s - T_a} \qquad (5.1)$$

Where Z is the measurement error and T_s is the true surface temperature, T_i is the indicated temperature and T_a is the temperature of the surrounding. Due to the lack of such an equation for thermistors it was decided to use equation 5.1 to analyse and compare experimental results of ETS yarns in this chapter.

Since the thermistor is not in direct contact with skin/wound when it is embedded within the ETS yarn, it is important to understand how the micro-pod and the yarn filaments effect the surface temperature measurement. Once the ETS yarn is made it will be incorporated into a textile fabric, the fabric will further impact the temperature measurements. Other external factors such as distance of the sensor from the skin, wind speed (Cengel, 2002), different ambient temperatures

(Psikuta et al., 2013), humidity, and orientation of the ETS yarn (Cengel, 2002) could all impact the temperature measurements.

5.3 Experimental procedure

Test equipment was constructed study the performance of ETS yarns; this consisted of a controllable heating and cooling source and thermocouples. An ECHOTHERM™ IC50 digital Chilling/Heating Dry Bath (henceforth known as dry bath) from Torrey Pines Scientific Inc (Carlsbad, United States) was used as the heating and cooling source for the experiments (information about the dry bath is given in appendix 16). This was selected as it could be used as a heating as well as a cooling source. The dry bath also has a high accuracy of ± 0.2 °C. One of the possible applications of the ETS yarns would be to monitor the temperature of feet when exposed to temperatures around 5 ^{o}C. If ones feet are exposed to such temperatures for a prolonged period of time this could result in non-freezing cold injuries. Therefore, it was decided to test the performance of ETS yarns at temperatures around zero degrees.

Initially it was essential to ensure that there were no hot or cold spots on the surface of the dry bath, and to determine if the surface temperature remained uniform throughout the dry bath surface. This was analyzed with a FLIR i7 hand held thermal camera (FlIR®, Oregon, United States); images of the dry bath were recorded with the dry bath set to 40 °C.

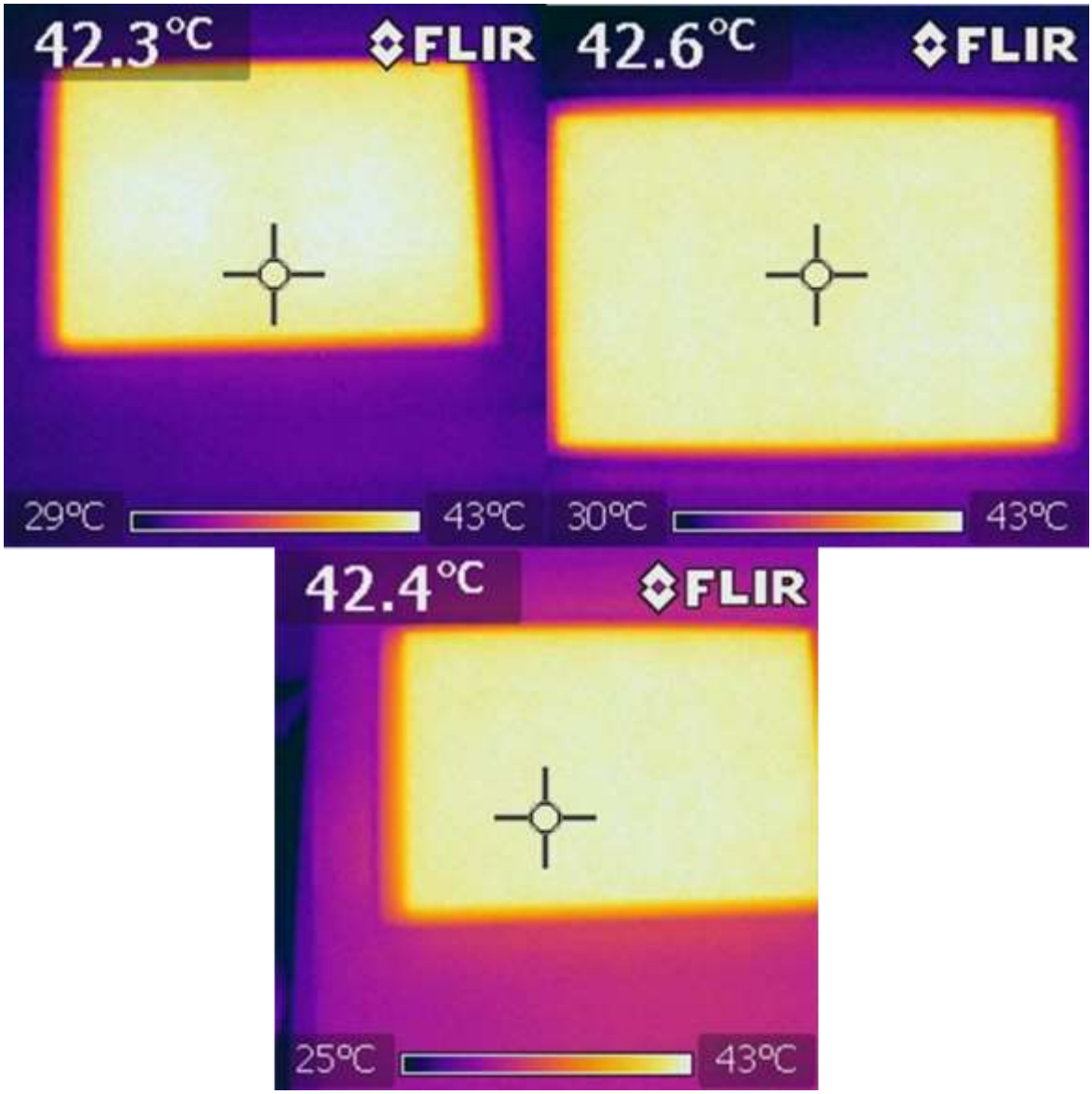

Figure 5-1: Thermal images of the surface of the Ecotherm dry bath set to 40°C recorded with the FLIR thermal camera

The thermal images given in Figure 5.1 shows that the temperature of the dry bath remained uniform throughout the surface, with the temperature varying by less than 0.3 °C. The accuracy of the FLIR i7 given by the manufacturer is ±2 °C and the temperature differences shown in images of figure 5.1 falls within this tolerance band. Therefore it was regarded that the surface of the dry bath provided a uniform heating surface for the samples to be tested during experiments.

The preliminary experiments were carried out by placing the ETS yarn, two thermistors soldered to copper filaments and a k type thermocouple on the surface of the dry bath as shown in Figure 5.2**.** The two NCP15XH103F03RC SMD thermistors soldered onto copper wires were positioned on either side of the ETS yarn (5 mm apart). The K type thermocouple was positioned 40 mm to the left of the ETS yarn. In-order to capture the room temperature another k type thermocouple was positioned 40.0 cm to the right of the dry bath, this ensured that this thermocouple's measurements were not influenced by the dry bath. The thermocouples were connected to a PICO-

TC08 unit from PICO (Pico Technology, St Neots, UK). The resistance of the thermistors and the ETS yarn were determined with a potential divider circuit and a NI USB 6008 DAQ unit (as described in chapter 3 section 3.6.1). The voltage out from the three potential divider circuits which contained the two thermistors and the ETS yarn were connected to the analogue inputs (AI0, AI1, AI2) of the NI USB 6008 DAQ unit. The PIC0-TC08 and the NI 6008 DAQ both were interfaced to the same PC. The values of the resistors used in the potential divider circuit were determined with an Agilent 34410A 6 ½ digital multi-meter which has a precision of 0.01 Ω. The LabVIEW program developed in chapter 4 section 4.2.3 was used to obtain the temperature. The software was enhanced to capture the voltage from the several analogue inputs.

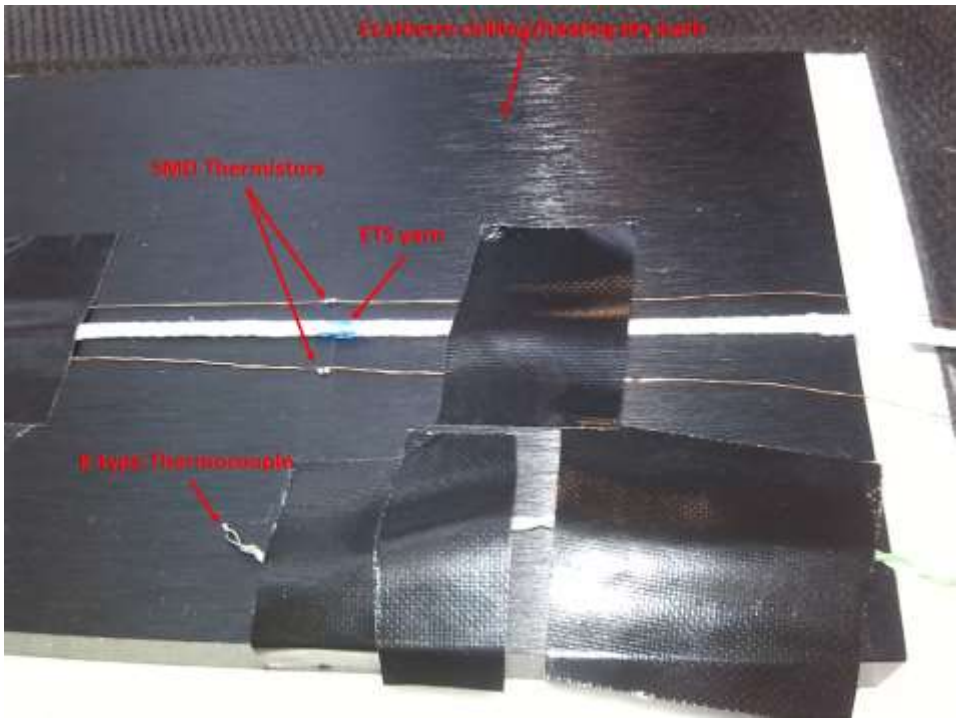

Figure 5-2: The ETS yarn, SMD thermistors and the k type thermocouple attached to the Ecotherm dry bath

5.4 Determination of the steady state error

The first preliminary experiment was done to identify whether the ETS yarn recorded the correct room temperature when the dry bath was switched off; and the experiment was carried out the following day allowing the dry bath's surface to settle overnight to the room temperature. This was carried out in order to identify if the ETS yarn, the thermistors soldered onto copper wire and the thermocouple (k type) recorded the same temperature. The average temperature recorded by the two thermistors were plotted along with the temperature recorded by the ETS yarn and the two thermocouples, and it is given in figure 5.3.

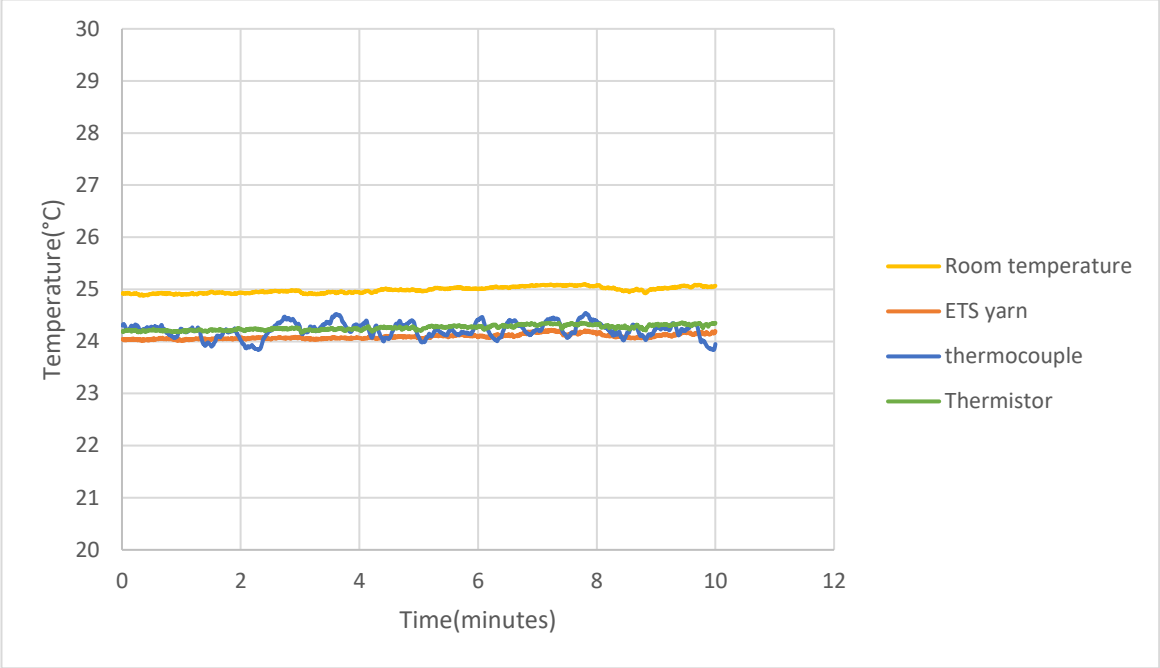

Figure 5-3: Temperature measurements from the ETS yarn, SMD thermistors and the k type thermocouple when the Ecotherm dry bath is switched off and left at room temperature.

It can be observed from the results in figure 5.3 that the temperature measurements of the ETS yarn, the NTC thermistors and the K type thermocouple positioned on the plate recorded the same temperature when it was left in room temperature. The k type thermocouple that is measuring the room temperature seems to be one degree higher than the rest. This maybe as a result of the 1.5 °C tolerance of the k type thermocouples.

Thereafter it was important to identify the response of the ETS yarn, the NTC thermistor and the thermocouple when the dry bath was switched on and set to different temperatures. The response of the three different types of sensors were recorded once the sensors have reached their steady state. Steady state occurs when the variables which define the behaviour of a system is not changing with time ("Steady state," 2016).

Dynamic errors could occur when measuring the surface temperature of a body. Usually this occurs when temperature readings are captured from a sensor before it has reached thermal steady state after coming into contact with the surface being measured. This error is generally eliminated if the sensor is in contact for a sufficient time for steady state to occur (Michalski, 2001). Therefore for steady state to occur it is essential to keep the sensors at a constant temperature for a prolonged period of time. For that reason the dry bath was set to 0 °C, 25 °C and 80 °C and left for 135 minutes at each of the temperatures and the results are given in Figure 5.4.

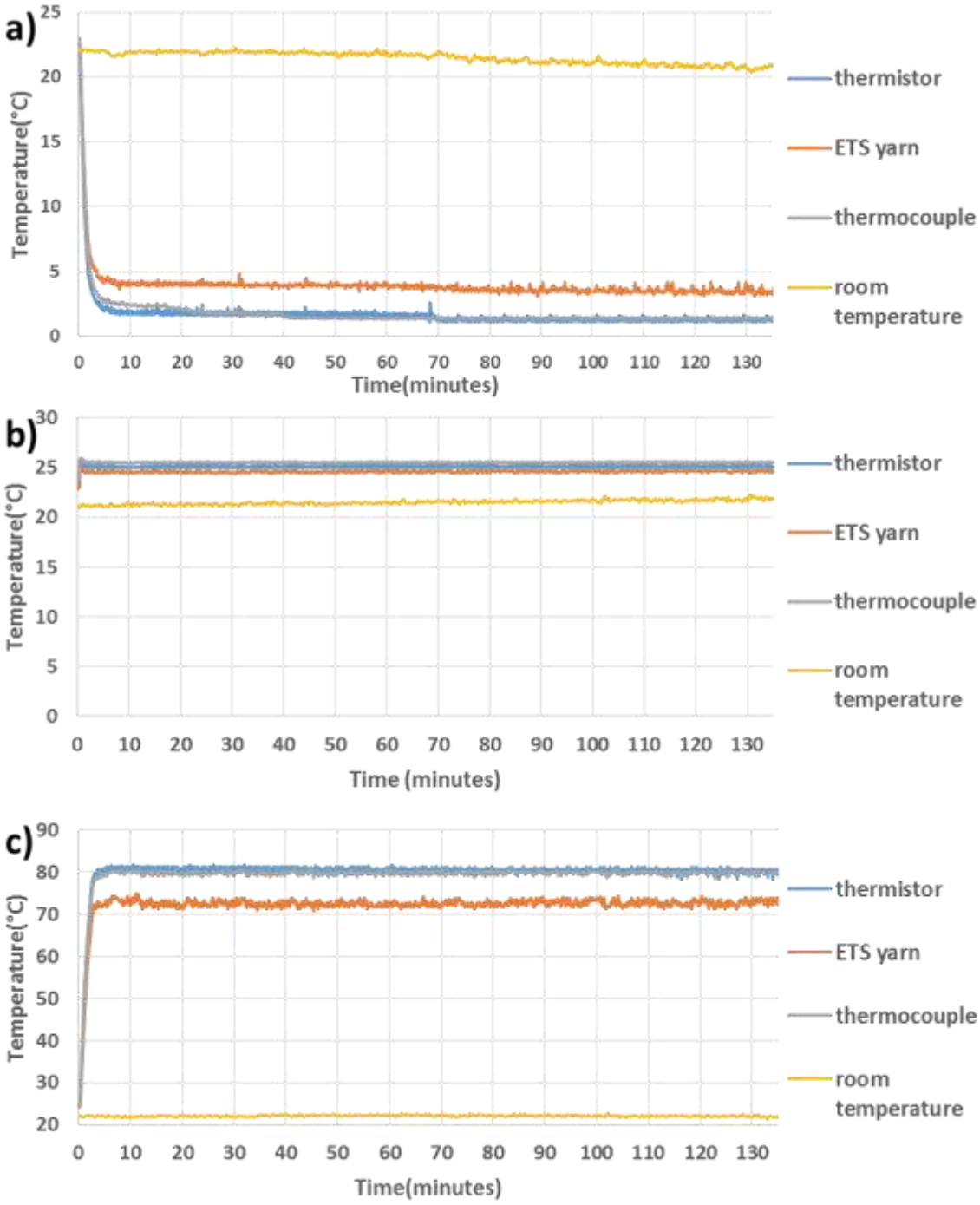

Figure 5-4: Temperature measurements from the ETS yarn, SMD thermistors and the k type thermocouples when a) the temperature of Ecotherm dry bath is set to 0 °C, b) when the dry bath temperature is set to 25 °C and c) when it is set to 80 °C.

As expected from the results in chapter 4 (section 4.2), the results of the experiments shown in figure 5.4a, b, c demonstrates that after the first 5-10 minutes a steady state is reached and when it is reached there is a difference in-between the temperatures recorded by the ETS yarn, the thermistors and the thermocouple. Therefore it was important to understand the cause of this difference in measurements.

In-order to estimate exactly when the steady state occurs the temperature of the dry bath was increased in steps of 10 °C every 10 minutes and the corresponding temperatures were recorded. The thermocouple and thermistor measurements were almost identical once steady state was reached in the previous set of experiments (shown in figure 5.4a, b, c). Therefore for this set of experiments the thermocouple on the plate was removed and the temperature captured from the ETS yarn was plotted along with the temperature recorded by the two thermistors and the k type thermocouple measuring room temperature. It is given in figure 5.5.

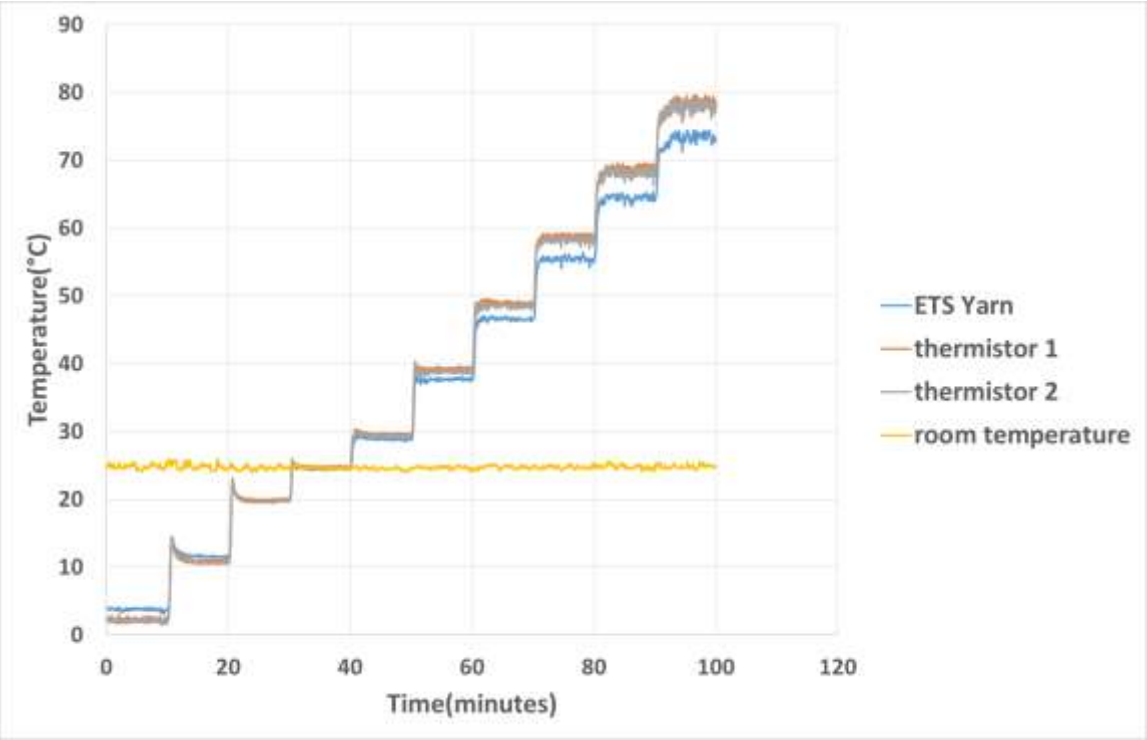

Figure 5-5: The temperature measurements from the ETS yarn, SMD thermistors and the k type thermocouple when the plate temperature is changed every 10 minutes by 10 °C

It can be observed from the results (figure 5.5) that in less than two minutes the ETS yarn and thermistors reach a steady state. Generally the temperature of a wound should be in the range 20 °C to 40 °C therefore, the main set of experiments were carried out for this temperature range. The temperature of the dry bath was increased from 20 °C to 40 °C by increments of 2 °C every 5 minutes. Some experiments were carried out in the range 0 to 40 °C in order to study whether ETS yarns could be used to monitor non-freezing cold injuries, which is common when one's feet are exposed to temperatures between 5-10 ^{o}C. .

For all the experiments stated below the LabVIEW program described in chapter 4 section 4.2.3 was used. However, the software was enhanced to read the voltage from more than one analogue input. Therefore for each experiment three or more samples were tested. Even though three samples was a low for a statistical analysis, given the difficulty to manufacture the samples it was regarded acceptable. However six or more samples were tested for the experiments in sections 5.4.2, 5.4.4, 5.5.1, 5.5.2, 5.5.3, 5.5.6. Each sample was connected to a separate potential divider circuit and to

different analogue inputs of the NI DAQ USB 6008 unit. The plate temperature was measured using two NCP15XH103F03RC SMD thermistors soldered onto copper filaments which was connected through individual potential divider circuits to the NI DAQ USB 6008.

The values of the resistors used in the potential divider circuit was determined with an Agilent 34410A 6 ½ Digital multi-meter (Agilent Technologies, USA) which has a precision of 0.01 %. The room temperature was measured using two k type thermocouples. The thermocouples were connected to a PICO-TC08 unit (Pico Technology, UK). The PIC0-TC08 and the NI 6008 DAQ both were interfaced to the PC.

The program provided 42 temperature readings each minute for each temperature sensors (the samples tested, the two thermistors and the two k type thermocouples). It is shown in appendix 17 table 8.7. The average temperature readings were calculated for each of the temperature sensors after it reached its steady state. It was seen from the previous experiment (figure 5.5) that the steady state was reached in less than 3 minutes after changing the temperature of the dry bath. Therefore the average temperature for each of the temperature sensors were recorded from the 84 readings recorded in between 3-5 minutes after changing the temperature of the dry bath.

Thereafter these averages were used to compute the average of all the samples and plotted, and the results were documented in graphs which are given in figures 5.7, 5.8, 5.9, 5.10, 5.11, 5.14, 5.15, 5.17, 5.19, 5.21, 5.24, 5.25. The confidence intervals were calculated from the sample average measurements and plotted in the graphs. The temperature measurements captured by the two thermistors were averaged and plotted along with the confidence intervals in figures 5.7, 5.8, 5.9, 5.10, 5.11, 5.14, 5.15, 5.17, 5.19, 5.24, 5.25. The temperature captured by the two k type thermocouples have been averaged and plotted along with confidence intervals as room temperature in figures 5.7, 5.8, 5.9, 5.10, 5.11, 5.14, 5.21, 5.23, 5.25 and in experiments where an environmental chamber is used it is plotted as chamber temperature in figures 5.15, 5.17, 5.19, 5.24.

5.4.1 Understanding the effects of the micro-pod on the steady state error

It is important to identify how the construction of the micro-pod of ETS yarn can impact the steady state error. Therefore the first set of experiments were carried out to understand the effects caused due to the polymer resin and the yarn filaments inside the micro-pod. For each of the experiments stated in sections 5.4.1.1, 5.4.1.2, 5.4.1.3 three samples were placed on the dry bath 5 mm apart. Two thermistors soldered to copper filaments were also placed on the two sides as shown in the figure 5.6 below. This was done to ensure that the dry bath surface temperature on either side of the samples remained uniform. Two k type thermocouples were used to capture the room temperature. The ETS yarns and the two thermistors were secured on to the surface of the dry bath using insulating tape (RS Stock No.134-7319, RS, Corby, UK).

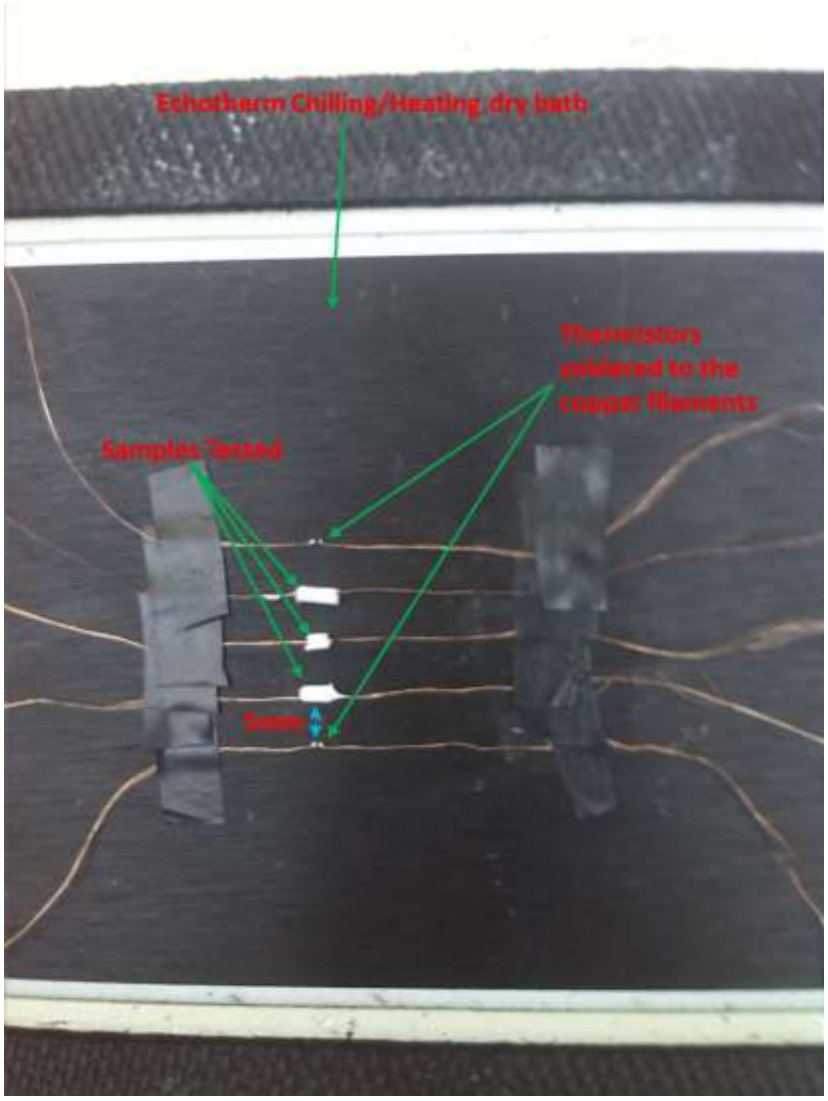

Figure 5-6: Samples and the SMD thermistors attached to the surface of the Ecotherm dry bath

5.4.1.1 Mico-pod formed using heat conductive polymer resin

It was important to identify if the thermal conductivity of the polymer resin used to create the micro-pod had any effect on the steady state error. Therefore the initial experiments were carried out with the micro-pods of different diameters, which were crafted using the heat conductive UV curable Multi-Cure® 9-20801 resin (data sheet in appendix 8). The samples that were used in section 4.2.1 in Chapter 4 were also used for these experiments. As discussed in section 4.2.1 a 5.00 mm diameter micro-pod was too large for an ETS yarn. Therefore a 5.00 mm diameter micro-pods have not been evaluated for the experiments stated in sections 5.4.1.1 and 5.4.1.2. Hence, the testing was limited to cylindrical micro-pods of 0.87 mm and 1.53 mm diameters.

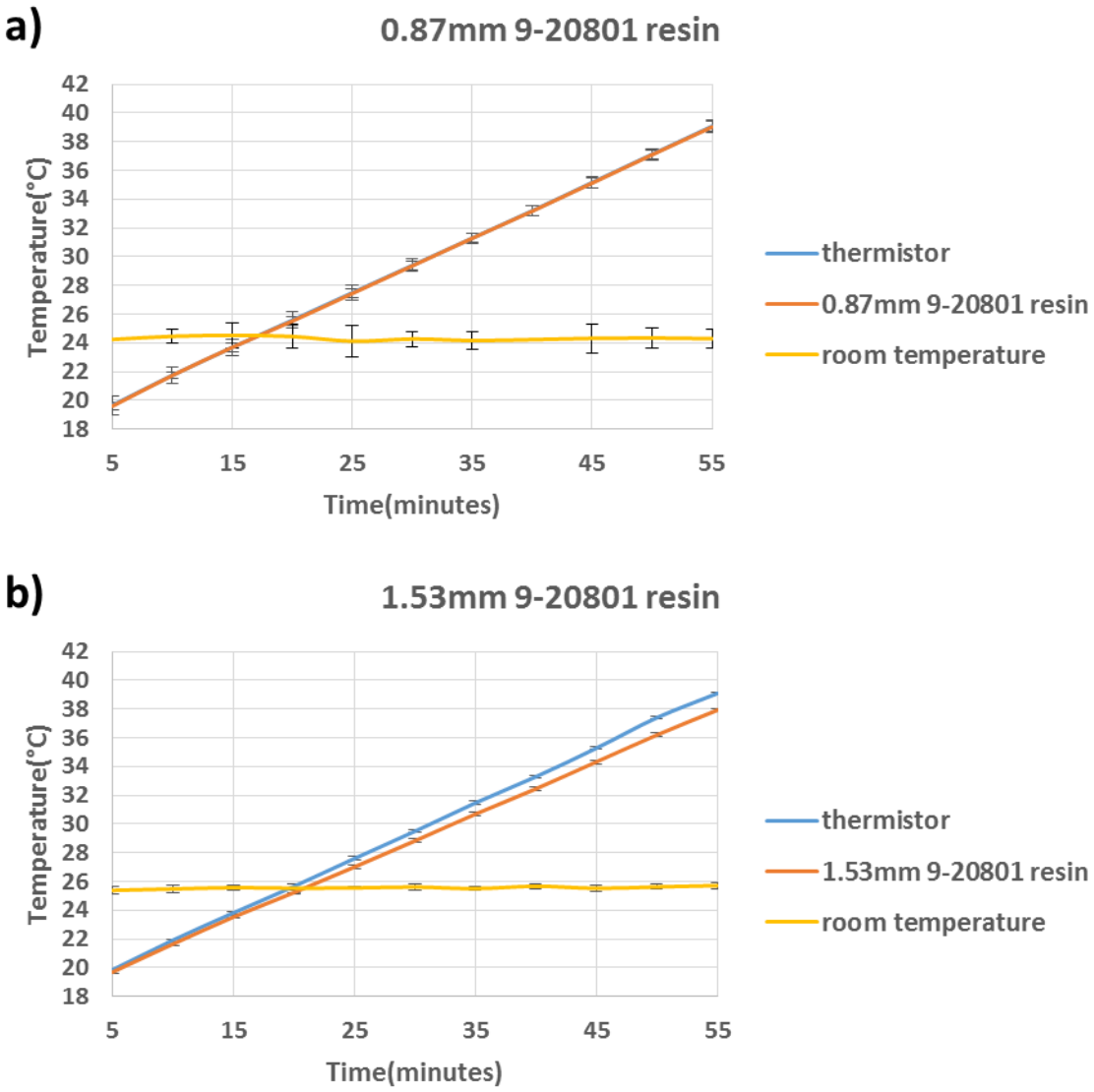

Figure 5-7: The results from the experiments where the average temperature recorded by the three samples is plotted when it is encapsulated by 9-20801 resin to form a cylindrical micro-pod of diameter a) 0.87mm and b) 1.53mm

The 9-20801 polymer resin as seen in figure 5.7a seem to have no impact on the temperature measurements with a 0.87 mm diameter cylindrical micro-pod. It can be seen from the figure 5.7b that there is a difference between the measurements of the thermistors on the dry bath surface and the thermistors positioned within the 1.53 mm diameter micro-pod (in the temperature range of 26 °C to 40 °C). This error could be caused due to the increase in the distance between the thermistor in the micro-pod and the dry bath surface, when a 1.53 mm diameter micro-pod is used. Assuming that the heat flow through the micro-pod is due to thermal conduction. Fourier's law of heat conduction can be used to show that the difference in temperature (ΔT) between the dry bath surface and the thermistor surface is directly proportional to Δx the location of the thermistor with regard to the dry bath surface. Fourier's law of heat conduction is given in equation 5.2 (Cengel, 2002)

$$\Delta T = -\frac{\Delta x Q_{Cond}}{kA} (5.2)$$

Where k is the thermal conductivity of the material (in this case the 9-20801 polymer resin), A is the heat transfer area and Q_{Cond} is the rate of heat conductance (Cengel, 2002).

It can be concluded from the results in figure 5.7 that the 0.87 mm diameter is the optimum diameter for the micro-pod since it does not bring about a steady state error. Therefore it can be stated that a 0.87 mm micro-pod created using thermally conductive 9-20801 polymer resin brings about no measurement error in the thermistor measurements.

5.4.1.2 Micro-pod formed using non-heat-conductive polymer resin

The next set experiments were carried out with samples having a 0.87 mm, 1.53 mm diameter cylindrical micro-pods formed using a non-conductive UV curable resin Multi-Cure® 9001-E-V-3.5 resin (data sheet in appendix 9).

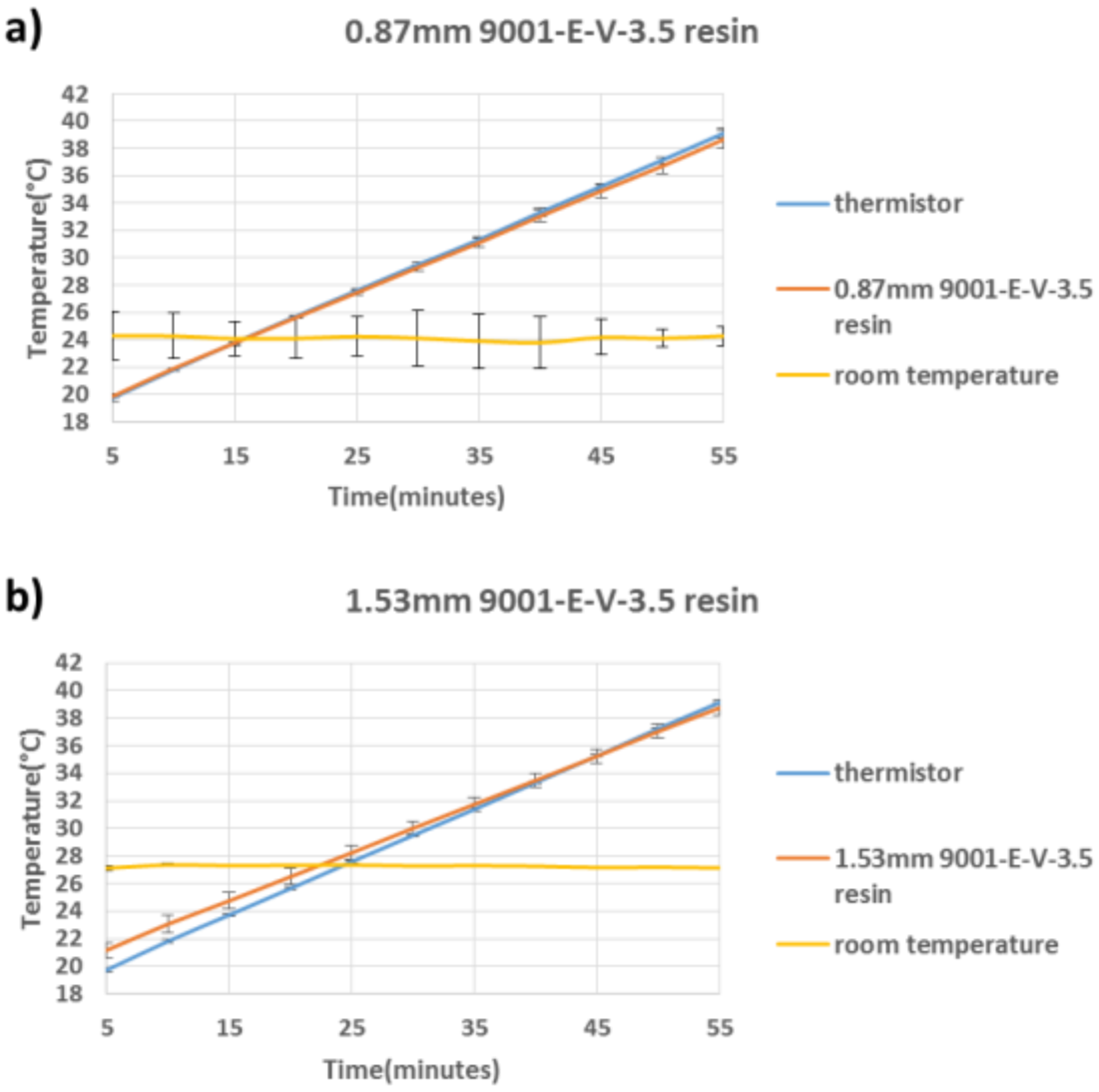

Figure 5-8: The results from the experiments where the average temperature recorded by the three samples is plotted when it is encapsulated by 9001-E-V-3.5 resin to form a cylindrical encapsulation of diameter a) 0.87 mm and b) 1.53 mm

It can be observed from the results in figure 5.8a that the thermally non-conductive 9001-E-V-3.5 resin has no impact when the diameter of the micro-pod is 0.87 mm. However increasing the diameter of the micro-pod makes the sample measurements deviate from the thermistor measurements as expected. However as discussed earlier for the optimum diameter of 0.87 mm there is no change in the measurements. Therefore it can be stated that the thermally non-conductive 9001-E-V-3.5 does not bring about a steady state error, when it is used to create a micro-pod of 0.87 mm diameter.

5.4.1.3 Micro-pod formed using 9-20801 polymer resin and yarn fibres

The following set of experiments were carried out to see how the fibres within the 0.87 mm micro-pod effect the steady state error.

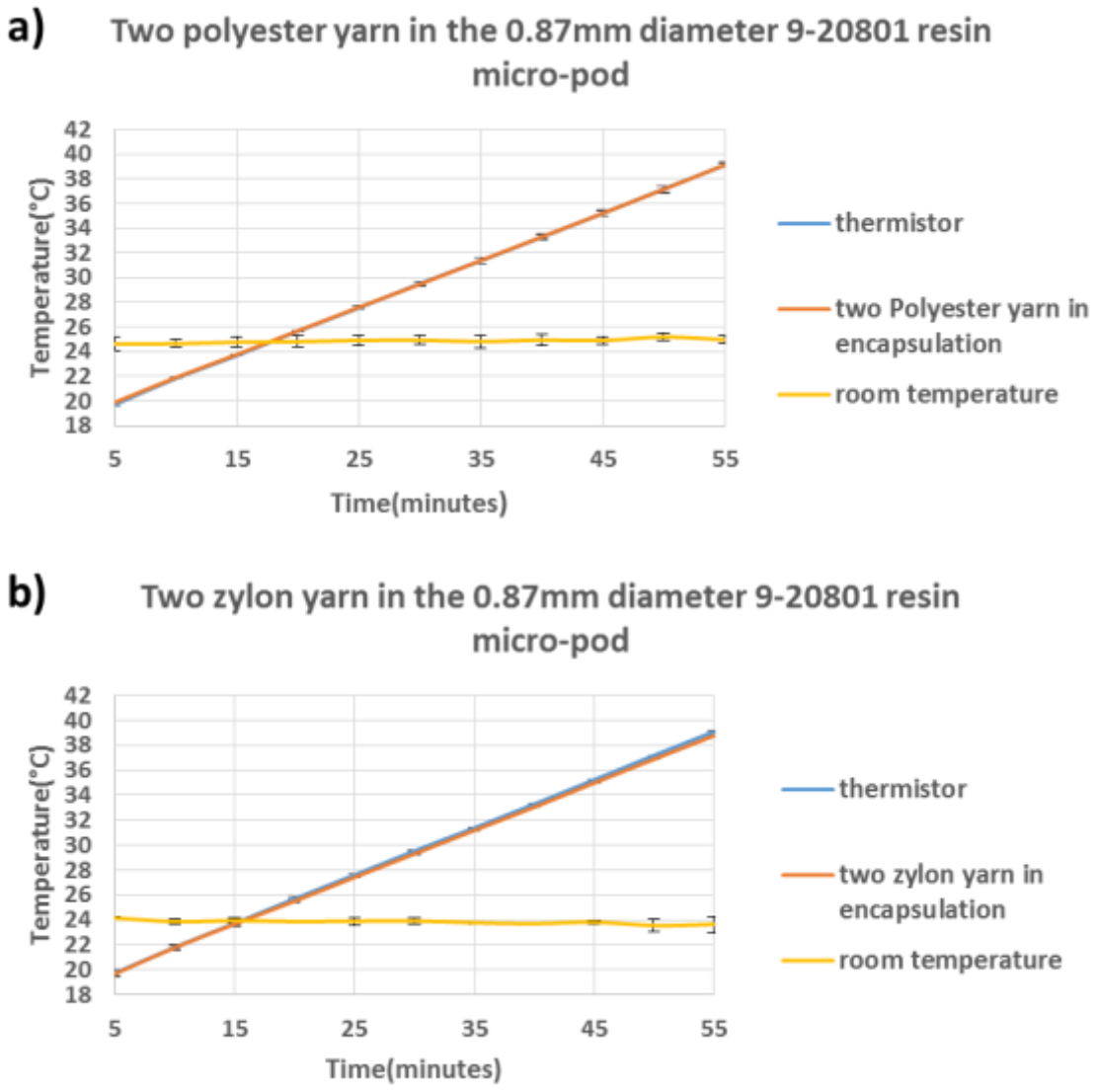

Figure 5-9: The results from the experiments where the average temperature recorded by the three samples is plotted when it is encapsulated by 9-20801 resin to form a cylindrical micro-pod of 0.87 mm diameter containing a) two polyester b) two zylon yarn inside the micro-pod.

It could be concluded from the graph in figure 5.9 that the fibres within the micro-pod does not seem to create a steady state error.

Therefore it can be concluded that the polymer micro-pod containing the polyester/zylon fibres and the polymer resin 9-20801 does not create a measurement error in the measurements.

5.4.2 Study of the effects of the knit braided fibre sheath and packing fibres on the steady state error

The next step was to identify the impact on the temperature measurements caused due to the packing fibres and braided yarn layer. Therefore six ETS yarn were positioned 5 mm apart on the surface of the dry bath with two thermistors soldered to 8 strands copper wire placed on either side of the six ETS yarn. The thermistors were positioned 5 mm apart from the nearest ETS yarn. The temperature of the dry bath was changed from 0 °C to 40 °C in steps of 2 °C every 5 minutes and the measurements of the ETS yarn and the SMD thermistors were recorded. The k type thermocouples used to capture the room temperature were positioned 40 cm to the left of the dry bath (this ensured that this thermocouples measurements were not influenced by the dry bath).

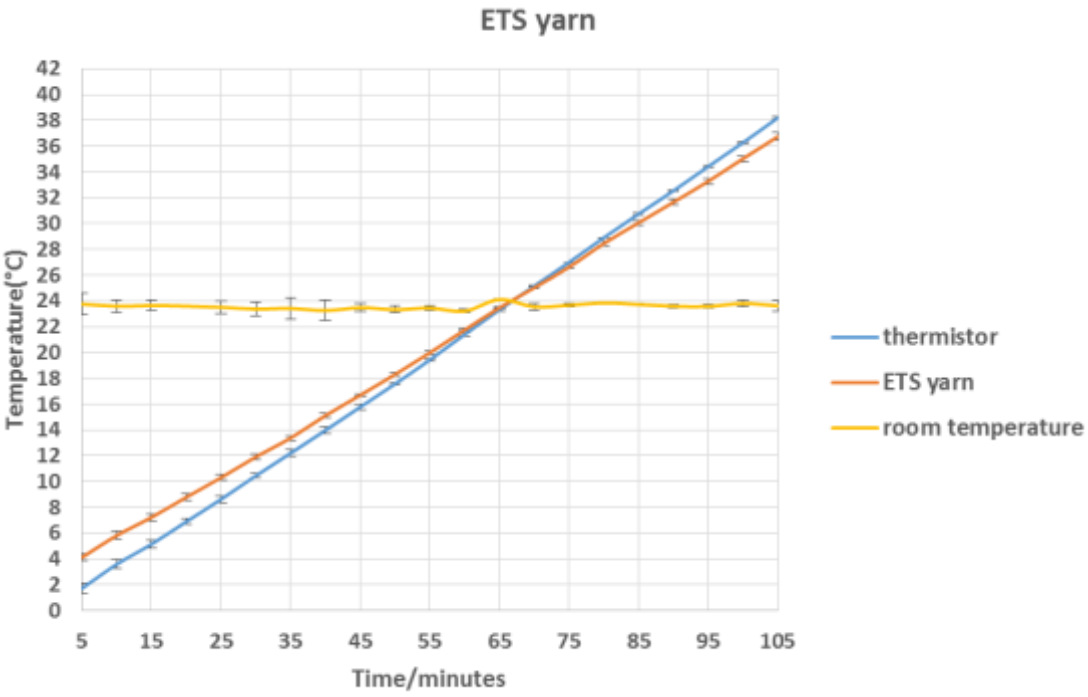

Figure 5-10: The average temperature recorded by the six ETS yarns were plotted along with the average temperature recorded by the two SMD thermistors and the average temperature recorded by the two k type thermocouples, when the temperature of the Ecotherm dry bath was changed from 0 °C to 40 °C in steps of 2 °C

The graph in figure 5.10 shows that the packing fibres and the braided yarn layer impact the temperature measurements. The temperature of the thermistor and the yarn is constant at room

temperature but when the temperature difference in-between room temperature and dry bath temperature increases, the difference between the temperature captured by the ETS yarn and the thermistor increases. This is brought about as a result of the increase in distance between the thermistor surface and the dry bath surface due to the layer packing fibres and the knit braided layer. Equation 5.2 in section 5.4.1.1 states that the difference in temperature (ΔT) between the dry bath surface and the thermistor surface is directly proportional to Δx the location of the thermistor with regard to the dry bath surface. Therefore it can be said that the packing fibres and the braided yarn layer causes a steady state error in the temperature measurements of the ETS yarn.

The measurement error caused due to the packing fibres and the braided yarn can be calculated as 0.12±0.006 using equation 5.1 given in section 5.2. Therefore by using this value and the equation 5.1 the actual temperature of the surface can be obtained from the temperature captured by the ETS yarn.

5.4.3 Understanding the effects of positioning ETS yarn at different distances away from the surface being measured

Textile yarns in a textile fabrics or garments may not always be in contact with the wearer's skin. There might be a small air gap in between the inner side of the fabric and the skin of the wearer. Therefore it is vital to understand the impact on the temperature measurements caused due to it. By holding the ETS yarn at different heights above the surface of the dry bath, it is possible to mimick this effect. However, it is impossible to estimate the exact height of the air gap since this would depend on the fabric content, position of the ETS yarn and also the fit of the garment on the wearer's body. Therefore for the following set of experiments the ETS yarn was positioned 0.0 mm (directly on the plate), 0.5 mm, 1.0 mm, 2.0 mm, 5.0 mm and 10.0 mm above the plate of the dry bath. In-order to achieve this small block of silicon 10 mm by 10 mm with varying heights (0.5 mm, 1.0 mm, 2.0 mm, 5.0 mm and 10.0 mm) was positioned on the two edges of the dry bath. The ETS yarn were positioned on top of the silicon blocks and the sensing element (micro-pod) of the ETS yarn was positioned in the middle of the dry bath (50 mm away from both the silicon blocks). These experiments were carried out on different days in a room that was not environmentally controlled therefore the room temperatures for each day was different. Hence the average room temperature was plotted with the maximum and minimum room temperatures plotted in green on the error bars in figure 5.11 below.

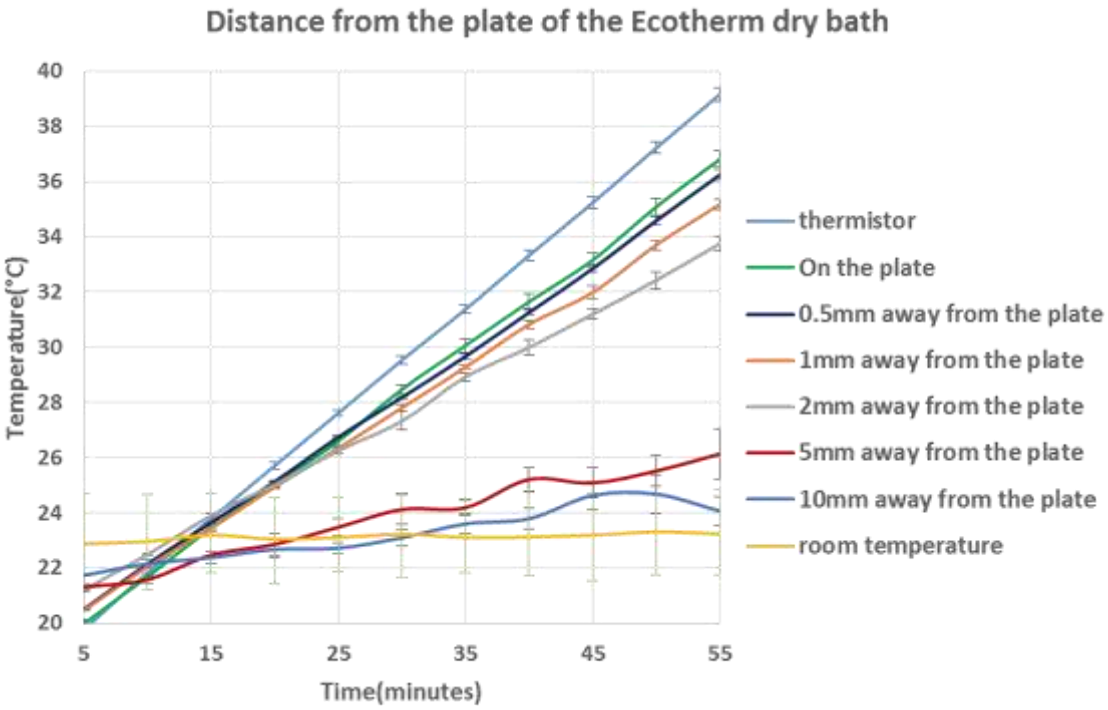

Figure 5-11: Temperature measurements of the ETS yarn when it is held at different heights above the surface of the Ecotherm dry bath

It can be observed from the results in figure 5.11 that keeping the ETS yarn at different heights from the surface of the dry bath increases the measurement error. It can also be seen from figure 5.11 that when the ETS yarns were kept at 5 mm and 10 mm above the plate, the ETS yarns were almost capturing room temperature. Therefore it can be concluded that these ETS yarns do not capture any significant measurements when it is positioned more than 5 mm away from the surface being measured. The graph 5.12 below gives the relationship between the distance of the ETS yarn from the surface of the dry bath and the measurement error (measurement errors when the ETS yarn is kept 5 mm and 10 mm away from the dry bath have not been included since they are irrelevant).

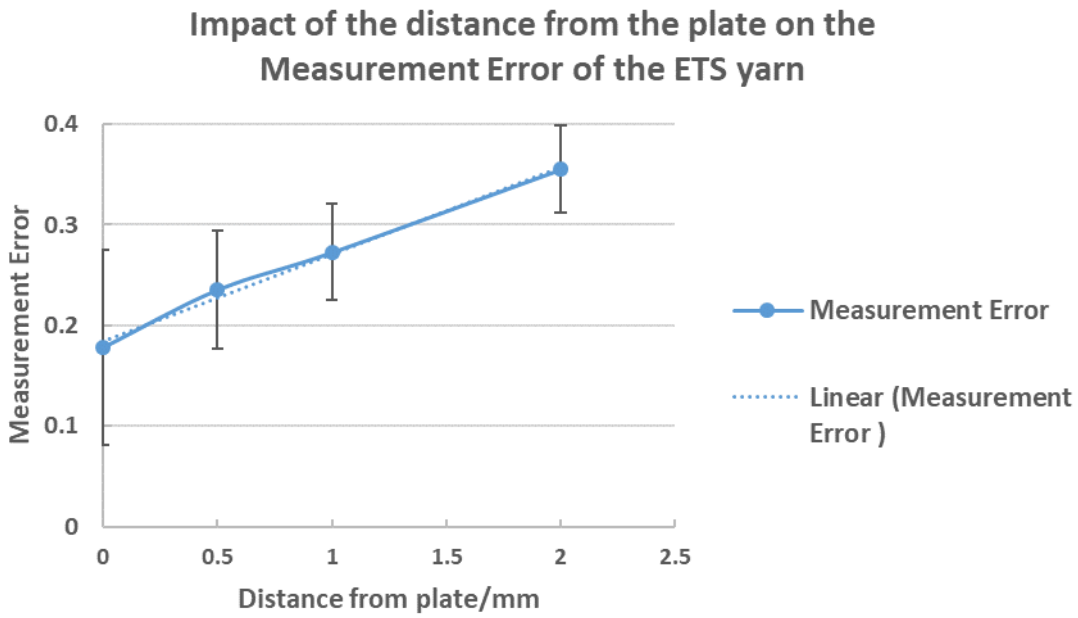

Figure 5-12: Relationship between the measurement error (measurement error calculated using equation 5.1 in section 5.2) and the distance of the ETS yarn from the surface of the dry bath

It can be observed from figure 5.12 that the measurement error increases linearly with the increase in the distance from the plate. This effect can be related to Fourier's law of heat conduction given in equation 5.2 (section 5.4.1.1) where, the difference in temperature between the ETS yarn and the dry bath surface is directly proportional to the distance in between them. However this is assuming that the air in-between the dry bath surface and the ETS yarn is dead air and there is no convection. Also assuming that the white fibres and the white micro-pod make a light and shiny surface. Light and shiny surfaces have the lowest absorption and emission of radiant heat (McMullan, 2012), (Avison, 2014).

Even when the ETS yarn is kept 0.5 mm away from the dry bath the measurement error increases to 0.24±0.03. Therefore it is crucial to ensure that any garment knitted or woven using ETS yarn is held in contact with the skin surface when taking temperature measurements. However when used as a wound dressing it is envisaged that the ETS yarn will be held in contact with skin/wound due to the bandage that would be wrapped around the wound dressing.

5.4.4 Effects of incorporating the electronic temperature sensing yarn in a textile fabric

The ETS yarn has to be knitted or woven into a fabric so that it could be applied as a wound dressing or worn as a garment. Since the ETS yarn is currently produced in small quantities it is difficult to knit using the ETS yarn. Therefore a new method was developed within the Advanced Textiles Research Group to incorporate ETS yarn post knitting, where 2.0 mm diameter channels were formed in fabrics during the knitting process, in order to insert ETS yarn. This enabled positioning of the thermistors accurately to predetermined locations of the fabric or garment. Using this technology a fabric was knitted with 8 channels positioned one after the other using 3/24 combed

100% white cotton yarn in a E14 Stoll ADF 32W knitting machine (Stoll, Reutlingen, Germany). For these experiments eight ETS yarn were positioned within the knitted fabric. The knitted fabric was held onto the dry bath surface using fabric tape as shown in figure 5.13 below.

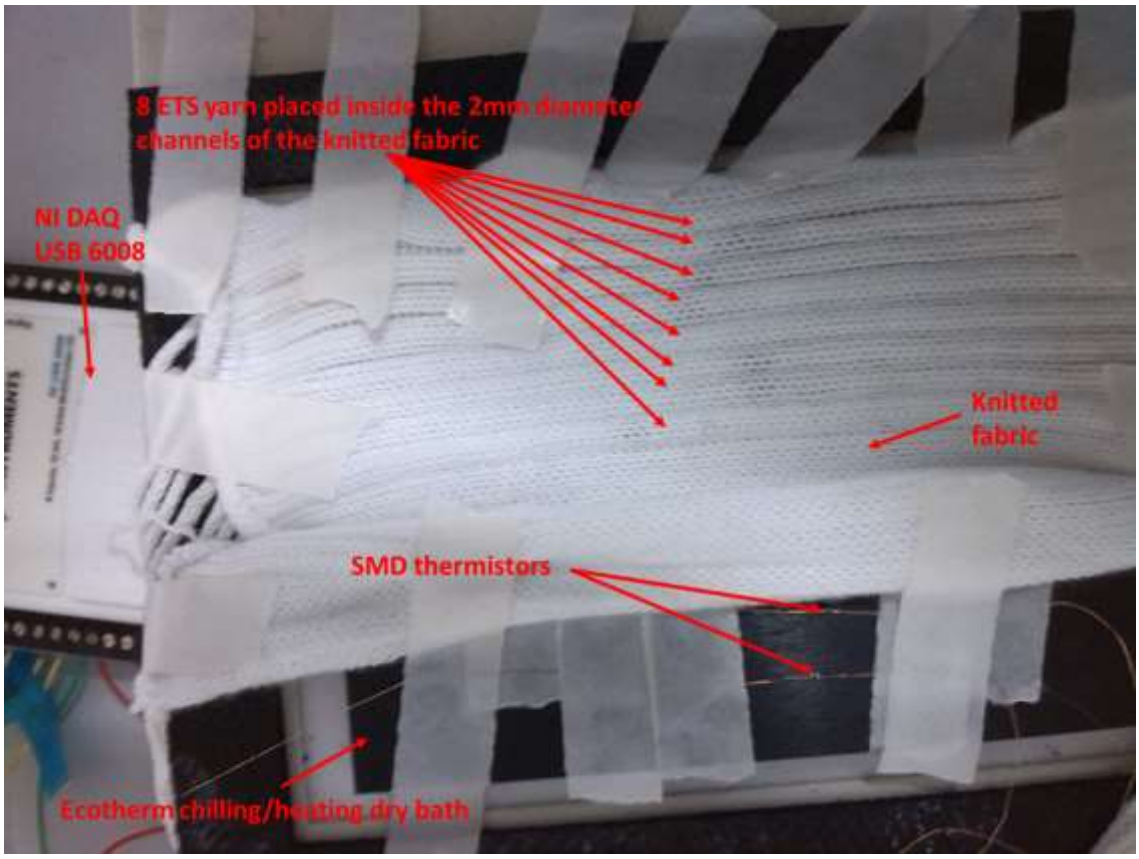

Figure 5-13: Eight ETS yarn positioned in the knitted fabric and attached to the surface of the Ecotherm dry bath

The plate temperature was changed from 0-40 °C in steps of 2 °C every five minutes. The temperature measurements after the steady state has occurred were recorded and has been plotted in the figure 5.12 below.

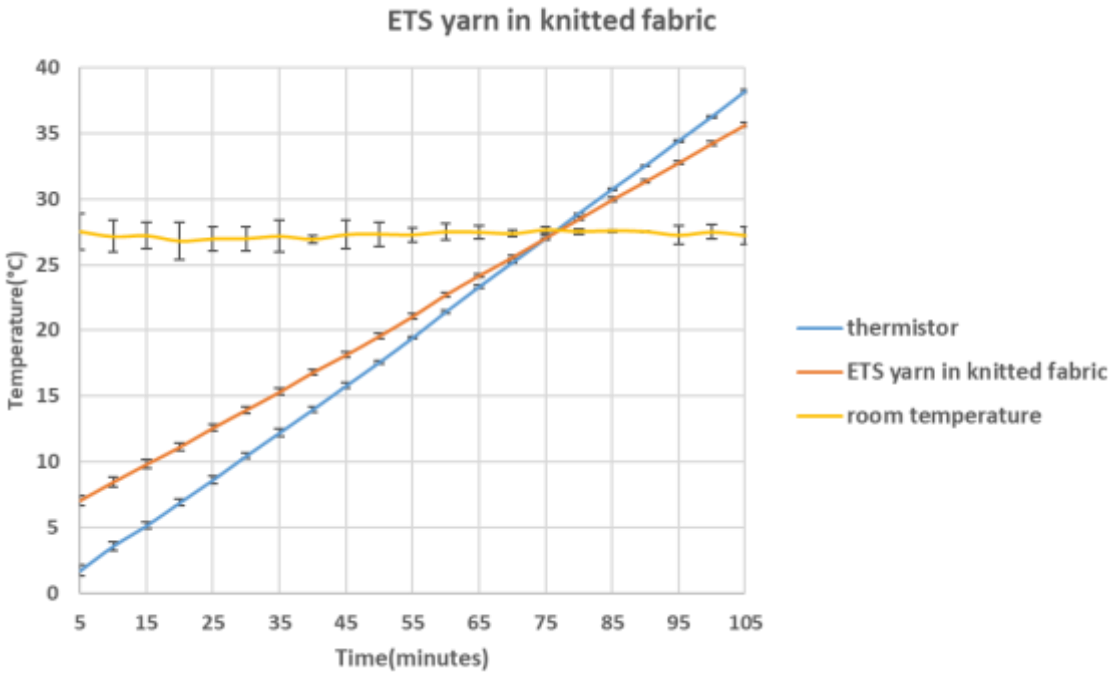

Figure 5-14: The average temperature recorded by the eight ETS yarn within a knitted fabric was plotted along with the average temperature recorded by the two SMD thermistors and the average temperature recorded by the two k type thermocouples.

The graph (figure 5.14) above demonstrates that when the ETS yarn was placed inside the knitted fabric it increased the steady state error. The measurement error increases to 0.24±0.06 (using equation 5.1 in section 5.2) when compared to the measurement error of 0.12±0.006 when the ETS yarn was used (given in figure 5.10). This might have been caused due to the ETS yarn being further away from the surface of the plate and due to the insulation bought about by the layer of cotton in-between the ETS yarn and the surface of the dry bath.

5.5 External factors that influence temperature measurement

For the next set of experiments the ETS yarn positioned within the knitted fabric has been used.

5.5.1 Effects of ambient temperature

The surface temperature measurement will be influenced by ambient/room temperature (Psikuta et al., 2013). Therefore it is important to understand the effects of ambient temperature on the temperature measurements of the ETS yarn. Hence a Benchtop Environmental Chamber from Thermotron (Thermotron(R), Michigan, USA) was used to provide different ambient/chamber temperatures. The Ecotherm dry bath was placed inside the environmental chamber and the temperature of the dry bath was set to 37 °C. The knitted fabric containing 8 ETS yarn was held on top of the plate using fabric tape. The chamber temperatures was set to 0 °C, 10 °C, 20 °C, 25 °C, 30 °C, 40 °C, 50 °C and at each of the temperatures the dry bath was kept for 10 minutes and the measurements were obtained during the last two minutes. This was done in-order to ensure that

everything reached equilibrium (steady state). The temperature inside the thermotron chamber was measured using thermocouples. The relative humidity was set to 60%.

The chamber temperature of the thermotron did not reach 0 °C, the minimum temperature it reached was 7.0 °C. At 50 °C water droplets formed on the surface of the dry bath. This effected the readings of the two thermistors soldered onto the copper wires. Therefore the measurements at 50 °C were taken after the first five minutes. The x axis of the graph (figure 5.15) below gives the chamber temperature whereas the y axis gives the temperature measured by the thermistor and the ETS yarn.

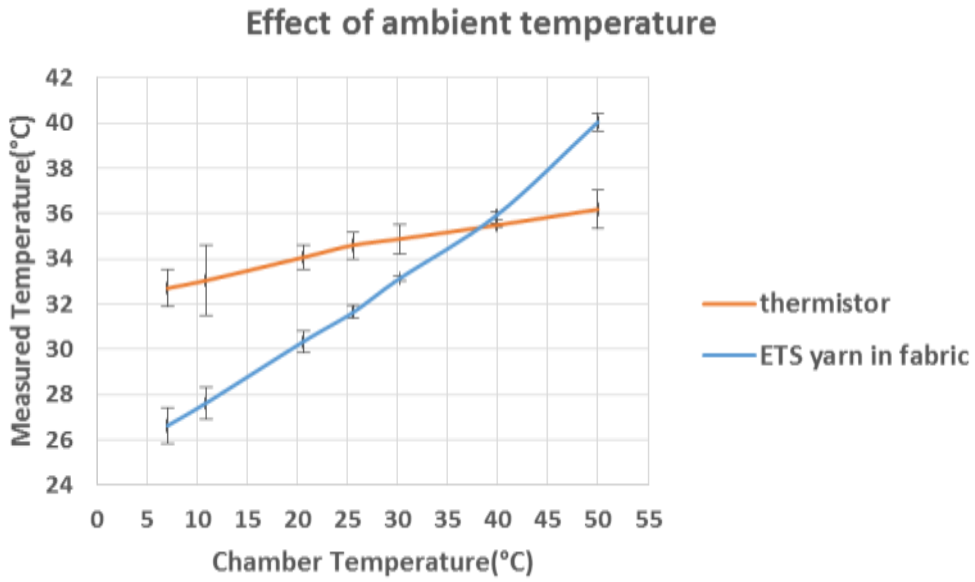

Figure 5-15: Effects of ambient temperature on the ETS yarn (average temperature recorded by the eight ETS yarns have been plotted) and the thermistor (average temperature recoded by the two SMD thermistors) measurements

It can be observed from the graph (figure 5.15) that the ambient temperature has an effect on the measurements of both the thermistor and the ETS yarn. The ambient temperature effects the ETS yarn more than the thermistor. By using equation 5.1 (section 5.2) the measurement error can be calculated as 0.26±0.03 which is similar to the measurement error obtained (0.24±0.06) when the knitted fabric was placed at room temperature and the dry bath surface temperature was changed (given in figure 5.14). This proves the impact of ambient temperature on surface temperature measurement and validates the equation 5.1 which is used in this chapter.

5.5.2 Effects of using an insulating material to cover the fabric

It is envisaged that the wound dressing made using ETS yarn would be positioned in contact with the wound and that there would be a bandage positioned on top of it giving it insulation. The experiments carried out by Buono and Ulrich (Buono and Ulrich, 1998) in various environmental conditions has shown that thermistors when covered record higher body temperatures compared

to when the thermistors were not covered. Therefore the following test were carried out to identify how the material used to cover the dressing would impact on the temperature captured.

Three different material were chosen to cover the knitted fabric containing the ETS yarn for these experiments; a knitted fabric, a knitted spacer fabric and an aluminium plate. The knitted fabric used as the cover was a 1 x 1 rib structure knitted using an acrylic 2/28 nm yarn using the E14 Stoll ADF 32W 3 machine. The thickness of the knitted fabric was measured at 2.2±0.1 mm using a Shang Hai Heng Liang micrometer. The spacer fabric was knitted using 167dtex/48filament polyester yarn using an E16 Stoll CMS822HP machine. The spacer structure was 4 ends and 16 tucks spacer of thickness 5±0.1 mm measured using a Shang Hai Heng Liang micrometer. The thickness of the aluminium plate used to cover was measured at 0.99±0.02 mm using an Electronic digital calliper. In order to ensure that the covering fabric (knitted fabric/spacer fabric) or metal plate is held in place two 50 g weights were placed on either side of the covering fabric/sheet as shown in the figure 5.16 below. The metal weights were kept on the edge of the plate to ensure that their thermal conductivities have minimum impact on the temperature readings captured by the ETS yarn.

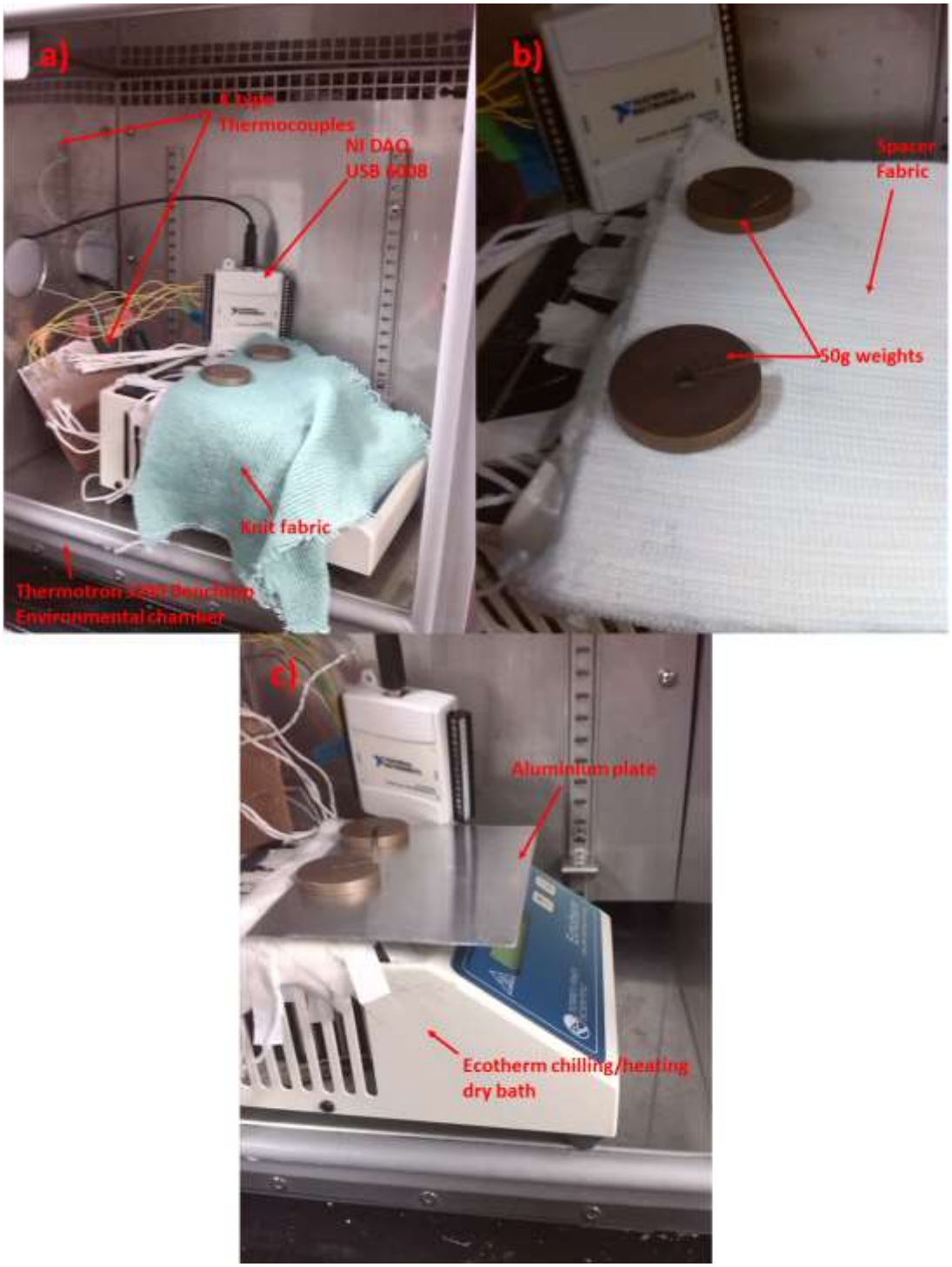

Figure 5-16: The ETS yarn in the knitted fabric covered by a) knitted fabric, b) Spacer fabric and c) Aluminium plate

These experiments were carried out inside the Thermotron Environmental chamber and the chamber temperature was set to 25 °C and the relative humidity was set to 60%. The temperature of the dry bath was changed from 20-40 °C in steps of 2 °C every 10 minutes. The time interval for each temperature step was increased from 5 minutes to 10 minutes to ensure that both the chamber temperature and the plate temperature reached a steady state. The temperature measurements after the sensors reached steady state was recorded.

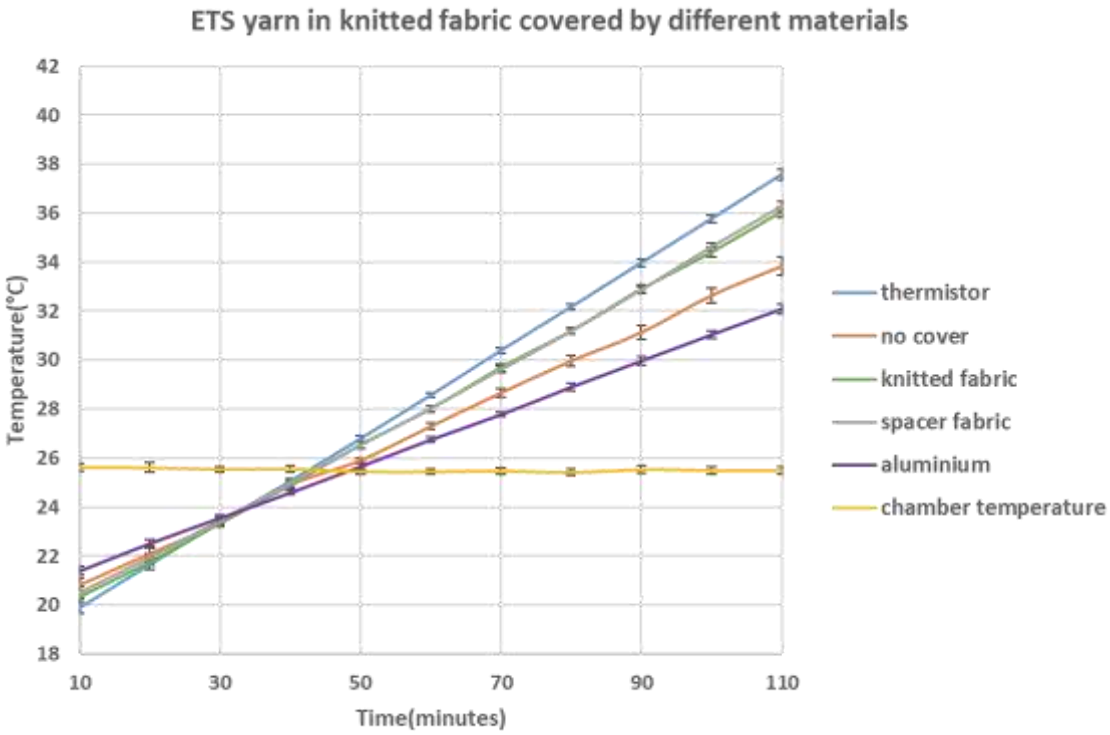

Figure 5-17: Effects on the temperature measurements given by the ETS yarn (average of the temperature recorded by the 8 ETS yarns plotted) due to covering the knitted fabric containing ETS yarn with different materials

The results seen in figure 5.17 has shown that covering the knit fabric with an insulator (knitted fabric or a spacer fabric) reduces the measurement error whereas covering it with a conductor (aluminium) increases it. This is expected according to Fourier's law of heat conduction given in equation 5.2. The thermal conductivity of the material used to cover the ETS yarn is indirectly proportional to the temperature difference between the knitted fabric and the surrounding. Therefore increasing the thermal conductivity of the material increases the heat flow from the ETS yarn to the surrounding assuming all the other variable remain constant. Thus the increase steady state error when aluminium is used to cover the knitted fabric. When the knitted fabric and the spacer fabric are used to cover the knitted fabric the steady state error decreases because they (knitted fabric and spacer fabric) are insulators and they reduce the amount of heat flowing from the ETS yarn to the surrounding. There is no significant difference between the temperatures recorded when the knitted structure is covered using the knitted structure and the spacer fabric.

However when ETS yarn are used in wound dressings it is envisaged that the bandage that will be wrapped around the dressing would be an insulator and provide insulation to the ETS yarn.

5.5.3 Measuring temperature from a vertical surface

The orientation of the ETS yarn when worn in a garment will depend on the posture of the wearer. If the yarn is placed on the stomach of the wearer and the wearer is standing against gravity the yarn will be oriented vertically however if the wearer is lying down the ETS yarn will be oriented

horizontally. Therefore, it is important to identify if the orientation of the ETS yarn impacts its measurements.

Literature has shown that the orientation of the surface could impact the heat transfer from that surface. The heat transfer from the human body to the atmosphere can take place by conduction, radiation and natural convection in the absence of forced convection. The transfer of heat due to natural convection from a surface depends on the geometry of the surface as well as its orientation. Natural convection occurs when a hot surface heats up the air adjacent to it by conduction causing the adjacent air to have a lower density. At constant pressure the density of a gas is inversely proportional to its temperature. This causes the lower density air to rise allowing high dense cooler air to take its place. This process repeats itself cooling the surface. The opposite happens if a cold object is placed in a hot room. A widely used simple correlation for the average Nusselt number (Nu) in natural convection is given by the equation 5.3 (Cengel, 2002).

$$Nu = \frac{hL_c}{k} = CRa_L^n \qquad (5.3)$$

Where h- average heat transfer coefficient of the surface, Lc- characteristic length of the geometry (in the case of the ETS yarn the micro-pod length), C and n depends on the geometry of the surface and the flow regime. Ra_L is the Rayleigh number and it is a product of Grashof (Gr_L) and Prandtl (Pr) numbers and is given in the equation 5.4.

$$Ra_L = Gr_L Pr = \frac{g\beta(T_s - T_a)L_c^3}{v^2} Pr \qquad (5.4)$$

Where g- gravitational acceleration, β-coefficient of volume expansion, T_s- Temperature of the surface, T_a-temperature of fluid sufficiently far from the surface, L_c - characteristic length of the geometry (micro-pod length) and v- kinematic viscosity of the fluid.

Assuming that the ETS yarn is cylindrical, the Nusselt number for natural convection off a cylinder surface when it is vertical and horizontal are given by the equations 5.5 and 5.6 respectively.

$$Nu = \left(0.825 + \frac{0.387 Ra_D^{\frac{1}{6}}}{\left(1+\left(\frac{0.492}{\mathrm{Pr}}\right)^{\frac{9}{16}}\right)^{\frac{8}{27}}} \right)^2 \qquad (5.5)$$

$$Nu = \left(0.6 + \frac{0.387 Ra_D^{\frac{1}{6}}}{\left(1+\left(\frac{0.559}{\mathrm{Pr}}\right)^{\frac{9}{16}}\right)^{\frac{8}{27}}} \right)^2 \qquad (5.6) \text{ (Cengel, 2002)}$$

The Nussel number is used to calculate the average convection coefficient (h) using equation 5.3 and then rate of heat transfer from natural convection (Q_{conv}) can be identified by using the Newton's law of cooling given in equation 5.7.

$$Q_{conv} = hA_s(T_s - T_a) \quad (5.7)$$

Where A_s - heat transfer surface area and h- average heat transfer coefficient of the surface

The results from equation 5.7 show the rate of cooling/heating due to the atmosphere will be higher when the ETS yarn is held vertical when compared to when it is held horizontal (since the Nussel number is higher for a vertical surface assuming all other factors remained constant). Therefore it was assumed that the ETS yarn used to measure the temperature of a vertical surface would give a higher steady state error when compared to when it's held horizontal.

The figure 5.18 given below shows how the experiment to measure the temperature of a vertical surface was set up.

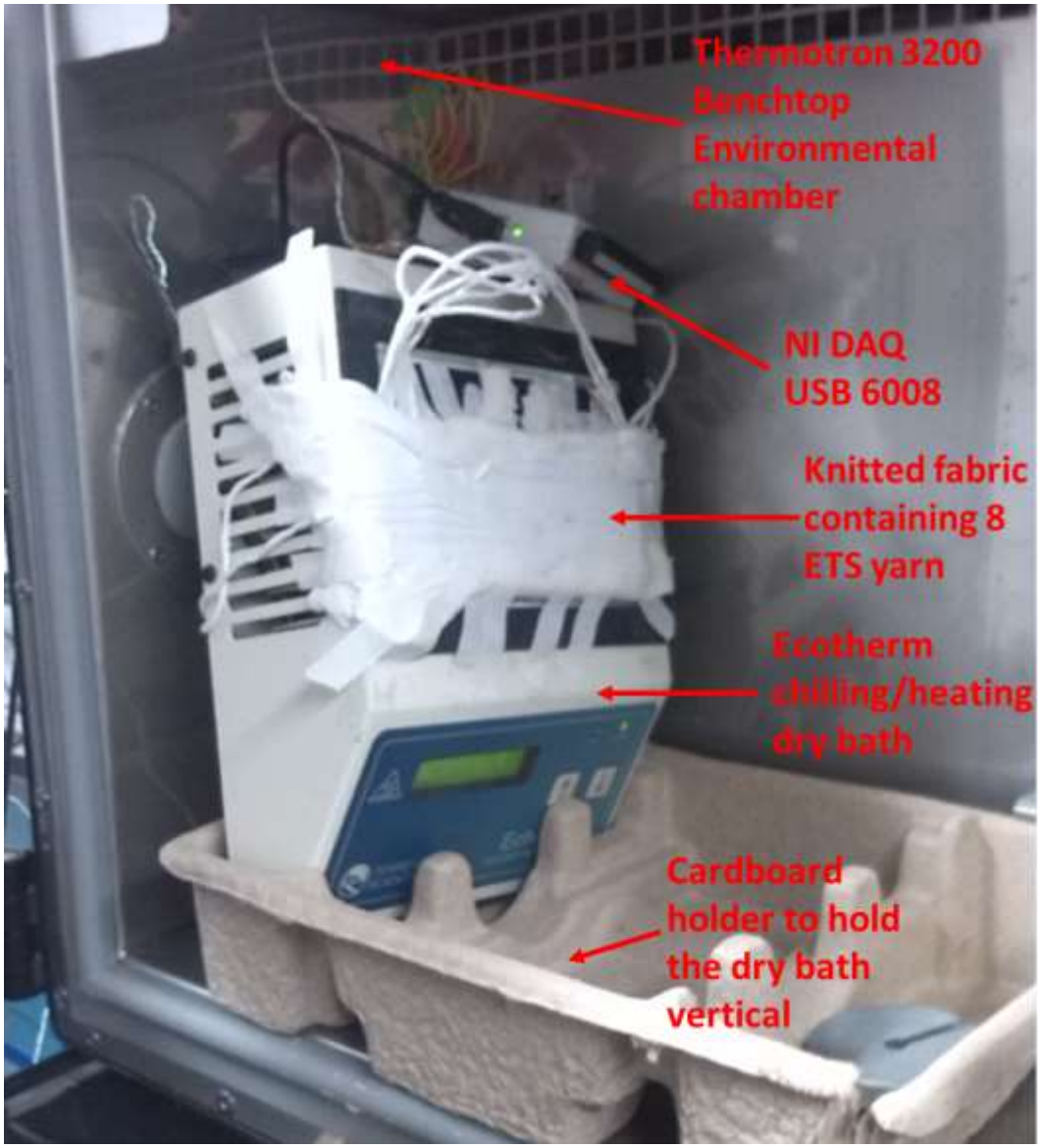

Figure 5-18: Ecotherm chilling/ heating dry bath held vertically inside the Thermotron Environmental chamber

The Thermotron temperature was set to 25 °C and the relative humidity was set to 60 %. The temperature of the Ecotherm dry bath was changed from 20-40 °C in steps of 2 °C every 10 minutes and the temperature once the sensors reached steady state was recorded.

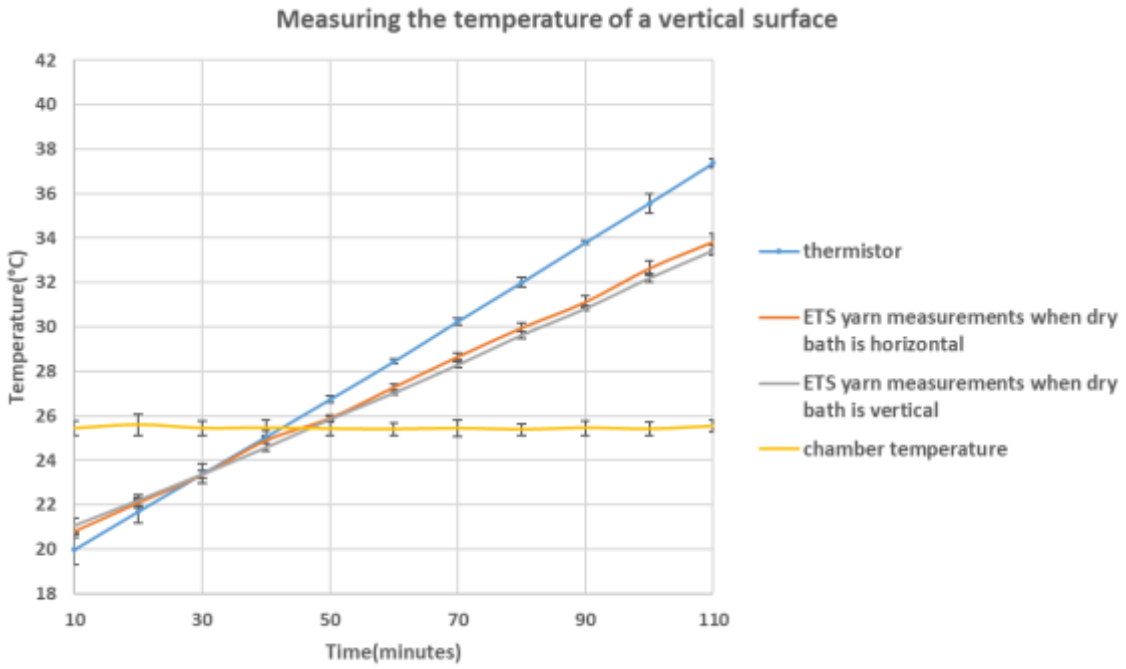

Figure 5-19: Effects of holding the plate vertical rather than horizontal (the average of the temperature recorded by the 8 ETS yarns have been plotted)

It can be observed from figure 5.19 that there was no significant difference between the ETS yarn measurements when the dry bath was held vertical and when it was held horizontal. This maybe as a result of the minute length of the micro-pod Lc which is only 2.17 +/- 0.07 mm (given in chapter 3 section 3.5.2). Therefore it can be concluded that the orientation of the skin where the temperature is being measured does not make a significant difference in the measurements of the ETS yarn.

5.5.4 Effects of moisture content on the temperature measurements

The amount of moisture in the wound dressing could also impact temperature measurements. Wounds are generally moist and moisture levels are known to be critical for wound healing (Winter, 1962). Therefore it is vital to understand the effects of moisture on the measurements of the ETS yarn.

Initially a preliminary experiment was carried out by positioning a knitted fabric containing three ETS yarn in a beaker of ionised water. The temperature of the water in the beaker was measured by a k type thermocouple and the room temperature was also measured using another k type thermocouple. The 600 ml of water was placed in the beaker and the knitted fabric containing the ETS yarn and the k-type thermocouple was positioned 300 ml below the surface of the water as shown in the figure 5.20 below.

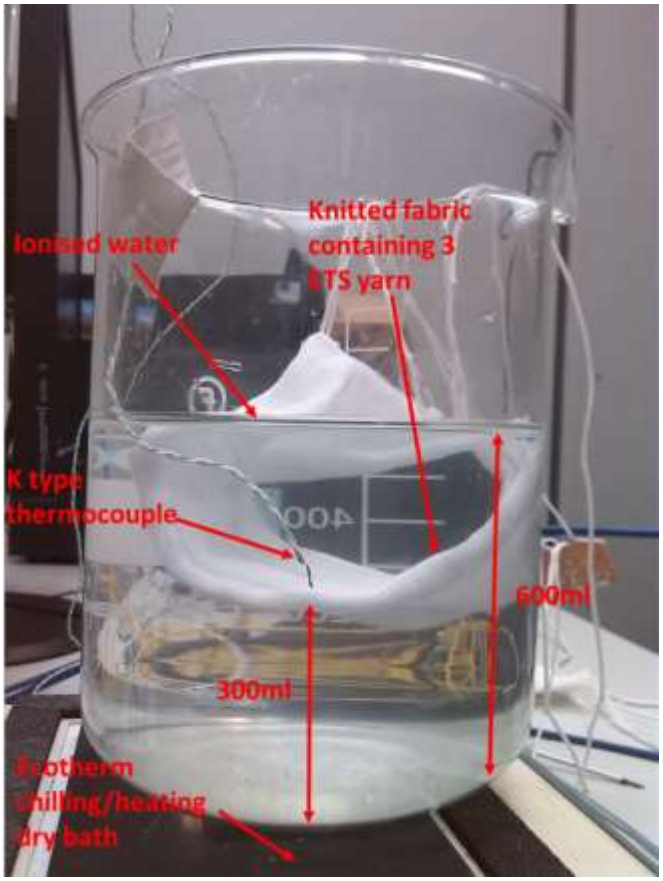

Figure 5-20: Experiment to measure temperature from the Beaker containing Ionised water

For this experiment the beaker containing ionised water was heated using the Ecotherm dry bath and the temperature captured by the k type thermocouple and the ETS yarns were recorded. The dry bath temperature was set to 100 °C in order to heat the water in the beaker. The beaker was left on the dry bath for several minutes in order to ensure the temperature distribution throughout the water was uniform. Then the measurements from the ETS yarns and the thermocouples were obtained during the process of heating the water. The average ETS yarn measurements obtained from the three ETS yarns are given in blue and the error bars which displays the confidence intervals are plotted in black. The results are given in figure 5.21 below.

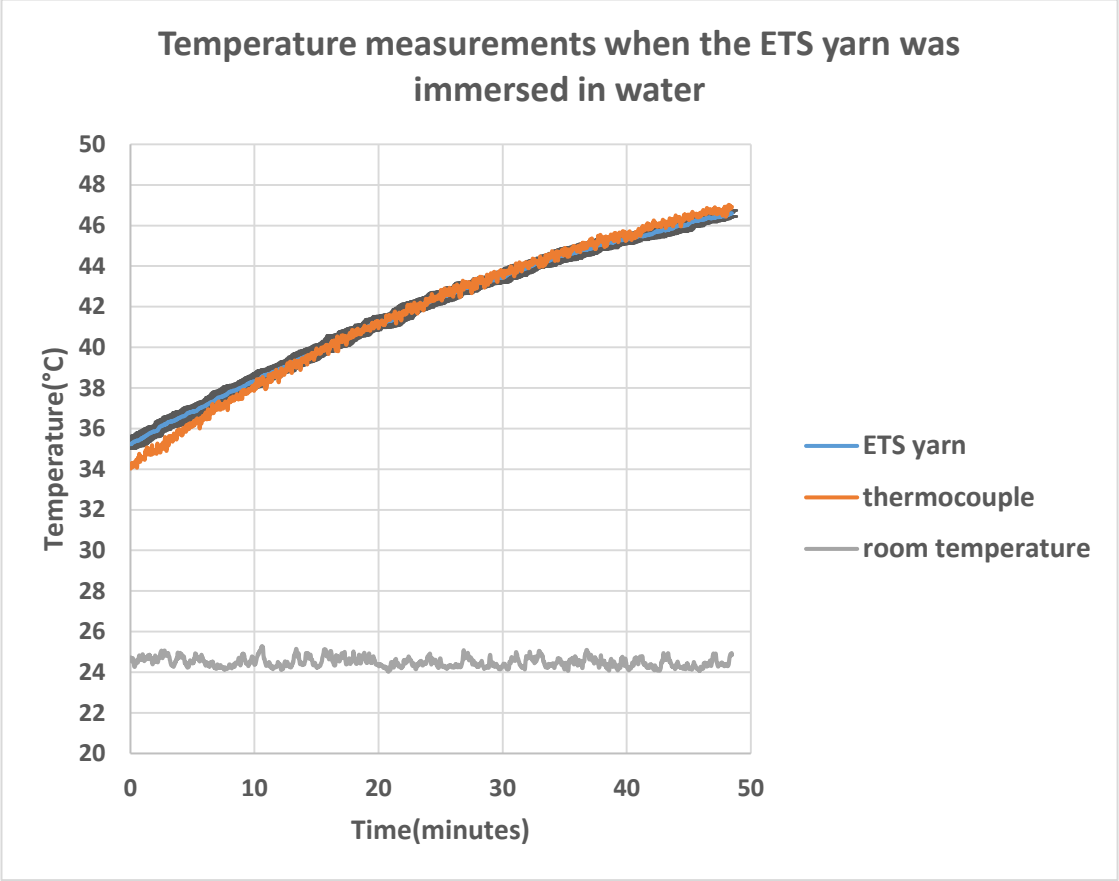

Figure 5-21: Temperature measurements when the ETS yarn is immersed in water

The results in figure 5.21 show that the temperature recorded by the k type thermocouple (plotted in orange) lies exactly on top of the average temperature of the three ETS yarns (shown in blue) and its confidence intervals (shown in black). The difference of 1.2 °C during the start of the experiment may have been caused due to the different in response times of the sensors or the temperature of the water not being uniform. However, it can be concluded from the results that the moisture content would not impact the ETS yarn measurements significantly. The thermistor when positioned in water stops functioning hence it can be argued that the polymer micro-pod protects the thermistor from moisture.

5.5.4.1 Effects of absorbing moisture on the temperature measurements

When used in wounds it is highly unlikely that the wound dressing would be submerged in moisture like in the previous experiment. Therefore, as a wound bed could not be used, a more practical experiment was designed using a Gravimetric Absorbing System from MK Systems, (Model MK 251, M/K GATS, Peabody, MA, USA) where a knitted fabric containing ETS yarn was placed on top of its porous plate and the effects on the ETS yarn measurements when the water was absorbed was recorded. The M/K GATS is used widely by academia and industry. The M/K GATS accurately measures liquid absorption rates and total capacity. The M/K GATS has been designed to comply with ISO 9073-12:2002 entitled 'Apparatus for Demand Absorbency, Apparatus for USA Patent

6,048,123, Tappi T-561, ASTM D5802', which also has the new M/K System's USA Patented liquid interface (MKSystems).

To make it more realistic the temperature of the ionised water used in the M/K GATS system was heated to 37 °C using the Ecotherm chilling/heating dry bath. However it was difficult to maintain the water temperature when the water was placed in the reservoirs of the M/K GATS. Therefore a thermocouple was placed in the lower reservoir of the M/K GATS to measure the temperature of the water.

Since the ETS yarn had to be connected to the NI DAQ special care had to be taken to prevent the water from flowing into the interface circuit. Therefore a stand was used to position the PCB board above the porous plate. However this effected the contact between the porous plate and the knitted fabric sample. One solution suggested was to use a wire mesh on top of the knitted fabric to enhance the contact (Mbise, 2015). However the weight of the wire mesh was insufficient to hold the sample in place. Therefore a weight of 119.17 g measured using an Adam balance (PW 214 Adam equipment PW analytical balance, Adam Equipment Ltd, USA) was placed on top of the wire mesh as shown in figure 5.22.

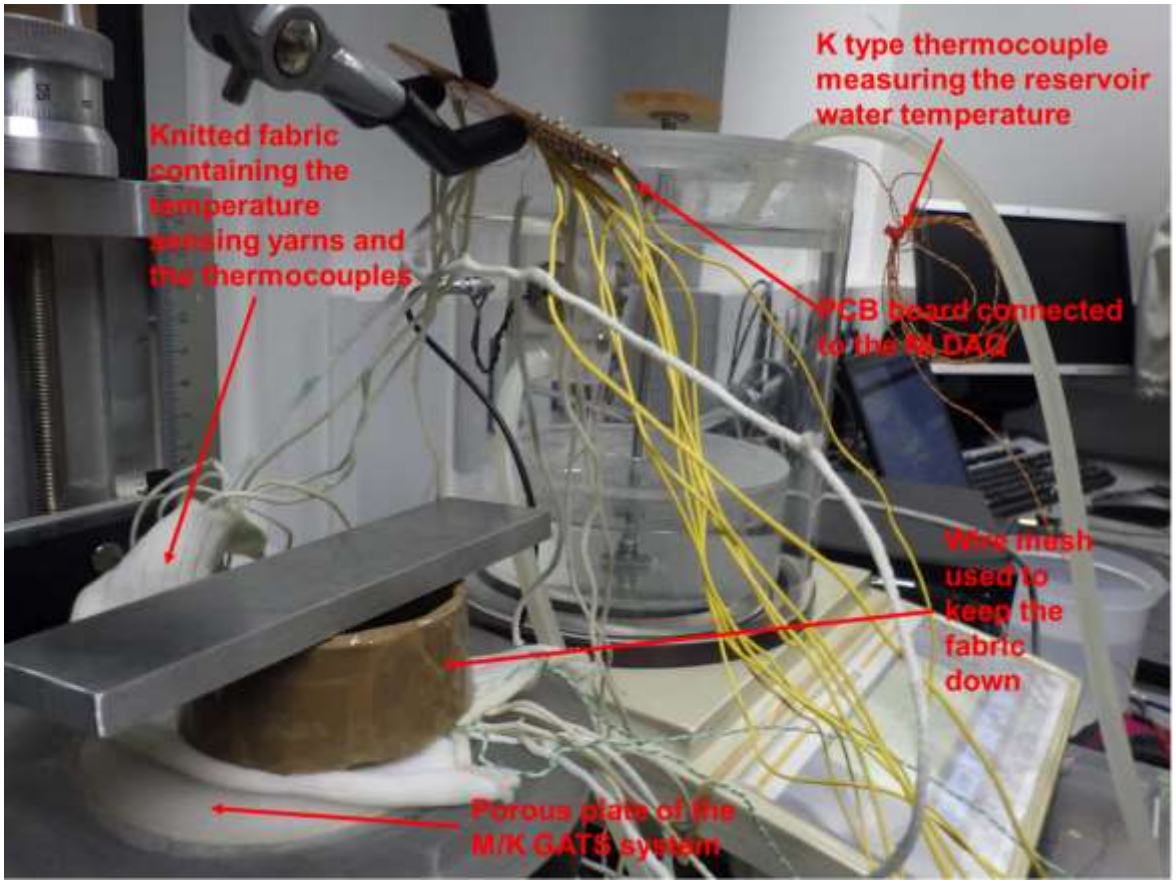

Figure 5-22: The setup used for the moisture experiment using the M/K GATS.

The knitted fabric containing 3 ETS yarns that was used in the preliminary experiment, was also used for this experiment. Four k type thermocouples were used for the experiment. One was used

to measure the room temperature, another was used to measure the water temperature in the lower reservoir. The final two thermocouples were positioned within two channels of the knitted fabric on either side of the three ETS yarns. The temperature measurements by the ETS yarns and the thermocouples were obtained using the program developed in LabVIEW.

The amount of water absorbed was measured using the software MK systems GATS 3.4.0 provided by M/K systems. Once the knitted fabric reached saturation, the knitted fabric was taken away from the porous plate and left to dry. The temperature measurements from the ETS yarn and thermocouple when the knitted fabric was absorbing water and when it was drying were recorded and it is given in figure 5.23a. The rate of water absorbed by the knitted fabric was also recorded and is given in figure 5.23b.

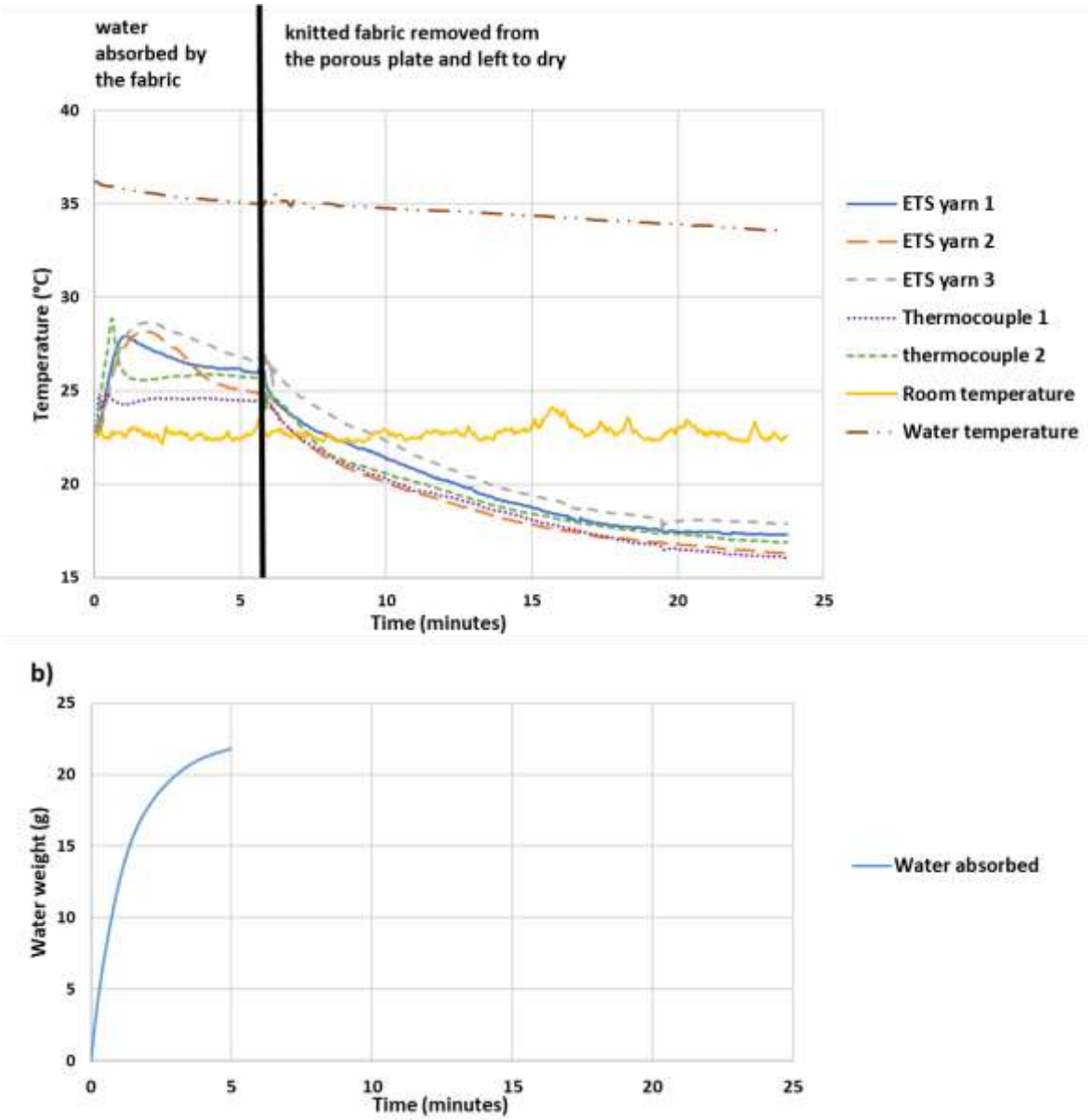

Figure 5-23: a) the temperature captured by the three ETS yarns and the thermocouples when the water is absorbed by the knitted fabric and when it is left to dry, b) the rate at which the water absorbed by the knitted fabric.

As demonstrated in figure 5.23a the temperature rises when the warm water is absorbed by the knitted fabric. But after the first few minutes the temperature decreases this may be as a result of water evaporating and cooling the knitted fabric. The thermocouple measurements follow the same pattern as the ETS yarn measurements however the low temperature measurements by the thermocouples might have been as a result of there being no fibres in the channels containing the thermocouples. This would result in the absence of wicking in these channels and therefore it can be argued that the water did not properly wick through the channels containing the thermocouples.

Finally when the knitted fabric is taken away from the plate the temperature captured by both the ETS yarn and the thermocouples decreased as illustrated in figure 5.23a, this is most likely caused due to evaporation.

As expected the polymer micro-pod appears to protect the thermistors in the ETS yarn from moisture. Therefore it can be established that the ETS yarns could be used to measure temperature in wound dressings or in any other application that involves moisture.

5.5.5 Effects of relative humidity

The humidity of a room could also affect the temperature measurement. Therefore it is important to understand the effects of relative humidity on the temperature measurements. The Thermotron 3200 environmental chamber was used to change the relative humidity from 30% -80% in steps of 10 %. The plate temperature was kept constant at 37 °C and the chamber temperature was kept constant at 25 °C. The temperature captured by the ETS yarn and the thermistor were recorded.

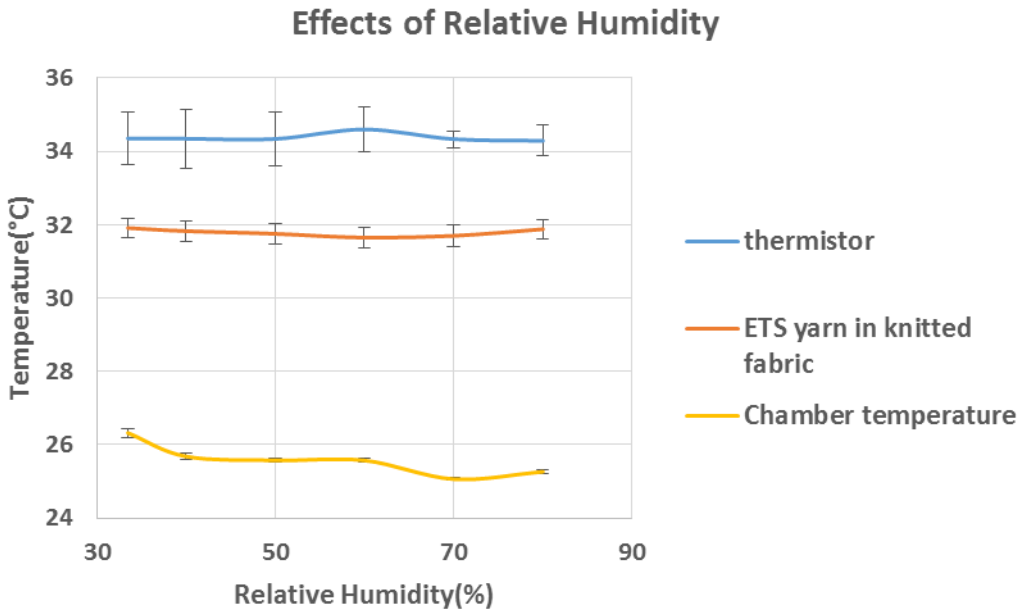

Figure 5-24: Effects of relative humidity on the temperature measurements of the ETS yarn (average temperature recorded by the eight ETS yarn has been plotted) in the knitted fabric

As expected the results above (figure 5.24) exhibits that the humidity level has no significant impact on the ETS yarn and thermistor measurements.

5.5.6 Influence of wind speed

Wind speed is another factor that would affect surface temperature measurements. Forced convection is used to increase heat transfer from a surface (Cengel, 2002). Therefore it would be interesting to identify the effects wind speed on the temperature measurements of the eight ETS yarn in the knitted fabric. To get different wind speeds a Micromark fan (batch No. 259369/0504, London, UK) was used to blow air across the dry bath for this set of experiments. The fan initially was turned to its lowest speed (1) and kept 25 cm from the sample. Wind speed was measured at 1.22 m/s above the sample. Thereafter the fan was set to 3 and the wind speed was measured at 2.06 m/s. An anemometer the rotating vanes LCA301 from AIRFLOW™ Instruments (Buckinghamshire, UK) was used to measure the wind speed.

These set of experiments were not carried out in an environmentally controlled room therefore the room temperature varied for each experiment. In the graph (figure 5.25) below the average room temperature has been plotted and the maximum and minimum room temperatures recorded for the experiments have been plotted on the error bars in green.

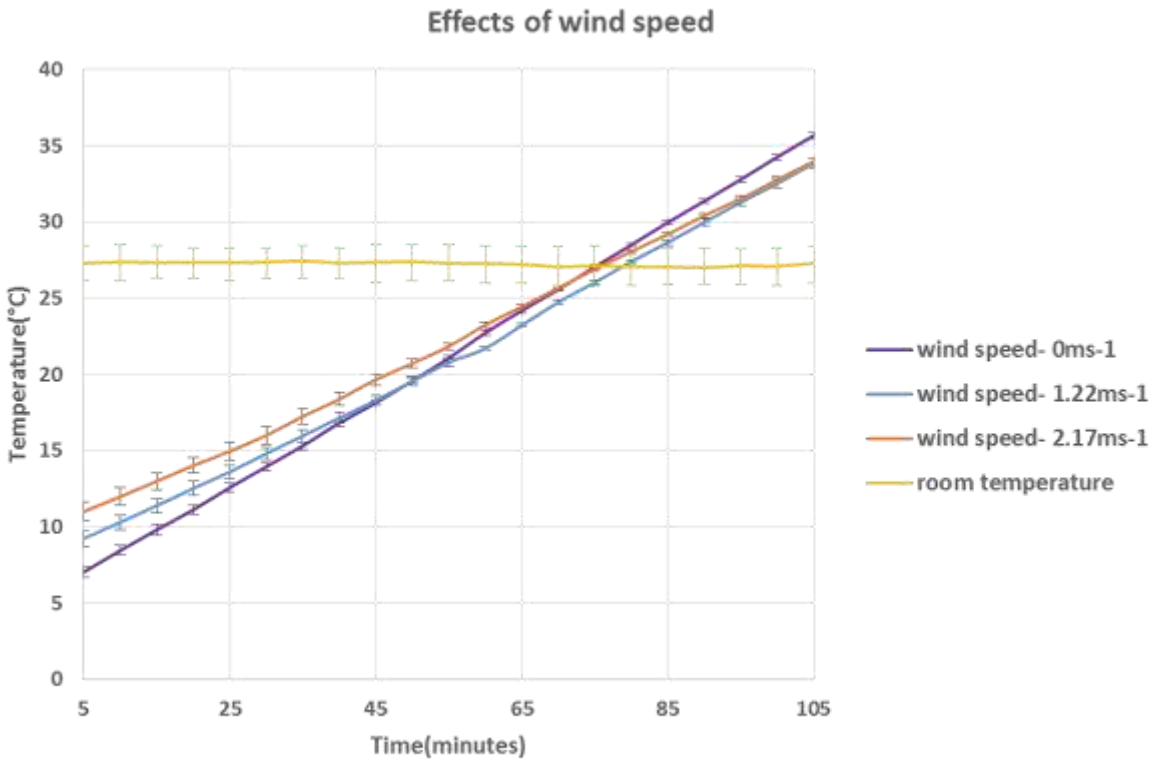

Figure 5-25: Effects of different wind speeds on the temperature measurements of the ETS yarn (the average temperature recorded by the 8 ETS yarns have been plotted).

As it can be seen in the graph (figure 5.25) the speed of the wind has an impact on the steady state error. The measurement error increased to 0.26±0.06 and 0.30±0.06 when the wind speed was set to 1.22 ms^{-1} and 2.17 ms^{-1} respectively. The higher the wind speed the higher the measurement error. This is caused as a result of the increase in heat transfer from the knitted fabric due to the forced convection bought about by the fan. However when used in wound care it is likely that the patient will be in the house/hospital therefore will not be effected by wind. This becomes problematic if the fabric is used to monitor body temperature of athletes or personnel that are exposed to high wind speeds for example mountain climbers.

5.6 Summary

From all the experiments above it can be seen that there are many variables effecting the temperature measurement from the ETS yarn therefore one can conclude that getting highly accurate temperature readings using the ETS yarn is difficult. However if placed in same conditions they provide precise readings therefore a relative reading can be obtained using the ETS yarn. If the ETS yarn is to be used for accurate temperature measurements the yarn has to be calibrated depending on the factors discussed in the chapter.

However for the intended application where the temperature deviation among certain points of a wound is captured, this sensor is ideal. Since all the ETS yarns used would be in a single wound dressing which will ensure that all of them are in similar conditions. Therefore the measurements obtained by the ETS yarn would be precise and if there is a change in temperature between certain points (localised temperature measurement) it would be indicated. If highly accurate measurements are required the smart wound dressings will have to be calibrated depending on the material used to make the wound dressing, the type of bandage used and the temperature of the room the patient is staying in.

5.7 References

- Avison, J., 2014. The World of Physics. Nelson Thornes.
- Buono, M.J., Ulrich, R.L., 1998. Comparison of mean skin temperature using “covered” versus “uncovered” contact thermistors. Physiol. Meas. 19, 297–300. PMID: 9626693.
- Cengel, 2002. Heat Transfer: A Practical Approach, 2nd Ed edition. ed. Higher Education, Boston.
- Childs, P.R.N., Greenwood, J.R., Long, C.A., 2000. Review of temperature measurement. Rev. Sci. Instrum. 71, 2959–2978. doi: 10.1063/1.1305516.
- Deng, Z.-S., Liu, J., 2008. Effect of fixing material on skin-contact temperature measurement by wearable sensor, in: 5th International Summer School and Symposium on Medical Devices and Biosensors, 2008. ISSS-MDBS 2008. Presented at the 5th International Summer

School and Symposium on Medical Devices and Biosensors, 2008. ISSS-MDBS 2008, pp. 137–140. doi: 10.1109/ISSMDBS.2008.4575037.

- Kuznetsov, G.V., Mukhammadeev, K.M., 2010. Numerical estimation of errors of temperature measurements by thermocouples using special glues and pastes. J. Eng. Thermophys. 19, 17–22. doi: 10.1134/S1810232810010030
- Liu, Y., Zhang, J., 2016. Model Study of the Influence of Ambient Temperature and Installation Types on Surface Temperature Measurement by Using a Fiber Bragg Grating Sensor. Sensors 16, 975. doi: 10.3390/s16070975
- Manual on the Use of Thermocouples in Temperature Measurement, 1993. ASTM International.
- Mbise, E., 2015. The development of a quick dry fabric for outdoors garments (PhD thesis). Nottingham Trent University, Nottingham.
- McMullan, R., 2012. Environmental Science in Building. Macmillan International Higher Education.
- Michalski, L., 2001. Temperature Measurement. John Wiley & Sons.
- Psikuta, A., Niedermann, R., Rossi, R.M., 2013. Effect of ambient temperature and attachment method on surface temperature measurements. Int. J. Biometeorol. 58, 877–885. doi: 10.1007/s00484-013-0669-4.
- Steady state, 2016. Wikipedia Free Encycl. URL https://en.wikipedia.org/wiki/Steady_state (accessed 8.9.16).
- Winter, G.D., 1962. Formation of the Scab and the Rate of Epithelization of Superficial Wounds in the Skin of the Young Domestic Pig. Nature 193, 293–294. doi: 10.1038/193293a0.

6. Design and manufacture of temperature sensing apparel

6.1 Introduction

This chapter discusses the integration of the Electronic Temperature Sensing (ETS) yarn into a textile garment to monitor wearer's skin temperature. The chapter consists of the following subsections:

- Preliminary testing of the behaviour of ETS yarn on skin;
- Making prototype garments using the ETS yarn;
- Development of hardware and software for data capture and processing;
- Small scale user trials carried out using temperature sensing garments.

6.2 Testing the ETS yarn on skin

6.2.1 Positioning an ETS yarn in the hand

It was important to observe how the ETS yarn would behave when taking skin contact temperature measurements. Therefore, a preliminary experiment was carried out to observe the effects of using the ETS yarn for temperature measurements on different points of the hand. This task was conducted to study the response of ETS yarn on human skin temperature measurement.

The ETS yarn was placed at different positions in the hand (side, front, back) as shown in figure 6.1. Two 100 g weights were attached to the ETS yarn to give it tension. Each of these positions provided different contact surfaces for the ETS yarn. In order to compare the measurements two k type thermocouples were positioned on either side of the ETS yarn and also a Raytek Raynger MX Infrared Thermometer (Raytek® Fluke Process Instruments, California, USA) having an accuracy of ±1 °C was also used to obtain the non-contact temperature measurements.

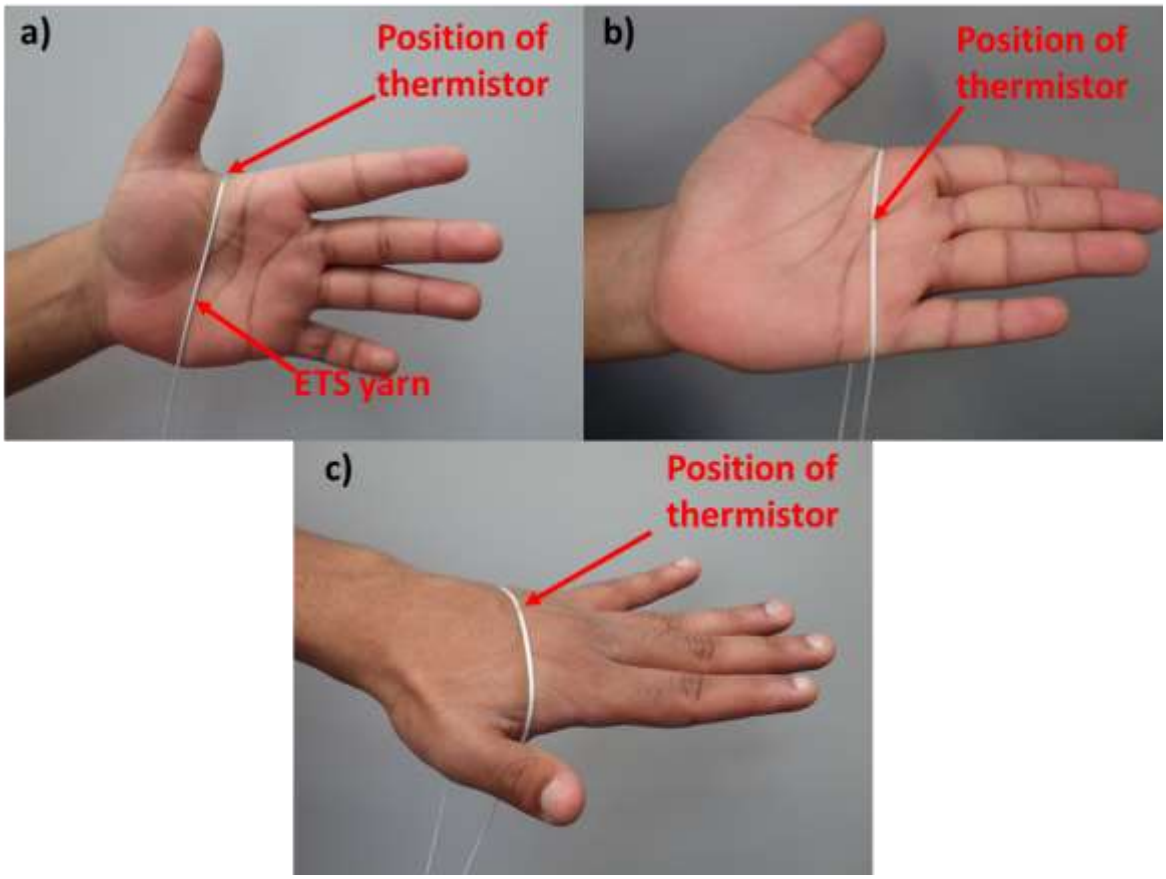

Figure 6-1: Positioning the ETS yarn a) side, b) front and c) back of the hand

The experiments were carried out on three separate volunteers and on each volunteer the measurements were taken using three different ETS yarns, placed in the three positions of the hand. The thermocouples were pasted onto the skin using insulating tape (RS Stock No.134-7319, RS, Corby, UK) on either side of the ETS yarn during each experiment. The program used in chapter 5 section 5.3 was used to capture the temperature from the ETS yarns and the thermocouples. The ETS yarn was kept in each position for two minute and the average temperature measurements during the last thirty seconds were calculated. This was done to ensure that a steady state was reached before the measurements were taken. Thereafter from the measurements of the three ETS yarn the average and the standard deviation was calculated for each position in each of the volunteers and it is given in table 6.1. The average measurements captured by the thermocouples and the infrared thermometer are also recorded in table 6.1 and the difference in between the thermocouple temperature measurements and that of the ETS yarn are calculated and presented on the last row for each of the volunteers in the table 6.1. The recorded room temperatures (the room temperature was recorded using another k type thermocouple) is also is also presented in table 6.1.

Table 6-1: ETS yarn, thermocouple and Infrared thermometer measurements at different positions on the hand, on the three different volunteers.

Volunteer 1			
Position on the hand	Front	Back	Side
ETS yarn (°C)	28.01±0.12	28.77±0.07	28.72±0.31
Thermocouple (°C)	29.90±0.04	30.13±0.07	29.84±0.23
Infrared thermometer (°C)	30.50±0.53	30.00±0.26	29.37±0.06
Room temperature (°C)	22.95±0.03	23.02±0.07	23.00±0.08
Difference (thermocouple-ETS yarn) (°C)	1.89±0.12	1.36±0.10	1.12±0.39
Volunteer 2			
Position on the hand	Front	Back	Side
ETS yarn (°C)	31.93±0.25	31.35±0.12	33.23±0.25
Thermocouple (°C)	34.27±0.13	34.04±0.23	34.46±0.63
Infrared thermometer (°C)	34.97±0.25	33.77±0.31	35.27±0.25
Room temperature (°C)	23.30±0.10	23.21±0.02	23.31±0.07
Difference (thermocouple-ETS yarn) (°C)	2.34±0.28	2.68±0.26	1.22±0.68
Volunteer 3			
Position on the hand	Front	Back	Side
ETS yarn (°C)	31.74±0.15	31.78±0.34	32.08±0.19
Thermocouple (°C)	33.73±0.20	32.65±0.22	32.84±0.51
Infrared thermometer (°C)	34.20±0.40	33.67±0.12	33.57±0.21
Room temperature (°C)	22.42±0.02	22.72±0.21	23.13±0.03
Difference (thermocouple-ETS yarn) (°C)	1.99±0.25	0.87±0.41	0.76±0.55

From the results in table 6.1 the average temperature difference between the ETS yarn measurements and the thermocouple measurements for each position, from all the three volunteers were calculated as 2.07 °C, 1.63 °C, 1.03 °C for the front, back and side respectively. These results illustrate that the difference between the ETS yarns and the thermocouples were at a minimum when the ETS yarns were positioned on the side of the hand. This was most likely due to the lower radius of curvature at the side of the hand when compared to other positions, which provides a higher surface contact pressure between the ETS yarn and skin according to Laplace pressure equation (see equation 6.1) when taking temperature measurements.

$$p = \frac{2*\sigma}{r} \qquad (6.1)\ (KRUSS, 2018)$$

Where p is the pressure, σ is the surface tension and r is the radius of curvature.

The ETS yarn had minimum contact pressure with the skin when it was placed in the front of the hand since it had the largest radius of curvature and as expected it gave the largest difference. However, this effect will most likely be reduced when the ETS yarn is placed in a fabric. It is important to ensure that the pressure on the fabric is uniform. When the ETS yarn is used to capture temperature this would be another important area to look into, however when the ETS yarn is used as a tool to compare the temperature measurements at specific points in-between two feet for example, the radius of curvature is most likely to remain similar hence this can be ignored.

6.2.2 Developing Prototypes using the ETS yarn

The ETS yarn will be knitted or woven into a fabric before it will be used to measure temperature. The process of making ETS yarn is a manual process (as discussed in chapter 3 section 3.5) therefore they are produced in small quantities. Hence it was decided for this research that the best way of including ETS yarn in garments was by knitting structures containing 2mm diameter channels which allowed the ETS yarn to be inserted and positioned accurately in the structure. It was also regarded important to identify the best interface hardware (voltage divider circuit, analogue to digital converter) to use when using the ETS yarn.

Another major concern when using ETS yarn was making the connection between the ETS yarn and the interface hardware. Connecting soft and hard electronics is a key challenge even faced in the flexible hybrid electronics industry. The connectors generally hinder the flexibility of the device and are also prone to interconnect issues (Khan et al., 2016)

In-order to device the best method of connection between interface hardware and ETS yarn and also to device the most suitable interface to the hardware, a series of different Prototypes were created using ETS yarn. For each prototype the interface hardware, the method of connection and the software interface was varied.

6.2.2.1 Arm band

The first prototypes made using ETS yarn were Arm bands. Three prototype arm bands were made and for each prototype the hardware used was changed and the method of connection between the ETS yarn and the hardware was altered. For all these prototypes the software in LabVIEW was also changed according to the hardware used. Figure 6.2 shows the images of all the three arm band prototypes.

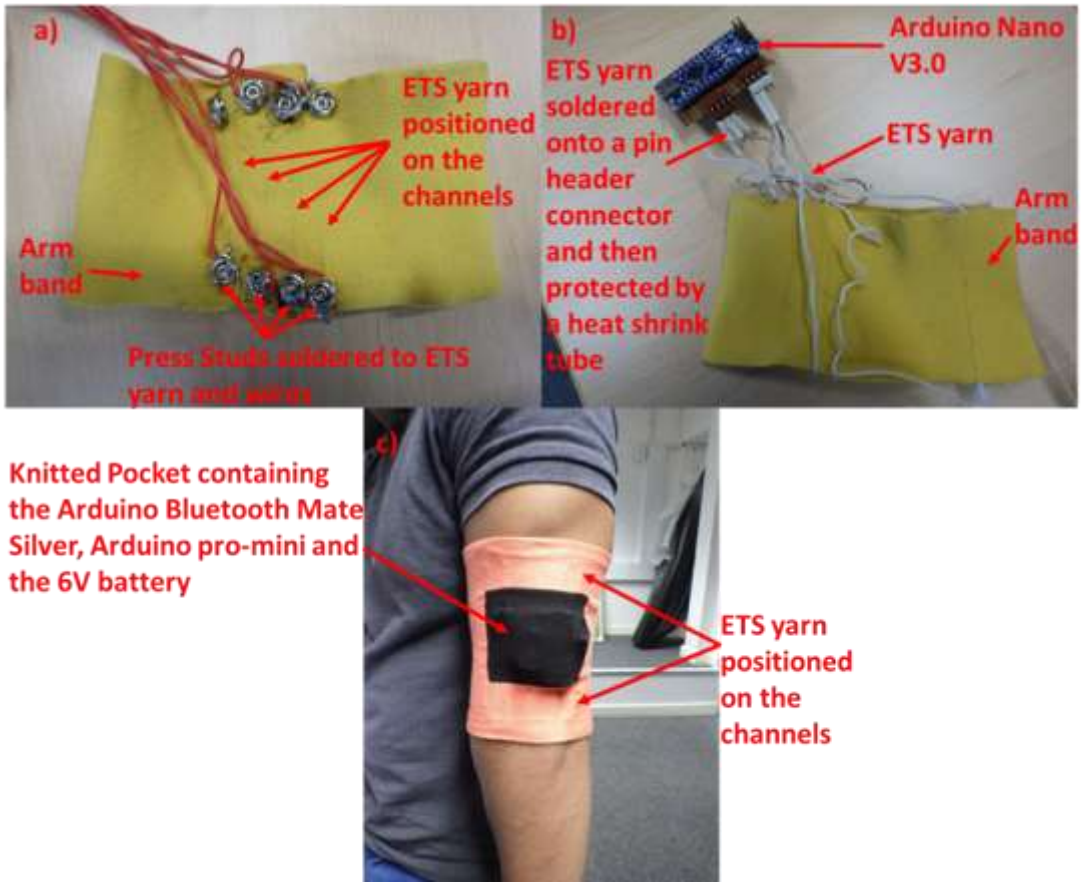

Figure 6-2: Prototype armbands knitted containing channels with ETS yarn placed in them. Where a) Prototype 1 b) Prototype 2 and c) Prototype 3

6.2.2.1.1 Armband Prototype 1

In the first prototype the ETS yarns were connected to the interface hardware by using press studs. Press studs have been used in several electronic textile applications to make electrical connections (Gould, 2003), (Munro et al., 2008). The ETS yarns were soldered onto the female parts of the metal studs as shown in the figure 6.2a. Thereafter wires were soldered onto the male parts. Then these wires were soldered onto a potential divider circuit which was then connected to an NI DAQ USB 6008. The LabVIEW program used in chapter 5 section 5.3 was modified to get the voltage out from the four ETS yarns.

The main issues when using this approach was the bulky size of the NI DAQ USB 6008 unit (84.98 mm by 64.01 mm by 23.19 mm) which caused the connections at the press studs to fail. Another

issue was due to the large size of the press studs which prevented the ETS yarn being positioned in close proximity in a fabric.

6.2.2.1.2 Armband Prototype 2

The next armband was also knitted using the same material. Instead of using press studs the fine multi-strand copper wire of ETS yarn were soldered directly onto male header connectors, and the solder joints were encased in heat shrinkable sleeves. This also enhanced the mechanical strength of the connection. An Arduino Nano (Arduino, Turin, Italy) having dimensions of 43.18 mm × 18.54 mm was used as the microcontroller in place of the NI DAQ USB 6008 unit. The Nano was then connected to the computer using a mini b USB jack.

The LabVIEW program in chapter 5 section 5.3 was modified to read the data from the Arduino Nano. To do this the LabVIEW interface for Arduino add-on was installed from the VI package manager. The VI package manager is a software that makes using and distributing an NI LabVIEW add-ons simple (National Instruments, 2013).

Then the analogue read pin VI was used to capture the voltage out from the voltage divider circuit and thereafter it was converted to the temperature reading using the LabVIEW program. The block diagram of the program is given in appendix 11 figure 8.19.

6.2.2.1.3 Armband Prototype 3

The prototype 3 was developed with wireless connectivity between the ETS yarns in the arm band and the PC. This prototype was made with a knitted pocket to include the interface hardware. An Arduino Pro Mini (Arduino, Turin, Italy) was used as the microcontroller due to its minute size of 17 mm by 33 mm. It was then connected to a Bluetooth module from Sparkfun Bluetooth Mate Silver (SparkFun Electronics, Colorado, USA). This Bluetooth module was chosen due to its low power consumption; however, it uses a class 2 Bluetooth Module RN-42 which limits the transmit range.

The main problems when using the armband to obtain temperature measurements was the random drop in the Bluetooth signal.

6.2.3 Prototype Glove

A prototype temperature sensing glove was also designed and produced. The glove was knitted with five channels to accommodate ETS yarns. The thermistors in the ETS yarn were positioned on the tips of the five fingers.

The same interface hardware that was used for Armband Prototype 3 (section 6.2.2.1.3) was used with the glove. However instead of the Bluetooth Mate Silver, a Bluetooth Mate gold module was used. This uses a RN-41 Bluetooth module which increases the range of transmission. The software in LabVIEW was modified to provide the user with a better user interface. A picture of a hand was

included onto the front panel of the program, in which colour boxes were placed on the positions of the thermistors in the glove. The allows the user to set temperature limits so that once the temperature went above the limit the box turned red and when it went below the colour box turned blue, otherwise it remained green. The user interface for the glove and the glove are shown in figure 6.3.

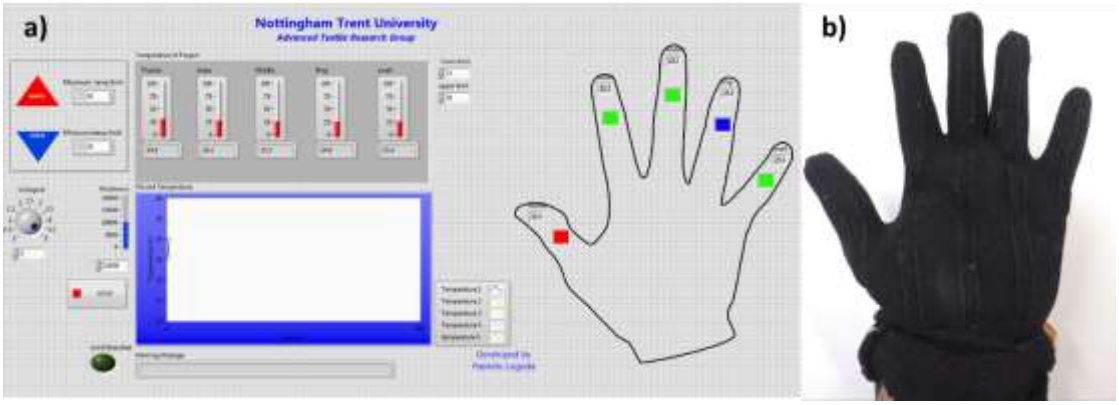

Figure 6-3: a) The LabVIEW software user interface for the glove and b) the prototype glove.

6.2.4 Development of a temperature sensing sock for early detection of Non Freezing cold injury

6.2.4.1 Design and manufacture

The electronic temperature sensing (ETS) yarn was then used to produce a sock that can detect temperature at five different points of a foot. As with all knitted materials, the structure relaxes and shrinks in size after manufacture and may then be stretched when worn. Therefore, to ensure that the thermistor micro-pods of the ETS yarn are positioned correctly when worn, a simulated foot with metal studs as location markers was created by using Plaster (Gypsum). The simulated foot is shown in figure 6.4.

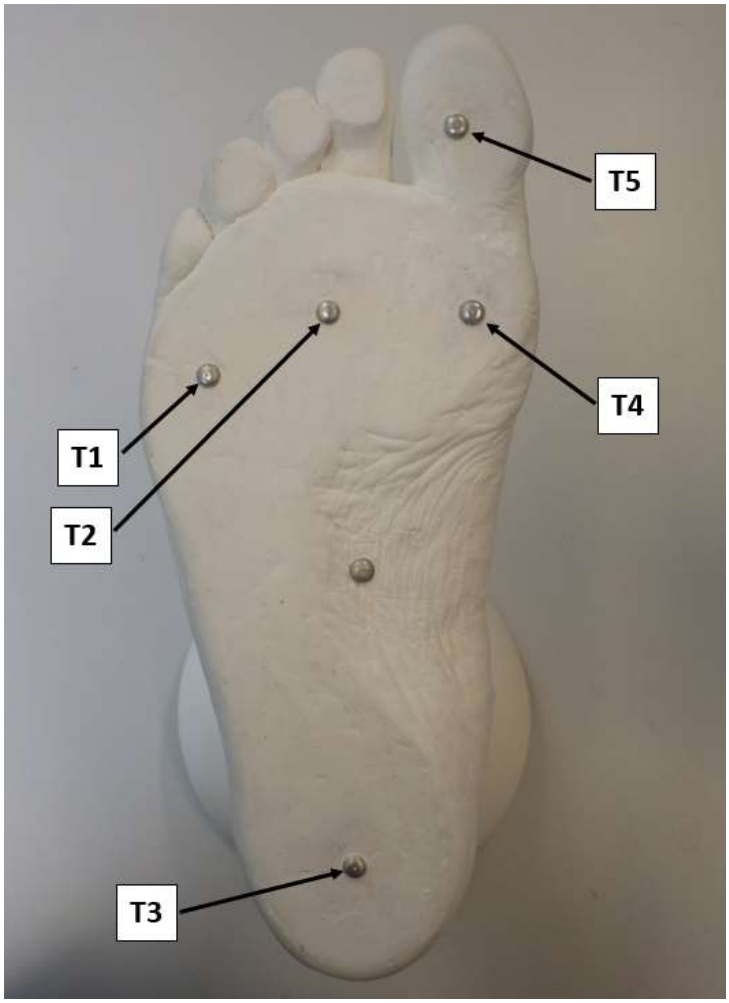

Figure 6-4: Simulated foot used for sensor location.

The knitted sock with channels was pulled on to the simulated foot and five ETS yarns were inserted into the channels of the sock and positioned so that the thermistor micro-pods are aligned with the studs of the simulated foot. Figure 6.5 indicates the path of a typical ETS yarn.

Figure 6-5: Path of a typical ETS yarn. The hexagon represents the location of a thermistor.

The fine multi-strand copper interconnects of thermistors of the ETS yarns were connected to a potential divider circuit to determine their resistance using an USB 6008 DAQ unit from National

Instruments interfaced to a PC. The values of the resistors used in the potential divider circuit were determined with an Agilent 34410A 6 ½ Digital multi-meter to a precision of 0.01 %. The software developed for the glove (section 6.2.3) was modified to be used with the sock. On the front panel instead of having an image of a hand an image of a foot was used. The corresponding temperatures from the thermistors were computed from the resistance values recorded with the DAQ, using the temperature conversion equation provided by the thermistor manufacturer. The temperatures were saved onto a spreadsheet. On the location of each of the sensors on the knitted sock, intensity graphs were positioned as indicators on the foot image. Intensity graphs were used instead of colour boxes due to its gradual change in colour with the change in temperature. The ramp of each of the intensity graphs were set to change from dark blue to red with increasing temperature as shown in figure 6.6 below.

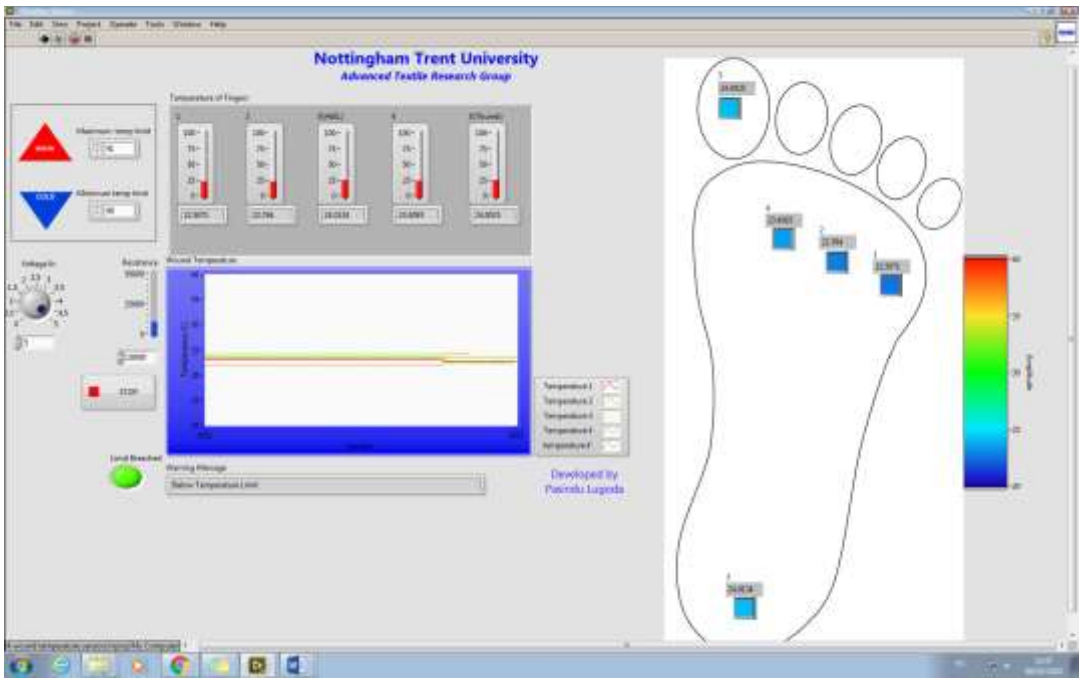

Figure 6-6: User interface for the Temperature monitoring sock

6.2.5 Wearable thermograph

The final prototype created was the wearable thermograph. The main focus was to create a fabric-based thermograph with several ETS yarns placed within the textile. The application of the wearable thermograph was to monitor wounds therefore a commercially available wound dressing was purchased to understand the construction of it. The structure of the commercially available wound dressing was a double layer woven structure. However, it was decided to employ a knitted spacer structure for the wound dressing since the expertise in the advanced textiles research group (ATRG) was knitting. A spacer structure was knitted containing sixteen channels to accommodate ETS yarns. Depending on the wound size and the requirement, the spatial resolution required can be varied.

However, to demonstrate the feasibility of creating a temperature sensing wound dressing sixteen ETS yarns were used to fabricate the dressing.

6.2.5.1 Design and manufacture

The wearable thermograph had dimensions of 122 mm by 100 mm and the ETS yarn were positioned as shown in the figure 6.8 below. The thermistors in the ETS yarn were positioned in the middle of the spacer fabric. The Spacer fabric was knitted using the Stoll CMS ADF 3 32W E14 knitting machine (Stoll, Reutlingen, Germany) using 3 polyester 167/48 Dtex yarns twisted together. The structure of the spacer fabric is given below in figure 6.7. The thickness of the spacer fabric came to 3.00±0.03 mm (measured using a Shang Hai Heng Liang micrometer).

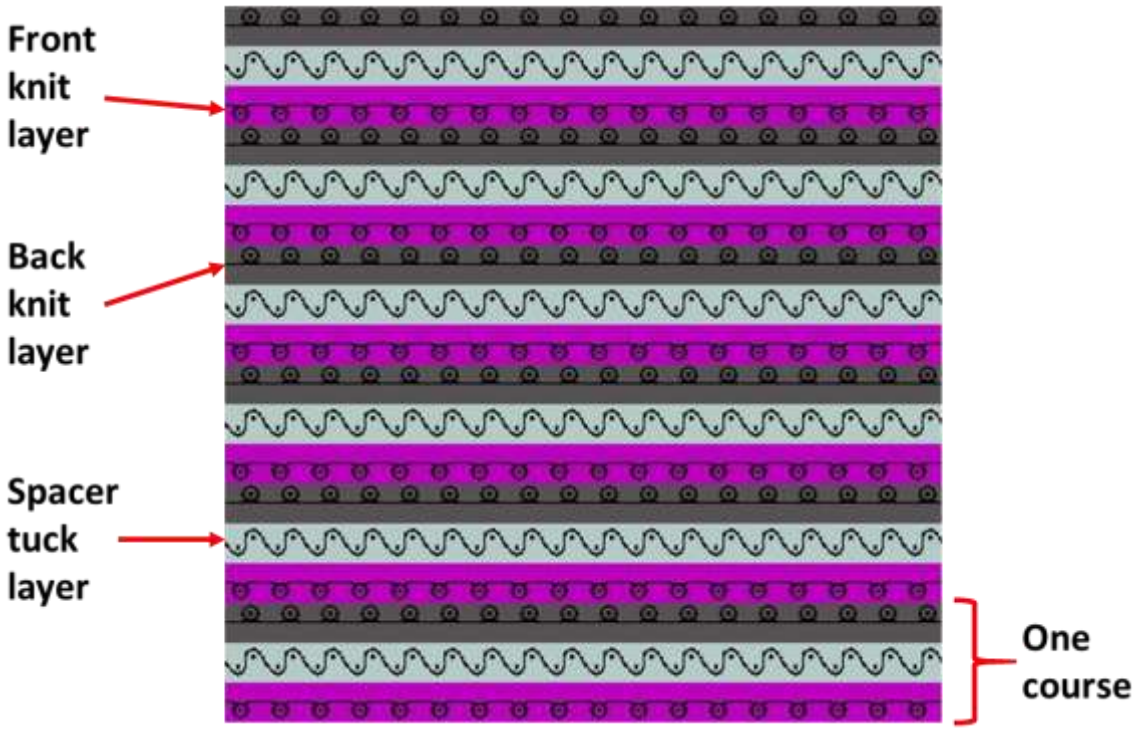

Figure 6-7: Structure of the Spacer fabric

In-order to create the wearable thermograph, ETS yarns were manually inserted when the spacer structure was knitted in the Stoll knitting machine. The ETS yarns were positioned in-between the front knit layer and the spacer tuck layer (shown in figure 6.7). This method ensured that the distance in between two ETS yarn remained constant for the whole sample. The figure 6.8 below demonstrated the process of positioning ETS yarn in the Spacer structure.

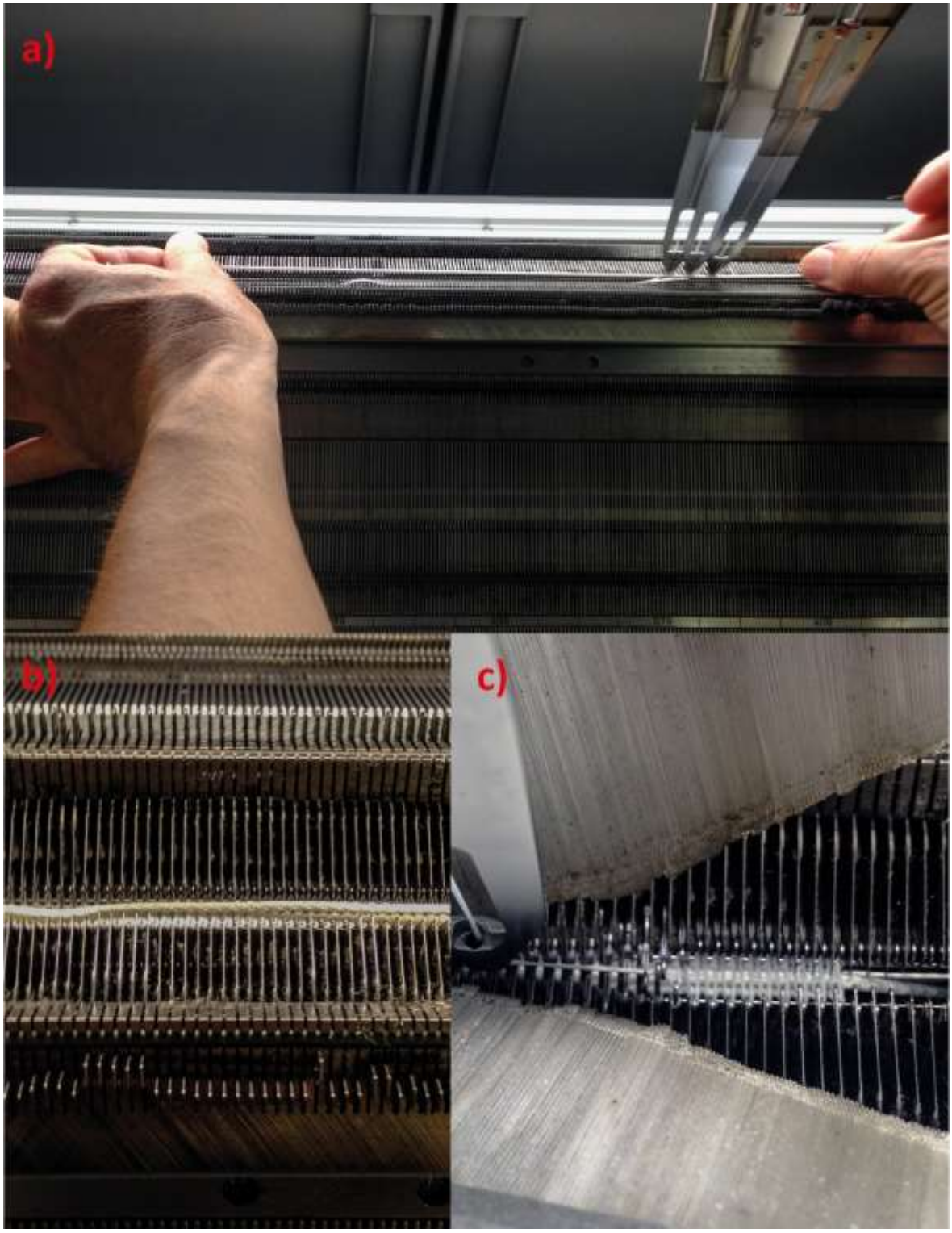

Figure 6-8: Positioning the ETS yarn in the spacer structure where a) manually positioning the ETS yarn, b) ETS yarn positioned on the machine and c) Spacer tuck layer knitted on top of the ETS yarn which holds the ETS yarn in place.

The distance between two ETS yarn can be altered by changing the number of courses in between two ETS yarn. A course consisted of a front knit layer, back knit layer and a spacer tuck layer as shown in figure 6.7. In-order to understand the optimum number of courses between two ETS yarn, three trail samples were knitted varying the number of courses (1 course, 2 courses and 3 courses) between two braided yarn. For the trial samples, braided yarns were positioned in the spacer structure instead of ETS yarns. Braided yarns were made by only using the 8 strand copper wire as

the core yarn and then covering it with the packing fibres and the knit braided fibre sheath. Braided yarns were used since manufacturing ETS yarns were time constraining.

When the number of courses between the two braided yarns were one, the yarns were almost positioned one after the other. Even though this provided a good spatial resolution, this resulted in the fabric being too stiff. For the next trial two courses were kept in-between two braided yarns. This added a gap of 1.345±0.036 mm (measured using VHX Digital microscope (Keyence, Milton Keynes, UK)) in-between two braided yarns. This caused a lower spatial resolution for the wearable thermograph however this gave a better feel to the sample. The last trial was done by leaving three courses in between two braided yarns. This gave the best feel to the fabric however it increased the distance between two braided yarns to 2.284±0.038 mm (measured using VHX Digital microscope), hence this decreased the spatial resolution even further. Therefore, a compromise was reached and the wearable thermograph prototype was knitted with two courses in between two ETS yarns. The figure 6.9 gives the structure of the spacer fabric containing the ETS yarns.

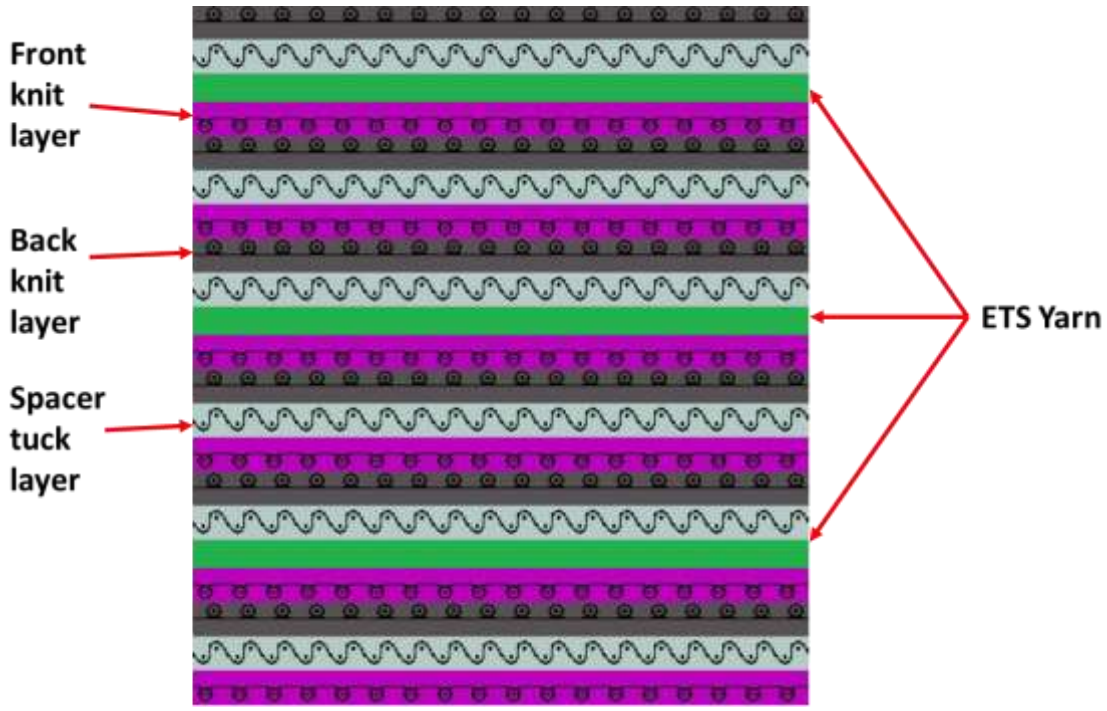

Figure 6-9: Spacer structure containing ETS yarns

The wearable thermograph was knitted with 16 ETS yarns and it had a thickness of 3.36±0.02 mm (measured using a Shang Hai Heng Liang micrometer) in the area containing the ETS yarns and a thickness of 3±0.03 mm (measured using a Shang Hai Heng Liang micrometer) in the area where there were no ETS yarn. The separation between two ETS yarns were measured at 1.157±0.023 mm. The measurements were taken using a VHX Digital microscope. The figure 6.10 below shows the

positioning of the ETS yarn (the ETS yarns were coloured in green for easy identification) in the wearable thermograph.

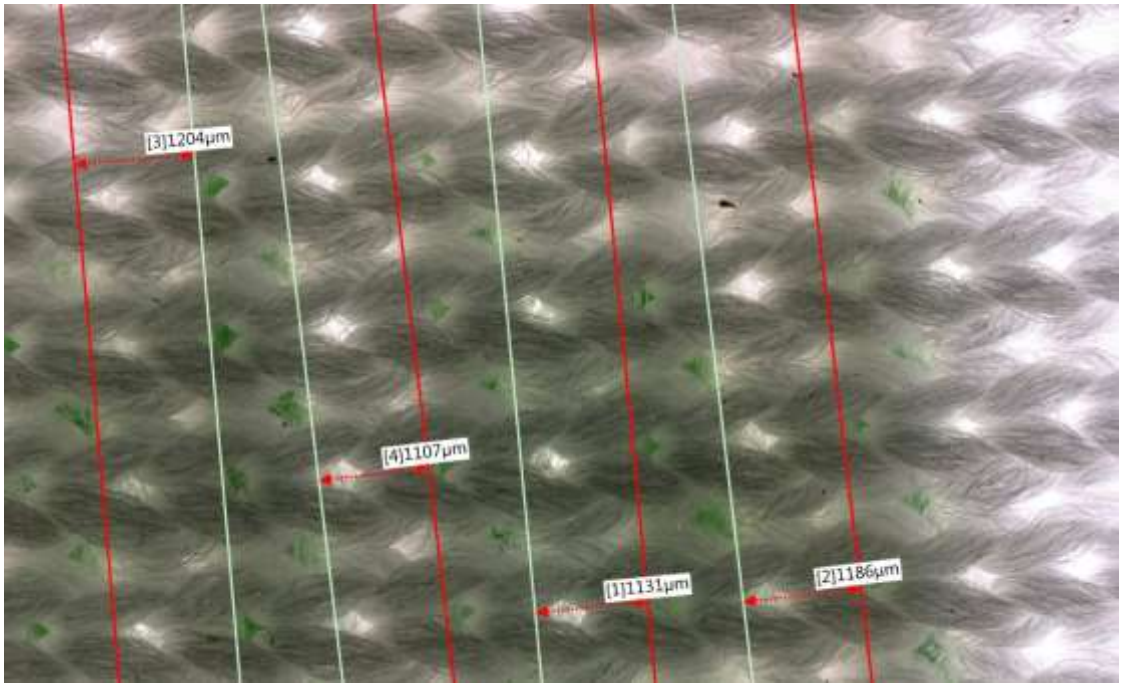

Figure 6-10: An image of the wound dressing containing 16 ETS yarns taken from the VHX digital microscope. The distance indicated between the red and green lines shows the distance between each of the ETS yarn (coloured in green) in the wound dressing.

6.2.5.1.1 Interfacing Hardware

The hardware comprised of a 16 channel multiplexer (Analog/Digital MUX Breakout - CD74HC4067, SparkFun, Colorado, United States). The 16 channel pins of the Analog Multiplexer were used to connect the 16 ETS yarns. The four digital input channels of the multiplexer were connected to the four digital output of an Arduino Pro Mini (Arduino, Turin, Italy). The signal output (sig. pin) from the multiplexer was connected to the Analogue input (AI0) of the Arduino Pro Mini. A 10 kΩ resistor was used to ground the analogue input (AI0) of the Arduino Pro Mini (the 10 kΩ resistor was used as the load resistor to complete the potential divider circuit). The Arduino Pro Mini was also connected to a SparkFun Bluetooth Mate Gold (SparkFun Electronics, Colorado, USA) which provided the Bluetooth connectivity.

The ETS yarns were soldered onto male header connectors which were then protected using heat shrinkable sleeves.

6.2.5.1.2 Software

The software that was used for the wearable thermograph was the same as the one used for the glove (section 6.2.3) with the following differences. A new SubVI was created in the main VI called thermistortemperature.vi. In this SubVI a for-loop was used and inside the for-loop a flat sequential structure (flat sequential structure contains one or more frames that execute sequentially) was

created. In the first frame the iteration number of the for loop was converted to a Boolean array using the function in LabVIEW called “Number To Boolean Array”. The Boolean array was then broken down into its array elements using another function in LabVIEW called “index array”. Each array element was connected to the “digital write pin VI” which can be found in the LabVIEW interface for Arduino library. This ensured that with the increase in the for-loop count (i) the channel input chosen by the Multiplexer would differ. This provided the digital output required by the Multiplexer in order to select the different channels.

The next frame in the flat sequential structure contained the “analog read pin VI” (also found in LabVIEW interface for Arduino library) which was used to obtain the voltage from Analogue input (AI0) (Vout from potential divider circuit). In the last frame the temperature was calculated using the help of two formula Express VI’s (formula Express VI’s are used to apply operations and variables to the data recorded). One of the Formula Express VI’s was used to calculate the thermistor resistance (R_t) using the voltage divider formula (given in equation 3.7 in chapter 3 section 3.6.1) and the other was used to calculate the temperature in Kelvin using the thermistor equation (given in equation 3.1 in chapter 3 section 3.3). Thereafter 273.15 was deducted from the temperature in Kelvin to obtain the temperature in °C. This temperature was then stored in an array outside the for-loop.

The user interface in the front panel of the main VI was also changed. It contains a control that allows the user to define the x and y coordinates of the thermistors in the wearable thermograph. The temperatures captured by the 16 ETS yarn are presented individually on thermometers as shown in figure 6.11. The temperature is also plotted in a graph, which would change colour depending on if the temperature limits set by the user are breached (as described in chapter 3 section *3.6.2.1.6)*. It also represented the temperature as a thermograph using a 3D graph, this gave a 3D representation of the temperature distribution in the fabric as shown in figure 6.11 below.

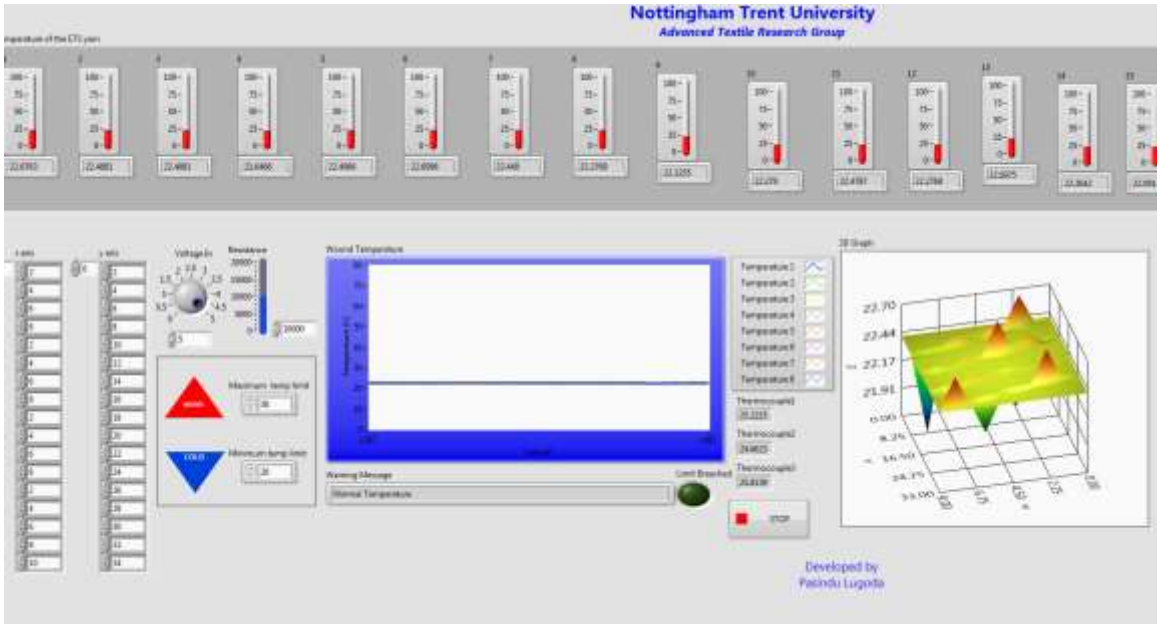

Figure 6-11: User interface of the labVIEW program devoloped for the wearable thermograph

6.3 User trials carried out using temperature sensing garments

6.3.1 User trials on the Sock

Experiments were conducted with the temperature sensing sock on five volunteers in three different scenarios (worn, worn under a shoe, worn under a shoe while walking). The sock was also tested on a simulated foot before experiments. An additional condition was also evaluated on Volunteer 5, where a second cotton sock was worn on top of the temperature sensing sock. These experiments were carried out to understand the limitations of taking foot skin temperature measurements with a textile-based temperature sensor. The sock with interface is shown in figure 6.12.

Figure 6-12: Sock with USB 6008 DAQ from national instruments

The shoes worn by the volunteers are given in figure 6.13 below

Figure 6-13: The shoes worn by the five volunteers for the trial

Results from each of the test conditions have been detailed below.

6.3.1.1 The sock worn on the simulated foot

The results for when the sock was not worn by the volunteers, but instead worn on a simulated foot are presented in Figure 6.14. It was essential to capture and present the ambient temperature, since ambient temperature has an impact on skin contact temperature measurements (as shown in the literature (Psikuta et al.,2013)). These experiments were not conducted in a climate-controlled room and therefore daily variations had to be understood when comparing volunteer data.

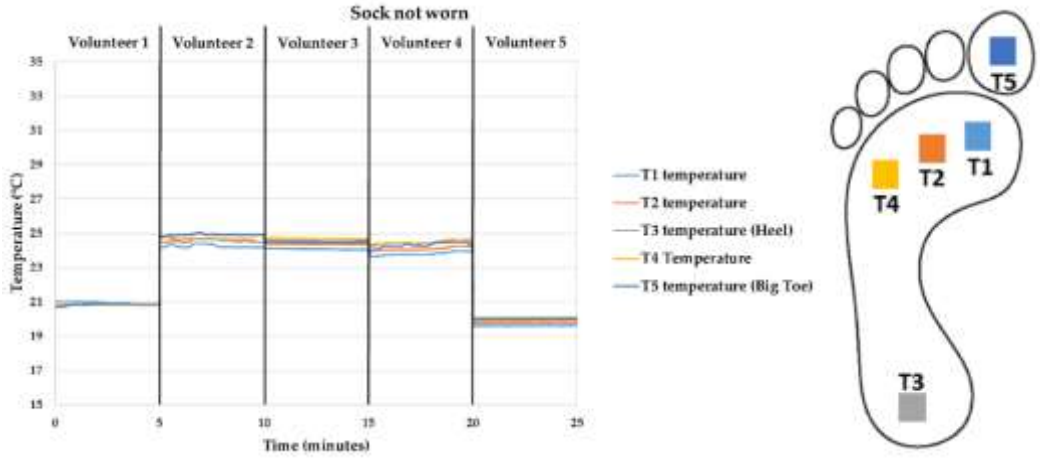

Figure 6-14: Temperature measurement from the temperature sensing sock when the sock was not worn by a volunteer. Temperatures were recorded prior to testing on all the volunteers: Volunteer 1, Volunteer 2, Volunteer 3, Volunteer 4, Volunteer 5.

Figure 6.14 shows that there were minor variation of >1 °C between the temperature measurements of the five temperature sensing yarns. This variation falls within the ± 1.37 °C accuracy of the thermistor, which has been specified by the thermistor manufacturer. It should also be noted that the user trails were not carried out on the same day, therefore, as seen in Figure 8, the ambient temperatures recorded prior to testing on each volunteer were different. Despite this, in the cases of the second, third and fourth volunteers the ambient temperatures captured were within a ± 1 ˚C and this provided similar test conditions for these three volunteers.

6.3.1.2 The sock when worn by the volunteers

Trials were subsequently carried out with the temperature sensing sock worn by volunteers. The temperatures captured by the temperature sensing yarns in the sock when the sock was worn by each of the volunteers, is presented in Figure 6.15.

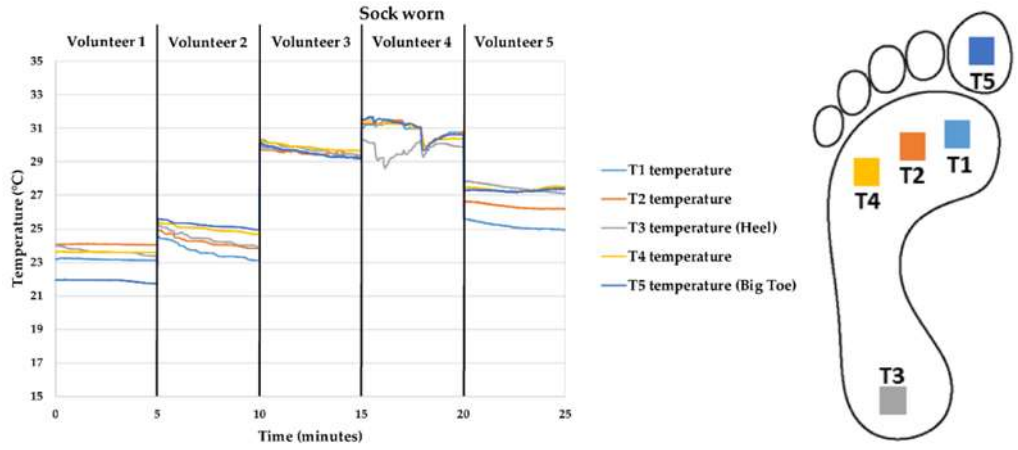

Figure 6-15: Temperature measurements from the temperature sensing sock when the sock was worn by each of the volunteers: Volunteer 1, Volunteer 2, Volunteer 3, Volunteer 4, Volunteer 5.

It can be observed in Figure 6.15 that when the sock was worn the temperature increased for all the volunteers. It was also seen that for all the volunteers, except for Volunteer 1, the foot

temperature measurements gradually decreased with time, this may have been caused due to cooling bought about by the room temperature.

For the first two volunteers the temperature measurements were below 28 °C, which was outside of one standard deviation of the mean measured foot temperatures presented in the literature (30.6 ± 2.6 °C) (Nardin et al., 2010). This may have been due to poor contact between the sock and the foot. The socks were made for a UK size 9 foot but the feet size of the first two volunteers were size 7 and 5 respectively. The temperature recorded from the next two volunteers were within the mean measured foot temperatures presented in the literature. This was most likely due to the sock fitting well to the wearer's feet. The foot size of the third and the fourth volunteers were 8.5 and 9 respectively. For the fourth volunteer the heel temperature (T3) was notably lower during the first three minutes compared to the other temperature sensing yarns. This may have been caused due to improper contact between the temperature sensing yarn and the heel. It was also observed that for the fourth volunteer there was a significant fall in the temperature readings after the first three minutes. This might have been due to the volunteer changing the position of their foot during the experiment.

The fifth volunteer had size 11 feet, implying that the temperature sensing sock would have had a close fit. The temperatures obtained from the fifth volunteer were not within the expected range (30.6 ± 2.6 °C). The fit of the sock might have affected the positioning of the thermistors in the temperature sensing yarns (especially in the cases of T1 and T2) and this could have led to improper contact between the foot and the temperature sensing yarns. The lower ambient temperature observed in the case of the fifth volunteer (as seen in Figure 6.14) would have also lowered the temperatures captured by the temperature sensing yarns in the sock.

Therefore, it can be argued that to obtain highly accurate or relative measurements the socks have to be well fitted to the wearer's feet.

6.3.1.3 The sock worn by the volunteers when a shoe was worn over it

Temperature measurements taken by the temperature sensing yarns from all of the volunteers when a shoe was worn on top of the sock are given in Figure 6.16.

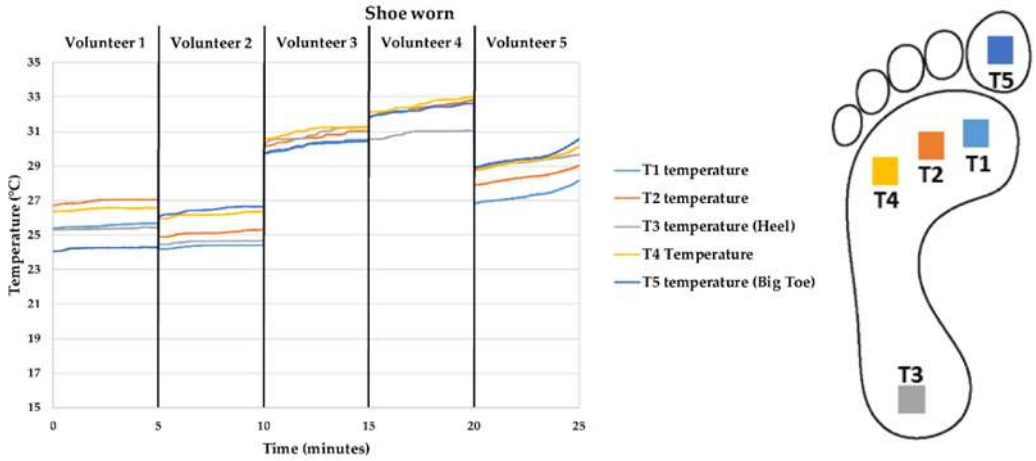

Figure 6-16: Temperature measurement from the temperature sensing sock when the sock was worn under a shoe for all of the volunteers: Volunteer 1, Volunteer 2, Volunteer 3, Volunteer 4, Volunteer 5.

The temperatures recorded increased for all the volunteers when a shoe was worn on top of the sock. The shoes provided insulation against the lower ambient temperature and reduced the heat flow from the foot to the atmosphere. The most significant rise in the temperature measurements were observed in the fourth volunteer (this volunteer wore a boot), where the temperature rose by 1.5 °C in four of the five sensors (T1, T2, T4 and T5). This may have been caused due to the extra insulation provided by the boot.

This data clearly showed that the shoes anatomy also had an impact on the temperatures captured by the temperature sensing yarns in the sock. It can be concluded that wearing a shoe over the sock alters the temperature measurements captured by the sock and that the anatomy of the shoe may also have an impact on the measurements.

6.3.1.4 Walking while the sock was worn and a shoe is worn on top

The results from walking while wearing the temperature sensing sock and a shoe for all the volunteers is presented in Figure 6.17.

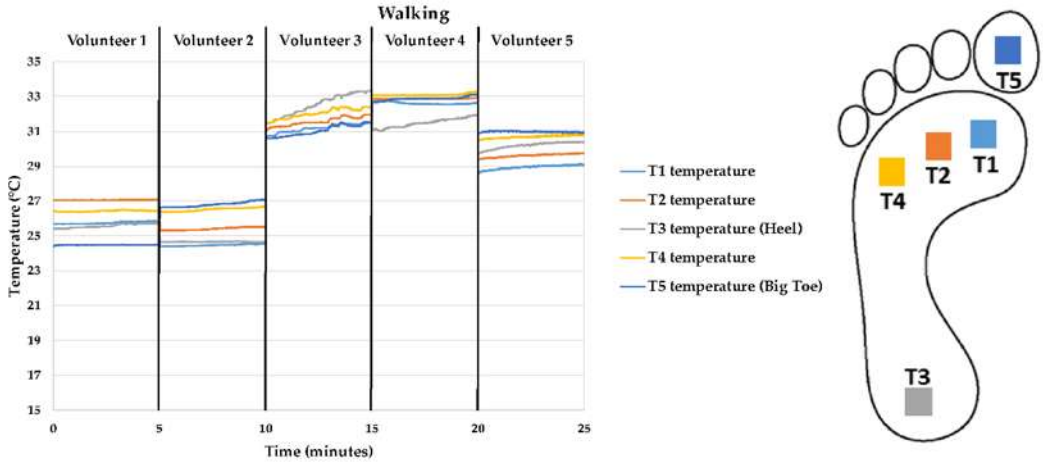

Figure 6-17: Temperature measurement from the temperature sensing sock when the sock worn under a shoe while walking for all of the volunteers: Volunteer 1, Volunteer 2, Volunteer 3, Volunteer 4, Volunteer 5.

As illustrated in Figure 6.17, walking bought about dissimilar changes in the temperatures recorded for each of the volunteers. For Volunteer 1 the temperature measurements were the same when the feet were moving compared to when they were stationary. For Volunteer 2 there was a minimal increase in the temperature recorded by four temperature sensing yarns (T1, T2, T4 and T5) when the user started walking. The temperature of the foot rose by the greatest amount for Volunteer 3. This may have been due to the fact that the volunteer moved their feet faster than the rest of the volunteers. This resulted in an up to a 3 °C temperature difference compared to when the sock was just worn (i.e. no movement and no shoe worn). In the case of Volunteer 4 motion bought about a small increase in temperature. For Volunteer 5 the temperature recorded by four of the temperature sensing yarns (except for the sensor on the Big Toe; T5) increased slightly. It can therefore be concluded that walking with these temperature sensing socks brought about changes in the temperatures captured. The changes in temperature depend on the individual wearing the sock as well as the walking speed, however further experiments would be needed to fully quantify this effect.

6.3.1.5 Wearing an additional sock over the temperature sensing sock

The results for when Volunteer 5 wore the temperature sensing sock and when an additional sock was worn on top of the temperature sensing sock were recorded and are shown in Figure 6.18.

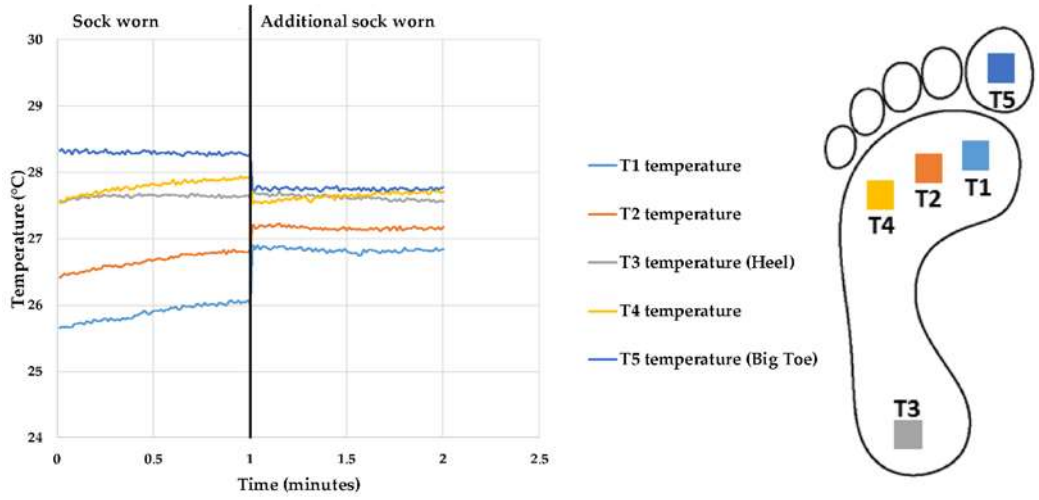

Figure 6-18: Temperature captured when the temperature sensing sock was worn (presented in the 1st minute) and when an additional sock was worn on top of it (presented in the 2nd minute).

Figure 6.18 showed that wearing another sock on top of the temperature sensing sock reduced the difference between the temperature captured by the five temperature sensing yarns significantly. Wearing an additional sock provided insulation to external environmental conditions, and enhanced the contact between the skin and the temperature sensing sock.

6.3.1.6 Discussion

Foot temperature measurements could be successfully captured for all of the volunteers at five points on the feet.

It was observed that the temperature captured from the first two volunteers were significantly lower than for the last three volunteers. This could be a result of the socks being too large for the feet of the first two volunteers, leading to poor contact between the sock and the skin. The temperature readings from Volunteers 1 and 2 were outside of the expected range for foot skin temperature, whereas the temperature readings from the last three volunteers were closer to this figure. This proved that the fit of the sock is critical to obtaining meaningful and realistic absolute temperature measurements. This supports the earlier experiments in this chapter showing the importance of contact pressure between the temperature sensing yarn and the skin. Therefore, in-order to ensure that the temperature sensing yarn provides precise temperature measurements, it would be advisable that the socks were made to fit the users' feet, guaranteeing good contact between the sock and the skins surface.

It was also observed that critical factors external to the sock, such as the type of footwear worn or movement of the feet had an effect on the absolute temperature readings. Work by Reddy et al. has shown that walking increases the foot temperature and has highlighted the importance of creating evidence-based healthcare guidelines for managing diabetic foot ulcerations (Reddy et al., 2017).

The temperature changes recorded in this section were not necessarily relative, for example in the case of Volunteer 3, walking induce a ~1 °C between points T3 and T4, when they had been in agreement when the foot was static. This would have influenced relative temperature measurements also.

For the last three volunteers (Volunteers 3, 4 and 5) it was observed that the temperatures recorded for the five temperature sensing yarns varied compared to each other by about ± 2 °C when the socks were worn.

Wearing another sock on top of the temperature sensing sock would enhance the contact between the temperature sensing sock and the skin, and act as an insulating layer between the sock and the external environment. The results have shown that the additional sock did reduce the recorded temperature differences between points on the foot. The differences between the points were still present when a shoe was worn (which would have provided some degree of thermal insulation), and therefore the change was likely due to better contact between the foot and the thermistors in the sock. This again highlighted the importance of the fit of the sock on the viability of taking foot skin temperature measurements.

Ultimately, highly accurate temperature measurements were only achieved when the sock had a very close fitting to the foot. Wearing a shoe and walking also bought about dissimilar changes in the temperature measurements from the volunteers (this resulted in an average change of 1.23 °C

in the five temperature sensing yarns in Volunteer 3). To obtain highly accurate and statistically relevant measurements the socks would have to be well fitted and calibrated depending on the individual and anatomy of the wearers shoe. The fit of the sock could be improved by custom knitting socks using scan-to-knit technology (Power, 2014).

For applications such as non-freezing cold injury detection where large temperature changes may be observed, and the exposure time to the lower temperatures is regarded important (Hope et al., 2014), these socks may provide an ideal solution. Currently there are no tools available that are capable of remotely monitoring foot temperature over a prolonged period of time in operational conditions. These socks would provide a powerful tool for the UK military to monitor, record and analyse the development of non-freezing cold injury in soldiers.

A California based start-up company Siren Care (Siren Care, 2017) showed interest in the sock for monitoring temperature in diabetic high risk patients (shown in figure 6.19). Therefore, prototypes of the sock were provided to them. They created an interface hardware consisting of a microcontroller, Bluetooth device and battery pack. The battery pack can be charged using a power socket, once charged it can last for 15 hours. They also created a smart phone application that provided the user with temperature measurements from each of the ETS yarn in the socks.

Figure 6-19: a) Socks and hardware developed by Siren care, b) Mobile application for the sock developed by Siren care (Siren Care, 2017).

6.3.2 User trials on the wearable thermograph

The thermograph created responded almost immediately to heated object and touch. The thermograph could not be tested on wound conditions without clinical approval, and during the course of this project it was not possible to evaluate the temperature sensing wound dressing in a clinical environment. However, in the future it is envisaged that the wound dressing will be tried on wound conditions. The clinical trials could help to determine the efficacy and suitability of the sensors.

6.4 Summary

The ETS yarn has been successfully used to create several garments. The sock for early detection of foot ulcers and the wound dressing that functions as a wearable thermograph. It can be stated that ETS yarns in fabrics give accurate relative measurements. To obtain highly accurate measurements an algorithm has to be used which would differ depending on the material used for the fabric, the atmospheric temperature, type of insulation on the fabric and depending on if the individual is walking/running/stationary. The limited user trials done with the socks have shown that for ideal use, the socks containing ETS yarn should fit the feet of the user. This would ensure proper contact between the ETS yarn and the feet of the user.

It is envisaged that the wound dressing created would be tested in wound conditions in the future. There have been no standards defined for wound temperature measurement. However, to commercialise and to use the wound dressing in clinical settings the ISO80601-2-56:2009 (en) (ISO80601-2-56:2009 (en) Medical electrical equipment— Part 2-56: Particular requirements for basic safety and essential performance of clinical thermometers for body temperature measurement) standard would have to be met. Companies such as URGO medical (Loughborough, UK) have shown interest in the wound dressing.

6.5 References

- Gould, P., 2003. Textiles gain intelligence. Mater. Today 6, 38–43. doi: 10.1016/S1369-7021(03)01028-9.
- Hope, K., Eglin, C., Golden, F., Tipton, M., 2014. Sublingual glyceryl trinitrate and the peripheral thermal responses in normal and cold-sensitive individuals. Microvasc. Res. 91, 84–89. doi: 10.1016/j.mvr.2013.11.002.
- Khan, Y., Garg, M., Gui, Q., Schadt, M., Gaikwad, A., Han, D., Yamamoto, N.A.D., Hart, P., Welte, R., Wilson, W., Czarnecki, S., Poliks, M., Jin, Z., Ghose, K., Egitto, F., Turner, J., Arias, A.C., 2016. Flexible Hybrid Electronics: Direct Interfacing of Soft and Hard Electronics for Wearable Health Monitoring. Adv. Funct. Mater. 26, 8764–8775. doi: 10.1002/adfm.201603763.
- KRUSS, 2018. Laplace pressure [WWW Document]. URL https://www.kruss-scientific.com/services/education-theory/glossary/laplace-pressure/ (accessed 2.23.18).
- Munro, B.J., Campbell, T.E., Wallace, G.G., Steele, J.R., 2008. The intelligent knee sleeve: A wearable biofeedback device. Sens. Actuators B Chem. 131, 541–547. doi: 10.1016/j.snb.2007.12.041.
- Nardin, R. A., Fogerson, P. M., Nie, R., Rutkove, S. B., 2010. Foot temperature in healthy individuals: effects of ambient temperature and age. J. Am. Podiatr. Med. Assoc., 100, 258–264. doi: 10.7547/1000258.

- National Instruments, 2013. VI Package Manager - National Instruments [WWW Document]. URL http://www.ni.com/tutorial/12397/en/ (accessed 2.23.18).
- Power, E. J. 2014. Yarn to Fabric: Knitting, in: Sinclair, R. (Ed.), Textiles and Fashion. Woodhead Publishing, Cambridge.
- Psikuta, A., Niedermann, R., Rossi, R. M., 2013. Effect of ambient temperature and attachment method on surface temperature measurements. Int. J. Biometeorol. 58, 877–88. doi: 10.1007/s00484-013-0669-4.
- Reddy, P. N., Cooper, G., Weightman, A., Hodson-Tole, E., Reeves, N. D., 2017. Walking cadence affects rate of plantar foot temperature change but not final temperature in younger and older adults. Gait Posture. 52, 272–279. DOI: 10.1016/j.gaitpost.2016.12.008.
- Siren Care, 2017. Smart Diabetic Socks [WWW Document]. Siren. URL https://siren.care/ (accessed 2.23.18).

7. Conclusion

This is concluding chapter of the thesis and it has been broken down into the following subsections in-order to give a clear overview.

- Problems encountered during the research
- Summary and conclusion
- Contribution to knowledge
- Future work

7.1 Problems encountered during the research

In this research project there were many difficulties that were encountered and had to be overcome. The main complications are listed below.

- Manufacture of the ETS yarn- The process of making a single ETS yarn during the course of this research took close to an hour due to the difficulty in getting rid of the short circuit in between the solder pads of the thermistor.
- Robust Connection between ETS yarns and the interface hardware- Creating a robust connection between the fine copper wires and the interfacing hardware proved troublesome. One solution implemented was to use heat shrinkable sleeves to give the connections more mechanical strength.
- Proper Contact between the ECHOTHERM™ IC50 digital Chilling/Heating Dry Bath plate and the samples tested- It was difficult to ensure that the samples tested were in proper contact with the plate of the dry bath. Insulating tape was used to hold the ETS yarn samples down and fabric tape was used to hold down the knitted fabric.
- Water wicking onto the interface hardware during the moisture absorption test on the M/K Gats system - This equipment required the fabric samples to be placed on top of the porous plate for absorption to occur and the ETS yarn had to be connected to the NI DAQ unit for measurements to be taken. This resulted in water from the knitted fabric flowing onto the interface circuit. Hence a stand was used to position the PCB board above the porous plate but this effected the contact between the porous plate and the knitted fabric sample. A solution suggested by Mbise et al (Mbise, 2015) was to use a wire mesh on top of the knitted fabric to enhance the contact but the weight of the wire mesh was insufficient to hold the sample in place. Therefore a weight of 119.17 g was placed on top of the wire mesh to ensure proper contact between the knitted fabric and the porous plate.

7.2 Summary and Conclusion

7.2.1 Exclusive Summary

A novel technology for monitoring skin temperature, with a potential to identify complications (such as Non Freezing Cold Injury formation, wound infection and early detection of diabetic ulceration) has been presented. A unique electronic temperature sensing (ETS) yarn has been developed and characterised. The yarn was designed to ensure that the sensor response time and accuracy was sufficient to collect physiologically relevant measurements.

Initially a geometrical model of the ETS yarn was designed. This was used to calculate the theoretical minimum diameter of the cylindrical micro-pod needed to encapsulate the thermistor at the heart of the yarn and it was calculated as 0.732 mm. Practically it was not possible to create such a small micro-pod, therefore the next best diameter was decided as 0.87 mm. Thereafter the ETS yarn was made in three stages; interconnection formation stage, micro-pod creation stage and covering stage.

Experiments were conducted to investigate the effect of the micro-pod creation stage on the response and recovery times of the ETS yarn, where it was shown that the volume of micro-pod had an insignificant effect on the response and recovery times of the sensor, this also held true in the presence of filaments within the micro-pod. The micro-pod, packing fibres and the braided yarn sheath however increased the response and recovery time by 310%, although the final thermal time constant was only 12.1 s. This can be regarded as adequate when the ETS yarn is used for body monitoring applications where readings will take place over a time course of hours. A test rig was used to demonstrate that temperature measurements made using the ETS yarn were comparable to traditional temperature measurements and that the system was well suited to making long term temperature measurements. The ETS yarns accuracy was determined to be accurate with ± 0.5 °C, which was suitable for detecting a difference of 2 °C, for 63 % of measurements taken. The polymer micro-pod was shown to protect the yarn from applied strain using cyclical strain tests, which was essential as garments are subjected to constant strain during the manufacturing process.

External conditions (such as ambient temperature, insulation using other material, wind speed and the contact between the surface and the textile) influence the absolute temperature measurements captured using ETS yarn in a temperature sensing fabric. If the external conditions are known, then the system can be calibrated against a known temperature sensor. If the temperature sensing fabrics are used in homes or hospitals, where the environmental conditions would remain fairly constant, this would not be problematic. These external conditions will have minor impact for the applications specified in the thesis (i.e. diabetic foot ulceration or wound infection), because a temperature difference monitoring system is what is required. Ideally, if all

the sensors are in proper contact with the skin then all of the sensors would be effected by the same environmental conditions. If the environmental conditions remain almost constant they can be ignored when taking measurements of temperature differences across the skin.

Finally, temperature sensing prototype garments have been produced using a network of ETS yarn. Temperature sensing socks and a smart wound dressing capable of functioning as a wearable thermograph were created and both work as expected. The user trial carried out using the socks shows how these prototypes can be used to monitor skin temperature. The creation of a representative temperature difference monitoring device for skin measurements opens a number of exciting possibilities for both clinical and pre-clinical studies.

7.2.2 Conclusion

In conclusion this research has shown that a novel electronic temperature sensing yarn could be created by embedding miniature thermistors within the fibres of a textile yarn. The yarn could be used to make textile fabrics or garments and it does not seem to affect the textile characteristics of the textile (such as its ability to bend, drape and shear), however experiments will have to be conducted in the future to quantify the effects of the micro-pod on the textile characteristics. The electronic temperature sensing yarn is well suited for making long term measurements of temperature when incorporated into a garment creating an innovative skin temperature difference monitoring device. It is also capable of providing remote, continuous temperature measurements at given points on the skin. The miniature size of the thermistor makes it invisible to the wearer and well suited for wearable applications.

Even though there are many wearable temperature sensors in the market most of these are not textile-based and geared for truly discrete temperature measurements. The few textile-based temperature sensors that have been produced are unable to provide localised temperature measurements. Therefore the electronic temperature sensor yarn developed in this research would provide clinicians with a powerful tool when dealing with pathologies such as wound care, early detection of diabetic ulcers and non-freezing cold injury detection.

7.3 Contribution to knowledge

- Critical analysis in the literature of the temperature sensors that are currently used for temperature measurement.
- A new method of producing electronic yarns using a silicone, silicon carbide, carbon (SiO, SIC, C) mould and a General Purpose Resin (GPR) mould has been demonstrated.
- A theoretical model has been created to study the heat flow through the ETS yarn and it's been validated using experimental results.

- The effects of the yarn filaments and the polymer resin on the response and recovery time of the sensor has been analyzed and understood.
- The effects of the yarn filaments and the polymer resin on the accuracy of the thermistor have been examined.
- The effects of tensile stress on the temperature measurements of the ETS yarn has been evaluated.
- The effects of environmental conditions on temperature sensing fabrics have been explored.
- Production of prototype garments using the ETS yarn; Armbands, gloves, socks, wound dressings.

7.4 Future work

The prototype socks created as part of this work have been tested on healthy individuals however, a statistically significant user trail with healthy individuals would have to be carried out in-order to sort out any potential issues with the textile fabrication process. The socks could be used for non-freezing cold injury detection however, in order to do so ethical approval has to be taken. The smart socks could also be used for early detection of diabetic ulcers, in-order to proceed further it will be important to involve clinicians in this project. Clinical trials must be conducted on the socks before it can be used by diabetic patients. The smart wound dressing will also have to be tested on patients with open wounds, this too requires clinical approval. Future work will exploit this innovation to address the apparent absence in the literature for guidance of the temperature variation for wound infection. Since the current clinical trials in wound temperature measurement have not been carried out using a localized, continuous temperature monitoring system, they have been unable to provide clinicians with a powerful tool when dealing with wounds.

The wearer comfort level is another important aspect that must be looked into before the sock is used by diabetic patients. Experiments will have to be carried out to quantify the effects of the micro-pod on the textile characteristics (such as its ability to bend, drape and shear). The design of the software and the interconnecting hardware must also be improved in-order to make it more appealing to the wearer.

Another crucial area that has to be dealt with is the automation of the yarn manufacturing process. This would enable the production of large quantities of ETS yarn. This project is currently carried out by the Advanced Textiles Research Group (ATRG) of Nottingham Trent University. At the time of writing a semi-automated production process is in place were one ETS yarns can be produced in less than 15 minutes. The craft process carried out in this research took more than 1 hour to produce one ETS yarns. Automation of the process will also improve the repeatability of the production process and in theory this will create more reliable yarns.

One more vital factor that must be looked at is the miniaturization of the diameter of the ETS yarn. In-order to integrate it into any textile structure the yarn ideally should be capable of fitting through the head of a sewing needle. The project of miniaturizing these electronic yarns are currently been done by the Advanced Textiles Research Group in collaboration with Southampton University.

The temperature error that can occur due to the tolerances of the Murata thermistor (model) is quite high and in the future would be advisable to use a temperature sensor with a higher accuracy.

For the applications specified in the thesis highly accurate absolute temperature measurements were not required however if it was desired a method has to be devised to enhance the contact between the temperature sensing textile and the skin. It is also essential to minimize the effects of the atmospheric temperature. An ideal solution would be to have an algorithm in the monitoring hardware that equates the actual temperature captured depending on the level of insulation, atmospheric temperature and wind speed but this is quite impractical because of the requirement of additional sensors. Assuming that the temperature sensing textile will be used in homes and hospitals where the room temperature would be fairly constant the ETS yarn could be calibrated against a known temperature sensing system.

It is also vital to minimize the size of the interconnecting hardware. In the future it is likely that the monitoring hardware would be small enough to be included within the yarn itself. Until then it is important to develop a small, light and comfortable hardware interface. It is also crucial to find a strong and robust way to connect the ETS yarn onto the interface hardware. A miniaturized alternative power source (preferably self-sustainable) will have to be developed to power it. The flexible ribbon like perovskite solar cells developed by Li et al (Li et al., 2016) might be a solution.

Lastly, the sustainability of temperature sensing textiles have to be addressed before it goes into mass production (McLaren et al., 2017).

7.5 References

- Li, C., Islam, M.M., Moore, J., Sleppy, J., Morrison, C., Konstantinov, K., Dou, S.X., Renduchintala, C., Thomas, J., 2016. Wearable energy-smart ribbons for synchronous energy harvest and storage. Nat. Commun. 7, 13319. doi: 10.1038/ncomms13319.
- Mbise, E., 2015. The development of a quick dry fabric for outdoors garments (PhD thesis). Nottingham Trent University, Nottingham.
- McLaren, A., Hardy, D.A., Hughes-Riley, T., 2017. Electronic textiles and product lifetimes: exploring design strategies for product longevity. Presented at the Product Lifetimes And The Environment (PLATE) Conference, Delft, Netherlands.

8. Appendix

8.1 Appendix 1: Fibre Optic thermometers

8.1.1 Fibre Bragg gratings (FBG)

They are formed by a periodic perturbation of the core refractive index of an optical fibre. Hence coupling between the nodes can be achieved. A common FBG couples a forward-propagating mode into its contradirectional propagating version. FBG's use the thermooptical effect where the change in refractive index due to thermal effects is used to calculate the temperature. The reflection spectrum centre wavelength shift can be used to calculate the sensing parameters and it's given by the resonance or Bragg condition (given in equation 8.1).

$$\lambda \mathbf{B} = 2n_{eff}\Lambda \quad (8.1)$$

Where, Λ - spacial refractive index perturbation period and n_{eff} - effective refractive index of the mode in consideration.

The sensitivity of the FBG sensor for a change in temperature with regard to change in reflected wavelength can be computed using equation 8.2.

$$\frac{\lambda(\mathrm{B,T})}{\lambda \mathrm{B}} = \frac{1}{\lambda \mathrm{B}}\frac{d\lambda \mathrm{B}}{\mathrm{dT}} = \left(\frac{1}{n_{eff}}\frac{\partial n_{eff}}{\partial T} - \frac{\partial {n_{eff}}^2}{2}(p_{11} + 2p_{12})\alpha T + \alpha T\right) \quad (8.2)$$

Where, ΔλB,T /λB - relative change in centre wavelength per temperature change (K), ∂neff/∂T - thermooptical coefficient, p_{11} and p_{12} are Pockel's coefficients which represents the photoelastic effect and αT - thermal expansion coefficient of the fibre material.

FBGs have a very niche market due to the high technological effort required to manufacture them. They are generally embedded in carbon fibre reinforced plastic structures and used in aeronautics (Hoffmann et al., 2007).

8.1.2 Distributed temperature sensing using Raman Scattering

Optical fibre distributed temperature sensors enable to monitor the temperature profile along the length of a fibre continuously. This is achieved by sending a short laser pulse along the fibre and detecting the backscattering Raman light, with high temporal resolution. The Raman light intensity contains information about temperature and loss along the fibre, whereas the distance of the fibres can be measured by detecting the time taken for the back scattering signal to arrive after sending the pulse (Hoffmann et al., 2007).

8.1.3 Temperature sensing with an interferometric probe

Interferometric fibre optical temperature sensors can be divided into extrinsic and intrinsic sensor types. The main function of interferometric sensors is the variation of the optical resonator length. Intrinsic sensors use Fabry–Perot resonators which consists of a single-mode fibre with a partially

transmitting fibre end. Extrinsic sensors use a thin film Fabry-Perot resonator which is localized on the fibre end. The Fabry-Perot resonator of a temperature sensor generally comprises of multiple thin layers with alternating low and high refraction indices. The refractive index has a temperature dependence (Hoffmann et al., 2007).

8.1.4 Semiconductor band gap technology which depends on the band gap of semiconductor crystals

The photonic band gap for semiconductor-based photonic crystals are effected by temperature. The band gap shifts with temperature and is more pronounced in the structures where the refractive index changes more with temperature (Malik et al., 2013).

8.1.5 Brillouin Scattering distributed temperature sensors

Brillouin scattering is a “photon-phonon” interaction as annihilation of a pump photon creates a phonon and a Stokes photon simultaneously. The phonon created is the vibrational modes of atoms, it is also called an acoustic phonon/wave or a propagation density wave (Zou et al., 2015). Brillouin scattering strongly depends on the temperature in the medium, entropy, and the material density (Galindez-Jamioy and López-Higuera, 2012). Stimulated Brillouin scattering (SBS) which occurs in the core of an optical fibre can be used to construct a distributed temperature sensor (Culverhouse et al., 1989).

8.2 Appendix 2: Datasheet provided for the NCP15XH103F03RC (NTC) thermistor by Murata (Kyoto, Japan)

muRata INNOVATOR IN ELECTRONICS

Product Search Data Sheet

Note: This datasheet may be out of date.
Please download the latest datasheet of NCP15XH103F03RC from the official website of Murata Manufacturing Co., Ltd.
https://www.murata.com/en-eu/products/productdetail?partno=NCP15XH103F03RC

NCP15XH103F03RC

In Production | Recommended | RoHS | REACH

Appearance & Shape

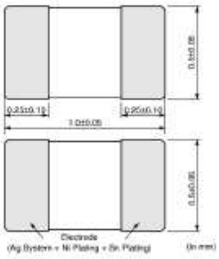

Features

1. Excellent solderability and high stability in environment
2. Excellent long time aging stability
3. High accuracy in resistance and B-Constant
4. Reflow soldering possible
5. Same B-constant in the same resistance in the three sizes (0805 size / 0603 size / 0402 size)
   Easy to use smaller size in the circuits
6. Lead is not contained in the product.
7. NCP series are recognized by UL/cUL (UL1434, File No.E137188).

Applications

Limited Usage	Consumer Grade
Other Usage	1. Temperature compensation for transistor, IC and crystal oscillator in mobile communications 2. Temperature sensor for rechargeable batteries 3. Temperature compensation of LCD 4. Temperature compensation in general use of electric circuits

Packaging Information

Packaging	Specifications	Minimum Order Quantity
RC	180mm Paper Tape	10000

NCP15XH103F03RC

Specifications

Resistance (25℃)	10kΩ
Resistance Value Tolerance (at 25℃)	±1%
B-Constant (25/50℃)	3380K
B-Constant (25/50℃) Tolerance	±1%
B-Constant(25/80℃)(Reference Value)	3428K
B-Constant(25/85℃)(Reference Value)	3434K
B-Constant(25/100℃)(Reference Value)	3455K
Permissive Operating Current (25℃)	0.31mA
Rated Electric Power (25℃)	100.0mW
Typical Dissipation Constant (25℃)	1mW/℃
Operating Temperature Range	-40℃ to 125℃
Size Code (in mm)	1.0x0.5mm
Size Code (in inch)	0.4x0.2inch
Shape	SMD
Mass	0.0012g

NCP15XH103F03RC

Product Data

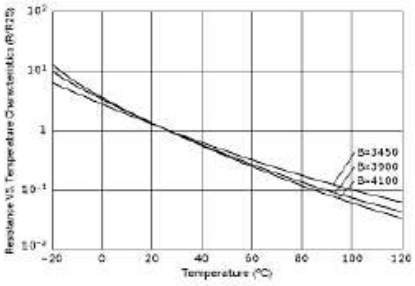

Resistance-Temperature Characteristics

Basic Characteristics

■ Basic Characteristics

1. Zero-power Resistance of Thermistor: R

$R=R_0 \exp B(1/T-1/T_0)$ ·····(1)

R: Resistance in ambient temperature T (K)
(K: absolute temperature)
R_0: Resistance in ambient temperature T_0 (K)
B: B-Constant of Thermistor

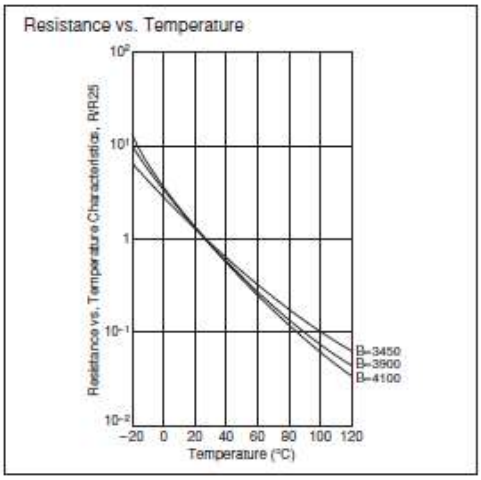

2. B-Constant

as (1) formula

$B=\ell n (R/R_0) / (1/T-1/T_0)$ ·····(2)

3. Thermal Dissipation Constant

When electric power P (mW) is spent in ambient temperature T_1 and thermistor temperature rises T_2, there is a formula as follows

$P=C(T_2-T_1)$ ·····(3)

C: Thermal dissipation constant (mW/°C)
Thermal dissipation constant is varied with dimensions, measurement conditions, etc.

4. Thermal Time Constant

Period in which Thermistor's temperature will change 63.2% of its temperature difference from ambient temperature T_0 (°C) to T_1 (°C).

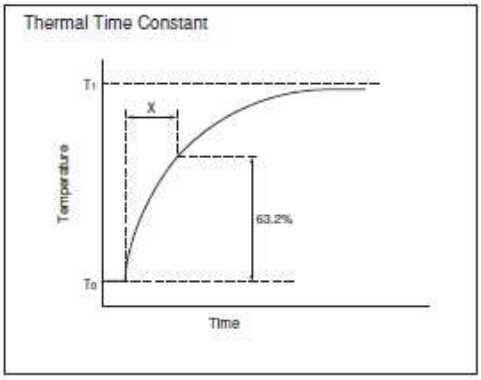

■ Performance

Item	Condition
Resistance	Measured by zero-power in specified ambient temperature.
B-Constant	Calculated between two specified ambient temperatures by next formula. T and T_0 is absolute temperature (K). $B=\frac{\ell n (R/R_0)}{1/T-1/T_0}$
Thermal Dissipation Constant	Shows necessary electric power that Thermistor's temperature rises 1°C by self heating. It is calculated by next formula (mW/°C). $C=\frac{P}{T-T_0}$
Rated Electric Power	Shows the required electric power that causes Thermistor's temperature to rise to a specified temperature by self heating, at ambient temperature of 25 °C.
Permissive Operating Current	It is possible to keep Thermistor's temperature rising max. 1°C.

Please inquire about test conditions and ratings.

8.3 Appendix 3: Diameter and resistance measurements from the eight strand copper wire

8.3.1 Diameter of the eight strand copper wire

In order to calculate the diameter of the copper strands, five strands from the eight strand copper wire was chosen. The diameter of the copper strand was measured using an Olympus BX41

microscope (OLYMPUS, Tokyo, Japan) given below in figure 8.1. The microscope was calibrated according to the manufacturer's specifications. The values obtained for the measurements and the average are given in table 8.1.

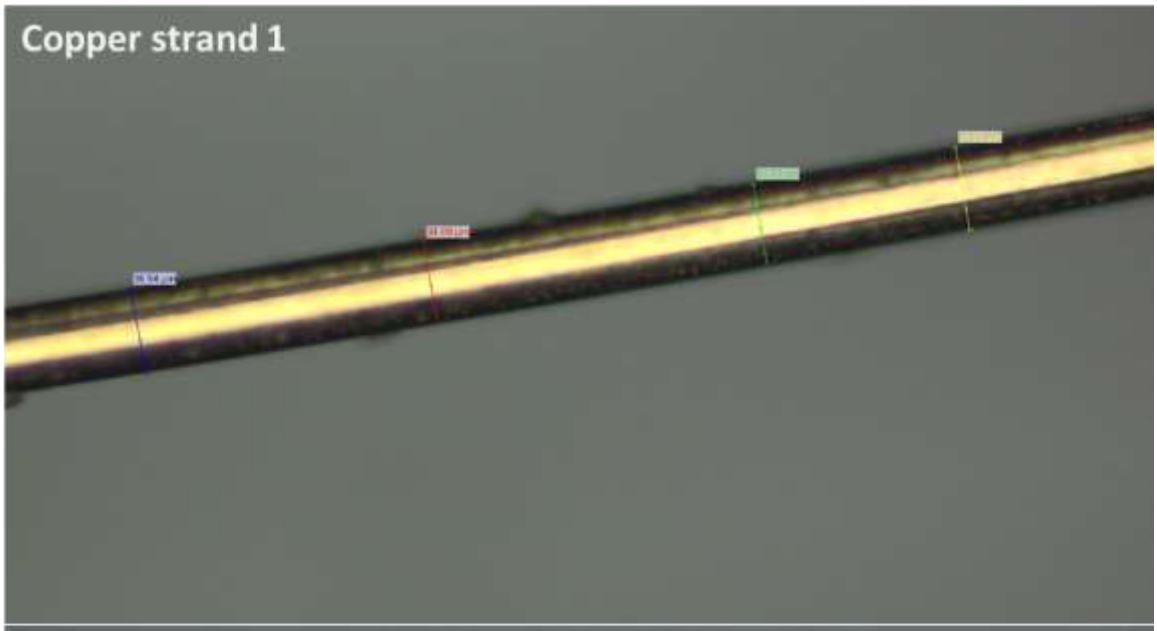
Copper strand 1

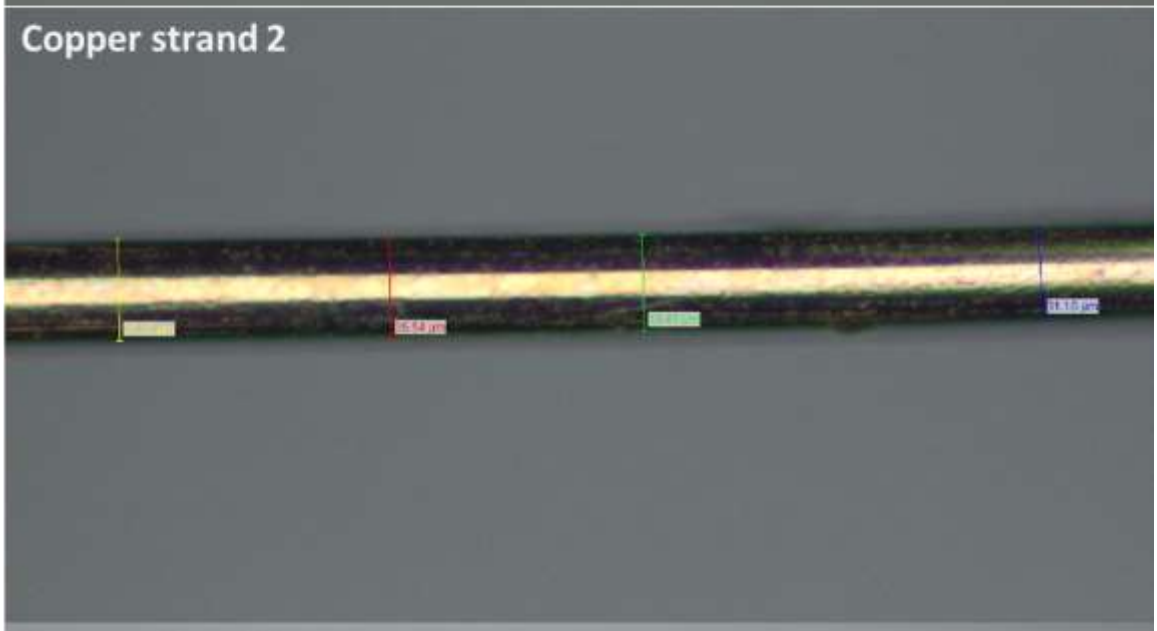
Copper strand 2


Copper strand 3

Figure 8-1: Images of the copper strands taken on the Olympus microscope

Table 8-1: Diameter of the copper strands

	copper strand 1	copper strand 2	copper strand 3	copper strand 4	copper strand 5
Diameter at location 1/µm	36.54	35.2	35.7	29.87	34.52
Diameter at location 2/µm	34.99	35.54	35.7	32.45	33.48
Diameter at location 3/µm	34.99	33.47	38.11	33.42	34.52
Diameter at location 4/µm	33.58	31.1	39.14	36.16	33.48
Average diameter of each copper strand/µm	35.025	33.8275	37.1625	32.975	34
Average diameter of a strand/µm			34.598		
Standard Deviation			2.16		
standard Error			0.48		

8.3.2 Resistance of the eight strand copper wire

The resistance of the copper wire was measured using an Agilent 34410A 6 ½ Digital multi-meter (Agilent Technologies, California, USA). The copper wire was measured against a meter ruler to obtain the length.

Table 8-2: Resistance of a meter of the 8 strand copper wire

Length/m	Resistance/Ω
1	16.66
1	16.55
1	16.461
1	15.1
1	15.01
Average resistance/Ω	15.9562
Standard deviation	0.74
Standard error	0.33

8.4 Appendix 4: Calibration curves for the Resistance vs Temperature of the six thermistors

The calibration graphs for each of the six thermistors are given below in figures 8.2-8.7.

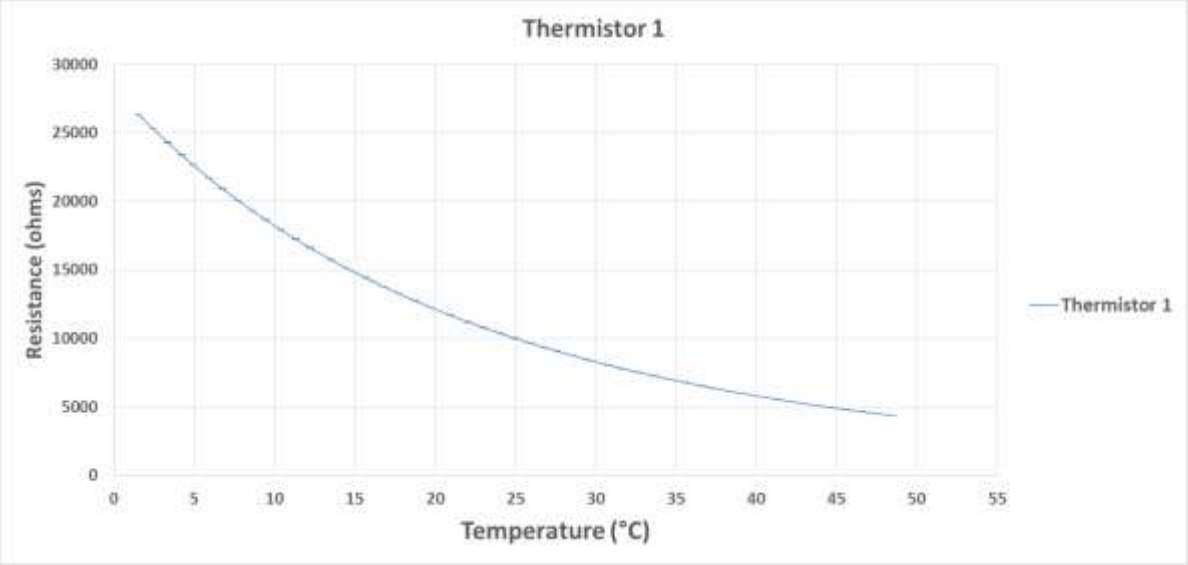

Figure 8-2: Calibration graph of thermistor 1

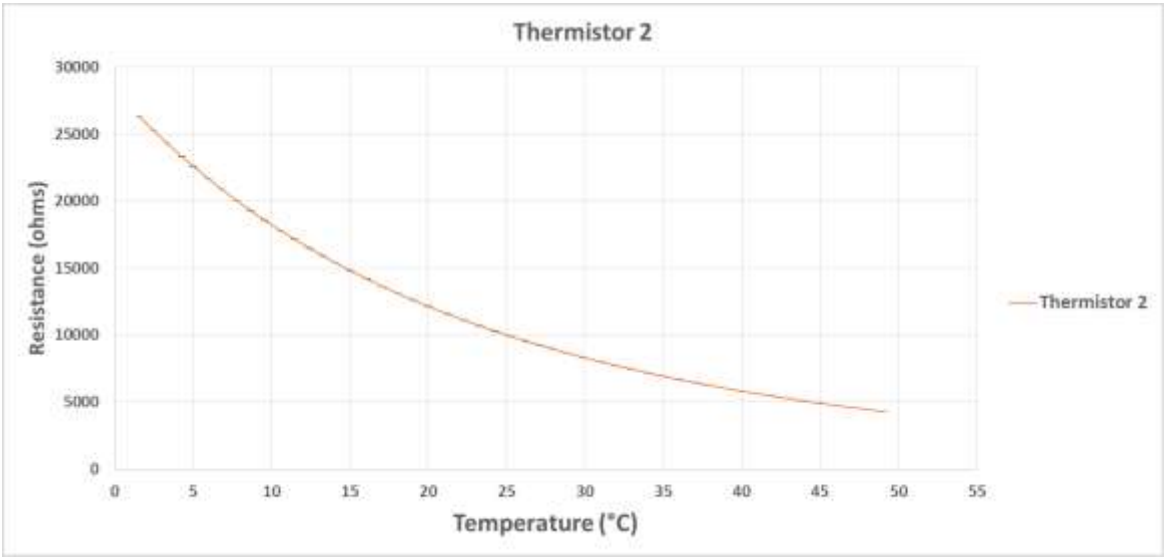

Figure 8-3: Calibration graph of thermistor 2

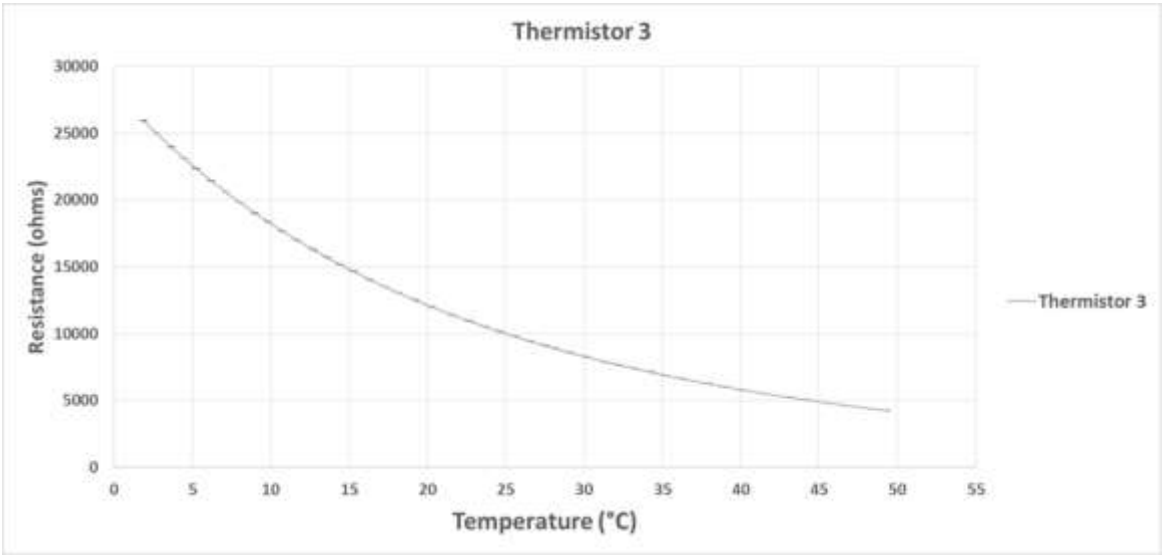

Figure 8-4 Calibration graph of thermistor 3

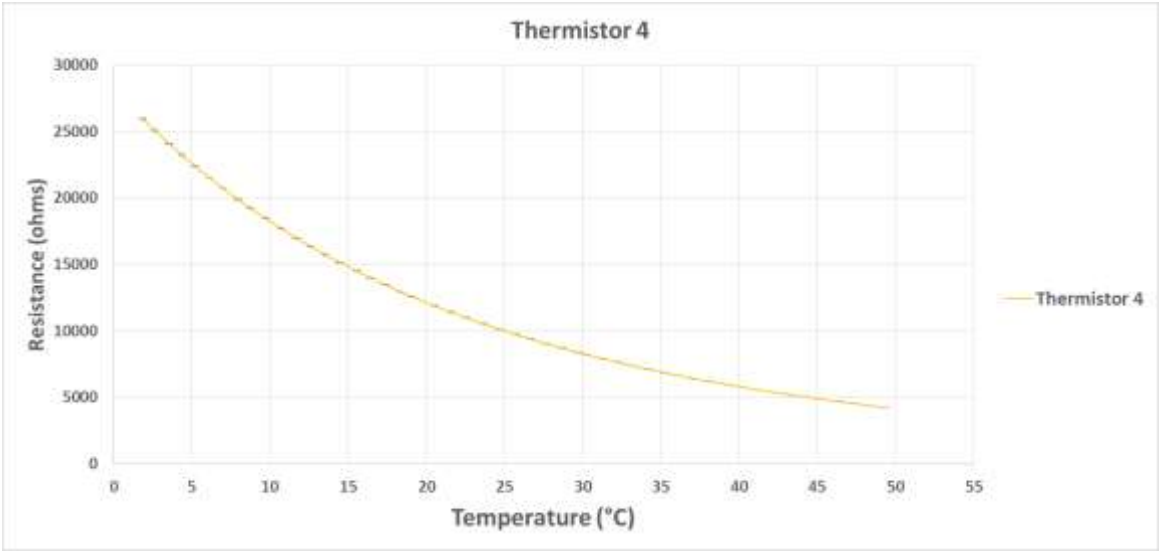

Figure 8-5 Calibration graph of thermistor 4

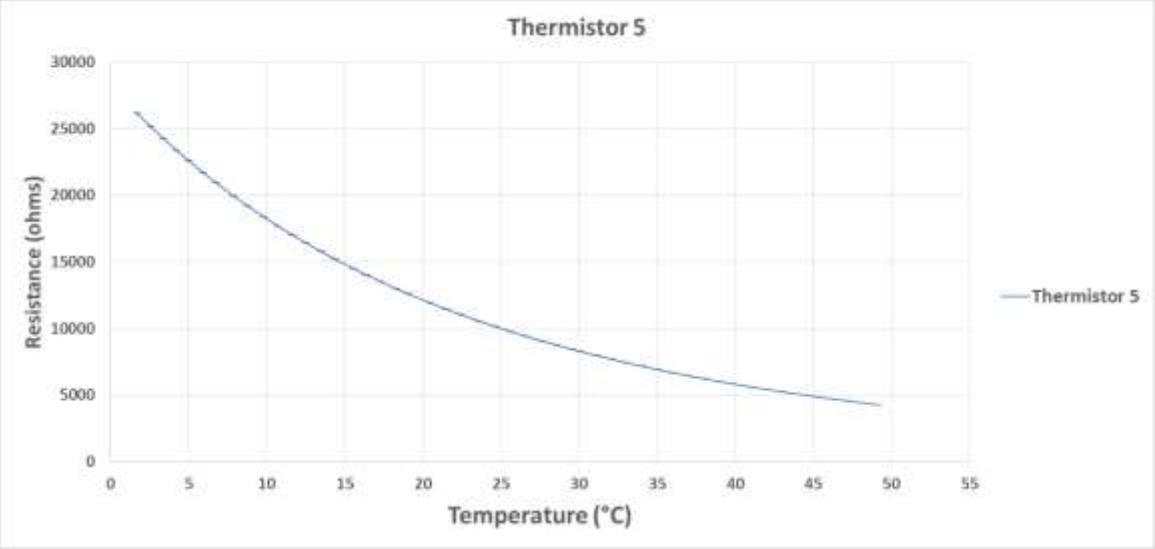

Figure 8-6 Calibration graph of thermistor 5

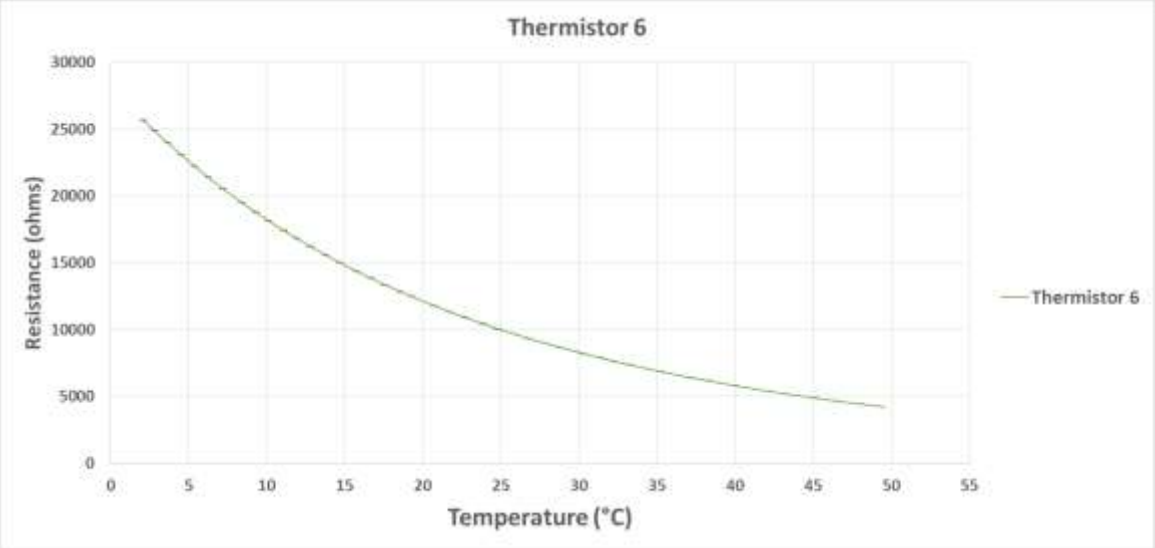

Figure 8-7: Calibration graph of thermistor 6

8.5 Appendix 5: MATLAB code for generating the Geometrical model

The MATLAB code for the Geometrical model.

8.5.1 Main Program

```
%Geometrical model of the ETS yarn
%calculates the minimum volume of resin, minimum radius of encapsulation
and also gives the volume of resin depending on the mass of resin used
Mr = 0.00141*(10^-3);%mass of resin
den = 2000;%density of resin[kg/m3]
Vr = 1.639*(10^-10);%Mr/den;%volume of resin
Lc= 1*(10^-3);%length of thermistor chip
Wc= 0.5*(10^-3);%width of thermistor chip
Hc= 0.5*(10^-3);%height of thermistor chip
Ls=Lc/4;%length of solder pad
Vc= Lc*Wc*Hc; %volume of thermistor chip
NCufillaments= 8;%number of copper strands
diameterofcopper     =     3.4598*10^(-5);%diametre     of     the     copper
filaments(8strand total 128microns)
nyarnc = 2;%number of yarn around the chip(used in the micro-pod creation
stage)
```

```
Nfibres = nyarnc*48; %Number of yarn multiplied by the filament count to
get the total number of filaments
diameterofpoly = 1.4464*10^(-5);%diametre of a fibre in the 1/167/48
polyester undyed yarn
nyarnb = 6;%number of yarn used in the braiding process
Volfraction = 0.5;%volume fraction of the braided layer
%calculate the whole volume
D_ofbraidingcylinder= 1*10^(-3);%diameter of the braiding machine cylinder
[Vw,r] = wholevolume3cylindrical1( Lc,Wc,Hc,diameterofcopper);
%calculate the minimum volume of solderpaste
[ Vol_solder,Vt ] =
min_vol_solderpaste( Lc,Wc,diameterofcopper,NCufillaments );
%calculate the volume of occupied by the polyester fibres
[Vp] = Vol_polyesterfibres2cylindrical1(diameterofpoly,Nfibres,Lc);
%calculate the optimum amount of resin
[ Opt_Vol_res ] = optimum_resinvol2(Lc,Wc,Hc,Vp,Vw,Vt);
%It also plots the ETS yarn according to the specifications of the user
%drawing the circle
Vw1= Vr+Vc+(Vt*2)+Vp; %whole volume sphere
rad = sqrt(Vw1/(Lc*pi));% radius of the cylinder
%call the plot chip function in matlab
plotchip( Lc,Wc,Hc );
%plot the resin in Matlab
plotresin2cylindrical1( rad,Lc,diameterofcopper )
%call the plot solder pads functions
plotsolderpads1(Lc,Ls,Wc,Hc);
plotsolderpads2(Lc,Ls,Wc,Hc);
%plot the copper filaments
copperfilaments(NCufillaments,Ls,Hc,diameterofcopper);
%plot the solder paste
plotsolderpaste1( Lc,Ls,Wc,Hc,diameterofcopper);
plotsolderpaste2( Lc,Ls,Wc,Hc,diameterofcopper);
%plot the  yarn fibres used before encapsulation(around the thermistor
%chip)
polyesterarnchip(Nfibres,Lc,Hc );
% plot packing fibre layer
plotpackingfibres( D_ofbraidingcylinder,Lc,radpolyesteryarn,diameterofcop
per )
%plot the number of yarn fibres used in the braiding process
[radpolyesteryarn]=
polyesteryarn2cylindrical1( nyarnb,Lc,Volfraction,diameterofpoly,Nfibres,
diameterofcopper,D_ofbraidingcylinder);
%change background colour
set(gca,'Color',[1 1 1]);
%label the axis
xlabel('width/m');
ylabel('length/m');
zlabel('height/m');
```

8.5.2 Functions

wholevolume3cylindrical1 function

```
function [Vw,r] = wholevolume3cylindrical1( Lc,Wc,Hc,diameterofcopper )
%calculate the optimum volume of the entire encapsulation
%calculate the Hypotenuse (add the width of the chip and the solder paste
width to the width
p= sqrt((Wc+diameterofcopper)^2+(Hc)^2);

r= p/2;%radius of the cylinder of resin
%calculate the whole cylindrical volume of micropod
Vw = (Lc)*pi*(r^2);
```

```
end
```

min_vol_solderpaste function

```
function [ Vol_solder,Vt] = min_vol_solderpaste( Lc,Wc,diameterofcopper,NCufillaments )
%calculating the minimum volume of solder paste required
%total volume= area of solderpad* diameter of copper filament
Vt= (Lc/4)*Wc*diameterofcopper;
%volume occupied by a copper filament (length of solder pad*radius squared*pi
radius_copper= diameterofcopper/2;
Vcu1= (radius_copper^2)*pi*(Lc/4);
%volume occupied by all the copper filaments
Vcu = NCufillaments*Vcu1;
Vol_solder= Vt-Vcu;
end
```

Vol_polyesterfibres2cylindrical1 function

```
function [Vp] = Vol_polyesterfibres2cylindrical1(diameterofpoly,Nfibres,Lc)
%Calculating the optimum volume of polyester fibres in the encapsulation.
Rp = diameterofpoly/2;
hp = Lc;
V1p = pi*(Rp^2)*hp;%volume of a single fibre
%volume of all the fibres
Vp = Nfibres*V1p;
end
```

optimum_resinvol2 function

```
function [ Opt_Vol_res ] = optimum_resinvol2(Lc,Wc,Hc,Vp,Vw,Vt)
%calculating the optimum volume of resin to cover the entire chip
%calculating the volume of the chip
Vc = Lc*Wc*Hc;
%volume occupied by solder paste and copper filaments
Vtp=Vt*2;
Opt_Vol_res= Vw-Vc-Vtp-Vp;
end
```

plotchip function

```
function plotchip( Lc,Wc,Hc )
%ploting the chip in matlab
p1 = [(Wc/2) (Hc/2) -(Lc/2)];
p2 = [(Wc/2) -(Hc/2) -(Lc/2)];
p3 = [-(Wc/2) -(Hc/2) -(Lc/2)];
p4 = [-(Wc/2) (Hc/2) -(Lc/2)];
%plot it rectangle by rectangle give the points of the rectangle and fill it using the fill3 function
x = [p1(1) p2(1) p3(1) p4(1)];
y = [p1(2) p2(2) p3(2) p4(2)];
z = [p1(3) p2(3) p3(3) p4(3)];
fill3(x, y, z, 'k');
xlabel('x'); ylabel('y'); zlabel('z');
hold on
p5 = [(Wc/2) (Hc/2) +(Lc/2)];
p6 = [(Wc/2) -(Hc/2) +(Lc/2)];
p7 = [-(Wc/2) -(Hc/2) +(Lc/2)];
p8 = [-(Wc/2) (Hc/2) +(Lc/2)];
x = [p5(1) p6(1) p7(1) p8(1)];
```

```
y = [p5(2) p6(2) p7(2) p8(2)];
z = [p5(3) p6(3) p7(3) p8(3)];
fill3(x, y, z, 'k');
hold on
x = [p2(1) p6(1) p7(1) p3(1)];
y = [p2(2) p6(2) p7(2) p3(2)];
z = [p2(3) p6(3) p7(3) p3(3)];
fill3(x, y, z, 'k');
hold on
x = [p2(1) p6(1) p5(1) p1(1)];
y = [p2(2) p6(2) p5(2) p1(2)];
z = [p2(3) p6(3) p5(3) p1(3)];
fill3(x, y, z, 'k');
hold on
x = [p7(1) p8(1) p4(1) p3(1)];
y = [p7(2) p8(2) p4(2) p3(2)];
z = [p7(3) p8(3) p4(3) p3(3)];
fill3(x, y, z, 'k');
hold on
x = [p5(1) p1(1) p4(1) p8(1)];
y = [p5(2) p1(2) p4(2) p8(2)];
z = [p5(3) p1(3) p4(3) p8(3)];
fill3(x, y, z, 'k');
hold on
end
```

plotresin2cylindrical1 function

```
function plotresin2cylindrical1( rad,Lc,diameterofcopper )
[x,y,z] = cylinder(rad);%setting the radius of the cylinder
resin   =   mesh(x-(diameterofcopper/2),y,z*(Lc)-(Lc/2));%x-(diameter   of
copper/2) because the mid point of the cylinder will not be at 0,
%The height of the cylinder will be similar to the height of the chip for
a
%perfect model
set(resin,'FaceColor',[0.55 0.5 1]);%sets the colour to the resin
set(resin,'edgecolor',[0.55 0.5 1]);%sets the colour to the resin
set (resin,'FaceAlpha',(.4)); %setting the transparency level of resin
set (resin,'EdgeAlpha',(.4)); %setting the transparency level of resin
r=rad;
teta=-pi:0.01:pi;
x=r*cos(teta);
y=r*sin(teta);
resincircle                                =                                fill3(x-
(diameterofcopper/2),y,zeros(1,numel(x))+(Lc/2.1),[0.55 0.5 1]);%creating
a circle of resin filling the cylinder
set  (resincircle,'FaceAlpha',(.4));  %setting  the  transparency  level  of
resin
set  (resincircle,'EdgeAlpha',(.4));  %setting  the  transparency  level  of
resin
end
```

plotsolderpads1 function

```
function plotsolderpads1( Lc,Ls,Wc,Hc )
%plotting the solder pads
p1 = [(Wc/2) (Hc/2) -(Lc/2)];
p2 = [(Wc/2) -(Hc/2) -(Lc/2)];
p3 = [-(Wc/2) -(Hc/2) -(Lc/2)];
p4 = [-(Wc/2) (Hc/2) -(Lc/2)];
x = [p1(1) p2(1) p3(1) p4(1)];
y = [p1(2) p2(2) p3(2) p4(2)];
```

```
z = [p1(3) p2(3) p3(3) p4(3)];
fill3(x, y, z, [0.65 0.65 0.65]);
hold on
p5 = [(Wc/2) (Hc/2) -Ls];
p6 = [(Wc/2) -(Hc/2) -Ls];
p7 = [-(Wc/2) -(Hc/2) -Ls];
p8 = [-(Wc/2) (Hc/2) -Ls];
x = [p5(1) p6(1) p7(1) p8(1)];
y = [p5(2) p6(2) p7(2) p8(2)];
z = [p5(3) p6(3) p7(3) p8(3)];
fill3(x, y, z, [0.65 0.65 0.65]);
x = [p2(1) p6(1) p7(1) p3(1)];
y = [p2(2) p6(2) p7(2) p3(2)];
z = [p2(3) p6(3) p7(3) p3(3)];
fill3(x, y, z, [0.65 0.65 0.65]);
x = [p2(1) p6(1) p5(1) p1(1)];
y = [p2(2) p6(2) p5(2) p1(2)];
z = [p2(3) p6(3) p5(3) p1(3)];
fill3(x, y, z, [0.65 0.65 0.65]);
x = [p7(1) p8(1) p4(1) p3(1)];
y = [p7(2) p8(2) p4(2) p3(2)];
z = [p7(3) p8(3) p4(3) p3(3)];
fill3(x, y, z, [0.65 0.65 0.65]);
x = [p5(1) p1(1) p4(1) p8(1)];
y = [p5(2) p1(2) p4(2) p8(2)];
z = [p5(3) p1(3) p4(3) p8(3)];
fill3(x, y, z, [0.65 0.65 0.65]);
end
```

plotsolderpads2 function

```
function plotsolderpads2( Lc,Ls,Wc,Hc )
%plotting the solder pads
p1 = [(Wc/2) (Hc/2) +(Lc/2)];
p2 = [(Wc/2) -(Hc/2) +(Lc/2)];
p3 = [-(Wc/2) -(Hc/2) +(Lc/2)];
p4 = [-(Wc/2) (Hc/2) +(Lc/2)];
x = [p1(1) p2(1) p3(1) p4(1)];
y = [p1(2) p2(2) p3(2) p4(2)];
z = [p1(3) p2(3) p3(3) p4(3)];
fill3(x, y, z, [0.65 0.65 0.65]);
hold on
p5 = [(Wc/2) (Hc/2) +Ls];
p6 = [(Wc/2) -(Hc/2) +Ls];
p7 = [-(Wc/2) -(Hc/2) +Ls];
p8 = [-(Wc/2) (Hc/2) +Ls];
x = [p5(1) p6(1) p7(1) p8(1)];
y = [p5(2) p6(2) p7(2) p8(2)];
z = [p5(3) p6(3) p7(3) p8(3)];
fill3(x, y, z, [0.65 0.65 0.65]);
x = [p2(1) p6(1) p7(1) p3(1)];
y = [p2(2) p6(2) p7(2) p3(2)];
z = [p2(3) p6(3) p7(3) p3(3)];
fill3(x, y, z, [0.65 0.65 0.65]);
x = [p2(1) p6(1) p5(1) p1(1)];
y = [p2(2) p6(2) p5(2) p1(2)];
z = [p2(3) p6(3) p5(3) p1(3)];
fill3(x, y, z, [0.65 0.65 0.65]);
x = [p7(1) p8(1) p4(1) p3(1)];
y = [p7(2) p8(2) p4(2) p3(2)];
z = [p7(3) p8(3) p4(3) p3(3)];
fill3(x, y, z, [0.65 0.65 0.65]);
x = [p5(1) p1(1) p4(1) p8(1)];
y = [p5(2) p1(2) p4(2) p8(2)];
```

```
z = [p5(3) p1(3) p4(3) p8(3)];
fill3(x, y, z, [0.65 0.65 0.65]);
end
```

copperfilaments function

```
function copperfilaments(NCufillaments,Ls,Hc,diameterofcopper )
%plotting the copper filaments
[x,y,z] = cylinder();
radcopper = diameterofcopper/2;%radius of the copper fibre
xa = x*radcopper;
ya = y*radcopper;
za = (z*5*1E-4)+(Ls);
diff = Hc/NCufillaments; %calculating the spacing between fibres
space = ((-Hc/2):diff:(Hc/2));%calculating the spacing between fibres
for i=2:1:NCufillaments%plotting the yarn fibres around a other side of
the thermistor
    copper    =    surf(xa-(radcopper+(Hc/2)),ya+space(i),za);%plots    the
filaments
    set(copper,'FaceColor',[1 0.62 0.40]);%sets the colour to the copper
    set(copper,'edgecolor',[1 0.62 0.40]);%sets the colour to the copper
    %plot the filling circles to complete the cylinder
    radcir=radcopper;
    teta=-pi:0.01:pi;
    xaa=radcir*cos(teta);
    yaa=radcir*sin(teta);
    fill3(xaa-
(radcopper+(Hc/2)),yaa+space(i),zeros(1,numel(xaa))+Ls+(5*1E-4),[1    0.62
0.40]);%creating a circle of resin filling the cylinder
end
%plotting the filaments at the bottom
xb = x*radcopper;
yb = y*radcopper;
zb = -(z*5*1E-4)-(Ls);
diff = Hc/NCufillaments; %calculating the spacing between fibres
space = ((-Hc/2):diff:(Hc/2));%calculating the spacing between fibres
for i=2:1:NCufillaments%plotting the yarn fibres around a other side of
the thermistor
    copper    =    surf(xb-(radcopper+(Hc/2)),yb+space(i),zb);%plots    the
filaments
    set(copper,'FaceColor',[1 0.62 0.40]);%sets the colour to the copper
    set(copper,'edgecolor',[1 0.62 0.40]);%sets the colour to the copper
    %plot the filling circles to complete the cylinder
    radcir=radcopper;
    teta=-pi:0.01:pi;
    xbb=radcir*cos(teta);
    ybb=radcir*sin(teta);
    fill3(xbb-(radcopper+(Hc/2)),ybb+space(i),zeros(1,numel(xaa))-Ls-
(5*1E-4),[1 0.62 0.40]);%creating a circle of resin filling the cylinder
end
end
```

plotsolderpaste1 function

```
function plotsolderpaste1( Lc,Ls,Wc,Hc,diameterofcopper)
%plot solder paste on top
p1 = [-(Wc/2) (Hc/2) +(Lc/2)];
p2 = [-(Wc/2) -(Hc/2) +(Lc/2)];
p3 = [-((Wc/2)+diameterofcopper) (Hc/2) +(Lc/2)];
p4 = [-((Wc/2)+diameterofcopper) -(Hc/2) +(Lc/2)];
x = [p1(1) p2(1) p4(1) p3(1)];
y = [p1(2) p2(2) p4(2) p3(2)];
z = [p1(3) p2(3) p4(3) p3(3)];
fill3(x, y, z, [0.25 0.25 0.25]);
```

```
hold on
p5 = [-(Wc/2) (Hc/2) +Ls];
p6 = [-(Wc/2) -(Hc/2) +Ls];
p7 = [-((Wc/2)+diameterofcopper) (Hc/2) +Ls];
p8 = [-((Wc/2)+diameterofcopper) -(Hc/2) +Ls];
x = [p5(1) p6(1) p8(1) p7(1)];
y = [p5(2) p6(2) p8(2) p7(2)];
z = [p5(3) p6(3) p8(3) p7(3)];
fill3(x, y, z, [0.25 0.25 0.25]);
x = [p2(1) p6(1) p8(1) p4(1)];
y = [p2(2) p6(2) p8(2) p4(2)];
z = [p2(3) p6(3) p8(3) p4(3)];
fill3(x, y, z, [0.25 0.25 0.25]);
x = [p2(1) p6(1) p5(1) p1(1)];
y = [p2(2) p6(2) p5(2) p1(2)];
z = [p2(3) p6(3) p5(3) p1(3)];
fill3(x, y, z, [0.25 0.25 0.25]);
x = [p7(1) p8(1) p4(1) p3(1)];
y = [p7(2) p8(2) p4(2) p3(2)];
z = [p7(3) p8(3) p4(3) p3(3)];
fill3(x, y, z, [0.25 0.25 0.25]);
x = [p5(1) p1(1) p3(1) p7(1)];
y = [p5(2) p1(2) p3(2) p7(2)];
z = [p5(3) p1(3) p3(3) p7(3)];
fill3(x, y, z, [0.25 0.25 0.25]);
end
```

plotsolderpaste2 function

```
function plotsolderpaste2( Lc,Ls,Wc,Hc,diameterofcopper)
%plot solder paste at the bottom
p1 = [-(Wc/2) (Hc/2) -(Lc/2)];
p2 = [-(Wc/2) -(Hc/2) -(Lc/2)];
p3 = [-((Wc/2)+diameterofcopper) (Hc/2) -(Lc/2)];
p4 = [-((Wc/2)+diameterofcopper) -(Hc/2) -(Lc/2)];
x = [p1(1) p2(1) p4(1) p3(1)];
y = [p1(2) p2(2) p4(2) p3(2)];
z = [p1(3) p2(3) p4(3) p3(3)];
fill3(x, y, z, [0.25 0.25 0.25]);
hold on
p5 = [-(Wc/2) (Hc/2) -Ls];
p6 = [-(Wc/2) -(Hc/2) -Ls];
p7 = [-((Wc/2)+diameterofcopper) (Hc/2) -Ls];
p8 = [-((Wc/2)+diameterofcopper) -(Hc/2) -Ls];
x = [p5(1) p6(1) p8(1) p7(1)];
y = [p5(2) p6(2) p8(2) p7(2)];
z = [p5(3) p6(3) p8(3) p7(3)];
fill3(x, y, z, [0.25 0.25 0.25]);
x = [p2(1) p6(1) p8(1) p4(1)];
y = [p2(2) p6(2) p8(2) p4(2)];
z = [p2(3) p6(3) p8(3) p4(3)];
fill3(x, y, z, [0.25 0.25 0.25]);
x = [p2(1) p6(1) p5(1) p1(1)];
y = [p2(2) p6(2) p5(2) p1(2)];
z = [p2(3) p6(3) p5(3) p1(3)];
fill3(x, y, z, [0.25 0.25 0.25]);
x = [p7(1) p8(1) p4(1) p3(1)];
y = [p7(2) p8(2) p4(2) p3(2)];
z = [p7(3) p8(3) p4(3) p3(3)];
fill3(x, y, z, [0.25 0.25 0.25]);
x = [p5(1) p1(1) p3(1) p7(1)];
y = [p5(2) p1(2) p3(2) p7(2)];
z = [p5(3) p1(3) p3(3) p7(3)];
fill3(x, y, z, [0.25 0.25 0.25]);
```

```
end
```

polyesterarnchip function

```
function polyesterarnchip(Nfibres,Lc,Hc )
%plotting the yarn around the chip
[x,y,z] = cylinder();
diameterofpoly = 1.464*10^(-5);%calculated using the microscope
radpolyester = diameterofpoly/2;%radius of the polyester fibre
xa = x*radpolyester;
ya = y*radpolyester;
za = (z*15*1E-4)-(0.75*Lc);
Cfibres = Nfibres/3; %number of fibres around one side of the chip
diff = Hc/Cfibres; %calculating the spacing between fibres
space = ((-Hc/2):diff:(Hc/2));%calculating the spacing between fibres
for i=2:1:Cfibres%plotting the yarn fibres around a side of the thermistor
    side1 = surf(xa+space(i),ya+(radpolyester+(Hc/2)),za);
    set(side1,'FaceColor',[0.5 0.8 0.5]);%sets the colour to the polyester
    set(side1,'edgecolor',[0.5 0.8 0.5]);%sets the colour to the polyester
    %plot the filling cirlce
    radcir=radpolyester;
    teta=-pi:0.01:pi;
    xaa=radcir*cos(teta);
    yaa=radcir*sin(teta);

fill3(xaa+space(i),yaa+(radpolyester+(Hc/2)),zeros(1,numel(xaa))+(15*1E-
4)-(0.75*Lc),[0.5  0.8  0.5]);%creating a circle of resin filling the
cylinder
end
for i=2:1:Cfibres%plotting the yarn fibres around a other side of the
thermistor
    side2 = surf(xa+space(i),ya-(radpolyester+(Hc/2)),za);
    set(side2,'FaceColor',[0.5 0.8 0.5]);%sets the colour to the polyester
    set(side2,'edgecolor',[0.5 0.8 0.5]);%sets the colour to the polyester
    %plot the filling circle
    radcir=radpolyester;
    teta=-pi:0.01:pi;
    xaa=radcir*cos(teta);
    yaa=radcir*sin(teta);
    fill3(xaa+space(i),yaa-
(radpolyester+(Hc/2)),zeros(1,numel(xaa))+(15*1E-4)-(0.75*Lc),[0.5    0.8
0.5]);%creating a circle of resin filling the cylinder
end
for i=2:1:Cfibres%plotting the yarn fibres around a other side of the
thermistor
    side3 = surf(xa+(radpolyester+(Hc/2)),ya+space(i),za);
    set(side3,'FaceColor',[0.5 0.8 0.5]);%sets the colour to the polyester
    set(side3,'edgecolor',[0.5 0.8 0.5]);%sets the colour to the polyester
    %plot the filling circle
    radcir=radpolyester;
    teta=-pi:0.01:pi;
    xaa=radcir*cos(teta);
    yaa=radcir*sin(teta);

fill3(xaa+(radpolyester+(Hc/2)),yaa+space(i),zeros(1,numel(xaa))+(15*1E-
4)-(0.75*Lc),[0.5  0.8  0.5]);%creating a circle of resin filling the
cylinder
end
end
```

plotpackingfibres function

```
function
plotpackingfibres( D_ofbraidingcylinder,Lc,radpolyesteryarn,diameterofcop
per )
rad1= D_ofbraidingcylinder-(radpolyesteryarn*2)%setting the radius of the
cylinder
[x,y,z] = cylinder(rad1);
packingfibres = mesh(x-(diameterofcopper/2),y,z*(Lc)-(Lc/2));%x-(diameter
of copper/2) because the mid point of the cylinder will not be at 0,
%The height of the cylinder will be similar to the height of the chip for
a
%perfect model
set(packingfibres,'FaceColor',[0  0  1]);%sets the colour to the packing
fibres
set(packingfibres,'edgecolor',[0  0  1]);%sets the colour to the packing
fibres
r=rad1;
teta=-pi:0.01:pi;
x=r*cos(teta);
y=r*sin(teta);
packingfibrecircle                          =                       fill3(x-
(diameterofcopper/2),y,zeros(1,numel(x))+(Lc/2.1),[0.55 0.5 1]);%creating
a circle of resin filling the cylinder
set(packingfibrecircle,'FaceColor',[0  0  1]);%sets the colour to the
packing fibres
set(packingfibrecircle,'edgecolor',[0  0  1]);%sets the colour to the
packing fibres
set (packingfibrecircle,'FaceAlpha',(.2)); %setting the transparency level
of packing fibre layer
set (packingfibrecircle,'EdgeAlpha',(.2)); %setting the transparency level
of packing fibre layer
end
```

polyesteryarn2cylindrical1 function

```
function                                                [radpolyesteryarn]=
polyesteryarn2cylindrical1( nyarnb,Lc,Volfraction,diameterofpoly,Nfibres,
diameterofcopper,D_ofbraidingcylinder)
%plotting the polyester yarn fibres for the braiding process for the
polyester yarn with 48 filaments
%167Dtex
[x,y,z] = cylinder();
radpolyester = diameterofpoly/2;%radius of the polyester fibre
radpolyesteryarn  =  sqrt(((radpolyester^2)*Nfibres)/Volfraction);%radius
of a braided yarn
xa = x*radpolyesteryarn-(diameterofcopper/2);%setting the radius of the a
cylinder which represents the braided yarn
ya = y*radpolyesteryarn;
za = (z*3*1E-3)-(1.5*Lc);
D= D_ofbraidingcylinder-(radpolyesteryarn*2);%calculates the radius of how
far the braided yarn should be from the centre
rad1= D;
R = rad1+(radpolyesteryarn);%setting how far away the yarn should be placed
from the middle(outside the encapsulation)

theta = (-2*pi:(2*pi/nyarnb):2*pi);%calculate how far apart it should be
placed
xc = R*cos(theta);%getting the xc
yc = R*sin(theta)-(diameterofcopper/2);%getting the yc
for i=1:1:nyarnb%plotting the number of fibres

    polyester = surf(xa+xc(i),ya+yc(i),za);%plots the fibres
    set(polyester,'FaceColor',[0.5  0.8  0.5]);%sets the colour to the
polyester
```

```
    set(polyester,'edgecolor',[0.5  0.8  0.5]);%sets the colour to the
polyester
end
end
```

8.6 Appendix 6: Diameter of a single polyester fibre in the 167 dtex/48 polyester yarn

In order to calculate the diameter of the polyester fibres, five fibres from the polyester yarn was chosen. The diameter of each fibre was measured using an Olympus BX41 microscope (OLYMPUS, Tokyo, Japan). Given below in figure 8.8 are the images of the polyester filaments. The values obtained for the measurements and the average are given in table 8.3

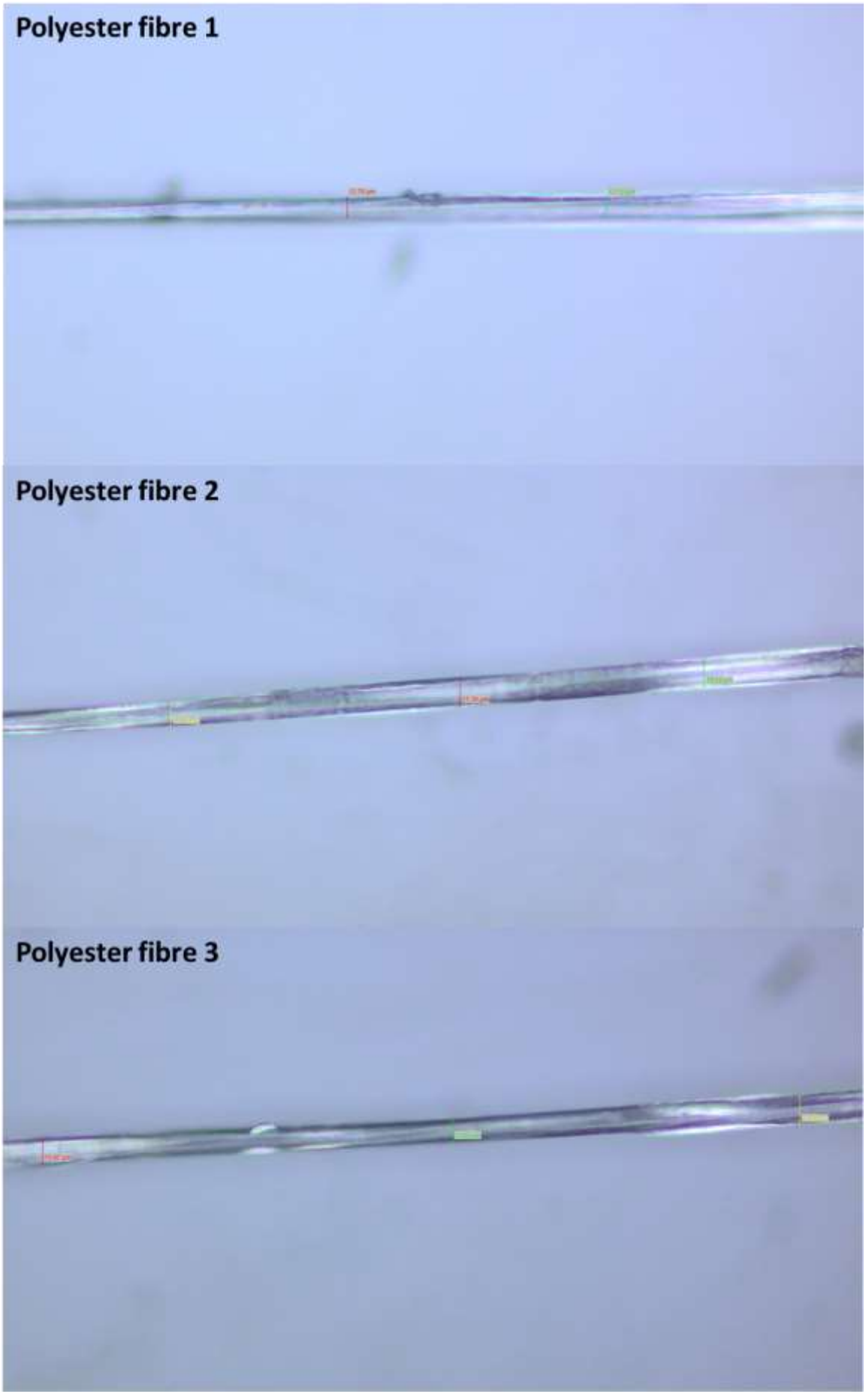
Polyester fibre 1
Polyester fibre 2
Polyester fibre 3

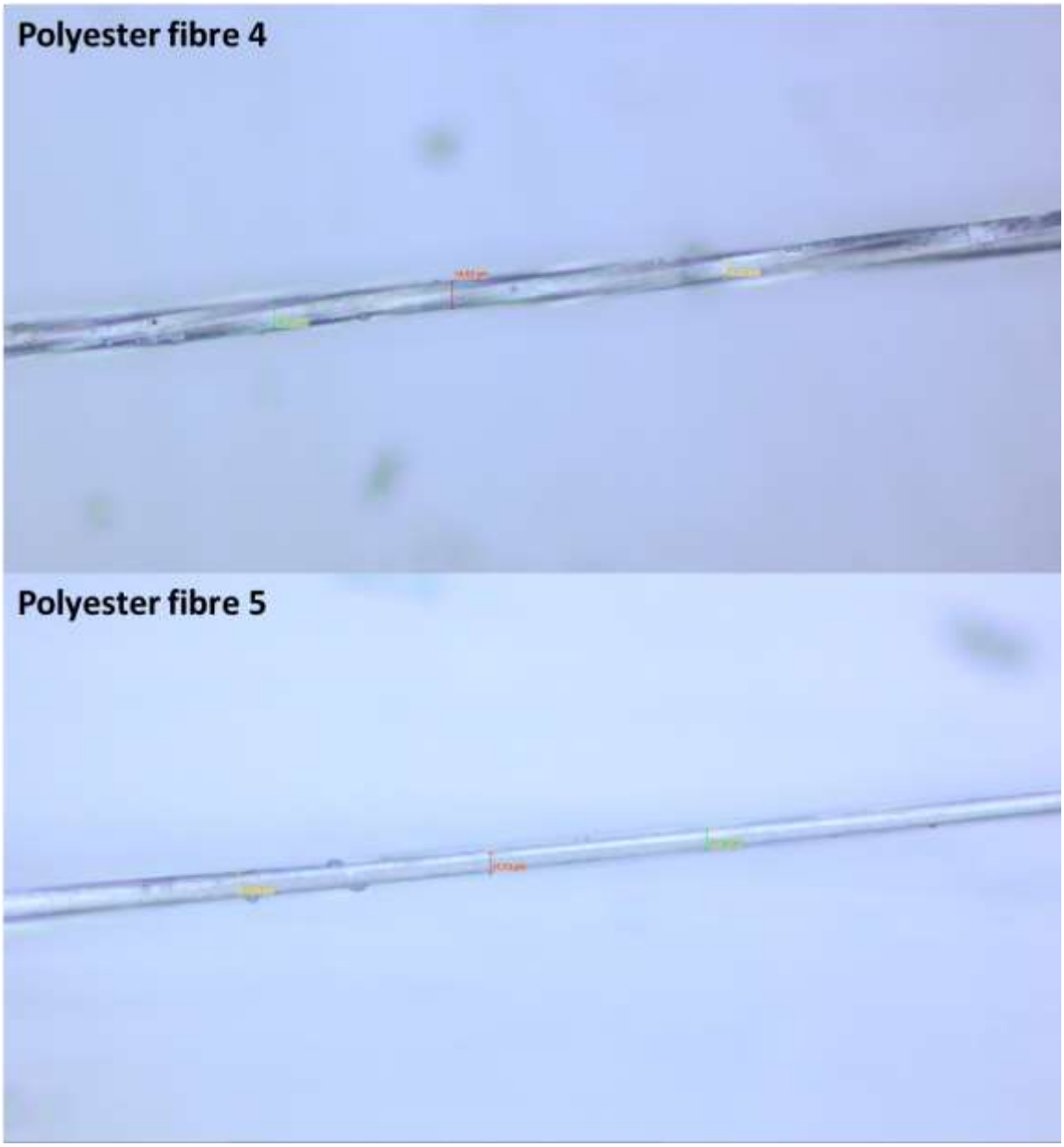

Figure 8-8: Images of the Polyester fibres taken on the Olympus microscope

Table 8-3: Diameter of the Polyester fibres

	Polyester fibre 1	Polyester fibre 2	Polyester fibre 3	Polyester fibre 4	Polyester fibre 5
Diameter at location 1/µm	12.76	15.18	15.87	16.21	13.8
Diameter at location 2/µm	12.76	17.25	13.8	14.83	11.73
Diameter at location 3/µm	-	18.28	18.63	11.73	11.38
Average diameter of each polyester fibre /µm	12.76	16.90	16.1	14.26	12.30
Average diameter of a polyester fibre /µm			14.46		
Standard Deviation			2.33		
Standard Error			0.62		

8.7 Appendix 7: Diameter of the ETS yarn

The diameter of ETS yarns were measured using an Olympus BX41 microscope (OLYMPUS, Tokyo, Japan). Given below in figure 8.9, 8.10 are images of the ETS yarn. The values obtained from the diameter measurements and the average are given in table 8.4.

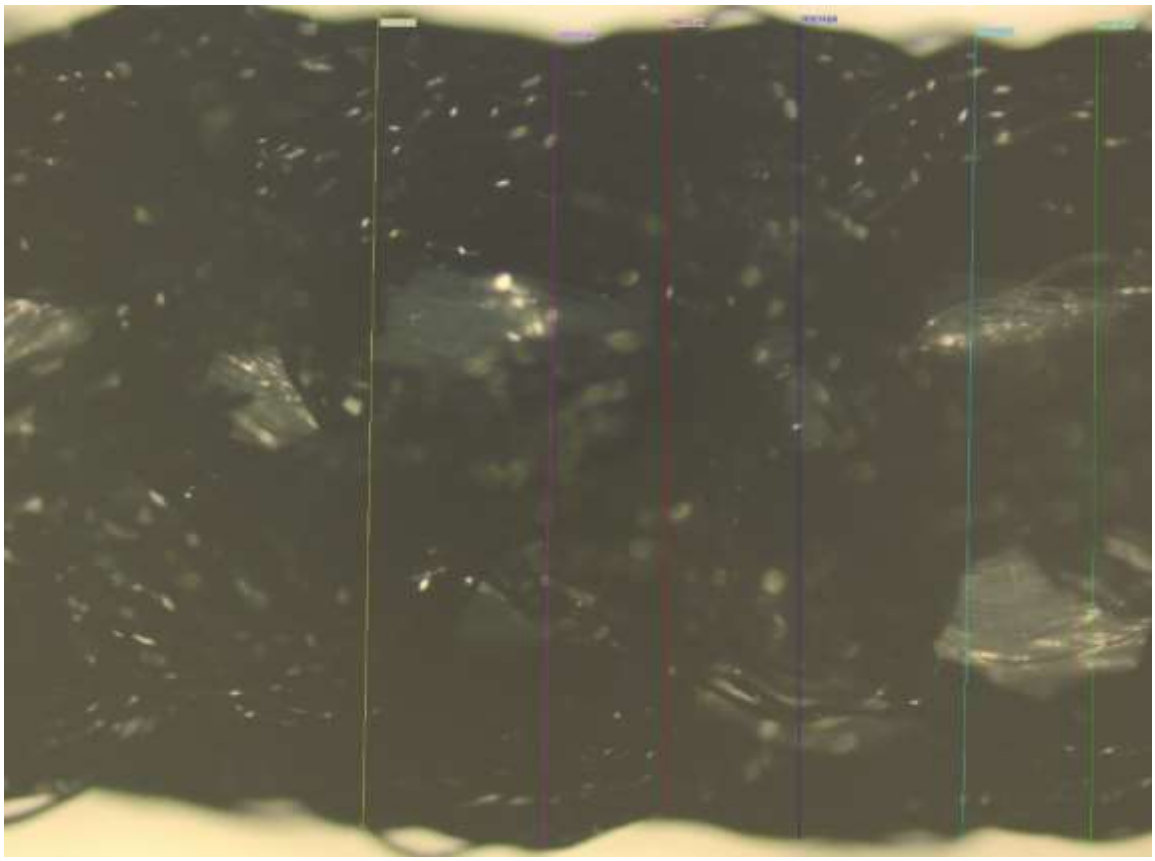

Figure 8-9: Image of ETS yarn 1 taken on the Olympus microscope

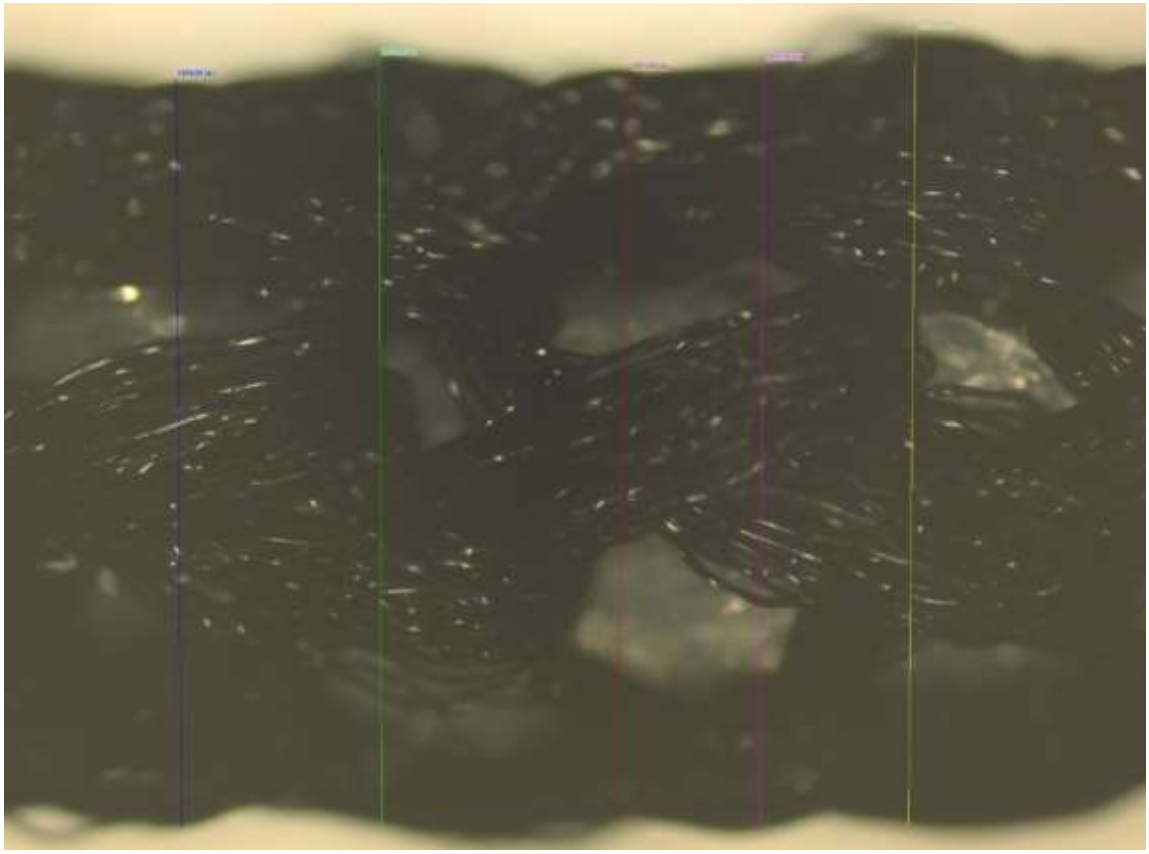

Figure 8-10: Image of ETS yarn 1 taken on the Olympus microscope

Table 8-4: Diameter of ETS yarn

Braided yarn diameter1/mm	Braided yarn diameter2/mm
2.0248	1.87685
2.02333	1.87165
1.96512	1.92236
2.03274	1.98728
2.00539	1.972987
Average diameter	1.9682507
Standard diviation	0.059587319
	0.031955838
standard error	0.018843165

8.8 Appendix 8: Data sheet for the Multi-Cure® 9-20801 resin provided by DYMAX Corporation (Torrington, CT, United States)

DYMAX®

ELECTRONIC CIRCUIT BOARD MATERIALS
9-20801 Product Data Sheet

Multi-Cure® 9-20801
Light-Curable Thermal Interface Material

APPLICATIONS

- Mounting Heat Sinks
- Bonding Heat Sensitive Components to PCBs

FEATURES

- UV Light Cure
- Secondary Activator or Heat Cure
- Highly Conductive
- Thixotropic for Easy Dispense and Placement Prior to Cure

OTHER FEATURES

- Superior Adhesion to FR4 and Many Metals
- Fast UV Cure for Immediate Fixture Strength

Dymax Multi-Cure® 9-20801 cures upon exposure to UV light, heat, and/or activator and is designed for rapid mounting of heat-sensitive components on printed circuit boards. Dymax 9-20801 is a Multi-Cure® material specially formulated to cure with heat or activator between opaque substrates. Most high-speed processes call for dispensing 9-20801 onto the substrate surface and then applying a thin layer of Dymax 501-E activator to the opposite component surface. The parts are mated and then exposed to light. This exposure cures the edges of the component in seconds so the parts are fixtured allowing for immediate handling and movement to the next step in the process. Material between the opaque surfaces will cure over time, typically minutes or hours. Dymax Multi-Cure® materials contain no nonreactive solvents and cure upon exposure to light. Their ability to cure in seconds enables faster processing, greater output, and lower processing costs. When cured with Dymax light-curing spot lamps, focused-beam lamps, or flood lamps, they deliver optimum speed and performance for bonding. Dymax lamps offer the ideal balance of UV and visible light for the fastest, deepest cures. This product is in full compliance with the RoHS Directives 2002/95/EC and 2003/11/EC.

UNCURED PROPERTIES *

Property	Value	Test Method
Solvent Content	No Nonreactive Solvents	N/A
Chemical Class	Acrylated Urethane	N/A
Appearance	Off White	N/A
Soluble In	Organic Solvents	N/A
Density, g/ml	2.0	ASTM D1875
Viscosity, cP (20 rpm)	110,000 (nominal)	ASTM D2556

ADHESION

Substrate	Recommendation
Lead Frame	✓
Ceramic	✓
PCB	✓
Flex	o
Silicon	✓

✓ Recommended o Limited Applications
st Requires Surface Treatment (e.g. plasma, corona treatment, etc.)

CURED MECHANICAL PROPERTIES *

Property	Value	Test Method
Durometer Hardness	D85	ASTM D2240
Tensile at Break, MPa [psi]	14 [2,100]	ASTM D638
Elongation at Break, %	NA	ASTM D638
Modulus of Elasticity, MPa [psi]	760 [110,000]	ASTM D638

OTHER CURED PROPERTIES *

Property	Value	Test Method
Boiling Water Absorption, % (2 h)	1.6	ASTM D570
Water Absorption, % (25°C, 24 h)	0.6	ASTM D570
Linear Shrinkage, %	0.39	ASTM D2566
Thermal Conductivity, W/m°K	0.9	ASTM D5470

* Not Specifications
N/A Not Applicable

RoHS Compliant

Dymax Corporation
860.482.1010 | info@dymax.com | www.dymax.com

Dymax Europe GmbH
+49 (0) 611.962.7900 | info_de@dymax.com | www.dymax.de

Dymax Engineering Adhesives Ireland Ltd.
+353.1.231.4656 | info_ie@dymax.com | www.dymax.ie

Dymax Oligomers & Coatings
860.626.7006 | info_oc@dymax.com | www.dymax-oc.com

Dymax UV Adhesives & Equipment (Shanghai) Co. Ltd.
+86.21.37285759 | dymaxasia@dymax.com | www.dymax.com.cn

Dymax UV Adhesives & Equipment (Shenzhen) Co. Ltd.
+86.755.83485759 | dymaxasia@dymax.com | www.dymax.com.cn

Dymax Asia (H.K.) Limited
+852.2460.7038 | dymaxasia@dymax.com | www.dymax.com.cn

Dymax Asia Pacific Pte. Ltd.
+65.6752.2887 | info_ap@dymax.com | www.dymax-ap.com

Dymax Korea LLC
+82.2.784.3434 | info_kr@dymax.com | www.dymax.com/kr

CURING GUIDELINES

Fixture time is defined as the time to develop a shear strength of 0.1 N/mm² [10 psi] between glass slides. Actual cure time typically is 3 to 5 times fixture time.

Dymax Curing System (Intensity)	Fixture Time or Belt Speed [A]
2000-EC (50 mW/cm²)[B]	7s
5000-EC (200 mW/cm²)[B]	5s
BlueWave® 75 (5.0 W/cm²)[B]	4s
BlueWave® 200 (10 W/cm²)[B]	4s
UVCS Conveyor with one 5000-EC (200 mW/cm²)[C]	2 m/min [6.5ft/min]
UVCS Conveyor with Fusion F300S (2.5 W/cm²)[C]	5 m/min [15 ft/min]

A *Curing through light-blocking substrates may require longer cure times if they obstruct wavelengths used for light curing (320-400 nm for UV light curing, 320-450 nm for UV/Visible light curing). These fixture times/belt speeds are typical for curing thin films through 100% light-transmitting substrates.*

B *Intensity was measured over the UVA range (320-395 nm) using a Dymax ACCU-CAL™ 50 Radiometer.*

C *At 53 mm [2.1 in] focal distance. Maximum speed of conveyor is 8.2 m/min [27 ft/min]. Intensity was measured over the UVA range (320-395 nm) using the Dymax ACCU-CAL™ 100 Radiometer.*

Full cure is best determined empirically by curing at different times and intensities, and measuring the corresponding change in cured properties such as tackiness, adhesion, hardness, etc. Full cure is defined as the point at which more light exposure no longer improves cured properties. Higher intensities or longer cures (up to 5x) generally will not degrade Dymax light-curable materials.

SECONDARY HEAT CURE

Heat can be used as a secondary cure mechanism where the adhesive cannot be cured with light. Light curing must be done prior to heat cure. The following heat-cure schedule may be used:

Temperature	Time*
110°C [230°F]	60 minutes
120°C [250°F]	30 minutes
150°C [300°F]	15 minutes

*Note: Actual heat cure time may vary due to part configuration, volume of adhesive applied, and oven efficiency.

ACTIVATOR CURE

Shadowed areas can be cured with activator.

Activator is placed on one surface and the adhesive on the mating surface. Curing takes place at room temperature when the parts are mated. Activator requires closely mated parts (up to 0.5 mm [0.02 in] gap). Closely mated parts fixture (achieve handling strength) in less than a minute. See Dymax Technical Bulletin "Guidelines for Activator Curing" for complete instructions for all activators.

CURING GUIDELINES (CONTINUED)

Dymax recommends that customers employ a safety factor by curing longer, at higher intensity, and/or at higher temperature than required for full cure. Although Dymax Application Engineering can provide technical support and assist with process development, each customer ultimately must determine and qualify the appropriate curing parameters required for their unique application.

DEPTH OF CURE

The graphs below show the increase in depth of cure as a function of exposure time with two different lamps at different intensities. A 9.5 mm [0.37 in] diameter specimen was cured in a polypropylene mold and cooled to room temperature. It was then released from the mold and the cure depth was measured.

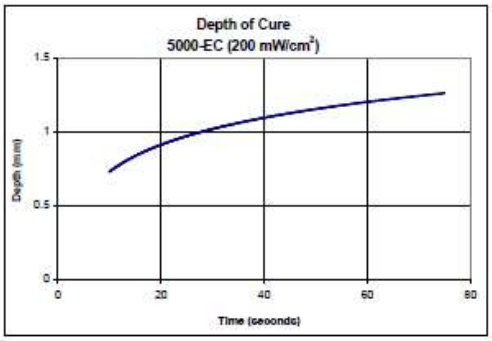

OPTIMIZING PERFORMANCE AND HANDLING

1. This product cures with exposure to UV light. Exposure to ambient and artificial light should be kept to a minimum before curing. Dispensing components including needles and fluid lines should be 100% light blocking, not just UV blocking.
2. All surfaces in contact with the material should be clean and free from flux residue, grease, mold release, or other contaminants prior to dispensing the material.
3. Cure speed is dependent upon many variables, including lamp intensity, distance from the light source, required depth of cure, thickness, and percent light transmission of components between the material and light source.
4. Oxygen in the atmosphere may inhibit surface cure. Surfaces exposed to air may require high-intensity (>100 mW/cm^2) UV light to produce a dry surface cure. Flooding the curing area with an inert gas, such as nitrogen, can also reduce the effects of oxygen inhibition.
5. Parts should be allowed to cool after cure before testing and subjecting to any loads or electrical testing.
6. In rare cases, stress cracking may occur in assembled parts. Three options may be explored to eliminate this problem. One option is to heat anneal the parts to remove molded-in stresses. A second option is to open any gap between mating parts to reduce stress caused by an interference fit. The third option is to minimize the amount of time the liquid material remains in contact with the substrate(s) prior to curing.
7. Light curing generally produces some heat. If necessary, cooling fans can be placed in the curing area to reduce the heating effect on components.
8. At the point of curing, an air exhaust system is recommended to dissipate any heat and vapors formed during the curing process.

DISPENSING THE MATERIAL

This material may be dispensed with a variety of manual and automatic applicators or other equipment as required. Questions relating to dispensing and curing systems for specific applications should be referred to Dymax Application Engineering.

CLEANUP

Uncured material may be removed from dispensing components and parts with organic solvents. Cured material will be impervious to many solvents and difficult to remove. Cleanup of cured material may require mechanical methods of removal.

PERFORMANCE AFTER TEMPERATURE EXPOSURE

Dymax light-curable materials typically have a lower thermal limit of -54°C [-65°F] and an upper limit of 150°C [300°F]. Many Dymax products can withstand temperatures outside of this range for short periods of time, including typical wave solder processes and reflow profiles. Please contact Dymax Application Engineering for assistance.

STORAGE AND SHELF LIFE

Store the material in a cool, dark place when not in use. Do not expose to light. This product may polymerize upon prolonged exposure to ambient and artificial light. Keep covered when not in use. This material has a six-months shelf life from date of manufacture, unless otherwise specified, when stored between 10°C [50°F] and 32°C [90°F] in the original, unopened container.

GENERAL INFORMATION

This product is intended for industrial use only. Keep out of the reach of children. Avoid breathing vapors. Avoid contact with skin, eyes, and clothing. Wear impervious gloves. Repeated or continuous skin contact with uncured material may cause irritation. Remove material from skin with soap and water. Never use organic solvents to remove material from skin and eyes. For more information on the safe handling of this material, please refer to the Material Safety Data Sheet before use.

8.9 Appendix 9: Data sheet for the Multi-Cure® 9001-E-V-3.5 resin provided by DYMAX Corporation (Torrington, CT, United States)

DYMAX

ELECTRONIC ASSEMBLY MATERIALS
9001-E-V3.5 Product Data Sheet

Multi-Cure® 9001-E-V3.5
Resilient, Clear Encapsulant

APPLICATIONS
- Encapsulation

FEATURES & BENEFITS
- UV/Visible Light Cure
- Secondary Heat Cure
- Flexible, Light-Curable Encapsulant
- Moisture and Thermal Cycle Resistance

SUBSTRATES
- FR4
- Flex Circuit
- Glass
- Kapton

Dymax Multi-Cure® 9001-E-V3.5 encapsulant is a performance upgrade of the flexible "instant curing" Dymax 9001 UV/Visible light-curable encapsulant, with improved moisture and thermal cycle resistance, and adhesion to various component substrates. Curing completely in as little as five seconds upon exposure to longwave UV and visible light, this material is environmentally resistant with good ionic and electrical properties. Multi-Cure® 9001-E-V3.5 encapsulant displays excellent adhesion to printed circuit boards and electronic components and is especially well suited for chip-on-board, chip-on-flex, and multi-chip modules. Dymax 9001-E-V3.5 is a Multi-Cure® material specially formulated to cure with heat in applications where shadowed areas exist. Dymax Multi-Cure® materials contain no nonreactive solvents and cure upon exposure to light. Their ability to cure in seconds enables faster processing, greater output, and lower processing costs. When cured with Dymax light-curing spot lamps, focused-beam lamps, or flood lamps, they deliver optimum speed and performance for encapsulation. Dymax lamps offer the optimum balance of UV and visible light for the fastest, deepest cures. This product is in full compliance with the RoHS Directives 2002/95/EC and 2003/11/EC.

UNCURED PROPERTIES *

Property	Value	Test Method
Solvent Content	No Nonreactive Solvents	N/A
Chemical Class	Acrylated Urethane	N/A
Appearance	Clear Liquid	N/A
Soluble In	Organic Solvents	N/A
Density, g/ml	1.06	ASTM D1875
Viscosity, cP (20 rpm)	17,000 (nominal)	ASTM D2556

CURED MECHANICAL PROPERTIES *

Property	Value	Test Method
Durometer Hardness	D45	ASTM D2240
Tensile at Break, MPa [psi]	5 [750]	ASTM D638
Elongation at Break, %	150	ASTM D638
Modulus of Elasticity, MPa [psi]	17 [2,500]	ASTM D638
Glass Transition T_g, °C	45	DSTM 256‡
$CTE_{\alpha 1}$, µm/m/°C	95	ASTM E831
$CTE_{\alpha 2}$, µm/m/°C	180	ASTM E831

OTHER CURED PROPERTIES *

Property	Value	Test Method
Refractive Index (20°C)	1.51	ASTM D542
Boiling Water Absorption, % (2 h)	2.6	ASTM D570
Water Absorption, % (25°C, 24 h)	1.0	ASTM D570
Linear Shrinkage, %	2	ASTM D2566

ELECTRICAL PROPERTIES *

Property	Value	Test Method
Dielectric Constant (1 MHz)	3.27	ASTM D150
Dissipation Factor (1 MHz)	0.046	ASTM D150
Dielectric Breakdown Voltage, kV/mm [V/mil]	500	ASTM D149
Volume Resistivity, 10^{12} ohm-cm	555	ASTM D257
Surface Resistivity, 10^{12} ohm	6,300	ASTM D257

* Not Specifications
N/A Not Applicable
‡ DSTM Refers to Dymax Standard Test Method

RoHS Compliant

Technical Data Collection Prior to 2009 Rev. 02/08/2012

Dymax Corporation
860.482.1010
info@dymax.com
www.dymax.com

Dymax Oligomers &Coatings
860.626.7006
oligomers&coatings@dymax.com
www.dymax-oc.com

Dymax Europe GmbH
+49 (0) 611.962.7900
info_de@dymax.com
www.dymax.de

Dymax UV Adhesives & Equipment (Shenzhen) Co Ltd
+86.755.83485759
dymaxasia@dymax.com
www.dymax.com.cn

Dymax UV Adhesives & Equipment (Shanghai) Co Ltd
+86.21.37285759
dymaxasia@dymax.com
www.dymax.com.cn

Dymax Asia (H.K.) Limited
+852.2460.7038
dymaxasia@dymax.com
www.dymax.com.cn

Dymax Korea LLC
82.2.784.3434
info@dymax.kr
www.dymax.co.kr

CURING GUIDELINES

Fixture time is defined as the time to develop a shear strength of 0.1 N/mm² [10 psi] between glass slides. Actual cure time typically is 3 to 5 times fixture time.

Dymax Curing System (Intensity)	Fixture Time or Belt Speed [A]
2000-EC (50 mW/cm²)[B]	3 s
5000-EC (200 mW/cm²)[B]	2 s
BlueWave® LED Prime UVA (10 W/cm²)[C]	2 s
BlueWave® 75 (5.0 W/cm²)[B]	1.4 s
BlueWave® 200 (10 W/cm²)[B]	1.2 s
UVCS Conveyor with one 5000-EC (200 mW/cm²)[D]	4.9 m/min [13 ft/min]
UVCS Conveyor with Fusion F300S (2.5 W/cm²)[D]	8.2 m/min [27 ft/min]

A *Curing through light-blocking substrates may require longer cure times if they obstruct wavelengths used for light curing (320-400 nm for UV light curing, 320-450 nm for UV/Visible light curing). These fixture times/belt speeds are typical for curing thin films through 100% light-transmitting substrates.*

B *Intensity was measured over the UVA range (320-395 nm) using a Dymax ACCU-CAL™ 50 Radiometer.*

C *Intensity was measured over the UVA/Visible range (350-450 nm) using a Dymax ACCU-CAL™ 50-LED Radiometer.*

D *At 53 mm [2.1 in] focal distance. Maximum speed of conveyor is 8.2 m/min [27 ft/min]. Intensity was measured over the UVA range (320-395 nm) using the Dymax ACCU-CAL™ 150 Radiometer.*

Full cure is best determined empirically by curing at different times and intensities, and measuring the corresponding change in cured properties such as tackiness, adhesion, hardness, etc. Full cure is defined as the point at which more light exposure no longer improves cured properties. Higher intensities or longer cures (up to 5x) generally will not degrade Dymax light-curable materials.

SECONDARY HEAT CURE

Heat can be used as a secondary cure mechanism where the adhesive cannot be cured with light. Light curing must be done prior to heat cure. The following heat-cure schedule may be used:

Temperature	Time*
110°C [230°F]	60 minutes
120°C [250°F]	30 minutes
150°C [300°F]	15 minutes

*Note: Actual heat-cure time may vary due to part configuration, volume of adhesive applied, and oven efficiency.

Dymax recommends that customers employ a safety factor by curing longer and/or at higher intensities than required for full cure. Although Dymax Application Engineering can provide technical support and assist with process development, each customer ultimately must determine and qualify the appropriate curing parameters required for their unique application.

DEPTH OF CURE

The graphs below show the increase in depth of cure as a function of exposure time with two different lamps at different intensities. A 9.5 mm [0.37 in] diameter specimen was cured in a polypropylene mold and cooled to room temperature. It was then released from the mold and the cure depth was measured.

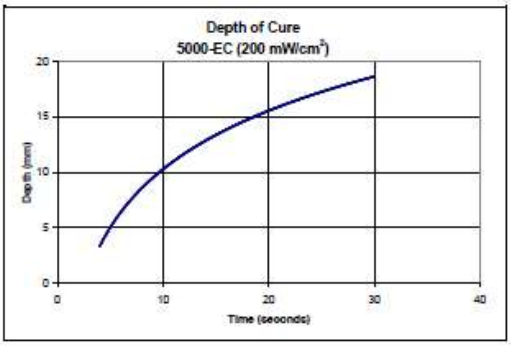

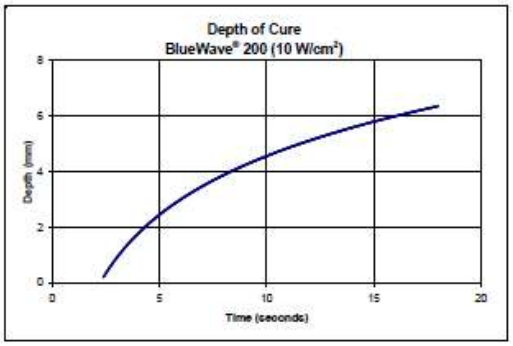

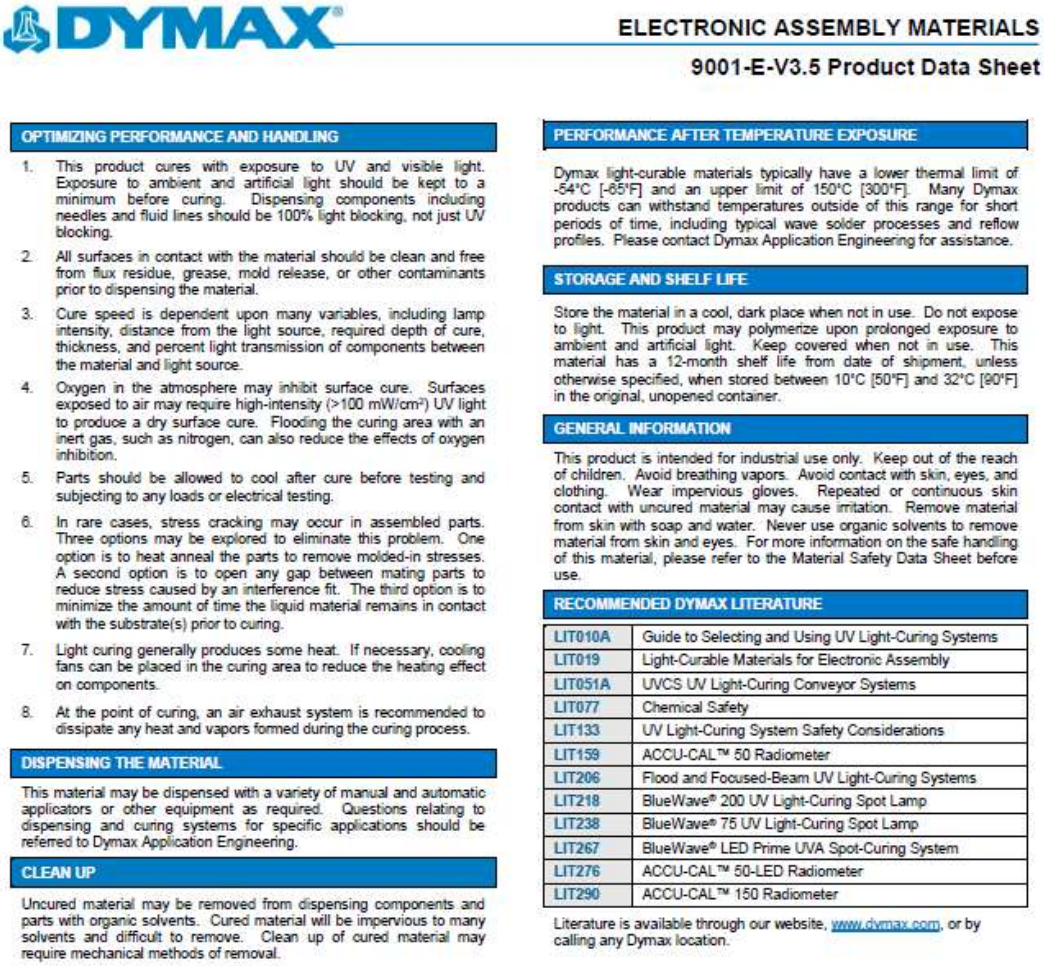

DYMAX

ELECTRONIC ASSEMBLY MATERIALS

9001-E-V3.5 Product Data Sheet

OPTIMIZING PERFORMANCE AND HANDLING

1. This product cures with exposure to UV and visible light. Exposure to ambient and artificial light should be kept to a minimum before curing. Dispensing components including needles and fluid lines should be 100% light blocking, not just UV blocking.
2. All surfaces in contact with the material should be clean and free from flux residue, grease, mold release, or other contaminants prior to dispensing the material.
3. Cure speed is dependent upon many variables, including lamp intensity, distance from the light source, required depth of cure, thickness, and percent light transmission of components between the material and light source.
4. Oxygen in the atmosphere may inhibit surface cure. Surfaces exposed to air may require high-intensity (>100 mW/cm²) UV light to produce a dry surface cure. Flooding the curing area with an inert gas, such as nitrogen, can also reduce the effects of oxygen inhibition.
5. Parts should be allowed to cool after cure before testing and subjecting to any loads or electrical testing.
6. In rare cases, stress cracking may occur in assembled parts. Three options may be explored to eliminate this problem. One option is to heat anneal the parts to remove molded-in stresses. A second option is to open any gap between mating parts to reduce stress caused by an interference fit. The third option is to minimize the amount of time the liquid material remains in contact with the substrate(s) prior to curing.
7. Light curing generally produces some heat. If necessary, cooling fans can be placed in the curing area to reduce the heating effect on components.
8. At the point of curing, an air exhaust system is recommended to dissipate any heat and vapors formed during the curing process.

DISPENSING THE MATERIAL

This material may be dispensed with a variety of manual and automatic applicators or other equipment as required. Questions relating to dispensing and curing systems for specific applications should be referred to Dymax Application Engineering.

CLEAN UP

Uncured material may be removed from dispensing components and parts with organic solvents. Cured material will be impervious to many solvents and difficult to remove. Clean up of cured material may require mechanical methods of removal.

PERFORMANCE AFTER TEMPERATURE EXPOSURE

Dymax light-curable materials typically have a lower thermal limit of -54°C [-65°F] and an upper limit of 150°C [300°F]. Many Dymax products can withstand temperatures outside of this range for short periods of time, including typical wave solder processes and reflow profiles. Please contact Dymax Application Engineering for assistance.

STORAGE AND SHELF LIFE

Store the material in a cool, dark place when not in use. Do not expose to light. This product may polymerize upon prolonged exposure to ambient and artificial light. Keep covered when not in use. This material has a 12-month shelf life from date of shipment, unless otherwise specified, when stored between 10°C [50°F] and 32°C [90°F] in the original, unopened container.

GENERAL INFORMATION

This product is intended for industrial use only. Keep out of the reach of children. Avoid breathing vapors. Avoid contact with skin, eyes, and clothing. Wear impervious gloves. Repeated or continuous skin contact with uncured material may cause irritation. Remove material from skin with soap and water. Never use organic solvents to remove material from skin and eyes. For more information on the safe handling of this material, please refer to the Material Safety Data Sheet before use.

RECOMMENDED DYMAX LITERATURE

LIT010A	Guide to Selecting and Using UV Light-Curing Systems
LIT019	Light-Curable Materials for Electronic Assembly
LIT051A	UVCS UV Light-Curing Conveyor Systems
LIT077	Chemical Safety
LIT133	UV Light-Curing System Safety Considerations
LIT159	ACCU-CAL™ 50 Radiometer
LIT206	Flood and Focused-Beam UV Light-Curing Systems
LIT218	BlueWave® 200 UV Light-Curing Spot Lamp
LIT238	BlueWave® 75 UV Light-Curing Spot Lamp
LIT267	BlueWave® LED Prime UVA Spot-Curing System
LIT276	ACCU-CAL™ 50-LED Radiometer
LIT290	ACCU-CAL™ 150 Radiometer

Literature is available through our website, www.dymax.com, or by calling any Dymax location.

8.10 Appendix 10: COMSOL model

The images of the simulations carried out on COMSOL for the different samples is given below in figures 8.11 to 8.16.

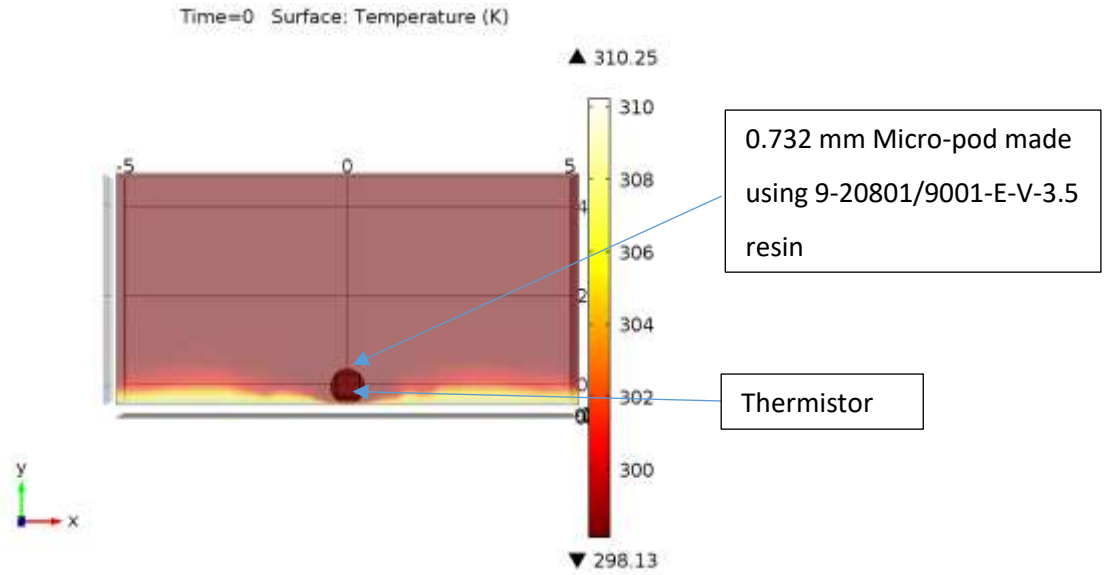

Figure 8-11: Thermistor encapsulated with 0.732 mm 9-20801 resin

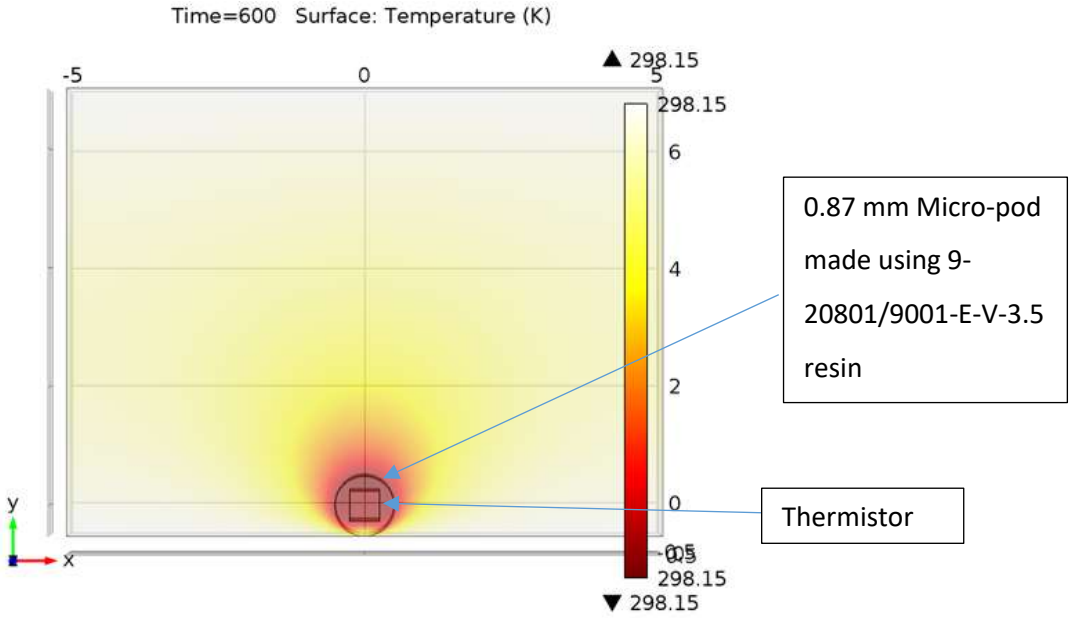

Figure 8-12: Thermistor encapsulated with 0.87 mm 9-20801/9001-E-V-3.5 resin

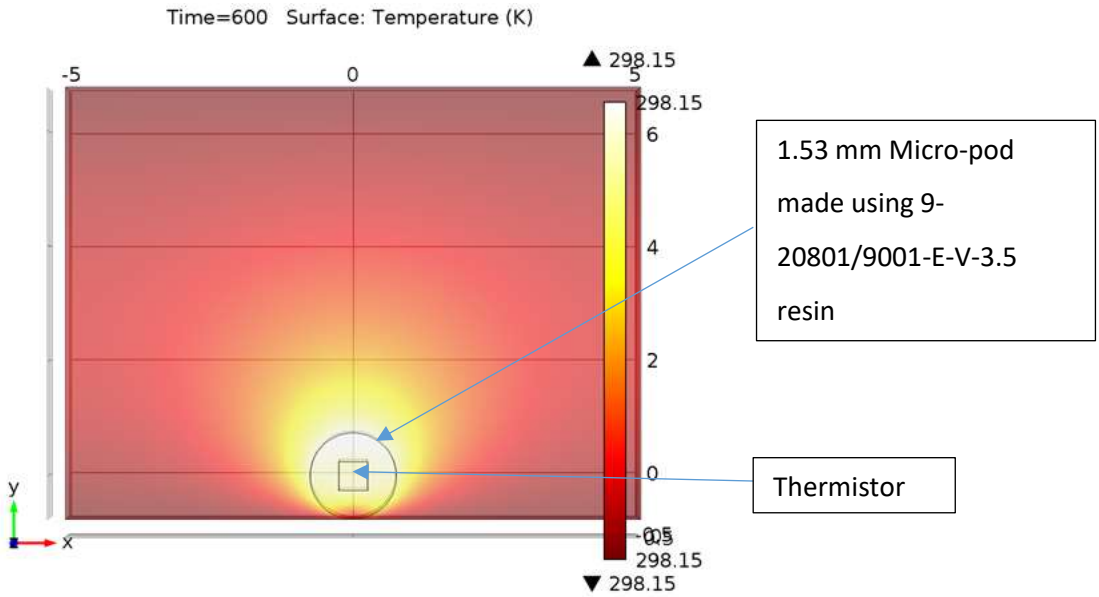

Figure 8-13: Thermistor encapsulated with 1.53 mm 9-20801/9001-E-V-3.5 resin

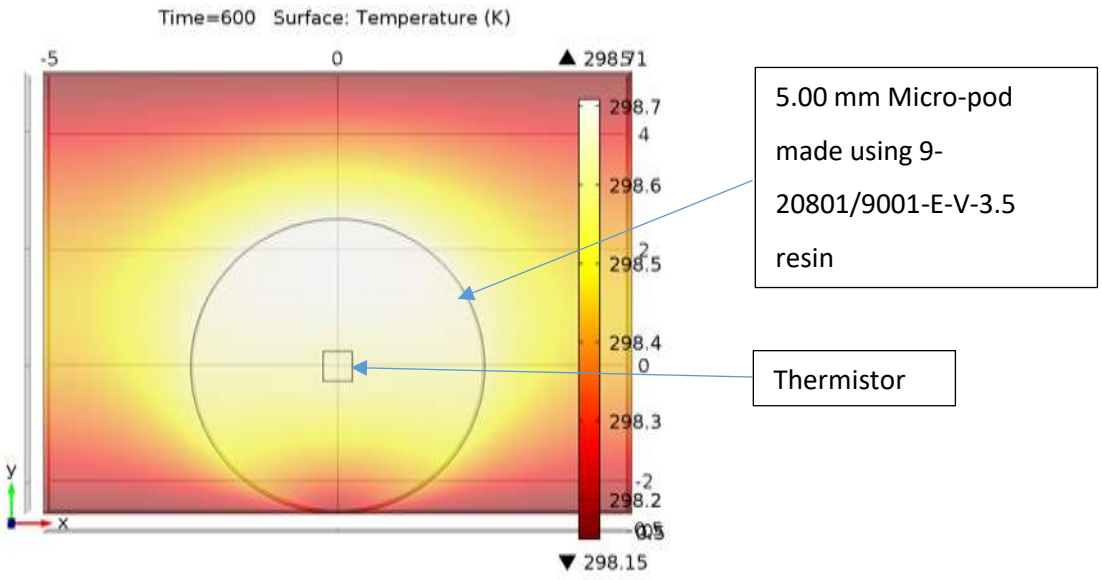

Figure 8-14: Thermistor encapsulated with 5.00 mm 9-20801/9001-E-V-3.5 resin

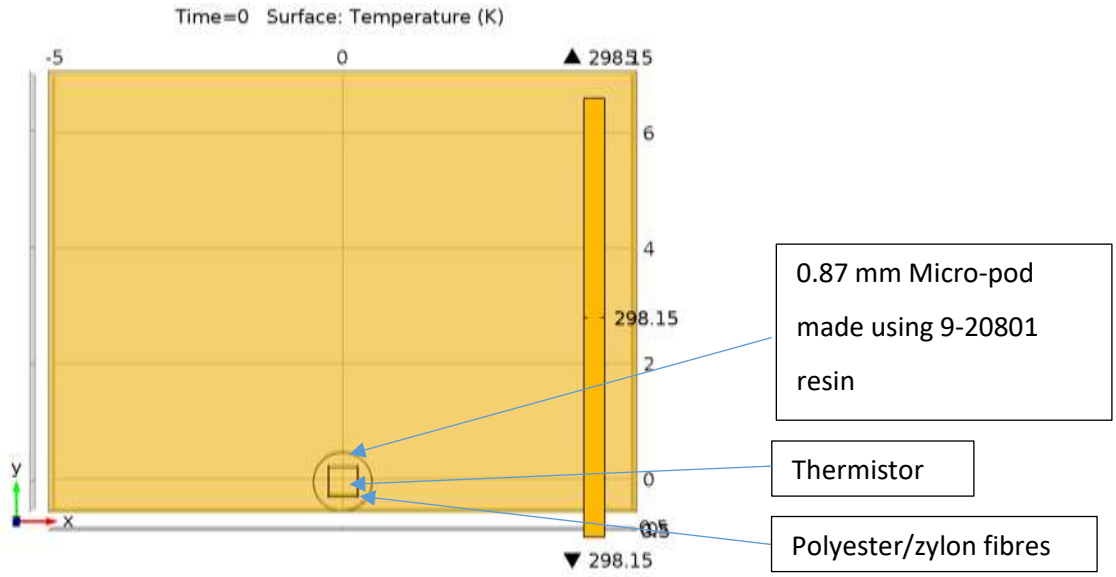

Figure 8-15: Thermistor and polyester/Zylon fibres encapsulated with 0.87 mm 9-20801resin

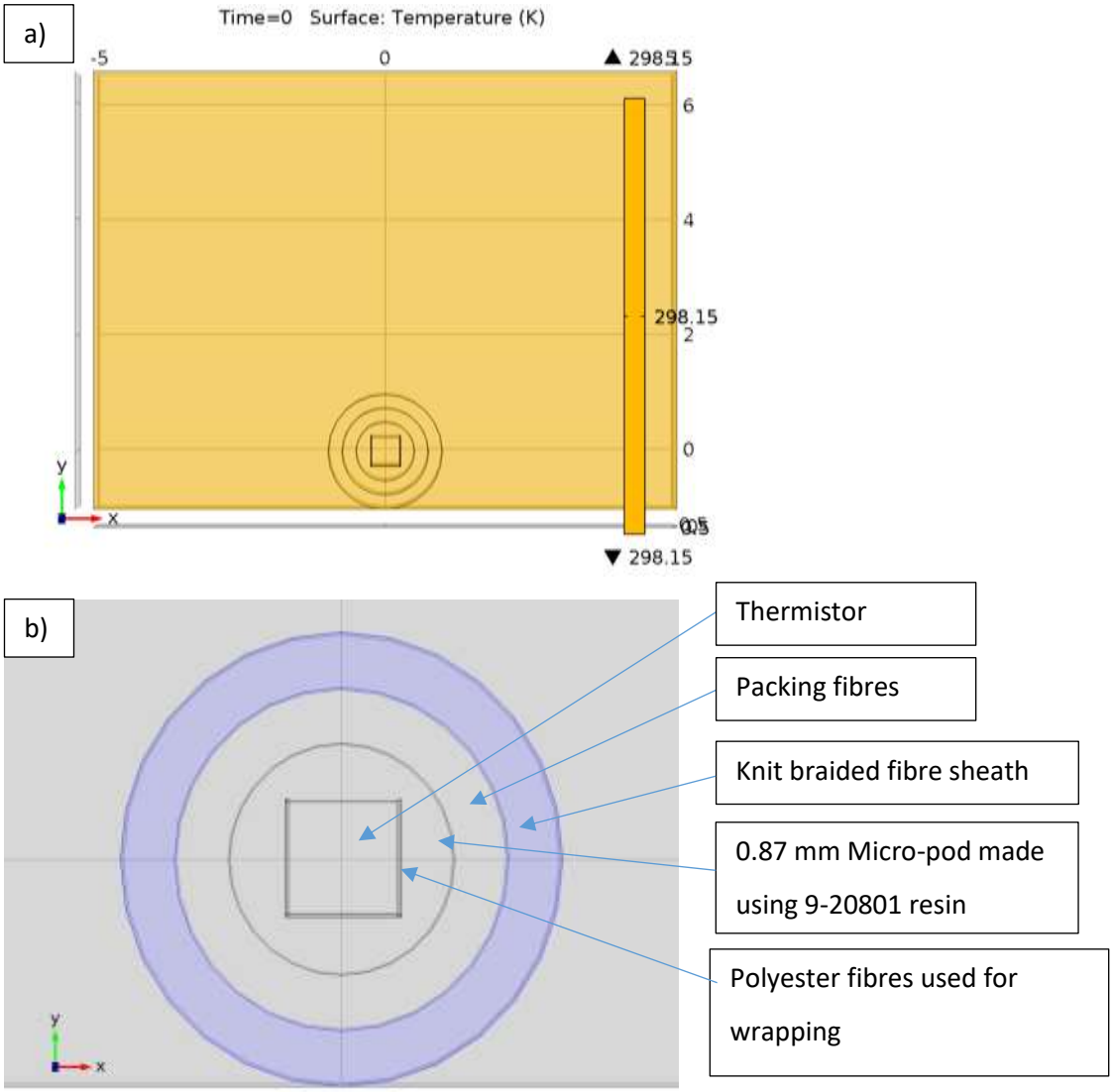

Figure 8-16: a) Final ETS yarn simulated and b) close up of the final ETS yarn

8.11 Appendix 11: LabVIEW Block diagrams of the USB_TC08 subVI

8.11.1 LabVIEW Block diagram for obtaining the temperature from an ETS yarn

The block diagram of the LabVIEW program to obtain the temperature from an ETS yarn is shown in figure 8.17.

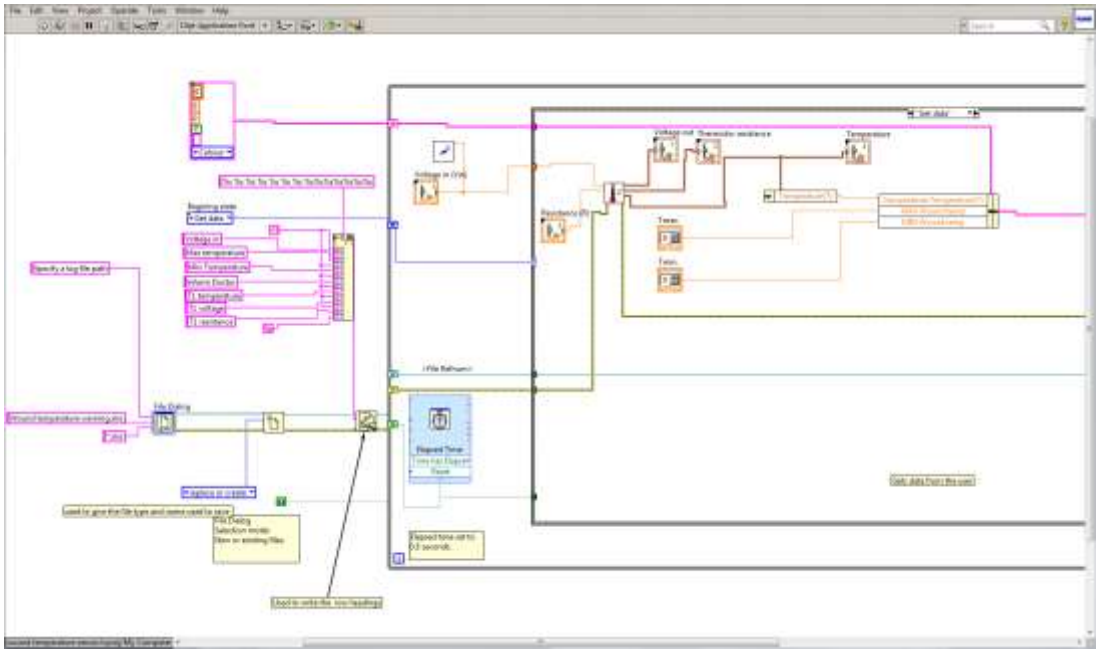

Figure 8-17: Block diagram of the LabVIEW program used for the ETS yarn

8.11.2 LabVIEW Block diagrams of the USB_TC08 subVI

The block diagram of the LabVIEW subVI used to communicate with the USB_TC08 is given below in figure 8.18.

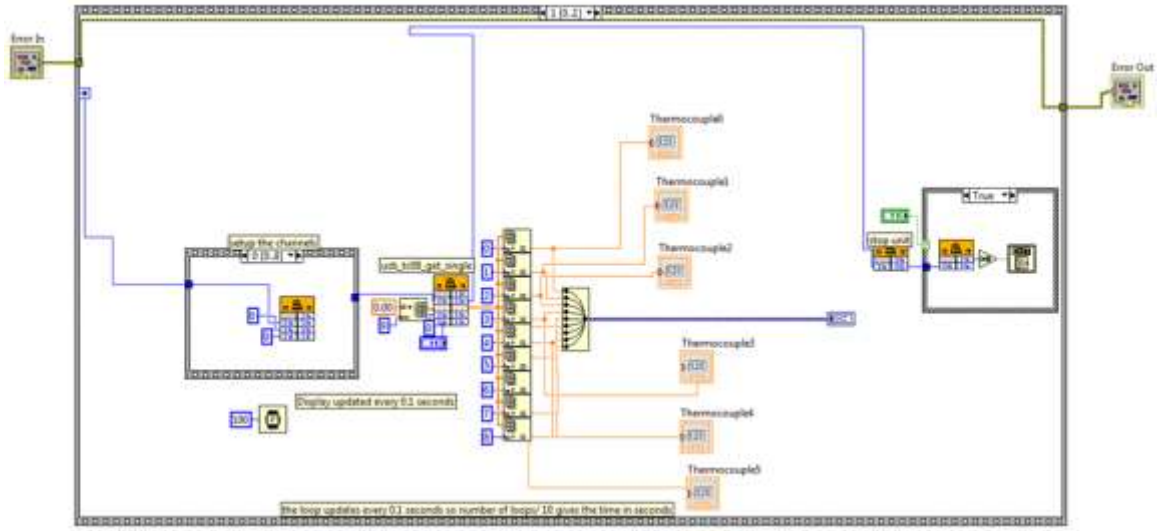

Figure 8-18: Block diagram of the USB_TC08 SubVI

8.11.3 LabVIEW Block diagrams of the USB_TC08 subVI

The block diagram of the LabVIEW program used to obtain data from the Arduino Nano is presented in figure 8.19.

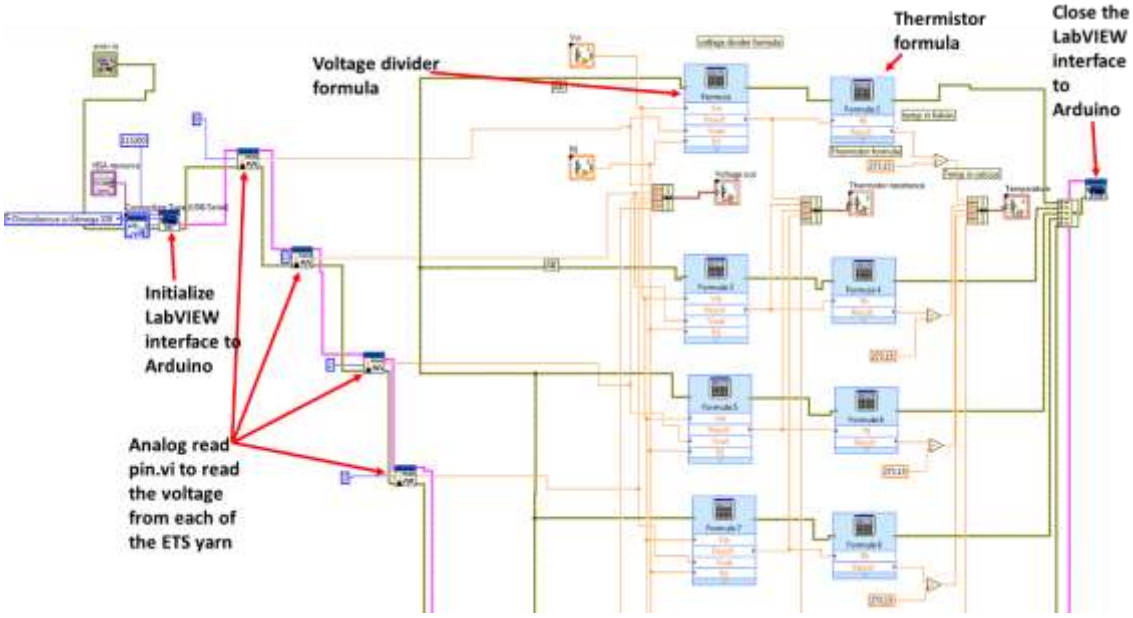

Figure 8-19: Block diagram of the LabVIEW program used to capture the temperature from the ETS yarn when connected to the Arduino Nano

8.12 Appendix 12: Step response time of the sensor

The step response time is another important parameter for temperature sensors. The step response time of a measuring system is the time duration taken by the measuring system to reach a final steady value once it is subjected to an abrupt change between two specified constant quantity values (JCGM, 2012). Therefore by using the simulated and experimental data acquired in chapter 4 the theoretical and experimental step response time was analysed.

8.12.1 Theoretical step response time

The step response times estimated by the simulations were all less than 350 s as shown in figure 4.2 (in chapter 4). This was deemed acceptably short for the desired application as temperature changes due to pathology would occur on a time scale of the order of hours. When the thermally conductive 9-20801 resin was used to form a cylindrical encapsulation of the optimum diameter (0.732 mm), the step response time for the heat to flow through the resin was found to be 3 s as shown in Table 8.5. Increasing the diameter of the cylindrical encapsulation resulted in an increase in the step response time as would be expected given the increased thermal resistance.

Similar results for the thermally non-conductive 9001-E-V-3.5 resin were observed giving an increase in the step response time of 3.9 s when compared to when the thermally conductive 9-20801 resin was used to form a cylindrical encapsulation of diameter 0.87 mm, which had no significant impact on the desired temporal resolution of the sensor which would be no less than 30

minutes. As would be expected this effect was more pronounced when a thicker encapsulation was used, with the 5 mm diameter encapsulation step response time changing between 181.0 s and 348.4 s depending on the type of resin used. The polyester (PE) fibres placed within the micro-pod appeared to have had minor impact of 0.3 s on the step response time. The packing fibres and the knit braid used for covering the micro-pod however increased the step response time by a further 27.7 s. As discussed previously this would not impede the performance of the device for the intended applications.

8.12.2 Experimental step response time

Due to the difficulty in creating a 0.732 mm diameter cylindrical micro-pod, 0.87 mm was considered as the minimum diameter of the micro-pod that could be manufactured reliably. When this was the case, the theoretical step response time only increased by 1.5 s when compared to using the optimum diameter of 0.732 mm, making 0.87 mm an acceptable diameter. Temperatures were calculated from resistance values using the information provided by the manufacturer although a calibration of the final ETS yarn was used to validate this approach. The graph plotted using the experimental results shown in Figure 4.3 (chapter 4) displayed a similar shape as the graph in the theoretical simulations (Figure 4.2).

The experimental results (Table 8.5) however showed a large difference between the step response times when the sensors were placed on the hot plate and when they were taken away from the hot plate. This change could be as a result of the silicon holder which was used to restrain the samples onto the hot plate. The properties (thermal conductivity, heat capacity and density) of the silicon sample holder were clearly different to those of air. So it can be said that the step response time was influenced by the silicon holder, when the samples were placed on the hot plate. This also explains the large standard deviation in the measured step response times given in the third row of Table 8.5. Hence, the step response time when the samples were taken away from hotplate was considered herein to be that of the samples.

Table 8-5: Theoretical and experimental step response times for the thermistor under different encapsulation conditions. Results have been extracted from the data presented in figures 4.2 and 4.3. The experiments were conducted on three different samples (except for 5 mm 9001 resin encapsulation) and five ETS yarn samples. The mean and the standard deviation has been stated in the table.

	Simulated step response time τ_S **(s)**	**Measured step response time (samples are placed on the hotplate)** τ_P **(s)**	**Measured step response time (samples taken away from hotplate)** τ_R **(s)**	**Effect of additional layers [** τ_R**(s)-3.9(s)*]**
Thermistor	Not Simulated	107.4 ± 50.7	20.8 ± 6.3*	0
0.732 mm 9-20801 resin	3	Not measured	Not measured	Not measured
0.87 mm 9-20801 resin	4.5	123.3 ± 10.7	29.8 ± 3.4	9.0 ± 3.7
1.53 mm 9-20801 resin	15.8	160.2 ± 34.8	61.8 ± 9.6	41.0 ± 18.8
5 mm 9-20801 resin	181	286.1 ± 15.8	163.0 ± 9.7	142.2 ± 51.8
0.87 mm 9001-E-V-3.5	8.4	142.5 ± 17.6	46.7 ± 6.5	25.9 ± 11.5
1.53 mm 9001-E-V-3.5	27.8	204.1 ± 8.7	65.7 ± 5.2	44.9 ± 17.2
5 mm 9001-E-V-3.5	348.4	275.5	240.3	219.5
Two polyester yarn (0.87 mm resin)	4.8	152.9 ± 32.5	27.9 ± 6.5	7.1 ± 3.8
Temperature sensing yarn	32.5	199.7 ± 19.8	55.0 ± 9.2	34.2 ± 16.1

The results of the first experiment given in Table 8.5 provided the step response time for the thermistor chip soldered onto the eight strands copper wire which was only 20.8 s. The theoretical model only gave the step response time taken by the heat to reach the surface of the chip, therefore to compare the simulation results with the experimental results the difference between the measurements of the sample and the thermistor were calculated. These values are presented in the last column of Table 8.5.

As in the theoretical simulations the experimental results demonstrated that the step response time increased with a larger diameter of encapsulation, this was due to the increase in the thermal resistance. The discrepancy between the step response times for the simulation and experiment results were most likely due to positioning of the thermistors within the encapsulation introducing a small error. The discrepancies seen with the larger encapsulations (5 mm) were due to simplifications made in the computer simulation. This was not investigated further since a 5 mm cylindrical encapsulation would mean that the volume of the micro-pod would be 46.6 times the minimum volume estimated in the geometrical model, and therefore the encapsulation would be too large to be included within a yarn and placed into a fabric.

The step response time only increased by 9.0 s when the thermistor was encapsulated using 9-20801 adhesive to form a 0.87 mm diameter cylindrical encapsulation and it was seen that the volume of resin brought about an increase in the step response time. When the thermally non-conductive 9001 –E-V-3.5 resin was used for the encapsulation, the step response time increased as in the theoretical simulations. For the optimum diameter of 0.87 mm there was an increase of only 16.9 s when compared to the thermally conductive 9-20801 resin.

As assumed by the theoretical simulations the polyester fibres within the encapsulation had no significant impact on the step response time in the experimental results compared to when a 0.87 mm 9-20801 resin was used. The minute difference in between the step response times of 7.1 s and 9.0 s when the fibres are included in micro-pod of 0.87 mm of 9-20801 resin and when they are not respectively may have been caused by the positioning of the thermistors within the micro-pod. Therefore, it can be argued that the PE fibres placed within the micro-pod have no significant impact on the step response time. This was due to the small volume of the PE fibres.

The step response time when the encapsulation was covered with packing fibres and the warp knitted outer covering (final yarn) was 34.2 s more than the step response time of the thermistor, this was 1.7 s longer than the theoretical estimate in Table 8.5 (last row of column 2). This may have been caused due to the estimations made about the volume fractions in the theoretical model. Regardless a step response time of 55.0 s for the ETS yarn (last row of the 4th column) can be regarded as acceptable since, as discussed earlier for long term monitoring applications, such a temporal resolution was not essential. It can be concluded that the volume and thermal conductivity of the polymer resin and the yarn filaments have an insignificant effect on the step response time of the sensor.

8.13 Appendix 13: Data sheet for Floormate 300A provided by Dow building solutions (MI, USA)

TECHNICAL DATA

DOW Building Solutions

Product data table for STYROFOAM™-A

CE

Properties	Standard	unit	CE Code	FLOORMATE™			ROOFMATE™		PERIMATE™
				300-A	500-A	700-A	SL-A	LG-A (foam)	DI-A
Thermal conductivity*									
≤ 70mm	BS EN 12667	W/mk	λ_D	0.033	0.034	0.034	-	-	-
71 – 80mm	BS EN 12667	W/mk	λ_D	0.033	0.035	-	-	0.033	-
81 – 100mm	BS EN 12667	W/mk	λ_D	0.034	-	0.035	-	-	-
101 – 120mm	BS EN 12667	W/mk	λ_D	0.034	-	-	0.034	-	0.034
≥ 121mm	BS EN 12667	W/mk	λ_D	0.036	-	-	0.036	-	-
Compressive strength at 10% or break (90 days)	BS EN 826	kN/m²	CS(10/Y)i	300	500	700	300	300	300
Design load 2% max. deflection (50 years)	BS EN 1606	kN/m²	CC (2/1.5/50) σ_c	130	180	250	130	-	-
Water vapour diffusion resistance factor	BS EN 12086	m	MUi	80-200	80-200	80-200	80-200	80-200	80-200
Water absorption									
Total immersion	BS EN 12087	% vol	WL(T)i	<0.7	<0.7	<0.7	<0.7	<0.7	<0.7
Diffusion	BS EN 12088	% vol	WD(V)i	<3	<3	<3	<3	<3	<3
Freeze/thaw, after 300 cycles	BS EN 12091	% vol	FTi	<1	<1	<1	<1	<1	<1
Dimensional stability									
48 hrs at 70C/90%RH	BS EN 1604	%	DS(TH)	<2	<2	<2	<2	<2	<2
168 hrs at 40kPa/70C	BS EN 1605	%	DLT(2)5	<5	<5	<5	<5	<5	-
Density (aim, foam only)	BS EN 1602	kg/m³	-	34	38	42	34	34	34
Dimensions									
Length	BS EN 822	mm	-	2500	1250	1250	1250	1200	1250
Width	BS EN 822	mm	-	600	600	600	600	600	600
Thickness	BS EN 823	mm	Ti	50, 75, 100, 125,150, 200	50, 75	50, 100	100, 120, 140, 160, 180**, 200**	90***	100
Fire classification - reaction to fire	BS EN 13164 BS EN 13501	-	Euroclass	E	E	E	E	E	E
Appearance									
Surface				skin	skin	skin	skin	mortar topping	grooved face & geotextile
Edge profile				butt edge	shiplap	shiplap	shiplap	tongue & groove	shiplap
Application				Floors - domestic and medium load bearing	Floors - high loadbearing	Floors - very highload bearing	Inverted roofs ballasted	Parapet/ Upstand	Basement walls external

The properties given are typical (unless stated otherwise).
* declared 90/90 value - BS EN 13164 ** length 2500 mm *** includes 10mm for the mortar topping

Note:
The information and data contained in this technical data sheet do not represent exact sales specifications. The features of the products mentioned may vary. The information contained in this document has been provided in good faith, however it does not imply any liability, guarantee or assurance of product performance. It is the purchaser's responsibility to determine whether these Dow products are suitable for the application desired and to ensure that the site of work and method of application conform with current legislation. No licence is hereby granted for the use of patents or other industrial or intellectual property rights. If Dow products are purchased, we advise following the most up-to-date suggestions and recommendations.

** Trademark of The Dow Chemical Company ("Dow") or an affiliated company of Dow

λ NEW

Dow Chemical Company Limited
Dow Building Solutions
Diamond House, Lotus Park
Kingsbury Crescent, Staines, TW18 3AG
Tel: 020 3139 4000
Fax: 020 3139 401

S06-291-01025-1212

8.14 Appendix 14: Python code for calibration

The python code to obtain the two calibration fittings and plot it along with the manufacturer's equation using the data obtained from the ETS yarns is given below.

```
#!/usr/bin/env python
# -*- coding: utf-8 -*-
"""
Spyder Editor
This is a temporary script file.
"""
"""
This is a trial fitting code with confidence intervals taken from here:
http://kitchingroup.cheme.cmu.edu/blog/2013/02/12/Nonlinear-curve-fitting-with-parameter-confidence-intervals/
"""
# Nonlinear curve fit with confidence interval
import numpy as np
from scipy.optimize import curve_fit
from scipy.stats.distributions import  t
import matplotlib.pyplot as plt
#from matplotlib.font_manager import FontProperti
from matplotlib import rc
#plt.rc('text', usetex=True)
plt.rc('font',**{'family':'serif','serif':['palatino linotype'],'size':30})
#Font
#cfont = {'fontname':'calibri'}
plt.rc('font', family='sans-serif')
plt.rc('font', serif='times new roman')
plt.rc('text', usetex='false')
plt.rcParams.update({'font.size': 12})
#Temperature
y2 = [22.25, 22.8, 24.35, 27.4, 30.95, 34.4, 38.2, 42.15, 45.8, 49.5, 54.45, 58.1, 62.15]
```

```
y1 = [0.046296296, 0.044444444, 0.041152263, 0.036630037, 0.032679739, 0.029542097, 0.026595745, 0.024154589, 0.022346369, 0.020898642, 0.018779343, 0.017528484, 0.016528926]

# YELLOW THERM y1 = [0.04494382, 0.043859649, 0.041067762, 0.03649635, 0.032310178, 0.029069767, 0.02617801, 0.023724792, 0.021834061, 0.02020202, 0.018365473, 0.017211704, 0.016090105] # 1/T

#Resistance

x2 = [11.181, 10.904, 10.293, 9.2921, 8.187, 7.23, 6.3066, 5.47, 4.8735, 4.335, 3.612, 3.16, 2.783]

#SECOND YARN

x3 = [11.212, 11.006, 10.37, 9.1721, 8.0063, 7, 6.0846, 5.331, 4.6713, 4.2908, 3.477, 3.1356, 2.804]

#THIRD YARN

x4 = [10.96, 10.737, 10.046, 8.8999, 7.7726, 6.8004, 5.9378, 5.1733, 4.5207, 4.2084, 3.3953, 3.0259, 2.7488]

#FOURTH YARN

x5 = [11.258, 10.981, 10.304, 9.1142, 8.004, 7.05, 6.1758, 5.3508, 4.772, 4.3402, 3.61, 3.1509, 2.797]

#FIFTH YARN

x6 = [11.283, 11.021, 10.36, 9.1645, 8.069, 7.1334, 6.2287, 5.4312, 4.8421, 4.305, 3.5996, 3.175, 2.8132]

#AVERAGE

x1 = [11.1788, 10.9298, 10.2746, 9.12856, 8.00778, 7.04276, 6.1467, 5.35126, 4.73592, 4.29588, 3.53878, 3.12948, 2.7892]

# NO ETS 1 x1 = [11.17825, 10.93625, 10.27, 9.087675, 7.962975, 6.99595, 6.106725, 5.321575, 4.701525, 4.2861, 3.520475, 3.12185, 2.79075]

# NO ETS 3x1 = [11.2335, 10.978, 10.33175, 9.185725, 8.066575, 7.10335, 6.198925, 5.39575, 4.789725, 4.31775, 3.57465, 3.155375, 2.7993]

xSD = [0.128560103, 0.116814811, 0.132150672, 0.143548208, 0.150991563, 0.161162676, 0.14198102, 0.114640778, 0.143177868, 0.053048016, 0.098152697, 0.059641906, 0.025132051]

#MANUFACTURER

Ro=10.000

T1=[]

inc=0

while inc<13:


   T1.append(1/((1/((np.log((x1[inc]*1000)/10000)/3395)+(1/298.15))) - 273.15))

   inc=inc+1

   #print(inc)

else:
```

```
   print(T1)



def func1(x1, e, f, g):
   'nonlinear function in a and b to fit to data'


  #                                return                                (12*a/30)*(2/((x1/30+(30/x1))))*((1-
(1/(((((x1/30)+(30/x1))/2)*(np.arcsin(2/((x1/30)+(30/x1)))))**6)))+b*((((((x1/30)+(30/x1))/2)*(np.a
rcsin(2/((x1/30)+(30/x1)))))**2)-(1/(((((x1/30)+(30/x1))/2)*(np.arcsin(2/((x1/30)+(30/x1)))))**4))))
# PROPER ONE!
   return e + f*np.log(x1)+g*(np.log(x1))**3
#initial_guess = [0.4, 0.02]
#initial_guess = [40, 40]
#pars, pcov = curve_fit(func, x, y, p0=initial_guess)
pars1, pcov = curve_fit(func1, x1, y1)
# this is the function we want to fit to our data
#def func(x, a, b):
   #second fitting function
def func(x1, a, b, c, d):
   'nonlinear function in a and b to fit to data'


  #                                return                                (12*a/30)*(2/((x1/30+(30/x1))))*((1-
(1/(((((x1/30)+(30/x1))/2)*(np.arcsin(2/((x1/30)+(30/x1)))))**6)))+b*((((((x1/30)+(30/x1))/2)*(np.a
rcsin(2/((x1/30)+(30/x1)))))**2)-(1/(((((x1/30)+(30/x1))/2)*(np.arcsin(2/((x1/30)+(30/x1)))))**4))))
# PROPER ONE!
   return a + b*np.log(x1/Ro)+c*(np.log(x1/Ro))**2+d*(np.log(x1/Ro))**3
#initial_guess = [0.4, 0.02]
#initial_guess = [40, 40]
#pars, pcov = curve_fit(func, x, y, p0=initial_guess)
pars, pcov = curve_fit(func, x1, y1)
#def func(x, a, b):
alpha = 0.05 # 95% confidence interval = 100*(1-alpha)
n = len(y1)    # number of data points
p = len(pars) # number of parameters
dof = max(0, n - p) # number of degrees of freedom
```

```
# student-t value for the dof and confidence level

tval = t.ppf(1.0-alpha/2., dof)

for i, p,var in zip(range(n), pars, np.diag(pcov)):

   sigma = var**0.5

   #print ('p{0}: {1} [{2}  {3}]')#.format(i, p,

                        #p - sigma*tval,

                        #p + sigma*tval)

xfit = np.linspace(2,12)

y2fit = func1(xfit, pars1[0], pars1[1], pars1[2])

#second polynomial equation

yfit = func(xfit, pars[0], pars[1], pars[2], pars[3])

"""NOTE: The confidence intervals DO NOT WORK in this version, I've not even tired to fix it. ~ Although I am getting values, so who knows?"""

#print 'p{0}: {1}'

print (pars)

#print "p{2}"

#plt.figure()

#plt.subplot(121)

#plt.subplot(122)

#plt.plot(x1,y1,'ko ')

plt.errorbar(x1,y1, color = 'k', xerr=[xSD, xSD], fmt='o', ecolor='k')

plt.plot(xfit,y2fit,'b-')

plt.plot(xfit,yfit,'k-')

#plotting the temperature from equation

plt.plot(x1,T1,'r-')

#plt.legend(loc=0, scatterpoints = 1)

plt.legend(['Data fitting 1','Data fitting 2','Manufacturers\nequation','Averaged data\nfor five ETS yarns'],loc='best',numpoints = 1)

plt.xlabel('Resistance (k$\Omega$)') #kΩ

plt.ylabel('1/Temperature (1/$^\circ$C)') # °C

font=dict(family='Courier New, monospace', size=35, color='#7f7f7f')

#plt.xlim(0,60)

#plt.ylim(0,0.03)
```

```
#plt.savefig('images/nonlin-curve-fit-ci.png')
plt.savefig('RvsT.png')
plt.show()
plt.plot(x2,y1,'bo ')
plt.plot(x3,y1,'ro ')
plt.plot(x4,y1,'go ')
plt.plot(x5,y1,'mo ')
plt.plot(x6,y1,'yo ')
plt.plot(xfit,yfit,'b-')
plt.legend(['Averaged data of five ETS yarns','Data fitting'],loc='best',numpoints = 1)
font=dict(family='Courier New, monospace', size=35, color='#7f7f7f')
plt.xlabel('Resistance (k$\Omega$)') #kΩ
plt.ylabel('1/Temperature (1/($^\circ$C)') # °C
plt.show()
plt.plot(x2,y2,'bo ')
plt.plot(x3,y2,'ro ')
plt.plot(x4,y2,'go ')
plt.plot(x5,y2,'mo ')
plt.plot(x6,y2,'yo ')
#plt.plot(xfit,yfit,'b-')
plt.legend(['ETS yarn 1','ETS yarn 2','ETS yarn 3','ETS yarn 4','ETS yarn 5'],loc='best',numpoints = 1)
plt.xlabel('Resistance (k$\Omega$)') #kΩ
plt.ylabel('Temperature ($^\circ$C)') # °C
plt.show()
```

The python code to compare the 2 polynomial equations and the manufacturers equation is given below.

```
# -*- coding: utf-8 -*-
"""
Created on Tue Nov  7 14:38:35 2016
@author: n0567598
```

```
"""
# Nonlinear curve fit with confidence interval
import numpy as np
import matplotlib.pyplot as plt
#from matplotlib.font_manager import FontProperti
#Font
#cfont = {'fontname':'calibri'}
plt.rc('font', family='sans-serif')
plt.rc('font', serif='palatino linotype')
plt.rc('text', usetex='false')
plt.rcParams.update({'font.size': 10})
#AVERAGE resistance
x1 = [11178.8, 10929.8, 10274.6, 9128.56, 8007.78, 7042.76, 6146.7, 5351.26, 4735.92, 4295.88,
3538.78, 3129.48, 2789.2]
#thermistor resistance
y2 = [22.25, 22.8, 24.35, 27.4, 30.95, 34.4, 38.2, 42.15, 45.8, 49.5, 54.45, 58.1, 62.15]
y1 = [0.046296296, 0.044444444, 0.041152263, 0.036630037, 0.032679739, 0.029542097,
0.026595745, 0.024154589, 0.022346369, 0.020898642, 0.018779343, 0.017528484, 0.016528926]
#standard deviation of the resistances
xSD = [128.560103, 116.814811, 132.150672, 143.548208, 150.991563, 161.162676, 141.98102,
114.640778, 143.177868, 053.048016, 098.152697, 059.641906, 025.132051]
Ro=10000
Rok=10
T1=[]
T2=[]
T3=[]
T1error=[]
T2error=[]
T3error=[]
Tvalue2=[]
Tvalue1=[]
Tvalue3=[]
T1mod=[]
T2mod=[]
```

```
T3mod=[]
TT1=[]
TT2=[]
TT3=[]
TT1error=[]
TT2error=[]
TT3error=[]
x2=[]
xSD2=[]
inc=0
b=3395
while inc<13:
    #resistancein kiloohms
    x2.append(x1[inc]/1000)
    #standard deviation in kiloohms
    xSD2.append(xSD[inc]/1000)
    #Manufacturers equation
    T1.append(1/((1/((np.log((x1[inc])/10000)/3395)+(1/298.15))) - 273.15))
    #1st polynomial equation
    T2.append(0.017598 - 0.003687*np.log(x2[inc])+0.002545*(np.log(x2[inc]))**3)
    #2nd polynomial equation
    T3.append(0.04057623 +
0.04170416*np.log(x2[inc]/Rok)+0.03051437*(np.log(x2[inc]/Rok))**2+0.00997951*(np.log(x2[in
c]/Rok))**3)
    TT1.append(1/T1[inc])
    TT2.append(1/T2[inc])
    TT3.append(1/T3[inc])
    #propagation of errors of T
    #t1 standard deviation assuming R0-1% and b=1% and T0-0%

T1error.append(((((((xSD[inc])/x1[inc])**2+1)**0.5)*(x1[inc]/Ro)/(x1[inc]/Ro))/(np.log(x1[inc])/R
o)+1)**0.5)*(np.log((x1[inc])/Ro)/b))
    #T2 error=()
```

```
T2error.append(((((xSD[inc])/x1[inc])*0.017598)**2+((3*((np.log(x2[inc]))**3)*((xSD2[inc])/x2[inc
])/(np.log(x2[inc])))*0.003687)**2)**0.5)

    # T3 error


T3error.append(((((0.04170416*((xSD[inc]/x1[inc])**2+1)**0.5)*(x2[inc]/Ro))/(x2[inc]/Ro))**2)+(
0.03051437*2*((np.log(x1[inc])/Ro)*((((xSD[inc]/x1[inc])**2+1)**0.5)*(x2[inc]/Ro))/(x2[inc]/Ro))*
*2)+(0.00997951*3*((np.log(x1[inc])/Ro)**2)*((((xSD[inc]/x1[inc])**2+1)**0.5)*(x2[inc]/Ro)/(x2[i
nc]/Ro))**2)**0.5)

    #T error calculation for T

    TT1error.append((-1)*(T1[inc])**(-2)*T1error[inc])

    TT2error.append((-1)*(T2[inc])**(-2)*T2error[inc])

    TT3error.append((-1)*(T3[inc])**(-2)*T3error[inc])

    #Tvalue calculation for T

    Tvalue1.append((TT1[inc]-y2[inc])/(TT1error[inc]*(5**0.5)))

    Tvalue2.append((TT2[inc]-y2[inc])/(TT2error[inc]*(5**0.5)))

    Tvalue3.append((TT3[inc]-y2[inc])/(TT3error[inc]*(5**0.5)))

    #modulus of each and every component

    T1mod.append(abs(Tvalue1[inc]))

    T2mod.append(abs(Tvalue2[inc]))

    T3mod.append(abs(Tvalue3[inc]))

    inc=inc+1

    #print(inc)

else:

    print(TT3)

    print(T2mod)

    print (T3mod)

    print(TT3)

    print(Tvalue2)

    print(T1error)

    print(T2error)

    print(T3error)


#calculating the mean T value for each equation by getting the modulus

T1mean= np.mean(T1mod, dtype=np.float64)
```

```
T2mean= np.mean(T2mod, dtype=np.float64)

T3mean= np.mean(T3mod, dtype=np.float64)


print(T1mean)

print(T2mean)

print(T3mean)

 #plotting the tvalues

plt.plot(y2,Tvalue1,'r-')

plt.plot(y2,Tvalue2,'g-')

plt.plot(y2,Tvalue3,'b-')

plt.legend(['manufacturers equation', '1st polynomial equation', '2nd polynomial equation'],loc='best',numpoints = 1)

plt.xlabel('Temperature ($^\circ$C)') #kΩ

plt.ylabel('T value') # °C

plt.show()

plt.plot(x1,TT1,'r-')

plt.plot(x1,TT2,'g-')

plt.plot(x1,TT3,'b-')

plt.show()
```

8.15 Appendix 15: Tensile test

The table 8.6 contains the results from the tensile test to get the breaking force.

Table 8-6: Results from the tensile test to get the breaking force

Test results:

Nr	Specimen no.	Date	L_v mm	F_H cN	R_H cN/tex	ε_H %	R_B cN/tex	W_H mJ	$W_{H,m}$ J/g	Titer tex
1	1	18/06/2015	50.18	10200	17.8	37	14.89	1152.79	40.02	574
2	2	18/06/2015	50.20	11500	20.0	44	20.00	1531.97	53.16	574
3	3	18/06/2015	50.16	10700	18.6	39	14.86	1263.36	43.88	574
4	4	18/06/2015	50.19	10800	18.9	41	14.77	1367.44	47.46	574
5	5	18/06/2015	50.29	10400	18.1	39	14.90	1250.48	43.32	574
7	6	18/06/2015	50.24	11800	20.6	44	17.67	1609.81	55.82	574
8	7	18/06/2015	50.21	12100	21.1	42	17.44	1390.53	48.24	574
9	8	18/06/2015	50.25	11400	19.8	40	19.27	1423.80	49.36	574
10	9	18/06/2015	50.34	11300	19.7	41	19.53	1426.98	49.38	574
11	10	18/06/2015	50.21	10800	18.8	40	15.62	1262.39	43.80	574

8.16 Appendix 16: Information about the Echotherm Chilling/Heating Dry Bath provided by Torrey Pines Scientific Inc (Carlsbad, United States)

ECHOTHERM™ IC50 DIGITAL, ELECTRONIC CHILLING/HEATING DRY BATH

Chill and heat biological samples from -10.0°C to 110.0°C (without sample block). Control the heating plate with internal temperature sensor, or control the sample block or the solution in a vessel directly using the temperature probe provided. Have precise sample control, even at ambient temperature, in your lab or in the field on a compact, versatile and inexpensive electronic chilling/heating dry bath.

Buy Now

Specifications

Accessories

Compare all models

IC50 $1595.00

FEATURES:

- Energy-efficient Peltier design
- Digital control to 0.1°C from -10.0C to 110.0°C w/o sample block
- Temperature settable and stable to 0.1C from -10.0C to 110.0C
- Accurate to +/- 0.2C
- Control plate surface with internal sensor
- Control sample block directly with temperature probe provided
- Control solution directly with temperature probe provided
- Control at ambient
- Hot surface indicator. Red LED on front panel illuminates at 50C
- 99-hour count down timer with audible alarm and user settable Auto-Off
- RS232 I/O port for computer control or data collection
- More than 30 standard sample blocks available
- Two-line, 16-character per line, backlit, alphanumeric display
- 12-month warranty
- Universal power supply provided for use anywhere in the world
- UL, CSA, and CE compliant

APPLICATIONS INCLUDE:

- Maintaining 14°C for ligation reactions
- Enzyme reactions and deactivations
- Maintaining 17°C for storing oocytes
- Hybridizations
- PCR sample preparation
- Reagent chilling at 4.0C with insulated blocks for 15, 50, 250, 2-250, and 500ml centrifuge tubes
- Storing samples at ice bucket temperatures
- Incubate samples in 96-well and 384-well assay plates, or in aluminum blocks holding 0.2 ml, 0.5 ml, 1.5 ml, 15 ml, 50 ml centrifuge tubes, test tubes and vials of all sizes
- Storing enzymes or DNA libraries at your work station
- Transporting samples from the field at exactly the right temperature
- Chilling or heating samples in the field
- Freezing and storing most any small sample at your workstation
- General molecular biology applications

PRODUCT DESCRIPTION:

The completely solid-state EchoTherm™ IC50 Digital Electronic Chilling/Heating Dry Bath is compact, versatile, reliable and easy to use. Simply use the UP or DOWN arrows on the front panel membrane switch to set the temperature desired and the unit will go to that temperature.

The chilling/heating surface is a 2.875" (7.3 cm) x 4.375" (11.1 cm) aluminum plate that is very flat for optimal contact with your sample. When unloaded, the plate surface will reach below 0°C in under two minutes. It will also heat to 37°C in approximately 2 minutes. This rate of chilling or heating may vary with the load on the plate. For instance, temperatures down to 4.0°C can be reached on a solid aluminum block as large as 4" (10.2 cm) x 3" (7.6 cm) x 6" (15.2 cm) in less than one hour. When insulated, these large blocks can be driven below 0°C. Temperature gradients from the center to the edge of any aluminum block mentioned will be less than 0.3°C at any temperature.

A sample cover is available for assay plates or aluminum blocks and other samples. These blocks and covers are available as accessories.

▼ PRODUCT SPECIFICATION:

Temperature:

Range	-10.0°C to 110.0°C (without sample blocks)
Readability	0.1°C
Accuracy	±0.2°C
Stability	±0.1°C
Sensor Type	Platinum RTD built into plate and probe
Controller Type	PID
Uniformity	±0.3°C

Timer:

Range	1 second to 99 hours, 50 minutes and 59 seconds
Readability	1 second
Audible Alarm	Yes, alarm sounds for 1 minute. Timer counts up until turned off.
Auto-Off	Yes, user settable.

Electrical:

Heater/Chiller	Peltier, 100 watts
Operating Voltages	100 to 265 VAC, 50/60 Hz input to universal power supply. 12 VDC output to chiller/heater module.
Power Consumption	100 watts maximum
Power Switch	Yes, for 12 VDC into heater/chiller module

Dimensions:

Chilling/Heating Module	
Width	6.5" (16.5 cm)
Depth	8.75" (22.23 cm)
Height	4.0" (10.16 cm)
Power Supply	
Length	6.5" (16.5 cm)
Height	3.2" (8.1 cm)
Width	2.2" (5.6 cm)
Weight (power supply & chiller/heater module)	6.5 lbs (2.9 kg)

8.17 Appendix 17: Samples tested on the Ecotherm Dry bath

Given below in table 8.7 is an example of the data recorded in the LabVIEW program.

Table 8-7: Data recorded by the LabVIEW program

Voltage in	sample 1	sample 2	sample 3	sample 4	sample 5	sample 6	Thermistor 1	Thermistor 2	Room temperature	Room temperature	number	time/mins
5	4.281716	4.206079	4.956373	3.91	5.043	4.441	1.631	2.178	24.211393	22.548	1	0.02381
5	4.281716	4.237025	4.973913	3.921	5.1	4.526	1.649	2.137	24.208035	22.633	2	0.047619
5	4.283932	4.135309	4.91909	3.901	5.04	4.419	1.672	2.205	24.127434	22.567	3	0.071429
5	4.270635	4.135309	4.921283	3.906	5.056	4.421	1.643	2.028	24.179272	22.542	4	0.095238
5	4.277284	4.133096	4.855459	3.888	5.038	4.428	1.656	2.078	24.220089	22.583	5	0.119048
5	4.275068	4.137521	4.780806	3.89	5.036	4.397	1.633	2.046	24.290333	22.664	6	0.142857
5	4.263986	4.124246	4.743459	3.899	5.003	4.399	1.627	2.091	24.38632	22.801	7	0.166667
5	4.139782	4.119821	4.721484	3.886	4.946	4.399	1.567	2.019	24.493536	22.878	8	0.190476
5	4.210776	4.119821	4.736867	3.879	4.832	4.393	1.471	2.005	24.383484	23.004	9	0.214286
5	4.055407	4.000257	4.554316	3.877	4.814	4.395	1.624	2.032	24.118742	23.181	10	0.238095
5	4.037634	3.960369	4.534501	3.85	4.812	4.382	1.503	1.987	23.935274	23.442	11	0.261905
5	4.030968	3.909377	4.543308	3.819	4.799	4.386	1.537	1.985	23.77758	23.612	12	0.285714
5	4.050964	3.920465	4.519087	3.806	4.812	4.388	1.59	2.001	23.755825	23.612	13	0.309524
5	4.073176	3.967019	4.593934	3.813	4.834	4.395	1.631	2.06	23.704659	24.172	14	0.333333
5	4.266203	4.097691	4.747854	3.884	5.005	4.41	1.624	2.048	23.712362	24.422	15	0.357143
5	4.26177	4.128671	4.747854	3.892	5.023	4.433	1.594	1.998	23.73827	24.401	16	0.380952
5	4.259553	4.124246	4.743459	3.884	4.992	4.393	1.574	1.969	23.874748	24.412	17	0.404762
5	4.263986	4.108756	4.747854	3.888	5.032	4.448	1.62	2.01	23.856697	24.375	18	0.428571
5	4.184159	4.079983	4.736867	3.897	5.014	4.43	1.638	2.001	23.890131	24.357	19	0.452381
5	4.055407	3.911594	4.538905	3.904	4.847	4.397	1.485	2.021	23.9751	24.24	20	0.47619
5	4.048742	3.909377	4.37584	3.895	4.797	4.39	1.432	1.944	23.898178	24.02	21	0.5
5	4.053185	3.911594	4.450795	3.892	4.799	4.395	1.535	2.003	23.890991	23.803	22	0.52381
5	4.037634	3.902724	4.51248	3.89	4.803	4.395	1.624	2.035	23.869242	23.509	23	0.547619
5	4.23295	4.126459	4.750051	3.899	4.937	4.41	1.558	2.014	23.93581	23.594	24	0.571429
5	4.164192	4.106543	4.721484	3.897	4.904	4.399	1.615	2.01	23.855019	23.631	25	0.595238
5	4.230733	4.119821	4.752248	3.89	4.986	4.401	1.631	2.001	23.748835	23.797	26	0.619048
5	4.110925	4.095477	4.776413	3.888	5.027	4.404	1.601	1.998	23.61655	23.679	27	0.642857
5	4.244036	4.122033	4.783002	3.89	5.04	4.466	1.643	2.007	23.605839	23.573	28	0.666667
5	4.25512	4.117608	4.754445	3.892	5.025	4.417	1.455	1.962	23.675915	23.536	29	0.690476
5	4.188596	4.073342	4.736867	3.813	4.953	4.388	1.418	1.941	23.661711	23.515	30	0.714286
5	4.148659	3.982531	4.626936	3.688	4.821	4.366	1.455	1.885	23.687468	23.338	31	0.738095
5	4.068734	3.929334	4.534501	3.67	4.801	4.224	1.409	1.832	23.827433	23.327	32	0.761905
5	4.039856	3.893852	4.46622	3.679	4.696	4.175	1.487	2.005	23.70636	23.287	33	0.785714
5	4.028746	3.86945	4.400097	3.677	4.685	4.177	1.592	1.98	23.50049	23.25	34	0.809524

8.18 Appendix 18: Research activity

During the course of this research I have taken part in various research, industrial and academic activities. I have been extremely lucky to be part of several research projects which has helped me to develop important skillsets. The skills developed during the research include product development, project management, team work, time management, writing publication (book chapters, Journal publications and conference publications), presentations skills, Arduino, computer simulation software such as COMSOL Multiphysics and computer programing languages such as LabVIEW and MATLAB. I have also been lucky to do two back to back internships with the Applied Sciences Group at Microsoft (Redmond, USA).

The list of research activities carried out during the course of the research are listed below.

I. Publications and Conferences

- Book chapter: Dias, T.; Lugoda, P.; Cork, C.R., 'Microchip technology used in textile materials', High Performance Apparel 1st Edition, Ed. John McLoughlin and Tasneem Sabir, Woodhead Publishing, 2017. 451- 471. Print.

- Journal Publication: Lugoda, P.; Hughes-Riley, T.; Morris, R., Dias, T., 'A Wearable Textile Thermograph', Sensors, Vol 18, Issue 7 (2018).

- Journal Publication: Lugoda, P.; Hughes-Riley, T.; Morris, R., Dias, T., 'Developing Novel Temperature Sensing Garments for Health Monitoring Applications', Fibers, Vol 6, Issue 3 (2018).
- Journal Publication: Lugoda, P.; Dias, T.; Hughes-Riley, T.; Morris, R., 'Refinement of Temperature Sensing Yarns', Proceedings, Proceedings, Vol 2, Issue3 (2018).
- Journal Publication: Hughes-Riley, T.; Lugoda, P.; Dias, T.; Trabi, C.; and Morris, R., 'A study of thermistor Performance within a Textile Structure', Sensors, Vol 17, Issue 8 (2017).
- Journal Publication: Lugoda, P.; Dias, T. and Morris, R., 'Electronic Temperature Sensing Yarn', Journal of multidisciplinary Engineering Science Studies (JMESS), Vol 1, Issue 1 (2015).
- Academia Paper Publication: Colin, C.; Dias, T.; Rathnayake, A. and Lugoda, P., 'Fibre Electronic Technology for Wearables', Academia (2015)
- Conference presentation: Lugoda, P.; Dias, T. and Morris, R., Conference presentation on 'Electronic Temperature Sensing yarn for medical Applications' at the College of Art & Design and Built Environment NTU PhD Conference (June 2016).
- Conference presentation: Lugoda, P.; Dias, T. and Morris, R., Conference presentation on 'Temperature Sensing Yarn For Remote Temperature Measurement' at IDtechEx Sensors Europe, Berlin (April 2016).
- Conference presentation: Lugoda, P.; Dias, T. and Morris, R., Conference presentation on 'Smart bandage for remote monitoring of temperature and the moisture content of wounds' at Sensors in Medicine, London (March 2015).
- Poster presentation: Lugoda, P.; Dias, T. and Morris, R., Poster presented at IDtechEx Sensors Europe, Berlin (April 2016).
- Poster presentation: Lugoda, P.; Dias, T. and Morris, R., Posters presented at the College of Art & Design and Built Environment PhD Conference at NTU (May 2014 & April 2015).

II. Research Internship

Feb 2017- Aug 2017 Research Intern at Microsoft (Redmond)

- Research in the Applied Sciences Group
- Part of the material science group
- Leading and developing concepts, for future products.

III. Training and Development

- Professional Research Practice Course at Nottingham Trent University (stage1&2 completed)
- LabVIEW software package training (Core1&2)
- Introduction to COMSOL 5.0 & application builder
- Material testing using Zwick/Roell tensile machine
- Microscopy using a digital 3D Keyence microscope

IV. Demonstrating & Facilitating Experience

- 2014-2016 Laboratory Demonstrator at NTU for LabVIEW, C and Matlab

Supervised students in the physics department and marked their projects.

- 2015 Facilitator at ArcInTex (5 day workshop in Nottingham)

Advised and worked with multidisciplinary groups to develop ideas and projects based on wearable electronics

- 2015 Facilitator at Lucerne week (5 day workshop in Nottingham)

Advised and worked with multidisciplinary groups to develop ideas and projects based on wearable electronics

8.19 References

- Culverhouse, D., Farahi, F., Pannell, C.N., Jackson, D.A., 1989. Potential of stimulated Brillouin scattering as sensing mechanism for distributed temperature sensors. Electron. Lett. 25, 913–915. doi: 10.1049/el:19890612.
- Galindez-Jamioy, C.A., López-Higuera, J.M., 2012. Brillouin Distributed Fiber Sensors: An Overview and Applications [WWW Document]. J. Sens. URL https://www.hindawi.com/journals/js/2012/204121/ (accessed 1.11.18).
- Hoffmann, L., Müller, M.S., Krämer, S., Giebel, M., Schwotzer, G., Wieduwilt, T., 2007. Applications of fibre optic temperature measurement. Temp. Mõõtmise Fiiberoptiliste Meetodite Raken. 13, 363–378.
- JCGM, 2012. International vocabulary of metrology- Basic general concepts and associated terms (VIM) (No. 3rd Edition). JCGM 200.
- Malik, J.V., Jindal, K.D., Kumar, V., Kumar, V., Kumar, A., Singh, K.S., Singh, T.P., 2013. Effect of Temperature on Photonic Band Gaps in Semiconductor-Based One-Dimensional Photonic Crystal [WWW Document]. Adv. Opt. Technol. URL https://www.hindawi.com/journals/aot/2013/798087/ (accessed 1.11.18).

- Zou, W., Long, X., Chen, J., 2015. Brillouin Scattering in Optical Fibers and Its Application to Distributed Sensors. doi: 10.5772/59145.